EUR 3347e

INVESTIGATIONS INTO THE CRITICAL HEAT FLUX IN BOILING WATER

by

F. MAYINGER, O. SCHAD and E. WEISS

(MAN)

1967

EUR 3347 e

INVESTIGATIONS INTO THE CRITICAL HEAT FLUX IN BOILING
WATER by F. MAYINGER, O. SCHAD and E. WEISS (MAN)

This work concerns the measurement of critical heat flux (burnout)
in boiling water, and especially the influence of flow prehistory and
inlet conditions together with the test-channel L/D ratio on nucleate
boiling and the onset of film boiling. The measurements were made at
pressures of 70 to 140 atm on internal-flow tubes of diameter 0.7 to
1.5 cm. With mass-flows of between 100 and 350 $g/cm^2/sec$ the test-
channel intake conditions ranged from 20 % subcooling to 20 % steam
quality.

Two physically quite distinct forms of burnout were observed. With the one form the pressure and mass-flow begin to fluctuate shortly before the onset of film-boiling ; this form is therefore called " pulsating burnout ". With the other form the hydrodynamic behaviour is completely stable until film-boiling suddenly begins. Pulsating burnout, which was observed only in the subcooled boiling range, leads to critical heat flux values 20 to 50 % below those for hydrodynamically stable flow.

With hydrodynamically stable burnout it was sometimes possible to increase the burnout up to 80 % by altering the inlet hydrodynamics (orifice plates or short swirl-vanes). Further it was found that reduction of the L/D ratio affects the burnout during boiling even more than do these hydrodynamic modifications.

A special study was made of the forces which play a major part in causing and damping the pressure and mass-flow fluctuations preceding pulsating burnout, and of the design and hydrodynamic methods of avoiding it.

EUR 3347e

INVESTIGATIONS INTO THE CRITICAL HEAT FLUX IN BOILING WATER

by

F. MAYINGER, O. SCHAD and E. WEISS

(MAN)

1967

SUMMARY

This work concerns the measurement of critical heat flux (burnout) in boiling water, and especially the influence of flow prehistory and inlet conditions together with the test-channel L/D ratio on nucleate boiling and the onset of film boiling. The measurements were made at pressures of 70 to 140 atm on internal-flow tubes of diameter 0.7 to 1.5 cm. With mass-flows of between 100 and 350 g/cm²/sec the test-channel intake conditions ranged from 20 % subcooling to 20 % steam quality.

Two physically quite distinct forms of burnout were observed. With the one form the pressure and mass-flow begin to fluctuate shortly before the onset of film-boiling; this form is therefore called " pulsating burnout ". With the other form the hydrodynamic behaviour is completely stable until film-boiling suddenly begins. Pulsating burnout, which was observed only in the subcooled boiling range, leads to critical heat flux values 20 to 50 % below those for hydrodynamically stable flow.

With hydrodynamically stable burnout it was sometimes possible to increase the burnout up to 80 % by altering the inlet hydrodynamics (orifice plates or short swirl-vanes). Further it was found that reduction of the L/D ratio affects the burnout during boiling even more than do these hydrodynamic modifications.

A special study was made of the forces which play a major part in causing and damping the pressure and mass-flow fluctuations preceding pulsating burnout, and of the design and hydrodynamic methods of avoiding it.

Note

The tests described in this report were carried out in the laboratory of the nuclear power division of M.A.N. Nürnberg Works.

The test facility was planned and built by Mr. H. Agena, and Mr. H. Baldauf.

The electrical equipment of the facility, the development of the burnout detectors, three-wire thermocouples and electrical measurement techniques were handled by Mr. D. Henkel.

The test section, layout and wiring of the instrumentation were made by Messrs. H. Grasser, R. Rupprecht and G. Sichermann.

Summary

The purpose of the present study has been the measurement of the critical heat flux (burnout) in boiling and, primarily, the effects of the history and the inlet conditions as well as the L/D ratio of the test channel on nucleate boiling and the inception of film boiling were investigated. The tests were made at pressures of 70 to 140 kgf/cm^2 using internally cooled tubes with diameters varying from 0.7 to 1.5 cm. The conditions at the test channel inlets covered mass flows between 100 and 350 g/cm^2s between a degree of sub-cooling of 20% and 20% steam quality.

Two types of burnout were observed which are completely different in their physical appearance. One type is characterized by the occurrence of fluctuations in the pressure and mass flow shortly before film boiling starts and therefore this was designated "pulsating burnout". The other type shows a hydrodynamically completely stable behaviour until film boiling suddenly occurs. Pulsating burnout which was observed only in the range of sub-cooled boiling was found to lead to critical heat flux levels 20 to 50% below those obtained with hydrodynamically stable flow.

With hydrodynamically stable burnout it was possible, by varying the hydrodynamic inlet conditions, to increase the critical heat flux up to 80%. The factors studied included primarily the influence of differently designed inlet openings as well as of orifices and short twisted tapes fitted in the inlet to the test channel. An even greater influence on the critical heat flux in boiling compared to these hydrodynamic measures was obtainable by a reduction of the L/D ratio. With very short test sections having an L/D ratio of 5 to 10 the critical heat flux is 4 to 5 times the value obtainable with long test channels having an L/D ratio of 80 to 100. The

physical and technical reasons for this improvement by a
change in the inlet conditions and shorter L/D ratios
could be clarified to a large extent by measuring probes
developed specifically in the course of the tests.

In respect of pulsating burnout, the question was given
special attention as to what forces are important for the
excitation and damping of the pressure and mass flow
variations which are preliminary to it and what the design
and hydrodynamic possibilities are to obviate it. It was
found that it is above all the existence of spaces filled
with compressible medium upstream of the test channel and
throttling of the flow at the test channel inlet that affect
the pulsations. Throttling has proved to be a reliable, if
uneconomical, means to avoid pulsating burnout. As increased
throttling invariably involves additional pumping power it
is sound policy to keep this pressure loss, allowed for
reasons of safety from pulsations, at the very minimum. For
this reason, extensive experiments were included in the work
carried out to study the minimum throttling effect necessary
for various design, thermal and hydrodynamic conditions.

Index
=====

1. Introduction (*)

The present report is intended to summarize the work carried out under the research contract No. 057-61-RDD/Q.D.No. III.1.8 made between the European Atomic Community and the Maschinenfabrik Augsburg-Nürnberg Aktiengesellschaft, Nuremberg Works. This contract had for its object the investigation of the critical heat flux in boiling in internally cooled tubes.

Work published during the last 10 years includes a multitude of studies of the problems in the vast and little known field of two-phase flow of which the greater part dealt with the phenomenon of film boiling or, more specifically, burnout. In spite of this large number of experimental studies and theoretical analyses, a clear understanding of the influence of important flow-mechanical, thermodynamic, and geometric parameters on the transition from nucleate to film boiling was lacking. Out of the numerous factors involved it was mainly the pressure, temperature, steam quality, mass flow and shape of the heated surface of which the effect on burnout had been the subject of both qualitative and quantitative studies. However, little, if no, data were available which would have permitted an evaluation of the influence of the hydrodynamic inlet conditions and the length/diameter ratio on the maximum heat flux in boiling.

It has, therefore, been the main aim of our work to define the influence of these parameters. With a view to simplifying the problem and to create clear cut test conditions, it was deliberately decided to adopt straightforward test conditions and, therefore, the tests were made on round, internally cooled, individual tubes. The form of the velocity profile and the thermal profile in the burnout zone were varied by providing different types of inlet sections and variously formed flow

disturbing elements such as twisted tapes and orifices as well
as by changing the length/diameter ratio of the heated section,
the test range covering pressures from 70 to 140 kgf/cm^2 mainly
in the range of sub-cooled boiling and low to medium steam
qualities. In addition to the main target of the tests, it was
possible to obtain results which provide information on the
influence of the parameters of pressure, mass flow and sub-
cooling on the boiling crisis.

During our investigations we observed two completely different
types of burnout. The term "burnout" as used in this report
is interpreted in the strict sense of the word, i.e. when
melting or destruction of the heated wall occurs due to
excessive temperature rise which is not necessarily identical
with the terms "film boiling" or "boiling crisis". The first
type burnout represents a genuine boiling crisis, i.e. film
boiling. The second type can conveniently be referred to as
"pulsating burnout" because it is caused by mass flow and
pressure variations and their consequences. The heat flux in
the case of the pulsating burnout, which tends to occur only
in a narrowly limited range, i.e. under conditions of sub-cooled
flow and at low steam qualities in the test channel is 20 to
50% lower than with the first type burnout. In pulsating burnout
pressure and mass flow fluctuations suddenly arise on a definite
heat flux level being reached without any change in the
circuit other than the slow and uniform increase in the heat
flux. The amplitudes of the pulsations increase rapidly and
lead to a crisis in the heat transfer process which eventually
causes burnout.

The physical conditions in either type of burnout show marked
differences. For this reason, and with a view to achieving a
clear and cohesive description of the phenomena, the first type

./.

burnout i.e. the boiling crisis under completely stable flow
conditions and the type two burnout,i.e. the pulsating
burnout, are discussed in separate chapters.

The task before us made it necessary to perform measurements
of certain hydrodynamic and thermodynamic factors without
time lag and with a reasonable degree of accuracy. In con-
junction with the work under the contract,various measuring
devices have been developed of which the three-wire thermo-
couples deserve special mention. These make it possible to
record the temperature variation on the surface of the
electrically heated test channel at the moment of the
extremely rapid burnout process without time lag and provide
valuable information on the hydrodynamic and thermodynamic
conditions during transition from nucleate to film boiling.

2. Test Facility and Measuring Equipment

The test loop in which the measurements of the critical heat
flux in boiling were made and in which heated channels of
any desired cross sectional flow area can be installed was
designed for the following main data:

Maximum permissible working pressure	220 kgf/cm^2
Maximum permissible working temperature	372 °C
Maximum flow	15 m^3/hr
Heating capacity available for the test channels	440 kW at 4000 A and 110 V
and	350 kW at 2000 A and 175 V

2.1 Description of Test Loop

2.1.1 Layouts and equipment in loop

In designing and proportioning the test loop care was taken
to permit operation of the plant both as a pressurized
water circuit, i.e. in the sub-cooled range, and as a
boiling water circuit with steam/water mixtures in the test
channel. The installation was of the closed circuit type, the
flowing medium being circulated by means of a centrifugal
pump. In its hydrodynamic stability behaviour it, therefore,
closely simulated the conditions prevailing in
pressurized water and boiling water reactors.

The arrangement of the circuit is shown in Fig. 1. Fully
demineralized and deaerated water is delivered by means of
the circulating pump 6 via one of three parallel flow-
measuring sections to the electrically heated preheater 7
where it is heated to the desired conditions at test channel
inlet and, depending on test conditions, may be partly
evaporated. From the preheater the medium flows into the
test section 1 incorporating the channel tube to be tested

for the maximum heat flux attainable. The water/steam
mixture produced in the channel can be separated into the
steam and liquid phases in the steam separator 2. The dry
saturated steam is passed into the condenser 4 where it
condenses and is slightly sub-cooled. The water obtained in
the steam separator flows to the cooler 3. Both part flows
can be determined by separate flow-measuring orifices.
Downstream of the flow-measuring orifices the two branch
flows combine to reach the initial point of the circuit
the pump 6 via the cooler 5. In the course of the tests, it
was found that, to obtain appropriate steady-state conditions
in the test circuit, it was preferable to cut out the steam
separator and to pass the water/steam mixture obtained in
the test channel directly to the condenser 4.

When measuring sub-cooled flow, the pressure in the circuit
was kept at the desired value by the electrically heated
pressurizer 8. A secondary circuit comprising a cooler 10,
a regenerative heat exchanger 11 and a mixed-bed filter 12
was provided to by-pass the pump 1 to "bleed" water from the
circuit for continuous cleaning under working pressure.

At temperatures up to $300^{o}C$ in the circuit, well water was
used as secondary coolant for the coolers and condensers,
whereas at higher temperatures, because of the high thermal
stresses arising in the tubes of these heat exchangers under
these conditions, it was necessary to interpose an inter-
mediate coolant circuit using Diphyl.

2.2 Equipment in the Test Loop

All parts of the test loop in contact with the primary
medium were made of stainless steel.

The circulating pump was of the glandless, three-stage
centrifugal type (made by KSB, Model LUVh) rated at about
120 m wg head and a maximum flow rate of 15 m^3/hr. The motor
was of the canned rotor type and protected from the high
temperatures in the pump section by a water-cooled heat
barrier. Additional cooling of the motor was provided via
a heat exchanger. Control of pump delivery was by means of
a by-pass fitted with a motor-operated control valve between
the pump inlet and discharge. A second possibility of control
was afforded by the throttling valves installed in the main
circuit.

The electrically heated preheater was formed by 4 tube banks
in series, each bank consisting of 6 parallel tubes. Heating
elements were concentrically arranged in these tubes. These
heating elements are resistance strips of AlSiCr embedded in
magnesium oxide and enclosed in a V2A tube. Coarse control
of heater capacity was by cutting in and out individual heating
rods and fine control was obtained by means of a regulating
transformer which provided infinitely variable control of
3 rods located at the outlet side of the heater.

The vertically arranged steam separator was of the combined
baffle and surface type. The two-phase medium entered the
vessel at the top and impinged on the baffle which divided
the inner space and was perforated at the bottom. As a
result, steam could pass unhindered into the steam space above
the liquid level. It then passed through a bank of Raschig
rings and through two steam strainers into the steam pipe
leading to the condenser. The saturated water was discharged
at the bottom of the vessel and carried into the intermediate
cooler.

./.

The coolers and condensers were of the shell-and-tube type with the tubes being expanded and welded into the tube plates at both ends. As previously mentioned, the coolant up to temperatures in the primary circuit of 300°C was boiling water at 1 kgf/cm^2 whereas, at higher temperatures, Diphyl was used at the secondary side of these heat exchangers. This was recooled in separate coolers by well water.

The pressurizer required for tests with steam-free water was a vertical cylindrical vessel designed to contain a steam cushion of 130 litres maximum. The pressure was controlled from the saturation temperature of the steam and the heat was supplied by 4 electrical heating elements welded into the bottom of the vessel and designed to permit a temperature increase of 50°C/h during start-up of the test facility. During operation, the saturation temperature required for the desired working pressure was regulated by on-off control of the heater rods.

Initial filling of the test loop, and refilling to account for variations in the working conditions was from a demineralization plant which was designed to supply fresh water with an electrical conductivity of 0.3 to 0.5 /u-Siemens/ cm.

2.3 Test Section

The design of the test section is shown in Fig. 2. It essentially consists of a thick-walled autoclave and the actual test channel, a tube carrying the circulating water and surrounded pressure-tight by the autoclave. By various design measures, a cylindrical space is provided between the test channel and the autoclave wall which is filled with

./.

nitrogen. The test channel 1 is brazed at the top in a lens-
shaped body which at the same time serves as the negative
pole of the power supply 2 and the upper airtight closure of
the nitrogen space. At the bottom end of the test channel
where the water is admitted there is another lens-shaped
body placed between two mating flanges which is designed
with a recess to attach expansion bellows 3. The expansion
bellows are arranged concentrically around a supporting tube
with a flange 4 fitted to its bottom end. This flange is
bolted to a mating flange and Klingerit gaskets and ceramic
spacers are provided for electrical insulation. It is in this
mating flange that the test tube is brazed in. These arrange-
ments provide a completely pressuretight closure of the
annular space filled with nitrogen against the circulating
water. The nitrogen pressure is maintained via an automatically
operating equalizing system,which is also shown in Fig. 2,at
the water pressure prevailing at the test channel inlet.
This relieves the test channel from any pressure and it is
possible to test tubes with thin walls similar to the
cladding tubes of the fuel elements in pressurized and boiling
water reactors. The test channel is directly heated
electrically by direct current with the test channel wall
serving as ohmic resistance. Direct current can be obtained
alternatively from 3 independent sources in the form of a
rectifier and 2 motor generator sets. The rectifier consists
of groups of parallel-connected silicon diodes connected in
a three-phase bridge circuit via a step-down transformer and
a regulating transformer with the 6 kV factory system.
Infinitely variable control of the d.c. voltage is possible
from 10 to 175 V with a maximum amperage of 2000 A which
provides a maximum heating power of 350 kW. The d.c. ripple
is about 4%. Cutting off of the power is by a circuit breaker
with a response time of about 12 ms. This short response

./.

time is achieved, inter alia, by an impulse tripping device
which releases the servo mechanism of the breaker within
3 ms after applying a release voltage impulse.

For tests which call for high constancy of the heating
voltage there is a motor generator set. It consists of two
d.c. shunt generators which are driven together by a slip-
ring motor. Both generators have a rated output of 220 kW
at an amperage of 2000 A and a terminal voltage of 110 V.
Each unit is equipped with a transistorized two-position
controller which regulates the current in the exciter winding
so that the desired voltage, which is infinitely variable in
a range from 7 to 110 V, is maintained constant with an
accuracy of 0.5%. Setting of the desired value is by means
of a multi-spiral Helipot potentiometer with precision drive.

Parallel connection of both units can be achieved by closing
the coupler switch. An automatic mechanism ensures that
both machines are regulated for equal voltage before parallel
connection and after connection are regulated in addition for
equal current. Shutting down is by means of quick-action
breakers of the same type as used in the rectifier plant
described further above.

The sensing elements for the test channel, such as thermo-
couples and voltage pick-ups, are welded onto the outer
non-cooled surface of the internally-cooled channels and are
brought out through specially designed electrically
insulated bushings which provide a pressuretight seal. This
bushing, which is shown in Fig. 3, consists of a cone of
Araldit which is pressed against a metal seat by the interior
pressure to be self sealing. The instrument leads are cast
into the cone.

./.

2.4 Measuring Techniques and Instruments

The critical heat flux in boiling depends on a number of hydrodynamic and thermodynamic parameters, such as mass flow density, system pressure, degree of sub-cooling or steam quality, respectively, which all have to be measured reliably and with accuracy. In addition, it is necessary to measure the power supplied to the test channel as well as the variation of the heating surface temperature. To protect the test channel from destruction a safety system is called for, a so-called burnout detector, which cuts off the power supply just before excessively high temperatures are reached.

2.4.1 Measuring the temperatures of the circulating medium

The following temperatures are measured in the main circuit by means of thermocouples:

Inlet and outlet temperatures at test channel
Inlet and outlet temperatures at preheater
Temperature at flow measuring orifices
Temperature at pressurizer

In the larger bore pipes of the circuit the thermocouples are distributed over the cross section on a traverse fitted between two flanges. Fig. 4 shows a section through a typical traverse. It consists of a ring with lens-shaped sealing surfaces with radial drilled holes and 3 or 4 branch-offs to which nipples are welded into which the steel-clad thermocouples are brazed. Projecting 30 to 40 mm into the flowing medium the measuring error caused by heat dissipation is negligible. In small-bore pipework of less than 50 mm inside diameter the fitting of temperature traverses is not

./.

possible. Therefore, a temperature measuring loop is used as shown in Fig. 5. For this purpose, a 90° knee is fitted into the pipe line in which a thermocouple is so arranged that it points against the flow and reliably indicates the temperature of the medium at this point.

The temperature readings of all these thermocouples were compared with that of a Pt-Pt-Rh couple which, in turn, was calibrated for high accuracy via several fixed points, such as the boiling point of water, the melting points of tin, zinc and cadmium. All temperatures to be measured were recorded during the test duration by means of two potentiometer recorders each with 12 channels. In addition, it was possible to obtain readings from each measuring point, via a selector switch, individually on a precision potentiometer recorder.

2.4.2 <u>Measuring the surface temperature of the test channel</u>

The best burnout criterion is the accurate and adequately fast measurement of the surface temperature of the test channel at the moment transition occurs from nucleate to film boiling. This calls for temperature probes with a correspondingly high rate of response. Conventional thermocouple arrangements, if they are applied to the current conducting test channel wall with electrical insulation interposed, are too sluggish or, if they are applied directly, a high error voltage is superimposed on the thermocouple e.m.f. which results from the voltage drop of the heating current in the test channel wall. The work under review therefore included the adoption of a special thermocouple system, a so-called three-wire thermocouple, the basic arrangement of which was given by Buchberg [1] ; but extensive developments were necessary in our laboratory before accurate and reliable functioning was obtained. This three-wire thermocouple which is schematically shown in

./.

Fig. 6 essentially consists of three wires welded directly
to the current conducting surface of the test channel and
spaced about 0.5 mm apart. The two outer wires consist of
like material whereas for the centre wire the material has
a different thermoelectric rating. The tube lengths between
the wires form a Wheatstone bridge together with the
resistors R_1 and R_2 which is so balanced that the error
voltage due to the heating current becomes zero and there is
only the thermoelectric e.m.f. in the galvanometer circuit.
The response time of these three-wire thermocouples is some
40 times shorter than that of a mica-insulated thermocouple.
As shown by the two graphs at the top of Fig. 6, a thermo-
couple insulated against the current-carrying wall by means
of a 0.1 mm thick mica layer using wires of 0.1 mm thickness
will take approximately 280 ms until an indication of 2/3 of
the actual value of a suddenly applied excess temperature
is obtained whereas the three-wire thermocouple gives the
same indication in 7 ms.

The Wheatstone bridge formed by the thermocouple system is
balanced by means of a Lissajous figure produced by a
cathode-ray oscilloscope. The use of this balancing method
calls for the d.c. used for heating having an a.c. voltage
component which can be produced, for instance, by super-
imposing an alternating current. To obtain the Lissajous
figure the voltage drops of the a.c. proportion across the
supply circuit and the galvanometer circuit of the Wheat-
stone bridge are applied to the r.c. coupled inputs of the
cathode-ray oscilloscope in a manner that the voltage of
the galvanometer circuit is applied to the vertical plates
and the voltage of the supply circuit to the horizontal
plates. The slope of the straight line appearing on the
screen relative to the horizontal screen axis is a measure
of the bridge unbalance. The system is balanced if the
straight line is parallel to the horizontal axis of the
screen.

Another possibility of balancing the three-wire thermocouples
is by suddenly shutting off the heating d.c. current by hand.
If the Wheatstone bridge is not balanced the galvanometer used
for the temperature measurement will show, in addition to the
thermal e.m.f. of the thermocouple, the unbalance voltage of
the bridge. If the shut-off process is recorded by means of
a recording oscilloscope there will initially be a sudden
voltage change in the thermocouple which originates from the
removal of the error voltage and then only does an
exponential drop of the reading occur, corresponding to the
temperature change due to the cooling of the heating
surface. A trace for such a thermocouple circuit which is
not accurately balanced is reproduced in Fig. 7a.

During operation, unbalance in the bridge circuit arises
due to temperature-dependent variations of the resistances
of the thermocouple wires as well as the resistances of the
channel sections between the junction welds of the thermo-
couple wires. Unbalance due to resistance variations in the
thermocouple wires can be eliminated by appropriate pro-
portioning of the resistors R_1 and R_2 shown in Fig. 6 which -
as explained in detail in 2 - have to be selected so that the
unbalance potential is below the class accuracy of the
measuring instruments used.

How much the bridge circuit is unbalanced due to resistance
changes in the channel section between the welds of the
thermocouple wires during nucleate boiling or a short time
before burnout occurs, has been examined on the same
principle which underlies the abovementioned calibration
method by means of shutting off the heating power. A few

./.

tenths of a second before burnout occurs, which mostly was preceded by statistical temperature variations, the heating power was therefore interrupted by hand. As is clearly shown in Fig. 7b the bridge was not unbalanced due to nucleate boiling or the boiling processes on inception of burnout because, at the moment of shutting off the power, there was immediately the exponential temperature drop and a sudden change resulting from a spurious voltage did not occur.

The recording instrument used to record the very fast temperature changes was a light-beam line recorder with 18 channels whose highly sensitive moving coil galvanometer is capable of tracing temperature variations up to a frequency of 8000 cps.

2.4.3 Pressure measurements

Measurements of the steady-state system pressure in the test loop were made by means of Bourdon tube pressure gauges of the accuracy class 0.6. These pressure gauges were calibrated before installation by means of a deadweight tester and their accuracy was checked at regular intervals. Furthermore, a piston-type pressure gauge was available for accurate measurements and this was used at the same time as the desired value transmitter for the control of the pressurizer heating system.

For measurements of high-frequency pressure variations, such as were liable to arise in the burnout process, two different types of differential pressure gauges were employed. The one relied on strain gauges and consisted essentially of a pressure diaphragm of austenitic steel onto which a strain gauge was glued. The one side of this diaphragm was

.../.

connected via a short tube branch with the points of the
test loop at which the pressure variations of the circulating
medium were to be measured. At the other side of the
diaphragm, a constant pressure was applied by means of the
abovementioned nitrogen pressure equalizing system which
corresponded to the mean value of the pressure in the
circulating medium. To correlate the voltage variation
indicated by the strain gauges with pressure differentials
this measuring system was statically calibrated before
installation by means of a mercury manometer.

Furthermore, a CEC differential pressure transmitter was used
which employs a modified strain gauge principle to sense
the pressure. In this instrument, the gauge wires subject to
strain are suspended from 4 movable bars connected by springs
and loaded via a diaphragm, a configuration designed to
ensure a linear relationship between the differential
pressure and the measuring voltage over the entire
measuring range. This transmitter was capable of sensing
pressure variations up to a frequency of 2000 cps.

2.4.4 Flow measurements

Measurement of flow rates was by means of orifice plates
to DIN 1952 [3] the dimensions of which were so selected
that an adequate indication was obtained in the differential
manometers for reasonable reading accuracy at the minimum
flow rate to be determined. The manometers were of the
mercury-filled U-tube differential type in which the
position of a steel ball floating on the mercury is sensed
magnetically.

To obtain information on high-frequency mass flow variations,
such as are caused by the boiling process in the test
channel, it is necessary to employ fast response sensing

elements. It was therefore decided, in addition to the
orifice measurements, to record the flow conditions by
means of a turbine flow meter. This instrument is basically
a small single-stage axial-flow turbine with a permanent
magnet rotating with the rotor to produce impulses in a
sensing coil outside and, thereby, generate an a.c. voltage
in proportion to the flow rate. This is converted in a
digital analog converter into a frequency proportional
direct voltage which can then be recorded on an oscillo-
graph against time. The response rate of this turbine flow
meter was approximately 10 ms and its measuring range
extended from 100 to 500 litres/hr.

2.4.5 Determination of steam quality

The steam quality at the test channel inlet was obtained
from the energy balance of the electric heater by the
formula:

$$x_{EM} = \frac{1}{r} \left[\frac{Q_{VW}}{M} - i^t + i_{Evw} \right] \qquad (1)$$

where

x_{EM}	steam quality at test channel inlet	-
r	heat of evaporation	kcal/kg
Q_{VW}	power supplied to the heater	kcal/h
M	mass flow	kg/h
i^t	enthalpy of water in state of saturation	kcal/kg
i_{Evw}	enthalpy of water at heater inlet	kcal/kg

The heat loss of the heater to the environment was
determined by calculation in advance and by thorough
calibration tests.

./.

The steam quality at the test channel outlet can be
determined by two alternative methods. The simplest and,
as was found during the test operation, most reliable
method relies on the energy balance of the test channel.
In this case, the abovementioned equation applies if the
corresponding magnitudes are referred to the test channel
instead of the heater.

It is also possible to determine the steam quality on the
basis of partial flows determined separately in flow
orifices downstream of the steam separator. However, this
method involves corrections for after-evaporation due to
the pressure drop in the pipework and for the condensation
due to the heat loss, and the efficiency of the steam
separator, i.e., the remaining humidity in the steam flow,
has to be taken into account.

2.4.6 Electric probe for locating steam bubbles

The time sequence of steam voids above the test channel
was determined by means of an electric probe of the type
employed by Nassos [4] . As shown in Fig. 8a it consists
of a glass-coated platinum wire having its end bent into
the flow direction and provided with a slender point which
projects from the insulation. If the probe is exposed to a
water flow containing steam bubbles it will be alternately
wetted with water and enveloped with steam. Both conditions
can easily be detected by means of a d.c.-fed resistance
or ohmmeter connected between the platinum wire and the
test channel wall. If enveloped with steam, the resistance
will be infinite and, consequently, the current zero whereas,
when wetted with water, the resistance and current, re-
spectively, will attain a value which essentially depends on the

./.

temperature-dependent electric conductivity of the water
as well as the volumetric ratio between water and steam in
the immediate vicinity of the platinum point. The circuit
arrangement in Fig. 8b shows the basic layout of the
electrical instrumentation. A d.c. source is connected in
series with the probe and a voltage divider R. The divided
voltage is fed to a high-ohmic input amplifier combination
to the output of which is connected the galvanometer of the
oscillograph.

2.4.7 Burnout detector

To protect the test channel from destruction on attaining
the critical heat flux due to melting or burning through,
a burnout detector was used the design of which is shown
in Fig. 9. In this connection, it should be emphasized
that this burnout detector served only as a safety device
and its response was not referred to as a criterion for
the inception of the boiling crisis. The latter purpose
was served by the temperature indication of the fast-
response three-wire thermocouples which - as discussed in
the following chapters - enabled satisfactory information
to be obtained on the inception and the pattern of the
burnout phenomenon.

In the burnout detector, the excessive temperature rise
at the moment of burnout is determined by comparing the
electrical resistance of the upper half of the test
channel with that of the lower half in a Wheatstone bridge
circuit. On inception of burnout, the previously balanced
bridge becomes unbalanced and the unbalance signal is
amplified in a differential amplifier with a very high
in-phase suppression and applied to a relay which,when a
preselected value is reached, closes a normally open
contact and, thereby, operates the quick-action breaker
explained in Chapter 2.4. Interference voltages with a
great width of the transition interval are largely
suppressed by the inductivity of the relay coil. The total
time required for cutting off the power was 20 to 30 ms.

./.

2.5 Error Analysis

For an evaluation of results it is necessary to consider possible errors and to determine the accuracy with which the individual results were obtained. The factors that enter directly into the results of the critical heat flux are the electric power applied as well as the heated surface of the test channel whereas other parameters - such as system pressure, temperature and the steam quality of the coolant respectively and the mass flow - are correlate factors. To define the overall measuring uncertainty it is necessary to know to what extent the various factors enter into the overall factor. The relative importance of the individual factors can be found by means of an equation to determine the critical heat flux in a manner that it is differentiated for the individual test parameters.

Using, for instance, the Bettis equation 7 shown in the Appendix 1 under Item 2

$$\frac{\Phi_{BO}}{10^6} = C_1 \left(\frac{H_{BO}}{10^3}\right)^{-2.5} \left(1 + \frac{G}{10^7}\right)^2 \cdot e^{-0.0012 \, L/D} \quad (2)$$

then the relative error for the heat flux is

$$\frac{\Delta\Phi_{BO}}{\Phi_{BO}} = 2.5 \cdot \frac{\Delta H_{BO}}{H_{BO}} + \frac{2}{10^7} \cdot \frac{G}{\left(1 + \frac{G}{10^7}\right)} + \Delta L/D \cdot 0.0012 \quad (3)$$

where

D	=	diameter	ft
G	=	mass flow	lb/hr-ft^2
H_{BO}	=	enthalpy at burnout point	Btu/lb
L	=	heated channel length	ft
Φ_{BO}	=	burnout heat flux	Btu/hr-ft^2

Regarding the system pressure, which in the Bettis equation is not allowed for, it is assumed, for the error analysis in the test range investigated by us from 70 to 140 kgf/cm^2, that it is linear so that $\frac{\Delta p}{p}$ can be taken for the

relative error. This term therefore has to be added to the abovementioned relative error. Before applying equation 3 it is, however, necessary to determine individual errors such as those in the enthalpy, the mass flow, the L/D ratio etc. which will be dealt with in greater detail in the following chapters.

2.5.1 Errors in the temperature measurements

Calibrated steel-clad nickel-nickel-chrome thermocouples as described in Chapter 2.4.1 were used for the temperature measurements in the test loop. The hot junctions of these thermocouples were connected via a multi-point selector switch against a common ice bath reference junction and the thermo-electric e.m.f. was measured by means of a potentiometer recorder with a class accuracy of 0.1. Inaccuracies result from reading errors of the measuring instruments and uncertainties in the calibration.

The measuring instrument had a reading accuracy of $\pm$ 0.02 mV which for the thermocouples used corresponds to approx. $\pm$ 0.5°. Calibration was made by comparing it with a platinum-platinum-rhodium couple which, in turn, had been calibrated by means of fixed points using a potentiometer recorder with a class accuracy of 0.01. This results in a maximum calibration error for the nickel-nickel-chrome thermocouple used in the tests of $\pm$ 1°C, and the total inaccuracy in measuring the temperature of the coolant would certainly not exceed $\pm$ 1.5°C.

2.5.2 Errors in determining the mass flow

As already mentioned in Chapter 2.4.4 mass flow was measured by means of orifices to DIN 1952 and turbine flow meters, both instruments being usually employed simultaneously. The orifice plate used for most of the measurements had an opening of 0.625 cm for a tube diameter of 2.32 cm. The flow rate was obtained by the equation

$$Q = 0.01252 \cdot \alpha \cdot \varepsilon \cdot m \cdot D_t^2 \sqrt{\frac{1}{\rho}} \cdot \sqrt{p_1 - p_2} \qquad (4)$$

where

α , ε , m	=	constants	-
D_t	=	tube diameter	mm
ρ	=	density	kg/m^3
$p_{1,2}$	=	pressure	kgf/m^2

With the low values of the mass flows measured by us the Reynolds number is below the limit of constancy stated in DIN 1952 of Re = $2.5 \cdot 10^4$. Therefore, the flow coefficient had to be determined experimentally. This was effected in a calibration section where the water flow per unit time was weighed and the differential pressure ($p_1 - p_2$) at the orifice was measured by a U-tube manometer. This resulted in a flow coefficient $\alpha = 0.608$ with a calibration tolerance of $\pm$ 1%. The further errors for flow measurements according to DIN 1952 are

Additional tolerance for tube roughness	$\pm$ 1%
Additional tolerance for edge bluntness	$\pm$ 1.7%

Consequently, the overall mean error for the orifice was $\pm$ 2.2%. The differential pressure $p_1 - p_2$ was measured in a mercury U-tube manometer with a reading error of $\pm$ 1 mm mercury. The deflection of this manometer with minimum flow was 100 mm Hg so that the maximum error in determining the differential pressure was $\pm$ 1%, it having to be borne in mind that the differential pressure under the root sign enters into the flow determination whereby this error source for the mass flow is reduced to $\pm$ 0.5%. The uncertainty in determining the density of the coolant in the flow measuring orifice attained values of approximately $\pm$ 0.5%.

All these factors taken together resulted in a mean error for the mass flow measurements of $\pm$ 2.3% according to the error propagation law.

The turbine flow meters had been calibrated by means of the flow measuring orifices. Therefore, it is necessary to add the reading error of the indicating instrument to the abovementioned uncertainty of the orifice plates for these instruments so that the inaccuracy in the flow results measured by the turbine flow meters is estimated at $\pm$ 3%.

2.5.3 <u>Errors in pressure measurements</u>

The maximum error of the Bourdon tube pressure gauges used to measure the system pressure was $\pm$ 0.6% of the maximum scale value. Added to this, is an observation error which for the given scale division is estimated at $\pm$ 0.25 kgf/cm^2. The scale ranges used in the pressure gauges were 0 - 100 kgf/cm^2 for the system pressure of 70 kgf/cm^2 and 0 - 250 kgf/cm^2 for the system pressures of 100 and 140 kgf/cm^2. Accordingly, the following overall error was arrived at for the pressure measurements in the individual ranges:

at   70 kgf/cm^2 $\pm$ 1.2%
at 100 kgf/cm^2 $\pm$ 1.8%
at 140 kgf/cm^2 $\pm$ 1.3%

The differential pressure transmitters used to sense high-frequency pressure oscillations during pulsating burnout were statically calibrated before installation by means of mercury manometers. On the basis of this calibration and the given observation accuracy on the oscillograph, the error in this dynamic pressure measurement is estimated at approximately $\pm$ 5%.

./.

2.5.4 <u>Errors in determining the degree of sub-cooling and steam</u>
<u>quality,respectively,at test section inlet</u>
The degree of sub-cooling and the steam quality of the
flowing medium is defined by $x = \dfrac{i-i'}{r}$ where

i	=	enthalpy of flowing medium	kcal/kg
i'	=	saturation enthalpy of water	kcal/kg
r	=	heat of evaporation	kcal/kg

With sub-cooled liquids, i.e. $i < i'$ the accuracy of the
abovementioned properties is dependent on the errors in the
pressure and temperature measurements. Most of the tests
were carried out in a pressure range between 70 and 140
kgf/cm^2 where the gradient $\dfrac{d\vartheta}{dp}$ is very small so that,
essentially, only the error in the temperature measurement
enters into the results which according to Chapter 2.5.1
amounts to $\pm$ 1.5°C. In the error analysis the specific heat
of the water in the enthalpy of the sub-cooled flow may as
a first approximation be assumed to be constant so that the
error for the enthalpy of the flowing medium is $\pm$ 1.5 kcal/kg.

The saturation enthalpy i' and the heat of evaporation r can
either be derived from a pressure measurement or a temperature
measurement using the water steam tables. A simple con-
sideration made by means of the steam pressure curve shows
that it is preferable to use as a basis the measured pressure
the error of which causes tolerances of $\pm$ 1 kcal/kg in the
saturation enthalpy and $\pm$ 1.5 kcal/kg in the heat of
evaporation. Thus, the error obtained, for instance, for the
degree of sub-cooling of x = -0.2 amounts to $\pm$ 0.01.

With two-phase flow at the test section inlet the steam
quality is determined via the energy balance of the heater

from the equation (1) explained in Chapter 2.4.5. If this
equation is differentiated for the error analysis with
respect to the individual magnitudes and divided by x_{EM},
the steam quality at the test channel inlet, then the
relative error is obtained by

$$\frac{\Delta x_{EM}}{x_{EM}} = \frac{1}{(\frac{Q_{vw}}{M} - i' + i_{vw})} \cdot (\frac{\Delta Q}{M} + \Delta M \frac{Q_{vw}}{M^2} + \Delta i' + \Delta i_{vw}) +$$

$$+ \frac{\Delta r}{r} \qquad\qquad (5)$$

The tolerances required in this equation for the mass flow,
the saturation enthalpy, the enthalpy of the sub-cooled
flow at the heater inlet as well as the heat of evaporation
can be taken from the Chapters 2.5.1 to 2.5.3. The error in
determining the heater output Q is essentially composed of
the instrument errors of the ammeters and voltmeters as
well as the heat loss of this heater to the surroundings.
On the basis of the class accuracy of 0.1 of the instruments
and measuring resistors used, the instrument error is
obtained as ± 1%. The heat loss can be taken from Fig. 10
which has been plotted on the basis of a thorough thermal
analysis.

2.5.5 Errors in determining the heat flux density

As already mentioned, the tolerance for the heat flux
density is composed of the error in determining the heat
emitting surface as well as the errors in measuring the
electric heating power. Added to this, there is an error
caused by the heat losses of the test channel to the power
leads as well as to the nitrogen cushion surrounding the
channel.

./.

The diameter of the test channel can be measured to within $\pm$ 0.0002 cm and its length to within $\pm$ 0.05 cm. Consequently, for a test channel diameter of 0.7 to 1.5 cm percentage errors are obtained between $\pm$ 0.5 and $\pm$ 1.5%.

The electric heating power supplied to the test channel was measured by means of ammeters and voltmeters with the accuracy class 0.2 in conjunction with precision shunts in accuracy class 0.1. Regarding the heat dissipated by the test channel wall to the static nitrogen cushion a rough calculation shows that, based on an assumed temperature difference between the test channel wall and the nitrogen of 100°, a heat transfer coefficient to the nitrogen of 5 kcal/m^{2}h degree, a test channel diameter of 0.7 cm and an L/D ratio of 40 this is 3.5 kcal/h. The total heating power supplied to the test channel immediately before inception of burnout, however, amounted to 10 kWh which corresponds to 8600 kcal/h so that the heat dissipated to the nitrogen can be perfectly ignored. Due to the different temperatures of the test channel wall and the electrical power leads at both ends of the test channel some heat dissipation would arise which has to be allowed for, above all with short test sections with L/D ratios of 5 and 10. The heat dissipated to the power leads by longitudinal heat conduction is dependent on the temperature profile at the point of transition from the test channel to this power lead. For the purpose of the error analysis, the wall of the round test channel, because of its small thickness, can be considered as a flat plate for simplicity, when the temperature distribution in the wall is defined by the expression

$$\frac{\delta^2 \vartheta}{\delta x^2} + \frac{\delta^2 \vartheta}{\delta y^2} + \frac{W}{\lambda} = 0 \qquad (6)$$

./.

(6)
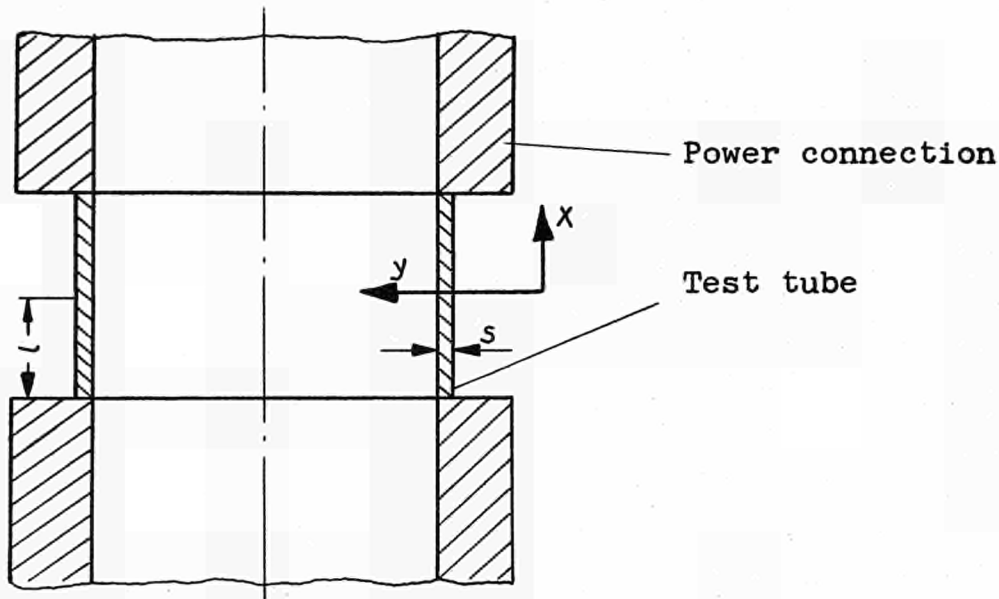
The symbols used in this equation have the following meanings:

ϑ = temperature   deg

x = coordinate in a direction longitudinal to the wall   m

y = coordinate in a direction transverse to the wall   m

λ = heat conductivity   kcal/m h deg

W = heat source   kcal/h

If it is assumed that the temperature distribution is symmetrical relative to the y-axis the boundary conditions will apply furthermore for

$$y = s; \quad 0 < x < 1 \qquad\qquad -\lambda\,\frac{\delta\vartheta}{\delta y} = \alpha\,(\vartheta - \vartheta_{Fl})$$

$$y = 0; \quad 0 < x < 1 \qquad\qquad \frac{\delta\vartheta}{\delta y} = 0$$

$$0 < y < s; \quad x = 0 \qquad\qquad \frac{\delta\vartheta}{\delta x} = 0$$

where $0 < y < s; \quad x = 1 \qquad\qquad \vartheta = \vartheta_{\infty}$

α = heat transfer coefficient   kcal/m^{2}h deg

ϑ_{Fl} = temperature of flowing fluid   deg

ϑ_{∞} = temperature of power leads   deg

./.

For a solution, the differential equation and the boundary conditions are re-written in the form of differences and integrated on an electronic computer by means of the relaxation method [5] . If the temperature profile across the whole cross section of the test channel wall is known, the heat loss can be computed by means of the temperature gradient at the line x = 1 by the equation

$$Q_V = 2 \cdot \lambda \cdot \pi \cdot d \int_{y=0}^{y=s} \frac{\delta \vartheta}{\delta x} \cdot dy \qquad (7)$$

For a test channel of L/D = 5 with 0.7 cm dia., 0.05 cm wall thickness and 940 W/cm^2 heat flux, the heat loss due to conduction to the power leads was therefore arrived at as approximately 1% of the total heating power applied.

2.5.6 Overall errors

If the individual errors dealt with in Chapters 2.5.1 to 2.5.4 are entered in the equation 3 a percentage error will be arrived at for the test section of L/D = 40 with D = 0.7 cm, an enthalpy at the burnout point of H_{BO} = 270 kcal/kg, a mass flow of G = 300 g/cm^{2}s and a system pressure of 70 kgf/cm^2 of $\pm$ 3.5% for $\emptyset_{BO}$. In addition to this error in the contributory factors, allowance has to be made as previously mentioned for the error arising direct in the measurement of the electric heating power; according to Chapter 2.5.5 this was calculated at $\pm$ 1 to $\pm$ 3% depending on the dimensions of the test channel.

3. First Type Burnout (under steady-state flow conditions)

3.1 Literature Review

The major part of the burnout studies in the recent years was essentially "project bound", in other words, they were usually made in order to obtain design criteria for a specific reactor project and to develop fuel elements with specific design features. These studies do not permit generally valid information to be derived on the influence of the thermal, hydrodynamic and geometric parameters on the transition from nucleate to film boiling. The reason for this little systematic approach is to be found in the rapid development of reactor engineering in the 'fifties which, in the absence of general empirical data obtained in basic research work, compelled the manufacturers to carry out in a minimum of time studies directed at specific objectives in a narrowly limited field. Only very recently have efforts been made to clarify the complex and difficult-to-appraise phenomena leading to burnout by means of systematic parameter investigations.

The simplest and quickest method of evaluating the multiplicity of these experimental data is to consider the different, almost invariably empirically obtained, equations by which it was attempted to represent the data analytically. In some cases, these equations are based on several thousand measuring points and, consequently, these provide a representative cross section through the experimental work. A number of these equations has been compiled in Appendix 1 (6-30). These equations mostly represent the mean of the test data, but some of them [13] define the lower envelope of the experimental data and are, therefore, specifically designed to assist the safety engineering of pressurized water and boiling water reactors.

./.

The test results which these equations represent were
mostly obtained in individual internally cooled tubes and
rectangular channels as well as in annuli heated at one
or both sides. The axial heat flux distribution of these
parallel flow elements was almost in all cases constant
and, therefore, did not simulate actual conditions prevailing
in a reactor. It is, therefore, not completely clarified
what correction factors have to be added to a large number
of these equations to extend their range of validity to
include multi-rod bundles with non-uniform heat flux
distribution. The study of rod bundles involves a large
number of additional hydromechanical and geometric
parameters which essentially influence the flow and heat
transfer conditions. Experimental studies on the burnout
behaviour of rod bundles were made by Janssen and Kervinen
[31] , Polimik and Quinn [32], Macbeth [33] , Waters, Hesson,
Fitzsimmons and Batch [34], Batch and Hesson [35], Matzner
and Neil [36], Hesson Fitzsimmons and Batch [37] , Alvensleben,
Caspar, Lochmann [38], Green, Maurer, Weiss [39], Bennett,
Collier and Lacey [40] as well as very recently by CISE [41] .
An attempt was also made by CISE to adapt an equation [11]
which is reproduced in the Appendix to cover the greater
part of the results of these experimental studies.

For a better understanding of the problem it is, however,
desirable initially to study the influence of the various
hydrodynamic, thermodynamic and geometric parameters in
simple internal flow channels. As previously mentioned, it
was a particular object of the work reviewed to study the
effects of the inlet flow conditions as well as the length/
diameter ratio. On these, there was hardly any information
to be found in the available literature. CISE [41] reported
on individual tests which had for their object an
investigation into the effects of throttling at the test

./.

channel inlet on the critical heat flux during boiling.
This throttling, however, primarily served to stabilize
the circulation and to obviate pulsations and it was not
primarily intended to influence the flow profile in the
heated channel by it. Similarly, CISE [42] carried out
analogy tests with argon-water mixtures which were to
provide information on the flow and steam bubble
distribution in internally-cooled channels. These tests
showed that pronounced disturbances in the flow will not
subside until after a length which corresponds to roughly
100 times the hydraulic diameter of the channel. They
afford only a qualitative insight into the flow conditions
to be expected. SNECMA [43] carried out investigations into
the effect of swirl produced at the test channel inlet on
the burnout behaviour. These tests which covered above all
the ranges of medium and high steam quality showed
appreciable increases in the critical heat flux levels with
tubes having an L/D ratio of 40. The length/diameter ratio
of the test channel is decisive for the hydrodynamic and
thermal profile of the flow at the burnout location and,
consequently, influences the density distribution and the
temperature gradient in the boundary layer governing the
heat transfer conditions. Tong, Currin and Engel [27] as
well as Lee and Obertelli [44] clearly stated the inter-
relationship between the critical heat flux and the L/D
ratio. The tests made by Tong, Currin and Engel were made
with internal flow tubes with a diameter of 1.1 cm at
70 kgf/cm^2 in a range between L/D 30 and 180 and the
results were explicitly stated for constant values of mass
flow and thermodynamic conditions at the inlets to the test
channel. Accordingly, the critical heat flux tends to
decrease very considerably initially according to an

exponential function as the L/D ratio increases and only
with an L/D ratio of 150 to 200 does the influence of this
parameter become negibly small. Lee and Obertelli who
carried out their investigations with internally-cooled
tubes of 0.5 to 1.2 cm diameter with L/D ratios of up to
400 found an even more sustained effect up to L/D ratios
of 400. For completeness' sake, a few short studies should
be mentioned on the other hydrodynamic and thermodynamic
factors. Studies of this type were made,inter alia,in the
laboratories of CISE [48], M.I.T. [49], A.E.E.W. [44,50] ,
W.A.P.D. [7] , A.N.L. [7,51] as well as in Russian
laboratories [52, 53, 54, 55, 24] . The effects of mass flow
and pressure on the critical heat flux in boiling are
coupled and cannot be considered separately. Starting from
atmospheric conditions, the critical heat flux initially
increases as the pressure is increased in order to decrease
once more on an optimum being reached. As Kazakova [45]
as well as Cichelli and Bonilla [46] concurringly found
this optimum with free convection,i.e. the so-called pool
boiling, is in a pressure range of 75 to 80 kgf/cm^2. In
forced-convection channels, the optimum shifts to smaller
pressures as the flow velocity is increased. Macbeth [22]
found this optimum for mass flow densities of 100 to
300 g/cm^2s between 20 and 40 kgf/cm^2. If one considers the
influence of the mass flow alone at constant pressure then
it is possible in this sub-cooled range to achieve a slight
improvement in the critical heat flux by raising the flow
velocity whereas from a steam quality of 10 to 50% by
weight the velocity increase tends to have a negative
effect. This tendency is clearly brought out by the data
furnished by Lee and Obertelli [44] as well as by Weather-
head [28]. This velocity influence in the sub-cooled range
with mass flows between 100 and 500 g/cm^2s is very small

./.

and only below a mass flow of 100 g/cm^{2}s is there a more pronounced decrease to be observed in the critical heat flux.

The effect of the test channel diameter is partly implicitly included in the considerations of the influence of the L/D ratio. If it is desired to represent it explicitly then the comparisons should be made for constant ratios of L/D and not for a constant absolute length of the test channel. The most pronounced effect is produced by small test channel diameters; according to Bergles and Rohsenow [47], who made tests between D = 0.05 and 0.5 cm with an L/D ratio of 25, the critical heat flux tends to decrease markedly as the channel diameter is increased. The drop becomes then smaller as the diameter is further increased and from a value of D = 2.0 cm decreases to zero. The same tendency was found by Lee and Obertelli [44] in their tests.

Where the studies perfectly agree is on the effect of the degree of sub-cooling or steam quality, respectively. As the sub-cooling decreases and steam quality increases the critical heat flux was found to decrease steadily.

3.2 Compilation of Results

All tests were made on individual vertically-arranged internally-cooled round tubes of 0.7 to 1.5 cm diameter. Essentially, they covered a pressure range from 70 kgf/cm^2 to 140 kgf/cm^2. Individual tests were also made at lower pressures down to 20 kgf/cm^2. The thermodynamic condition at the inlet to the test channel extended in most tests series from a maximum degree of sub-cooling of 60°C to a steam quality of 20%. In individual cases, the degree of sub-cooling was as high as 150°C. If the definition given on Page 22 is chosen for the degree of sub-cooling, viz.

$$x = \frac{i - i'}{r} \qquad\qquad (8)$$

./.

then the maximum degree of sub-cooling at the inlet will be $x_E = -0.3$ at 60 degrees or $x_E = -0.5$ at 150 degrees. Depending on burnout conditions and the test channel length, the outlet condition on the basis of these inlet conditions at the location of the boiling crisis, i.e. at the end of the heated length of the test channel, was $-0.2 < x_A < +0.5$.

For reasons of uniform test conditions, the test channel inside diameter was kept constant in the greater part of the tests, the diameter being 0.7 cm. Supplementary tests with test channel diameters of 1.1 and 1.5 cm rounded off the picture and provided information on the effect of the size of the flow area. All test channels had a wall thickness of 0.05 cm. The absolute length of the test channels was varied between 3.5 cm and 98 cm which corresponds to a range of the L/D ratio between 5 and 140. The value 140 was chosen as the upper limit of the L/D ratio on the strength of the findings that, above these, there was no longer any appreciable influence of the L/D ratio to be observed on the critical heat flux in boiling. True, L/D ratios of 5 have hardly any practical importance; but the tests made on these helped considerably to establish clearly the tendency of this factor.

The object of our tests was to determine the influence of various hydrodynamic conditions on the critical heat flux in boiling. As a basis for comparisons of these tests it is, however, necessary to have a number of reliable results under definite and clearly defined flow conditions in the test channel. For this reason, we initially carried out burnout tests over the entire thermodynamic range of interest where an inlet section preceding the heated length, the length of which was at least 100 times the diameter, ensured that the hydrodynamic profile was able to develop fully. In Figures 11 and 12 the results are compiled with these inlet conditions for various L/D ratios and mass flows. Fig. 11 shows the conditions at 70 kgf/cm^2 and Fig. 12 at 100 kgf/cm^2.

The test channel inside diameter in all these tests was
0.7 cm. In plotting the results the inlet quality was used
as the abscissa because it is much easier for the reactor
designer to decide or modify the conditions at the inlet to
the core than at the outlet. For this reason, almost all
other parameters were invariably referred to the inlet con-
ditions.

Basing on these tests, the influence of various inlet con-
ditions as well as the L/D ratio was studied in a large
number of test series, the individual results of which are
detailed in the tables 1 to 49[+). Table 1 gives a summary of
the tests made in the range of the first type burnout. In the
order of the L/D ratio the tests are initially given without
flow disturbing elements at the inlet of the test channel.
Subsequently, the data are given with twisted tapes and
orifice plates at the test channel inlet. The summary is
concluded by a test series where the test channel had a
sinusoidal heat flux distribution over its length.

As a next step, the question was of interest to find how the
maximum heat flux changes if the long inlet section is re-
moved and the flow is allowed to enter the test channel direct
via a sharp-edged inlet. In this case, both the velocity pro-
file as well as the thermal profile can develop only from the
start of the heated length onwards whereas, previously, in the
tests with a long inlet section, a fully developed velocity
profile existed. As explained in further detail in Chapter
3.3.1.2 the critical heat flux tends to increase by an
appreciable percentage only with short test channels with an
L/D ratio of 10 and less if the inlet section is omitted. With
an L/D ratio of 40 the improvement is so small already as to
be hardly measurable.

[+)It may be pointed out in this connection that, in applying the
numerical values, be it for purposes of comparison or as a basis
for design criteria, attention has to be paid to what hydrodynamic
inlet conditions existed such as undisturbed inlet, twisted tapes
or orifices at test channel inlet.

Orifice plates have a similar effect as a keen-edged inlet, namely, a contraction of the flow in the inlet, but they cause an additional pressure loss. The investigations into the influence of orifice plates on the critical heat flux in boiling were made in two test series with test channels of 0.7 cm diameter. Two different orifice plates were used , the dimensions and layout of which are shown in Fig. 13. The orifice plate of the first test series was located 4 cm upstream of the start of the heated length and had an opening of 0.4 cm. In the second test series, the orifice plate was located directly at the inlet of the heated length with an opening of 0.3 cm dia. The test channel with the No. 1 orifice plate had an L/D ratio of 80 and the one with the No.2 orifice plate an L/D ratio of 40. In Figures 14 and 15, the results of these tests at 70 and 100 kgf/cm^2 are compiled. A discussion of the influence of these flow disturbing elements is given in Chapter 3.3.1.4.

More success was achieved with twisted tapes. Three different types of twisted tapes were investigated with helix angles of 75, 56 and 48°, the definition of the helix angle being

$$\psi = \frac{h}{\pi\,D} \tag{9}$$

In this expression h is the length of one turn of the twisted tape and D the diameter of the test channel.

The exact arrangement of the twisted tapes is shown in Fig. 16.

For reasons of comparison, all these tests were made with test channels of 0.7 cm dia. and an L/D ratio of 40 was adopted. While smaller values of L/D promise an improved effect they are not so interesting from the practical point of view of their use in a nuclear reactor. Such twisted tapes suggest themselves as the simplest and cheapest elements in the core because they can readily be fitted in place of the spacers necessary at certain intervals

./.

between the fuel rods. The distance between two spacers
is usually 40 to 50 D. Typical results obtained with these
three twisted tapes are reproduced in Figures 17, 18 and 19.

Studies of the influence of the pressure on the transition
from nucleate to film boiling had been made to a sufficient
extent only under conditions of free convection, i.e., in
pool boiling. In forced convection channels no clear
information was available and we have, therefore, tried in
individual tests to obtain information on this. The pressure
influence varies as the mass flow increases as can be seen
from the results for 290 g/cm^2s and 350 g/cm^2s shown in
Figures 20 and 21. In both cases, the test channel had a
diameter of 0.7 cm and an L/D ratio of 80. The pressure
was varied from 20 to 100 kgf/cm^2.

Figures 22 and 23 represent the test results with test
channels of 1.1 and 1.5 cm dia. With their aid and the
data obtained with tubes with a diameter of 0.7 cm, it was
possible to determine the influence of the free flow area
on the critical heat flux.

During the tests described so far, the test channels
invariably had a constant heat flux distribution over their
length. Fuel rod bundles in pressurized water and boiling
water reactors show a sinusoidal heat flux distribution
caused by the neutron flux distribution and, therefore,
the question is of interest as to how far the results
obtained with constant heat flux are valid for sinusoidal
heat source distribution.

For this reason, the critical heat flux under conditions of
sinusoidal heat flux distribution was studied in a round
internally-cooled test channel of 0.8 cm inside dia and an
L/D ratio of 80 at 70 and 100 kgf/cm^2. For this purpose,
the test channel wall had been weakened correspondingly
by reducing the outside diameter stepwise, giving an as
near as possible approximation to the sine form within the
possible machining tolerances. The ratio from maximum to
minimum heat flux was 2 and the ratio of the maximum heat
flux to the mean heat flux 1.2. The results of these
investigations are summarized in Fig. 24.

3.3 Factors influencing first-type burnout

The factors liable to influence the transition from nucleate
to film boiling investigated in the scope of the present
work can be conveniently sub-divided into three groups, i.e.:

  hydrodynamic inlet conditions,
  L/D ratio,
  general thermodynamic and geometric parameters.

The first two groups are main objects of these studies.
Generally, these factors are not independent of each other,
but associated with each other by a series of complex
conditions.

In not too long test channels, the inlet conditions
determine the velocity profile and the thermal profile
at the location of the boiling crisis. The heat transfer
in single-phase non-boiling flow is essentially determined
by these profiles. The question, therefore, arises to what
extent they also govern the heat and material exchange in
boiling, and to what extent the critical heat flux is liable
to be affected by them. The L/D ratio of the test channel
contributes to establishing both the thermodynamic and the
hydrodynamic conditions at the burnout point. Other

                                                        ./.

thermodynamic and hydrodynamic parameters, such as the
degree of sub-cooling,or steam quality,respectively,
pressure and mass flow are generally decided by economy
considerations for the reactor and,in connection with
safety considerations arising out of the burnout problem,
are given parameters. In contrast to these, it is possible
by ingenious control of the inlet conditions to improve
burnout safety and/or to improve the output of a pressurized
water or boiling water reactor.

3.3.1 <u>Influence of the hydrodynamic inlet conditions</u>

Little information is available on the question of the
design of the core support plates and spacers in the core of
P.W. and B.W. reactors to achieve optimum heat transfer and
pressure loss conditions. Investigations and studies of this
problem have, however, to start on a sound understanding of
the influence and the effects of the hydrodynamic inlet
conditions on the conditions in two-phase flows. The tests
described in the following which were made on simple
geometries are intended to contribute towards this aim.

3.3.1.1 <u>Undisturbed inlet section</u>

In internally cooled tubes with single-phase media the
well-known turbulent velocity profile will have fully
developed after a distance of 40 to 50 D. In two-phase
flows, both the shape and the development of the velocity
profile are considerably dependent on the steam quality,
the density difference between the two phases and the mass
flow. After a distance of 100 to 200 D it can, however,
generally be anticipated that the inlet conditions have
subsided. In our tests on disturbed inlet channels, the
channel was therefore preceded by an inlet section with a
length of 100 to 200 D.

./.

The results obtained with these test channels were mentioned
earlier in Chapter 3.2 and are compiled in Fig. 11 and 12.
Essentially, they serve as a basis for comparison of the
studies discussed in the following of various inlet effects.

Essential information on the processes at the time of burnout
can be derived from the variation of the surface
temperature of the heated test channel during transition
from nucleate to film boiling.

We have tried by measuring the wall temperature at the
burnout point to obtain data on this. The sensing elements
were the three-wire thermocouples referred to in Chapter
2.5.2.Fig. 25 shows the variation of the temperature at
the test channel wall as well as the variation of the mass
flow at the moment of transition from nucleate to film boiling
for a flow with the abovementioned inlet conditions. The
heated length of the test channel had an L/D ratio of 40
so that up to the burnout location both the velocity
profile and the thermal profile,i.e. the density
stratification, were able to develop to a large extent. The
time as abscissa in Fig. 25 runs from right to left and the
distance between the two vertical lines entered there is
0.1 s. Furthermore, the step in the line at the top of the
oscillogram marks the time at which the burnout detector
cuts off the power by which the test channel is heated.
Considering the temperature variation ϑ_H, it can be clearly
seen at the right-hand side of the oscillogram how the wall
temperature suddenly changes by a small amount of about 5 to
10°C. Allowance has to be made for the fact, however, that
the sensing element was applied to the uncooled side of the
test channel wall and, therefore, does not directly indicate

./.

the temperature of the heat emitting surface. Subsequent
to this small temperature drop,brief statistical variations
develop which eventually,in an almost steplike rise,lead to
fully developed film boiling.

The slight temperature drop on inception of the boiling
crisis suggests an improvement in the heat transfer by
complete evaporation of the two-phase boundary layer
existing up to that point. Subsequent statistical temperature
variations are indicative of local steam blankets and,
consequently,hot spots developing which, initially, are
wetted again and again with liquid until eventually film
boiling prevails. The mass flow m is little affected by
these burnout processes and continues constant.

3.3.1.2 Sharp-edged inlet

In actual fuel elements of boiling and pressurized water
reactors, an undisturbed inlet flow such as was considered
in the previous chapter almost never exists. Usually, the
coolant enters through the core support plates direct into
the heat emitting channels of the fuel elements. Burnout
tests with channels having a sharp-edged inlet therefore
very closely approach conditions prevailing in practice.

In our tests with sharp-edged inlets, the test channel was
designed so that upstream of the start of the heated length
a large-bore tube was provided. By the sudden change from
the large flow area into that of the heated channel the
flow was contracted and considerably accelerated. The start
of the hydrodynamic inlet section therefore coincided with
the start of the heated length and the origin of the
thermal profile.

./.

As the test showed, the sharp-edged inlet brought about
an appreciable increase in the critical heat flux only
with test channels of small L/D ratios. This improvement
is shown in Figures 26 and 27 for an L/D ratio of 10 at
pressures of 70 and 100 kgf/cm^2. As shown by the tests,
it may amount to 8 to 15% and is not to a marked extent
dependent on the mass flow which was varied between the
values of 230 g/cm^2s and 350 g/cm^2s. As sub-cooling is
decreased and the state of saturation approached,
measured at the test channel inlet, this improvement
decreases which can be simply explained by the fact that,
as the steam quality increases,the inlet disturbances
subside more quickly due to the higher two-phase friction
and fail to take full effect up to the point of the
boiling crisis.

An omission of the unheated inlet section failed to
produce any noticeable increase in the critical heat flux
in the tests with L/D ratios of 40, 80 and more.

3.3.1.3 Orifice plates at the inlet

The fuel rods of the reactor core are mostly supported in
plates provided with holes through which the coolant is
admitted. These holes affect the inlet conditions in the
reactor core in a manner similar to orifice plates. They
cause a considerable constriction of the flow whose wake-
disturbances influence the heat transfer conditions down-
stream of the inlet point over a longer or shorter distance.
A constriction of the flow, if not to such a great extent,
also occurs with test channels having sharp-edged inlets
and, therefore, orifice plates can be expected to produce
a simpler effect on the burnout behaviour as was discussed
under Chapter 3.3.1.2 in connection with the tests without
an inlet section, i.e., with a sharp-edged inlet.

./.

Investigations on the influence of this type of inlet disturbances were included in our work and two different configurations of orifice plates at the inlet to the test channel were studied. The design of these two orifice plates was discussed earlier and shown in Fig. 13. The orifice plate No. 1 was fitted to a 0.7 cm inside diameter tube with an L/D ratio of 80. Between the orifice plate and the start of the heated section there was an extended space with a length of about 4 cm. This inter-space provided partial damping of the disturbances and the remainder had long subsided before reaching the burnout endangered point after a distance of 80 D. The orifice plate No. 2 was directly fitted at the inlet to the heated section and, in this case, the tube had an L/D ratio of 40. Fig. 28 shows the tests made with this orifice plate at a pressure of 100 kgf/cm^2. In the upper half of this figure are plotted the values for the critical heat flux versus sub-cooling. The lower half shows the relationship of the maximum attainable heat fluxes with and without orifice plates. As shown by the two curves plotted in this part for mass flows of 290 and 230 g/cm^{2}s the improvement enhances as sub-cooling decreases and steam quality increases. The effect of the orifice plate was found to be little dependent on the mass flow.

If this gain in heat flux level is compared to the additional amount of pumping power - the pressure loss at the orifice plate was 1 to 2 kgf/cm^2 - it can be seen that this type of flow control element does not provide an economic means of improving the burnout safety in nuclear reactors.

./.

3.3.1.4 Twisted tapes at inlet

Compared to the measures discussed so far to influence flow, a much better effect on the critical heat flux in boiling can be achieved by fitting short twisted tapes into the inlet of the heated section. These impart to the flow a swirl component which, depending on the helix angle and the amount of kinetic energy, will subside on its way through the heated channel more or less quickly.

The influence of the swirling flow on the burnout behaviour depends to a marked extent on the hydrodynamic and thermodynamic parameters of the flow conditions as well as the helix angle. Our tests were made on test channels with an L/D ratio of 40 with twisted tapes having three different helix angles viz. 75, 56 and 48°. The tape with the greatest helix angle was found to produce the least swirl and, in our tests, produced no noticeable effect on the critical heat flux in boiling. In contrast to this, it was possible with the two other twisted tapes, the twisted tape No. 2 with a helix angle of ψ = 56°, and the twisted tape No. 3 with a helix angle of ψ = 48° to achieve a remarkable improvement in the burnout heat flux level of the test channel. The figures of the critical heat flux obtainable when fitting these twisted tapes were referred to in Chapter 3.2 and are compiled in Figures 17, 18 and 19 mentioned there. It could be seen from Figures 18 and 19 that, with a steam quality of 5 to 8 percent by weight, measured at the inlets to the test channel, the curve of the critical heat flux with swirling flow shows a minimum and that there is partly considerable scatter of results. In isolated instances, it was noticed that in this range swirling flow may even adversely affect the burnout performance of the test channel.

The improving effect of the twisted tapes No. 2 and No. 3 is summarized in Figures 29 to 34. The order is according to the system pressure and the mass flow, Figures 29 to 32 showing the conditions at 70 kgf/cm^2 and the Figures 33 and 34 those at 100 kgf/cm^2. For a mass flow of 230 g/cm^{2}s at a pressure of 70 kgf/cm^2 Figures 29 and 30 show the improvements obtainable with these twisted tapes. The influence of swirling flow increases both as the steam quality increases and as sub-cooling decreases and, near the state of saturation, is zero with a helix angle of 56°. The twisted tape with 48° helix angle showed a sudden change in the critical heat flux loading with an inlet steam quality of approximately 5%. In the range of this low steam quality, slug flow prevails according to the measurements made by Baker [56], Collier [57], and Hewitt [58], a flow regime which most adversely affects swirl.

As steam quality increases the improvement obtainable by swirling flow is enhanced and, as shown in Fig. 30, in which the ratio of the critical heat flux is plotted with and without swirl, attains values of 30 to 50%, depending on the helix angle of the twisted tape, at a steam quality of x_E = 0.2 which, at the location of the boiling crisis, corresponds to x_A = 0.4. A higher mass flow also tends to improve the effect of swirling flow. Extrapolating the curves, entered in Figures 31 and 32 for a mass flow of 290 g/cm^{2}s, for a steam quality of x_E = 0.2 - as a comparison with the abovementioned values - an improving effect of these twisted tapes between 50 and 70% is arrived at for this condition. In contrast to this, the influence of the velocity on the effect of swirl is negligible in the region of sub-cooled flow.

./.

Fig. 33 shows a comparison for a system pressure of
100 kgf/cm^2 of the burnout values for test channels with
twisted tapes having a helix angle of 48°. Qualitatively,
the same trends as in the case of a pressure of 70 kgf/cm^2
appear, dependent on mass flow and steam quality, but,
quantitatively, the improvement is higher than in the
measurements previously discussed. Thus, as shown in
Fig. 34, an increase in the critical heat flux due to swirl
of about 20% was observed even in the region of minimum
swirl influence, i.e. at a steam quality of x_E = 0.05.
Under conditions of sub-cooled flow, a higher mass flow
tends to reduce the improving effect of swirl.

The improvement with high steam quality is to be attributed
to the centrifugal action of swirling flow because, in
this case, annular flow prevails in the test channel with
the steam flowing at the centre entraining water droplets.
These water droplets are thrown out to the heat emitting
wall and, thereby, improve the water supply at the heating
surface. As to the improvement observed in the sub-cooled
range, three reasons may be stated. Compared to the non-
swirling flow, there is a higher turbulence in the swirling
flow and, consequently, a more intense agitation of the
boundary layer adjacent to the wall, and the local
velocity is increased by the vector of the swirl components.
Furthermore, it appears that, in the sub-cooled range, too,
a steam film forming initially due to the centrifugal
action in the flow will again and again be penetrated by
liquid, whereby film boiling is shifted to higher heat
flux levels.

./.

The differences in the thermodynamic and hydrodynamic processes during boiling crisis in the case of swirling and non-swirling flow can be ascertained only by means of indirect measuring techniques. In connection with the present work, an attempt was made to obtain information on this by measuring the wall temperature at the burnout point. Figure 35 shows the variation of the temperature at the test channel wall as well as the variation of the mass flow at the moment of transition from nucleate to film boiling under conditions of swirling flow. If one compares with this, the temperature variation under conditions of non-swirling flow, which is shown in Fig. 25 and discussed in Chapter 3.3.1.1, essential differences will be found. As is shown by these tests, what is missing here is both the small temperature decrease which, with non-swirling flow, characterized the commencement of the boiling crisis as well as the statistical fluctuations. With swirling flow the temperature rise followed an exponential function with a nearly smooth rise. This suggests more stable heat transfer conditions during swirling flow compared to non-swirling flow. It appears that due to the swirl there exists a uniformly sub-cooled core flow which is separated from the heating surface by only a thin superheated boundary layer.

3.3.2 Influence of the L/D ratio

As explained in the preceding chapters, it was found during the investigations into the effect of the inlet conditions on the critical heat flux in boiling that twisted tapes proved most effective in improving the burnout performance of the channels. This increase in the critical heat flux has been attributed to a change in the conditions in the core flow and a reduced boundary layer thickness at the heat emitting wall. Similar conditions also prevail in the thermal inlet zone because the thermal profile on starting the heating will near the wall initially show a very steep density gradient and temperature gradient, respectively, which flatten out downstream. Consequently, a proportionate improvement in the critical heat flux, and a similar temperature variation in the heat emitting wall as with swirling flow, ought to be obtainable in the range of this thermal inlet zone. However, as the boiling crisis with uniform heating always occurs at the end of the test channel, it is necessary, in order to locate it in the thermal inlet zone, to adopt correspondingly short channels. In Fig. 36 the temperature variation during the boiling crisis at the wall of such a short test channel with an L/D ratio as small as 10 has been plotted. If a comparison is made with the temperature variation measured under conditions of swirling flow as shown in Fig. 35 and discussed in Chapter 3.3.1.4, the same smooth exponential rise in the temperature occurs in the short test channel as in the case of swirling flow although, in this case, a long unheated inlet section ensured that non-swirling flow prevailed and the normal turbulent velocity profile was able to develop fully.

Considering that the pattern of the burnout process in the thermal inlet zone is the same as under swirling flow, a similar improving effect on the critical heat flux level was to be expected as previously mentioned. In Fig. 37

./.

has been plotted the dependence of the critical heat flux on the length/diameter ratio with a mass flow of 290 g/cm^2s for pressures of 70 and 100 kgf/cm^2 as well as various degrees of sub-cooling at the inlet of the channel. This graph shows that the critical heat flux with a short test channel may be a multiple of that with L/D ratios of the order of 100 or more. The main influence is in the range of $0 < L/D < 100$. As the curves are referred to a constant degree of sub-cooling at the inlet,attention should be paid to the fact that as a second parameter,in addition to the L/D ratio,the steam proportion at the location of film boiling, which increases as the heated length is increased,enters into the results. Therefore, two further examples of constant steam quality at the outlet of the test channel, i.e. at the location of the boiling crisis have been additionally shown in Fig. 37 for the same mass flow. It can be clearly seen here that the curves from an L/D ratio of 100 onwards run almost parallel to the abscissa and, consequently, the slight drop observed previously for x_E = constant between L/D 100 and 140 can now be attributed only to the change in steam quality at the location of boiling crisis,and not to an increase in the L/D ratio. If one compares values of the critical heat flux given in Fig. 37,which were obtained with a channel with an L/D ratio of 5,with data obtained with an L/D ratio of 100,it will be found that these values differ by more than 300%. Whereas no information was available in the literature on the influence of the hydrodynamic inlet conditions on the critical heat flux in boiling a few studies had been published on the dependence on the L/D ratio. Out of recently published work mention should, above all, be made of the tests by Lee and Obertelli [44], by Tong, Currin and Engel [27] as well as Bergles and Rohsenow [47]. Fig. 38 shows a comparison of our data relating to the

./.

dependence of the critical heat flux on the L/D ratio with the data furnished by these authors. There is good agreement with these data, in particular, those made by Lee and Obertelli as well as Tong, Currin and Engel under conditions very well comparable with ours. It should be noted, however, that the 5 test series entered in Fig. 38 were carried out with test channels of various diameters and also at various pressures and mass flows. Therefore, only a qualitative comparison is possible and suitable corrections would have to be applied in order to bring about perfect quantitative agreements. In the values of the critical heat flux for L/D ratios greater than 100 there are slight differences compared to the data of Lee and Obertelli as well as Tong, Currin and Engel. Lee and Obertelli found a slight drop in the critical heat flux even up to L/D = 400 whereas the curve arrived at by Tong, Currin and Engel shows hardly any slope from L/D = 100 onwards.

In conjunction with the tests on very short test channels, the question arises as to what extent heat dissipation from the heated channel to the power leads has to be allowed for in the calculation of the heat flux. In the error analysis laid down in Chapter 2.7.5. it was already shown that, compared to the total heat supplied, the heat dissipated by conduction in the case of the tubes used by us with a wall thickness of only 0.05 cm is negligible even for L/D ratios as small as 5. If the wall thickness is increased to 0.1 cm and more, the heat conduction in the axial direction has to be taken into account in order to avoid errors which may then amount to several percent.

Fig. 39 shows the temperature distribution in the 0.05 cm thick wall of a test tube with an L/D ratio of 5 and an inside diameter of 0.7 cm as obtained by the method of

.∕∘

calculation explained in Chapter 2.7.5. For reasons of
symmetry, it is sufficient to consider only half the tube
length in the calculation. The heat dissipated to the power
leads by conduction can be determined from the temperature
gradient at the end of the heated length. In the case of our
tests, this is less than 1% and, consequently, is within the
measuring accuracy.

3.3.3 General thermodynamic, hydrodynamic and geometric parameters

In reviewing the burnout literature it will soon be found
that more, and more detailed, information is available on the
influence of sub-cooling, and steam quality, respectively,
system pressure, mass flow and channel diameter than was the
case in the previously discussed parameters. The reason for
this is partly in the fact that these are factors which are
of decisive importance in any design and optimization
calculation of P.W. and B.W. reactors. For a given pressure,
the degree of sub-cooling influences the thermodynamic
efficiency of a P.W. reactor and, in the case of B.W. reactors,
a detailed knowledge of the steam quality in the core is
indispensable for the nuclear and thermodynamic design. On
the mass flow depends the heating margin in the core in
P.W. reactors which, in turn, determines the heat stresses in
the core structure. Via the pumping power to be provided,
the mass flow also affects the economy of the plant. B.W.
reactors in operation, or under construction, mostly operate
at a system pressure of 70 kgf/cm^2 whereas P.W. reactors
normally are operated at pressures of 70 to 140 kgf/cm^2.
The burnout studies to be found in available literature are,
therefore, with few exceptions limited to this pressure
range. The diameter of the fuel rods and, consequently, the
hydraulic diameter of the test channel result, firstly, from
the nuclear calculations on neutron economy as well as fuel

./.

enrichment and burn-up and, secondly, from thermal calculations in respect of the heat transfer conditions in the core. Although the majority of actual reactors have hydraulic diameters varying only between 1 and 1.5 cm burnout studies are to be found in the literature on the influence of this parameter in a range of 0.1 to 3 cm.

3.3.3.1 Degree of sub-cooling and steam quality,respectively

Considering the influence of the degree of sub-cooling,and steam quality,respectively,on the critical heat flux in boiling it is important to accurately define the point in the core on which the study is based, in other words, a basic distinction must be made whether the conditions are considered at the inlet of the heated channel or those at the location of burnout. In investigations into the critical heat flux in boiling with uniformly heated channels, the condition at the channel outlet is almost always identical with the location of the boiling crisis because this invariably occurs at the end of the heated length.

Customarily, the test data on the critical heat flux in boiling are in the literature referred to the condition at the test channel inlet. There are two reasons for this: firstly, the results referred to the inlet condition can be presented with greater convenience and clarity than if they are referred to the outlet condition. Secondly, it is only the condition at the inlets of the core of a P.W. or B.W. reactor which can be directly controlled because the outlet condition depends on the interaction of nuclear thermodynamic and hydrodynamic parameters in the fuel element. This is also the reason why nearly all burnout correlations are based on the inlet condition.

./.

With undisturbed flow conditions, the critical heat flux
steadily decreases as sub-cooling diminishes and the steam
quality rises. This fact, which is known from the literature,
is confirmed by our data which are shown in Figures 11 and
12 discussed in Chapter 3.2 and reproduce the results of
tests with undisturbed inlet. If flow disturbing devices or
twisted tapes are fitted to the inlet of the heated section,
this will affect the pattern of the critical heat flux
variation versus sub-cooling, or steam quality, respectively,
and, from a steam quality of 5 to 8% onwards, an increase
will be found in the maximum heat flux level.

For a better understanding of the hydrodynamic and thermo-
dynamic processes leading up to boiling crisis, it is no
doubt important for the state and, in particular, the
steam quality, or sub-cooling, respectively, at the burnout
location to be exactly known. If its mean value is calculated
via the energy balance, this will by no means be representative
of the actual conditions because the various flow conditions,
the velocity difference between the steam and water as well
as the boiling and condensation delay are not taken into
account. Nor does it provide any information on the steam
bubble, or temperature, distribution in the flowing medium
across the test channel area at the location of burnout.

If the critical heat flux in boiling is plotted against the
steam quality at the outlet of the test channel, as this
was done in Fig. 40 for a pressure of 70 kgf/cm^2 as well
as various L/D ratios and mass flows, the curves show a
similar steady decrease as the steam quality x_A increases
as was observed in Fig. 11 in which the inlet quality was
chosen as the abscissa.

./.

Due to the manner of representation, the curves with the lower mass flows are invariably above those with higher velocities.

3.3.3.2 Pressure

The main emphasis of our measurements was in the pressure range between 70 and 140 kgf/cm^2. However, they extended down to 20 kgf/cm^2.

Studies on the influence of pressure on the transition from nucleate to film boiling had been carried out only under conditions of free convection i.e. with pool boiling. According to measurements made by Kazakova [45] as well as Cichelli and Bonilla [56] the critical heat flux in this case rises from about 60 W/cm^2 at 1 kgf/cm^2 to about 300 W/cm^2 at 75 kgf/cm^2 in order to decrease again at higher pressures. In forced convection channels, the location of this maximum of the critical heat flux is greatly dependent on the flow velocity. As the mass flow increases it shifts towards lower pressures. This is clearly shown by the work done by Macbeth [22] from which the representation of the pressure dependence of the critical heat flux has been reproduced in Fig. 41. According to this, the critical heat flux pattern shows a pronounced maximum at mass flows from 100 to 400 g/cm^2s between the pressures of 10 and 50 kgf/cm^2. As the mass flow decreases this maximum diminishes noticeably and, at 100 g/cm^2s, the critical heat flux in the region below 100 kgf/cm^2 is only little pressure dependent and only above this pressure decreases appreciably. These curves were interpolated from the measuring points entered in Figures 21 and 22. As can be seen from the graphs in Figures 42 and 43, the pattern found by us of the critical heat flux versus pressure corresponds to the interrelationship found by Macbeth.

./.

As is shown by these curves, the position of the optimum
is influenced also by the inlet quality, in addition to the
mass flow. While, in view of the relatively small difference
in the degree of sub-cooling, it is not possible to make
generally valid statements, it is clearly shown both with
a mass flow of 290 g/cm^2s and 350 g/cm^2s that the maximum
is shifted towards lower pressures as the sub-cooling
increases.

In Fig. 44, data found by Macbeth, Lee and Obertelli as well
as M.A.N. for a constant inlet quality $x_E = 0$ are compared.
Although the absolute values of the critical heat flux are
not directly comparable, because the measurements were made
at different L/D ratios, hydraulic diameters and mass flows,
there is clear agreement in the trend of the pressure
pattern, in particular, in the vicinity of the maximum. If
one compares the pattern at higher pressures, the measure-
ments by Lee and Obertelli tend to be slightly higher than
the figures of Macbeth and our own results.

3.3.3.3 Mass flow

The greater part of our measurements were made at mass flows
between 200 and 400 g/cm^2s. This range was extended down-
wards to 100 g/cm^2s in test channels with larger hydraulic
diameters. Comparing the test results compiled in Figures 11
to 24, where the mass flow is plotted as a parameter, it
will be found that a change in mass flow from 100 to
400 g/cm^2s influences the critical heat flux only. little.
This is confirmed by the data given, by Macbeth [22] and
Lee and Obertelli [44] which are shown in Fig. 45. Only at
mass flows of less than 100 g/cm^2s can a greater drop in
the critical heat flux level be observed.

./.

If the heat flux is plotted against the conditions at the
inlet to the test channel, as this has been done summarily
in Figures 11 and 12, it can be seen that in the sub-cooled
range a slight improvement can be achieved in the critical
heat flux whereas from a certain steam quality onwards the
velocity increase has a negative influence, a tendency
which agrees well with other tests such as those made by
CISE [11].In Figures 46 and 47, the interrelationship
between the critical heat flux and the mass flow at
various L/D ratios and degrees of sub-cooling has been
plotted for pressures of 70 and 100 kgf/cm^2. As shown by
the curves drawn there, it is possible in the sub-cooled
range to approximate the values with a high degree of
accuracy by a linear function. Two essential trends can be
observed, firstly, that the influence of mass flow
increases as the L/D ratio becomes greater and,secondly,
that its influence on the burnout heat flux becomes greater
as sub-cooling is increased.

3.3.3.4 Channel diameter

The quantitative influence of the test channel diameter on
the critical heat flux in boiling is not uniformly stated
in the literature. This is most evident if the various
burnout correlations are studied for their diameter
dependence such as has been done in Fig. 48 for the
correlations by Weatherhead [28], Menegus [23] as well as
Lee and Obertelli [44]. In these graphs the relative
values of the critical heat flux related to 1 cm channel
diameter are plotted against the hydraulic diameter. The
three curves show different trends. Whereas Menegus has
the critical heat flux constant from a test channel diameter
of 1 cm onwards,it continues to decrease at diameters above
2 cm according to Weatherhead as well as Lee and Obertelli.

./.

The results found by us with a constant L/D ratio in tubes
with 0.7, 1.1 and 1.5 cm inside diameter,which are plotted
in Fig. 49 for a mass flow of 230 g/cm^{2}s,show that this
influence increases exponentially below a channel diameter
of 1 cm as the channel area decreases. Furthermore, the
influence of the diameter is dependent on the system
pressure and the degree of sub-cooling at the inlets to the
test channel as can be seen from the curve families plotted
in Fig. 49 for 70 and 100 kgf/cm^2. As the pressure rises
the limit above which the diameter of the test channel has
no longer any influence, is shifted towards higher values.

3.3.4 The influence of non-uniform heat flux

If the burnout data obtained with test channels having a
uniform heat flux distribution are taken as a basis for
design calculations for pressurized water and boiling water
reactors whose fuel elements have a sinusoidal heat source
distribution over their length, it is usually assumed that
the differences in the heat flux distribution have only a
minor influence on the burnout behaviour. Recent measure-
ments with sinusoidal distribution of the heat flux over
the length of the test channel have been reported by
CISE [41] and the general conclusion may be summarized in
the statement that with equal dimensions and equal
thermodynamic and hydrodynamic conditions a heating channel
with sinusoidal heat flux distribution will transmit the
same total heat to the coolant as a channel with uniform
heat flux distribution. Supplementary to our measurements,
the critical heat flux was therefore studied for conditions
of sinusoidal heat flux distribution in a channel with a
length/diameter ratio of 80. For reasons of convenient
manufacture and better availability, a tube inside diameter
of 0.8 cm was adopted and, therefore, these tests are not
directly comparable with the previous measurements under

.   ./.

conditions of uniform heat flux distribution where the channel diameters were 0.7, 1.1 and 1.5 cm. However, from the three test series referred to, the conditions for a 0.8 cm channel inside diameter can be very easily interpolated. We have carried out this interpolation for 70 and 100 kgf/cm^2.

In Figures 50 and 51 the data so interpolated are compared with the data obtained with sinusoidal heat flux. As a basis for the comparison, the mean heat flux defined by Q_{total}/F was taken for the sinusoidal heat flux test channel. As can be seen from the data plotted in Figures 50 and 51, it is possible with sinusoidal heat flux distribution to transfer the same total amount of heat as with uniform heat flux and, consequently, an equal heat flux can be achieved.

3.4 Comparison with other Results and Analytical Representation of Data

In view of the equations compiled in Appendix 1, the question arises whether it is useful and desirable, at the present stage of our knowledge, to add to the number of already existing correlations for the critical heat flux in boiling a new, more or less empirically developed, function. On the other hand, if one evaluates the experimental test results, a sharp distinction should be made between the boiling crisis under absolutely stable flow conditions and burnout that is caused by instabilities such as periodical or singular changes in the pressure and mass flow. Boiling processes in the heated test channel tend to increase the pressure drop which, in the case of a not sufficiently steep delivery

./.

characteristic, is liable to lead to a sudden reduction of
mass flow and, consequently, burnout. The level of the
maximum heat flux obtainable under these conditions is,
as shown by the experiences accumulated by us in the course
of the tests, considerably lower than under conditions of
hydrodynamically perfectly stable flow. It does not have to
be pulsations always which reduce the critical heat flux,
there are also single sudden mass flow reductions which
influence the performance of a test channel and are liable
to cause burnout. It appears certain that the wide scatter
of the burnout data given in the published literature are
partly due to unstable flow conditions and not so much to
a lack of accuracy in measuring techniques.

The direct comparison of test data presented by other
authors is usually difficult because the test parameters
do rarely coincide completely. It appears convenient
therefore to make this comparison on the basis of a burnout
equation. We have initially used as a basis the burnout
correlation by CISE. This correlation was chosen because
its range of validity included almost all our test parameters
and because it is relatively recent and therefore takes
into account the latest data available at the time it was
formulated.

3.4.1 Comparison with CISE correlation

For the correlation of our test data the equation to be
used out of those presented by CISE is that applying to
the region of low steam quality. It reads:

$$\frac{W}{r \cdot H_{gl}} = \left(\frac{1 - \frac{p}{p_{cr}}}{(G/100)^{1/3}} - x_{in}\right) \frac{L}{L + 0.315 \left(\frac{p_{cr}}{p} - 1\right)^{0.4} \cdot D^{1.4} \cdot G} \quad (10)$$

./.

where:

W = the total heat flux necessary for producing film Watt
boiling

r = mass flow   g/sec

H_{gl} = heat of evaporation   kcal/kg

p = absolute system pressure   at

p_{cr} = critical pressure   at

G = mass flow per unit area g/cm^2s

x_{in} = enthalpy at test section inlet   kcal/kg

L = heated length of test channel   cm

D = hydraulic diameter   cm

The validity range given by CISE for this correlation is:

D > 0.7 cm

$45 \text{ kgf/cm}^2 \leq p \leq 150 \text{ kgf/cm}^2$

$100 \ (1 - \frac{p}{p_{cr}})^3 \ g/cm^2s < G < 400 \ g/cm^2s$

$x_0 > 0 : x_0$ = steam quality at test channel outlet

$x_{in} < 0.2$

The data measured by us in tubes with a diameter of 0.7 cm
are compared with the data predicted for corresponding
hydrodynamic and thermodynamic conditions by the CISE
correlation in Fig. 52. As abscissa are plotted the data
predicted according to CISE and as ordinate the data
measured by us which means that the predicted and measured
data coincide for all points which are on the 45° line.
For greater convenience, lines of constant deviation of
± 10% have been entered which start as a straight line from
zero. The graph shows that, for the test channel diameter

./.

of 0.7 cm shown here, the CISE correlation tends to
predict lower values for all L/D ratios studied than were
observed in our tests. While the differences between the
measured and predicted critical heat fluxes with L/D ratios
of 140 and 80 do not exceed 25% they tend to become greater
at smaller L/D ratios where they partly exceed 50%.

If, in contrast to this, the data found by us with test
channels of 1.1 and 1.5 cm diameter are compared with the
CISE correlation the agreement is very good as can be seen
from Fig. 53. The reason for the relatively poor agreement
between the predicted and measured data with test channel
diameters of 0.7 cm may be in the fact that this diameter
represents the lower limit of the validity range of the
CISE correlation. In addition, however, Fig. 52 showed that
the differences tend to become greater as the L/D ratio
becomes smaller. For a comparison, we then included the
data found by Lee and Obertelli 44 , as shown in the next
chapter, and it was then found that their data also are
higher, in the case of small test channel diameters and
small L/D ratios, than those predicted by means of the
CISE correlation. This has caused us to extend the validity
range of the CISE correlation by adding a few correction
factors to cover smaller test channel diameters and smaller
L/D ratios.

3.4.2 Extension of the CISE correlation

To preserve the original form of the CISE correlation, the
extension was carried out in a manner that only additional
terms were added. In the course of the work it proved
necessary, in addition to the two geometric parameters,
diameter and L/D ratio, also to apply small corrections

./.

for the influence of the pressure, the degree of sub-cooling at the inlet of the test channel and the mass flow. With these correction factors, the extended CISE correlation may be presented in the following form:

$$q_{Bo} = q_c \cdot K_{L/D} \cdot K_{x_E} \cdot K_m \cdot K_p \cdot K_D \qquad (11)$$

where:

q_c critical heat flux predicted from original CISE correlation (equation 10)

$K_{L/D}$ additional term to allow for influence of L/D ratio

K_{x_E} additional term to allow for influence of inlet steam quality on q_{BO}

K_m additional term to allow for influence of mass flow on q_{BO}

K_p additional term to allow for influence of system pressure on q_{BO}

K_D additional term to allow for influence of hydraulic diameter on q_{BO}

These additional or correction terms for the factors affecting burnout behaviour, viz. L/D ratio, inlet quality, mass flow, pressure and test channel diameter, were calculated on the basis of comparisons with numerous test results, and the following analytical equations were found for the individual factors:

./.

$$K_{L/D} = 1.444 - 5.919 \cdot 10^{-3} \, (L/D) + 2.907 \cdot 10^{-5} \cdot (L/D)^2$$

$$K_{x_E} = (1 + 1.2 \cdot x_E + 2.5 \cdot x_E^2) \, e^{-1.04 \cdot x_E} \, (2x_E + 1) \cdot (10 \cdot D/L)^2$$

$$K_m = e^{(m-290) \cdot (D/122.63 \cdot L)}$$

$$K_p = 1.6467 - 1.3591 \cdot 10^{-2} p + 6.3464 \cdot 10^{-5} \, p^2$$

$$K_D = (0.7/D)^{0.17}$$

The CISE correlation so extended is valid for the following range:

$$10 \leqslant L/D \leqslant 140$$

$$- 0.2 < x_E < + 0.2$$

$$100 \text{ g/cm}^2\text{s} \leqslant m \leqslant 400 \text{ g/cm}^2\text{s}$$

$$20 \text{ kgf/cm}^2 \leqslant p \leqslant 150 \text{ kgf/cm}^2$$

$$0.5 \text{ cm} \leqslant D \leqslant 1.5 \text{ cm}$$

At individual points, the correlation may perfectly well be extrapolated beyond the range indicated above. Thus, it is applicable, for instance, for L/D ratios of 5 with a high degree of accuracy in an x_E range between -0.15 and 0. The difference between the observed value and the predicted value is here $\pm$ 10% maximum.

3.4.3 Comparison of results with the extended CISE correlation

By adding the abovementioned correction terms it has been possible to extend the CISE correlation so that it reproduces all our test data with a deviation of less than $\pm$ 10%.

./.

Also, the data given by Lee and Obertelli [44] as well as a large part of the measurements of CISE [11 , 48] agree very well with the extended correlation. Some measurements by CISE, especially with small test channel diameters, appear to yield low values of the critical heat flux in boiling. This is also supported by a comparison with test data of other authors. Fig. 54 gives a comparison of the data obtained from our test channels with an inside diameter of 0.7 with the extended CISE correlation. For L/D ratios between 10 and 140 the agreement is better than $\pm$ 10%. Only with very short test channels having an L/D ratio of 5 and degrees of sub-cooling measured at the inlet to the test section below $x_E = -0.15$ does the correlation deviate to a greater extent from the observed values.

Fig. 55 shows a comprehensive comparison between data obtained by M.A.N., Lee and Obertelli [44] as well as CISE [11 , 48] and the extended CISE correlation. In conclusion, a few graphic comparisons have been carried out in Figures 56 and 57 between our test data and those given by CISE as well as Lee and Obertelli.

4. Second Type Burnout (Pulsating Burnout)

4.1 Definition and Symptoms

The second type of burnout differs from the first type
essentially by the fact that, on its inception, fluctuations
occur in pressure and mass flow and that the critical heat
flux attainable is 20 to 50% lower than in the case of first
type burnout. The object of the present work is not only to
reproduce data on the maximum attainable heat flux under
conditions of pulsating burnout, but also to explain how these
pulsations arise and by what parameters they can be controlled.

Looking at Figures 58 and 59 in which part of the burnout
data observed by us are plotted against the degree of sub-
cooling at the inlet of the test channel $x_E = \frac{i - i'}{r}$, it can
be clearly seen how the pulsating burnout suddenly arises in
the region of x_E = -0.05 to -0.08 and, from there, extends
into the region of higher sub-cooling. It was observed,
however, only in the case of test channels with relatively
great L/D ratios and, in fact, was not found to occur with
L/D ratios of 5 and 10. As can be further seen from
Figures 58 and 59 and as will be explained in greater
detail further below, second type burnout is greatly
dependent on the throughput, the system pressure, the
geometry of the test channel and also on the location of
various apparatus in the test loop, such as throttling valves
and pressure vessels filled with compressible media. It is,
therefore, important for a characterization of the test
results to clearly define these "layout-controlled" conditions,
in addition to the thermodynamic and hydrodynamic parameters.
The results shown in Figures 58 and 59 were observed with
the test loop so arranged that it proved to be most
susceptible to pulsations. This was the case when the
pressurizer, which is partly filled with compressible steam,
was connected between the circulating pump and the test

channel inlet and when, furthermore, there was no
sufficiently effective throttling point upstream of the
test channel.

An example of the pressure, temperature and flow pattern
during pulsating burnout is given by the traces in Fig. 60
which were recorded at atmospheric pressure. During the
pulsations, periods of pure water flow alternate with
relatively long periods of pure steam flow. This oscillogram
was recorded by means of the bubble probe described in
Chapter 2.5.6 and it also indicates that, between the two
types of flow regime, there was for a short time a two-phase
flow, the irregularities in the oscillogram suggesting that
the steam bubbles were not homogeneously distributed in the
water but combined in slug-type voids. In phase with the
flow pattern are the pressure measured at the test channel
inlet and the surface temperature of the test channel.

In order to find an answer as to how these pulsations arise
and by what forces they can be damped,and eliminated,
respectively,it is necessary first of all to consider the
physical processes during inception of these instabilities.

Fig. 61a shows the pattern of the pressure drop in a boiling
water flow under conditions of different rates of heating
and correspondingly different rates of evaporation. At small
rates of flow, a low heating rate is sufficient to evaporate
water,and steam generation is accordingly not very intensive
so that the resistance characteristic assumes the slightly
curved form of curve 1 in Fig. 61a. If the heating rate is
increased, evaporation occurs already at greater mass flows
and steam generation is noticeably accelerated so that the
pressure drop in the test channel increases sharply.

Accordingly, the curves 2, 3 and 4 plotted in Fig. 61a are obtained for the resistance characteristic. They are characterized in that there is a pronounced minimum and maximum in the two-phase region. These curves show that, in spite of decreasing mass flow due to the steam volume produced, the pressure drop in the two-phase flow increases. If, in Fig.61a, the delivery characteristic of the propulsive force produced by the pump is also entered, the operating points will be obtained as the intersections between the delivery and resistance characteristics. If it is assumed,for the present example,that the resistance characteristic is represented by the curve 3 entered in Fig. 61a the intersections are I, II and III. These operating points may be of a stable or unstable nature. According to Griffith [59], the stability criterion is obtained from the balance of the forces acting on the flow. This flow is stable if

$$\frac{\delta \Delta \, pf}{\delta \, m} - \frac{\delta \Delta \, pw}{\delta \, m} \leqslant 0 \qquad (12)$$

where:

$\delta \Delta \, pf$ = pressure drop produced by propulsive force

$\delta \Delta \, pw$ = pressure drop due to resistance in test channel

$\delta \, m$ = the variation of the mass flow.

If this criterion is applied to the example of curve 3 shown in Fig. 61a it can be readily seen that the points I and III are stable states whereas point II represents an unstable condition.

./.

If the heating rate is increased in a system which is in
the operating state I, whereby the resistance characteristic
shows, for instance, the pattern of curve 4, a new inter-
section of the delivery characteristic and the resistance
characteristic is at point I' where the stability criterion
is no longer fulfilled. This leads to a marked reduction in
mass flow down into the range of almost pure steam flow
which shows substantially poorer heat transfer conditions,
and point II' is obtained as a new stable operating state.
This instability is, however, not sufficient to produce
pulsations; it will produce a singular mass flow reduction
which, in turn, may result in burnout.

Pulsations are oscillating phenomena and caused by the inter-
action of exciting and damping as well as inertia and
resilience forces. Energy storage, corresponding to that in
a spring, is effected by the compression of compressible
media located upstream of the test channel. Such a space
filled with compressible medium is, for instance, the
pressurizer which is partly filled with steam. If, according
to Griffith [59], the test channel with the pressurizer
connected upstream is considered as a vibrating system, the
inception of pulsations can be explained by the following
process.

If, in increasing the heating rate, the point I' is reached
as mentioned above, and flow conditions in the test channel
become unstable as a result, this will lead to a marked
reduction in mass flow and simultaneous increase of the
pressure drop in the test channel. The quantity delivered
by the pump will then be split into two partial flows at
the point of connection of the pressurizer. One flow will
go into the pressurizer and the other will pass through the
test channel. Thereby, the pressure in the pressurizer is

./.

raised and, in a first approximation, it can be assumed that
the pressure rise follows the law of the adiabats. This
means that, at the beginning of the overflow, a greater
amount is received per unit time by the pressurizer for a
given pressure rise Δp than at the end of the compression
process. Consequently, the branched off volume flow becomes
smaller as time progresses. According to Griffith, water
will flow into the pressurizer until the gradient of the
pressure rise $\dfrac{\delta p}{\delta t}$ in the pressurizer becomes greater
than the resistance increase in the test channel and,
consequently, the pressure rise per unit time at the inlet
of the test channel. In the further process, water may even
overflow from the pressurizer into the test channel, whereby
an oscillation is initiated.

As a result of this pressure and mass flow storage in the
pressurizer, different delivery characteristics will be
obtained, as shown in Fig. 61b, at each moment of inflow and
outflow of the partial quantity from and to the pressurizer
which have different intersections with the resistance
characteristic, of the unstable or stable type. This makes it
possible for a system, which had changed from an unstable
condition II into the stable condition III, to return to
condition II by a change in the delivery characteristic. In
a boiling water system, the possibilities of energy storage
are very numerous and not limited to the compression of
steam in the pressurizer. Other possibilities of energy
storage are the evaporation heat of the steam bubbles as well
as the compressibility of the steam in the test channel
region.

There have been various attempts to explain the excitation of
pulsations from the evaporation process in nucleate boiling.
Heat transport during evaporation calls for a certain degree
of superheating of the boundary layer adjacent to the heat-
emitting wall. In the case of very smooth and polished sur-
faces, this may amount to as much as 30 to $50\,C^{\circ}$.This causes a

./.

bubble forming from a boiling nucleus to grow very rapidly
causing volume changes and pressure variations. However,
heating surfaces for engineering purposes, such as the
cladding material of fuel rods and the tube wall of test
channels, almost invariably have a sufficiently great
roughness, resulting from the manufacturing process, to
preclude any such high superheating temperatures in the
boundary layer. As superheating decreases the rate of growth
of the individual steam bubbles diminishes and the volume
change produced per steam bubble will no longer have
sufficient energy to cause appreciable pressure variations
in the channel so that the evaporation process cannot be
considered as a primary excitation cause for the pulsations.

Several authors have attributed the cause of the excitation
of the pulsations to the intermittent flow regime of
slug-type flow. The amplitudes of the pressure fluctuations
caused by this would have to correspond to the associated
pressure loss in the liquid or vapour phases, and their
frequency would be given by the time which it takes for a
liquid slug, or a steam void, to pass through the channel. Our
measurements at atmospheric pressure, where the flow regime
was studied by means of the bubble probe described in
Chapter 2.4.6, permit the conclusion that during pulsating
flow there is for a short time slug flow between the time
periods of the liquid and vapour phases. But pulsations also
occurred at higher pressures in regions where, according to
the experience reported in the literature, slug flow was not
assumed to occur.

In our measurements, which were made by means of the probes
described in Chapter 2, we were able to find clear differences
in the patterns of first type burnout and pulsating burnout.

./.

Fig. 62 compares the variation with time of the heating
surface temperature and the mass flow for either type of
burnout. The oscillogram in the upper part of this
illustration shows the conditions at the moment of first
type burnout, i.e., under hydrodynamically stable conditions
and that in the lower part those during pulsating burnout.
The time plotted as abscissa runs in both oscillograms from
right to left. Furthermore, the time when the burnout
detector cuts off the power which heats the test channel is
marked by the step in the line at the top of the oscillograms.

Looking at the oscillogram for the first type burnout
initially, it can be clearly seen from the temperature curve
at the right-hand side of the oscillogram how the wall
temperature suddenly decreases by a small amount. Subse-
quently, there are brief statistical fluctuations developing
which, in an almost steplike rise, lead to film boiling.
After shutting off the heating power, the wall temperature
subsides immediately according to an exponential function.
The mass flow is almost unaffected by the boiling crisis
during first-type burnout and remains constant.

Different conditions prevail during pulsating burnout which
is illustrated by the oscillogram in the lower part of
Fig. 62. Starting from completely stable conditions, mass flow
variations occur suddenly as the heat flux is increased, and
these increase sharply after a few periods. Also, the pattern
of the heating surface temperature variation differs
essentially from that during first-type burnout. Again, there
is a slight temperature discontinuity to be observed before
the actual temperature rise. But the rise is at a much
steeper angle than in first-type burnout and without the
statistical fluctuations observed there. A striking feature
is the initially very slow decrease of the heating surface

./.

temperature after cut-off of power whereas in first-type
burnout this decrease takes place almost without delay.
During pulsating burnout, the temperature curve shows the
anticipated decrease in the form of an exponential function
only after 0.1 to 0.2 seconds. This delay can be explained
only if one assumes that an extensive steam blanket is formed
in the test channel which, after cutting off the heating
power, has to be displaced by the flow first before cooling
of the heating surface is restored at an intensive rate. In
order to verify that this delay in the temperature drop is
due solely to the steam blanket existing in the test channel
a few theoretical studies were made which are set out in
Appendix 2. If the rate of displacement for this steam
blanket is equated with the mean velocity of the flowing
medium that existed before burnout the conclusion can be
derived from this that the test channel was almost completely
filled with steam over its entire length.

The pressure fluctuations at the moment of pulsating burnout
were found to attain amplitudes of approximately $\pm$ 1 kgf/cm^2
at a total pressure of the flowing medium of 70 kgf/cm^2. On
shutting off the heat supply by the burnout detector, the
pulsations receded at once, and stable flow conditions were
restored.

In several cases, the observation was made during our measure-
ments that periodical fluctuations occurred in the heating
surface temperature on inception of the burnout process
which showed an absolutely uniform frequency and which were
not, as in the case of the hydrodynamically stable burnout,
statistically distributed over time. An example of these
periodical temperature variations is shown by the oscillogram
reproduced in Fig. 63.

./.

4.2 Literature Review

A number of theoretical and experimental studies have been published on the stability of boiling water circuits. Almost none of these deals with the problem of a burnout risk due to instabilities in the coolant. Lowdermilk [60] and Aladiev [61] were among the first to observe that burnout may also be caused by pulsations in the flow. Recent investigations have been due to Silvestri [11] who already made a number of systematic tests. All three authors independently arrived at the conclusion that marked pressure fluctuations preliminary to burnout will substantially reduce the maximum attainable heat flux. It was attempted in those studies to reduce the liability for pulsations to arise by design modifications of the circuit. It was found, in particular, that eliminating all spaces upstream of the heated channel, which are filled with compressible media, as well as fitting of throttling devices at the inlet of the meating channel, tend to contribute substantially towards a stabilization of the conditions and, thereby, delay the inception of pulsations. The test facilities used by Lowdermilk, Silvestri and Aladiev differed essentially from the layout of our test loop. Whereas we used a closed circuit with a centrifugal pump to circulate the water the three authors used open circuit systems where the coolant, i.e. the water or the water/steam mixture were delivered from outside and, after passing the test section, were discharged through an automatically working or manually-operated throttling valve to atmosphere. Silvestri used a reciprocating pump to produce the flow, Aladiev fed steam into water, and Lowdermilk maintained the flow by means of a continuous pressure from a nitrogen cylinder acting on a plastic bag filled with water.

./.

Very recently, a number of other studies have been published
which, in addition to burnout measurements, deal mainly with
the instabilities in flowing two-phase mixtures.

Mention may be made of the investigations by Becker et al.
[62] , Griffith and Maulbetsch [59], Bergles et al. [62],
Weatherhead [64], Gouse and Andrysiak [65], Jeglic and
Grace [66], Bouré [67], Cesterline and Lee [68], Stenning
and Vezirglu [69], as well as the General Electric [70].
These authors have given criteria for the inception of
pulsations in the form of equations.Whereas Becker, Bouré
and Bergles based their stability considerations on the
three equations describing the conditions of flow in the
channel,i.e. the continuity equation, the theorem of momentum
and the energy balance,it was assumed by Jeglic and Grace
that it is the slug flow regime which is responsible for the
inception of pulsations. The latter worked on the basis of
the equation given by Yang and Clark [71] which defines the
growth of a steam bubble forming on the heated wall. Griffith
and Maulbetsch analysed the vibration behaviour of a system
consisting of a heated channel in conjunction with a vessel
connected directly adjacent to it upstream and filled with a
compressible medium and, starting from the delivery and
resistance characteristics provided stability criteria for
the flow of a two-phase medium. All these studies constituted
a substantial contribution towards a better understanding of
the problem within the scope of their validity. However, in
order to be able to establish criteria of broader validity
it will be necessary to carry out further tests. The number
of possible influence factors on the pulsations is so large
and the definition of the thermodynamic and hydrodynamic

./.

parameters so complex that a mathematical formula to cover the whole problem can, if at all, have a chance of success only if a clear picture is afforded by an adequate number of experimental results. We have therefore placed the emphasis in our investigations into the pulsating burnout clearly on the experimental side. In addition to a contribution towards a better understanding of this phenomenon it has been our secondary objective in these measurements to work out design criteria for pressurized water and boiling water reactors and, thereby, to provide further basic information for an increase in power and improvement in economy of these reactor types.

4.3 Presentation of Test Results

The parameters affecting pulsating burnout can be divided into 4 groups viz. thermodynamic, hydrodynamic and geometric factors and parameters which reflect the layout of the test loop. Our tests were made on round internally-cooled tubes with inside diameters of 0.7, 1.1 and 1.5 cm with a wall thickness of 0.05 cm and a length/diameter ratio of the heated section of 5 - 140. The mass flows studied extended through a range from 100 to 400 g/cm^2s at pressures between 70 and 140 kgf/cm^2. The maximum sub-cooling at the test channel inlet was 150° which corresponds to $x_E = -0.5$. In most cases, however, the degree of sub-cooling extended from 60° ($x_E = -0.3$) to the saturation line ($x_E = 0$). Pulsating burnout was observed to occur only under conditions of sub-cooled boiling as well as very low steam qualities.

./.

As already mentioned in Chapter 4.1, it was found at the beginning of the measurements that the pulsating burnout was greatly affected by the location of various equipment within the test loop. We therefore carried out our investigations initially with the loop arranged in a manner where it showed the greatest susceptibility to pulsations. This was the case when the pressurizer was connected directly upstream of the test channel and when as few throttling points as possible existed between the circulating pump and the test channel. A general survey of the test results obtained with this loop layout was given earlier in Figures 58 and 59 discussed in Chapter 4.1 which, at pressures of 70 and 100 kgf/cm^2, include values at L/D ratios between 40 and 140 and mass flows between 230 and 350 g/cm^{2}s. The difference between first type burnout and pulsating burnout is brought out clearly again in Fig. 64 in the example of a test series at 70 kgf/cm^2 and 230 g/cm^2. The L/D ratios were chosen as the parameter in these graphs with values of 40, 80 and 140. All tests referred to up to now were made with a channel diameter of 0.7 cm. Results for test channels of 1.1 and 1.5 cm diameter are shown in Figures 65 and 66. The L/D ratio there was 40 at pressures of 70 and 100 kgf/cm^2 and the mass flow was between 100 and 230 g/cm^{2}s.

With the layout producing maximum susceptibility to pulsations the influence was subsequently studied of various thermodynamic and hydrodynamic parameters such as pressure, degree of sub-cooling, mass flow and L/D ratio. These measurements are reproduced in Chapters 4.4.1 to 4.4.5.

./.

In our experimental studies, which, in fact, were intended to
provide design criteria for boiling water and pressurized
water reactors and to improve the burnout performance of
such installations, it was one of the objectives in the
investigations into the pulsating burnout to evaluate design
and flow-control measures that were apt to obviate
pulsating burnout. Out of a number of possibilities there
are two which offer practical engineering advantages: firstly,
to enhance the stiffness of the oscillating system in
reducing the compressibility of the flowing medium and,
secondly, to provide throttling points to increase the
damping forces. A large compressible volume is represented
by the pressurizer with its steam space which is an essential
component of all pressurized water reactors and acts as a
surge tank. The tests showed that the pulsations were far
more affected by measures taken to influence the flow and
oscillations upstream of the test channel than measures
applied at downstream points. The liability for pulsations
to arise decreases sharply, as explained in Chapter 4.5.1,
if a pressurizer connected upstream is relocated to a
location downstream of the test section, thereby eliminating
a large compressible volume between the circulating pump and
the test channel. The transition from first type burnout to
pulsating burnout was shifted as a result towards higher
degrees of sub-cooling. Throttling and, consequently, an
increase in the pressure drop immediately at the inlet to
the heated channel proved to be a reliable, if uneconomic,
means of controlling pulsating burnout. As a higher throttling
effect invariably penalizes pumping power the designer would
endeavour to keep the pressure drop required to improve
safety from pulsations to the absolute minimum. We have
investigated this minimum throttling effect required for
various design, thermodynamic and hydrodynamic conditions.

./.

The results are reproduced in Chapter 4.5.2. In these tests, a variable orifice was fitted to the inlet of the test section and the measurements were made with tubes of 0.7, 1.1 and 1.5 cm diameter at L/D ratios of 40 and 70 and pressures of 70 and 100 kgf/cm^2. Furthermore, fixed orifices were fitted to the inlet of the test channel and their influence on the pulsating burnout measured. For the sake of completeness, the effect of a throttling orifice located at the test channel outlet was also investigated.

The test objects and the principal test parameters of all test series referred to and carried out to study the pulsating burnout are conveniently tabulated in Table II. The individual results of these test series are to be found in the Tables 50 to 112. In the following chapters, the individual tests are explained in greater detail and the effects of the various factors are discussed.

4.4 Factors Controlling the Inception of Pulsations

For greater clearness, it is convenient to deal with the various test parameters in the following in separate chapters. In the Chapters 4.4.1 to 4.4.5 are discussed the results obtained with a layout of the test loop where maximum susceptibility to pulsation existed. The Chapters 4.5.1 to 4.5.4 are in respect of the measures by which pulsating burnout can be controlled.

4.4.1 The influence of the mass flow

The tests made by us covered the range which is of interest in reactor engineering, i.e., flow rates between 100 and 400 g/cm^{2}s. The observation was made that as the mass flow

./.

increases the effect of the pulsating burnout decreases to disappear eventually completely. This influence is exemplified in Fig. 67. With a mass flow of 230 g/cm^{2}s, the sudden transition from first type burnout to pulsating burnout can still be clearly seen here whereas with a mass flow of 290 g/cm^{2}s both types of burnout steadily blend into each other and, at 350 g/cm^{2}s, the maximum attainable heat flux in pulsating burnout hardly differs any more from the first type burnout. This influence of the mass flow can also be seen from the graphs 65 and 66 discussed previously in Chapter 4.3 where the data for test channels with diameters of 1.1 and 1.5 cm are plotted. Specifically, it will be noted that for the smallest mass flow measured of 100 g/cm^{2}s the pulsating burnout extends into the range of positive steam quality and the transition to first type burnout takes place only with a steam quality of 5 to 10% measured at the test channel inlet. This applies both for a pressure of 70 kgf/cm^2 and 100 kgf/cm^2. This observation that pulsating burnout does in fact occur under conditions of low steam qualities in the case of very small mass flows was made already by both Aladiev [61], and CISE [41]. Fig. 68 shows some data found by Aladiev [61] plotted for a mass flow of 40 g/cm^{2}s in a 0.8 cm diameter channel with an L/D ratio of 20 at a pressure of 100 kgf/cm^2.

If one were to assume with Jeglic and Grace [66] that the slug flow regime is contributary to the development of pulsations one could explain the decrease in the pulsation intensity with increasing mass flow from the fact that slug flow tends to occur to an appreciable extent only with low flow velocities. According to the findings of Bergles et al. [63] whose data are reproduced in Fig. 69 for a pressure of 70 kgf/cm^2 slug flow is possible only up to a mass flow of

./.

approximately 150 g/cm^{2}s and a steam quality between 5 and 40%.
A somewhat more obvious explanation is that the inertia forces
of the flow increase as the square of the flow velocity and
that therefore ever greater exciting forces are necessary for
the flow velocity to be reduced or even for its direction to
be reversed.

4.4.2 The influence of the degree of sub-cooling and steam quality

As already mentioned, the transition from pulsating burnout to
first type burnout will occur in the case of mass flows above
100 g/cm^{2}s only if sub-cooled flow prevails at the test
channel inlet. The change from one type of burnout to the
other was almost invariably observed with a sub-cooling of
x_E = -0.05 to -0.08. As the degree of sub-cooling is increased
the maximum attainable values of the critical heat flux in
pulsating burnout more and more approach those attained in
first type burnout until eventually there is hardly any
difference between the two types of burnout in respect of the
maximum heat flux. It was noticed in this range that points
which were on the curve of first type burnout nevertheless
showed slight oscillations in the mass flow.

This difficulty in discriminating between pulsating burnout
and first type burnout is clearly brought out by Figures 70
to 72. In Fig. 70 the maximum heat flux is plotted against
the degree of sub-cooling and two curves are drawn, one for
first-type burnout and the other for pulsating burnout. In
the region of high degrees of sub-cooling there are two
measuring points, one on the curve for pulsating burnout
and the other on the curve for first type burnout, marked
by the numerals 71 and 72. These numerals indicate the
Fig. Nos. of the oscillograms relating to each point which

./.

record the variation with time of the wall temperature, the mass flow and the pressure. With respect to point 1, which is on the curve of the pulsating burnout, and the relevant oscillogram Fig. 71 it follows both from its position in the qx-diagram and the oscillogram that it is clearly a pulsating burnout. In contrast to this, the point 72 is on the line of first type burnout, i.e., for hydrodynamically stable flow. But the oscillogram in Fig. 72 clearly shows pressure fluctuations,and periodically recurring temperature peaks are also to be observed in the temperature curve on inception of burnout so that,judging from its appearance,this measuring point ought to come under the heading pulsating burnout although in the qx diagram it is on the line of the first type burnout.

4.4.3 The influence of the system pressure

The tests made by us essentially covered a range from 70 to 140 kgf/cm^2. Individual tests were included at atmospheric pressure. The measurements showed that as the pressure rises the intensity of the pulsations decreases and that eventually at pressures above 100 kgf/cm^2 pulsating burnout generally fails to occur. As the pressure increases the difference in the maximum attainable heat fluxes between the two types of burnout diminishes. This is clearly shown in Fig. 73 in which the measurements at 70, 85 and 100 kgf/cm^2 have been entered for a mass flow of 300 g/cm^2s at an L/D ratio of the test channel of 40. At the point of transition from first type to second type burnout the values show the maximum difference at 70 kgf/cm^2 whereas at 100 kgf/cm^2 the difference is but a few percent. Also, the transition here is no longer sudden as at the lower pressures but both types of burnout blend steadily with each other.

./.

An increase in pressure also causes the transition point to be shifted towards higher degrees of sub-cooling as can be seen from Figures 74 and 75 for a test channel with an L/D ratio of 80 with mass flows of 300 and 350 $g/cm^2 s$.

This pressure-dependence of the pulsations can be explained by the fact that the volume expansion occurring during evaporation diminishes as the pressure increases. As a result, the amplitude of the excitation forces is reduced. An essential factor for the steam volume produced at constant heat flux is the dependence of the heat of evaporation on the pressure. A comparison shows that the specific volume of the steam at 70 kgf/cm^2 is higher by the factor of 1.5 than at 100 kgf/cm^2 whereas the heat of evaporation differs only by the factor of 1.14 between these two pressures, in other words, the steam quantity produced, measured in kg, is 14% higher at 100 kgf/cm^2 than at 70 kgf/cm^2, but the volume flow is reduced because of the lower density which is smaller by the factor of 1.5.

As the pressure increases the compressibility of the steam produced in the heated channel as well as in the pressurizer decreases, providing, as it were, a greater "stiffness" of the system. This enhances the frequency of the vibrations, leads to smaller amplitudes and changes the resonance behaviour of the circuit system.

4.4.4 <u>The influence of the test channel diameter</u>

The test channels studied during our investigations had diameters of 0.7, 1.1 and 1.5 cm. A comparison is afforded by Fig. 76 in which the measurements are plotted for channels with these 3 diameters for a mass flow of 230 $g/cm^2 s$ and a

./.

pressure of 70 kgf/cm^2. It can be seen that under conditions
of pulsating burnout the maximum heat flux is almost
identical for all three test channels, i.e. the diameter has
no influence. Also, transition from pulsating to first type
burnout is at the same degree of sub-cooling viz. at x_E =
-0.05. This conclusion, that the test channel diameter is of
no influence in the region of the pulsating burnout, differs
essentially from conditions under first type burnout where
the critical heat flux, at least in the range of small
diameters, is greatly affected by the channel area.

4.4.5 <u>The influence of the length/diameter ratio</u>
As shorter test channels are used there is less difference
in the maximum heat flux between pulsating and first type
burnout. Whereas with test channels having L/D ratios of
40, 80 and 140 this difference, as previously shown in
Fig. 64, amounts to 50% and more, no pulsating burnout was
observed in our tests with channels having L/D ratios of
5 and 10.

The resistance in the heated channel is composed of the
impact losses at the inlet to, and outlet from, the channel,
the friction of the single-phase flow, or two-phase mixture,
respectively, and the acceleration of the mixture
necessitated by the evaporation process. The relative
percentage of the inlet and outlet impact losses which in
their absolute magnitude remain the same increases as the
channel length is reduced. As a result, the effect of the
two-phase friction on the overall pressure drop is less
marked and its influence on the shape of the resistance curve
in the boiling range is diminished.

./.

4.4.6 Tentative analytical summary of test results at the transition from pulsating to first type burnout

It can be seen from Chapters 4.4.1 and 4.4.5 that, at the point of transition between the two types of burnout, there are partly substantial differences in the maximum attainable heat flux the value of which depends on the L/D ratio, the pressure and the mass flow. We have tried, for better predictability, to present this interrelation in the equation given further below. This equation permits the ratio of the maximum heat fluxes in hydrodynamically stable burnout and pulsating burnout at the point of transition to be calculated; it is valid, however, only for the thermodynamic and hydrodynamic as well as the geometric and physical design conditions existing in the test loop in which the test data here presented were obtained. For these test conditions, the equation reads

$$\frac{q_{stab}}{q_{puls}} = \frac{(1 L/D - 1801)^{1.6} + 157.5}{p \cdot m^{(0.743 - 0.31 \frac{L/D}{100})}} \cdot 1.42 \qquad (13)$$

where

q_{stab}	W/cm^2	critical heat flux in hydrodynamically stable burnout
p	kgf/cm^2	working pressure
L/D		length/diameter ratio of test channel
q_{puls}	W/cm^2	critical heat flux in pulsating burnout
m	$g/cm^2 s$	mass flow

./.

This correlation applies to pressures from 70 to 100 kgf/cm^2, mass flows from 230 to 350 g/cm^{2}s and L/D ratios of 40 to 140. With an L/D ratio of 40 and a pressure of 100 kgf/cm^2 it is limited upwards to a mass flow of 230 g/cm^{2}s because pulsating burnout will not occur for greater mass flows. Apart from that, the equation applies only to a design of the test loop where the pressurizer is connected upstream of the test section and where there is no additional throttling point at the test section inlet.

4.5 Measures to obviate Pulsating Burnout

As repeatedly stated, the test results discussed in Chapter 4.4 were obtained with a layout of the test loop that proved most liable to produce pulsations. By relocating compressible volumes upstream of the test channel to a location downstream and by the provision of throttling points directly at the inlet to the heated length of the test channel, pulsations can be obviated to a large extent. Fig. 77 gives a general picture of how such modifications of the loop layout tend to affect pulsating burnout.

The influence of these measures is proposed to be discussed in greater detail in separate chapters hereunder:

4.5.1 The influence of the location of the pressurizer connection

If the point of the pressurizer connection was relocated from an upstream position to a downstream location by opening the valve 7 shown in the schematic diagram of the test loop in Fig. 78 and closing the valve 6 the tendency for pulsations to arise decreased to a marked extent, and pulsating burnout

./.

was shifted into a region of higher degrees of sub-cooling. In addition to Fig. 77 already referred to, this is clearly to be seen from Fig. 79 in which the test data obtained with channels having L/D ratios of 40 and 80 have been plotted for various locations of the pressurizer. The mass flows in these tests were 230 and 300 g/cm^{2}s.

The improvement achieved in the stability of the circuit by relocating the pressurizer connection was explained repeatedly in the preceding chapters. As shown in Chapter 4.1 the total mass flow is split up in two partial flows when the pressure drop in the test channel increases due to the boiling process, one flowing through the test channel and the other flowing into the pressurizer. If then the pressurizer connection is relocated to a downstream point this momentary by-pass no longer exists and all water delivered by the pump flows to the test channel. Another important factor for the mass flow and pressure pulsations is that, when the compressible media are removed ahead of the test channel, the"stiffness" of the system will be greatly enhanced.

4.5.2 The influence of throttling points on pulsating burnout
Throttling action and, consequently, an increase in the pressure loss directly at the inlet of the test channel is a reliable, although in practice uneconomical, means of obviating pulsating burnout. Initial studies of this aspect were made, inter alia, by Silvestri [41], who fitted throttling devices at the test section inlet and, depending on the pressure loss produced, was able to shift the transition from pulsating burnout to first type burnout to ever higher degrees of sub-cooling. We have in our tests

./.

also applied throttling which, initially, was provided by
various orifice plates fitted to the test channel inlets
and outlets. The dimensions and arrangement of these orifice
plates is shown in Figures 13 and 80. The results obtained
with the orifice plate marked with the numeral 1 in Fig. 13
are plotted in Fig. 81. This provides qualitative confirma-
tion of the results obtained by Silvestri [41], to the
effect that the inception of pulsating burnout is shifted
towards higher degrees of sub-cooling. If, in addition to
such throttling action, the pressurizer connection is re-
located from an upstream location to a position downstream
of the test channel, the effects of the two measures will
be cumulative and, in fact, during all our tests with all
flow velocities, degrees of sub-cooling and pressures
investigated only first type burnout was experienced.

During the tests with the No. 2 orifice plate also shown in
Fig. 13 which caused a higher pressure drop than the No. 1
orifice plate, pulsating burnout was no longer observed
with the test channels used having L/D ratios of 40 and at
all flow velocities and all pressures irrespective of the
location of the pressurizer connection. For completeness'
sake, the influence of an orifice plate fitted to the test
channel outlet was also investigated. The entrance flow
conditions at the inlet of the channel were completely
undisturbed in these tests. As shown by the data reproduced
in Fig. 82, such throttling action at the test channel outlet
also influences pulsating burnout to the effect that its
inception is shifted towards higher degrees of sub-cooling
and completely obviated at higher pressures above 100 kgf/cm^2.
However, if the values obtained during these tests, which
apparently are on a line with first type burnout, and if
they are compared with other test results which were obtained

.../.

under completely identical conditions but without throttling
at the test channel outlet, it will be found that the test
points ascertained with outlet throttling are 25 to 30%
lower. As more detailed investigations by means of oscillograms
of the temperature variation and mass flow and pressure showed,
pulsations did in fact not occur but, shortly before
inception of burnout, a marked reduction in mass flow was
observed. This single and sudden mass flow reduction must
also be looked upon as an instability although this type of
burnout is not necessarily identical with the pulsating
burnout. It is therefore less useful to provide throttling
points at the outlet of the heating channel.

Increased throttling invariably costs additional pumping
power and the designer would therefore endeavour to keep
this additional pressure loss to the very minimum necessary.
We have, for this reason, made a number of investigations to
determine how great the pressure drop at the test channel
inlet has to be in order to obviate pulsating burnout under
given thermodynamic and hydrodynamic conditions or rather
to shift it towards higher heat flux levels. For this
purpose, an adjustable throttling device was fitted to the
test channel inlet which permitted infinite variation of the
pressure loss within wide limits. The design of this
throttling device is shown in Fig. 83.

It consists of two opposed pistons arranged perpendicular to
the flow direction and spaced 180° apart fitted in a lenticular
body located directly at the inlets to the test channel and,
at the same time, serving as a minus pole for the electric
power. Infinitely variable adjustment of these pistons which
at their inner end have a diameter of 8 mm, is by screw
extensions and permits the originally circular cross
sectional area of the test channel to be closed to any extent

./.

desired until the desired throttling action is obtained. The
pistons and their screw extensions are fitted in a pressure
tube and sealed by stuffing boxes against atmosphere. The
pressure drop across the throttling point is measured by
means of a single-leg mercury manometer connected to pressure
tappings upstream and downstream of the throttling point. The
tests with this type of adjustable inlet throttling included
tubes of 0.7, 1.1 and 1.5 cm diameter and L/D ratios of 40
and 71.5. At pressures of 70 and 100 kgf/cm^2 and mass flows
of 100 to 400 g/cm^2s, they covered a range of $-0.25 < x_E < 0$
inlet sub-cooling.

The Figures 84 and 87 show the observed burnout values in the
abovementioned test range for lines of equal pressure drop
at the test channel inlet. As throttling was increased the
inception of pulsating burnout was shifted towards ever higher
degrees of sub-cooling until, eventually, it failed to occur.
Considering in the abovementioned graphs a state of constant
inlet sub-cooling it will be found that as throttling is
increased the heat flux at which pulsating burnout occurs
tends to be at higher values. As sub-cooling is decreased
the throttling action required to obtain first type burnout
became increasingly smaller.

The question arises why pulsating burnout can be avoided by
throttling at the test section inlet and for what reason the
necessary pressure drop required for this becomes less as
sub-cooling diminishes. As already mentioned in Chapters 4.1
and 4.4.5 the well-known resistance characteristic applies
to two-phase flow in a heated channel which, depending on the
heat flux, may assume various shapes. By providing a throttling
point at the test section inlet a modified resistance
characteristic is obtained by superimposition of the S-shaped

./.

boiling curve on the curve for the pressure drop at the
throttling point which has the shape of a parabola. The use
of this measure - assuming that there is no compressible
volume between the throttling valve and the test section -
permits the unstable branch of the boiling characteristic
to be eliminated and, thereby, pulsations to be avoided.
Fig. 88 shows an example in which, by addition of the
curves 1 and 2, the curve 3 is obtained which permits stable
operation of the circuit.

Pulsating burnout cannot recur until the resistance
characteristic composed of the pressure drop at the throttling
point and two-phase friction again shows unstable operating
conditions in its interaction with the delivery characteristics.
However, this will now be the case only at much higher heat
flux levels than under conditions without throttling at the
test channel inlet.

Not in all cases do pulsations have sufficient energy to
cause burnout. The pressure and temperature traces re-
produced in Fig. 89 show that, as the heat flux is increased,
it is possible for pulsations which have already started to
subside again and that then the heat flux can be raised
until hydrodynamically stable burnout occurs.

For convenient representation, it has been attempted to give
an equation which permits the minimum pressure drop required
to attain hydrodynamically stable burnout as a function of
mass flow, pressure and sub-cooling. It is valid for an L/D
ratio of the test channel of 80 with upstream-connected
pressurizer.

./.

$$P_{min} = \left[\frac{(|m - 285|)^{2.08}}{1.2} + 10^4\right] \left[1.5 - 7.2 \cdot 10^{-3}p\right] \cdot |x|$$

$$- \left[\frac{(|m - 240|)^{2.75}}{1466} + 368\right] \left[0.467 + 7.62 \cdot 10^{-3}p\right] \tag{14}$$

where

P_{min}	mm Hg	minimum throttling
m	g/cm^2s	mass flow
p	kgf/cm^2	pressure
x	-	sub-cooling of flowing medium at inlet

This equation is valid for mass flows of 230 to 350 g/cm^2s, pressures of 70 to 100 kgf/cm^2 and a test channel diameter of 0.7 cm. If it is desired to apply it to other loop arrangements it is axiomatic that attention should be paid to hydrodynamic and design similarity of the system.

4.5.3 Frequency and amplitude of the pressure and mass flow variations preceeding pulsating burnout

Information on the frequency and the amplitude of the oscillating phenomena can be derived from the oscillograms taken of the temperature, pressure and mass flow at the moment of pulsating burnout. Both values are dependent on the damping, the compressibility and the inertia of the system. The greater the damping, the compressibility and the inertia the smaller the frequency of the pressure and mass flow variations. As the oscillograms discussed elsewhere in this report have shown, the frequency of the oscillations of pressure and mass flow agree completely in almost all cases. Figures 90 and 91 show examples of

the dependence of the frequency of these oscillations on
the degree of sub-cooling. The higher the degree of sub-
cooling the lower the medium steam quality in the test
channel which again, because of the decreasing compressibility
of the system, leads to higher frequency of oscillations.
The test data entered in Fig. 90 are based on a channel with an
L/D ratio of 40 whereas the channel in Fig. 91 had a ratio
of 80. This increase in the heated length has, as anticipated
and shown in the traces, a frequency-reducing effect on the
oscillations. The characteristic patterns of the pressure
and mass flow variations for two widely different degrees
of sub-cooling are again shown in Figures 92 and 93. If,
finally, the compressibility of the system is varied by
connecting the pressurizer upstream in one case and down-
stream in the other case, this measure will as shown in
Fig. 94 also affect the frequency of the pressure and mass
flow variations.

In the course of our studies, we also investigated the
dependence of the frequency and amplitude on the degree of
throttling at the test channel inlet. These tests were made
at a pressure of 70 kgf/cm^2 and mass flows of 240 and
290 g/cm^2s with a test channel having an L/D ratio of 40
and a diameter of 0.7 cm.

The system pressure in these tests was measured by means of
a high-frequency pressure pick-up directly at the test
channel inlet. Instead of the mass flow, the pressure
differential across the adjustable throttling device shown
in Fig. 83 was determined which is a measure of the
instantaneous flow through the test channel.

./.

The results which are reproduced in Figures 85 and 96 show that, as throttling at the test channel inlet is increased, both frequency and amplitude of the pressure and mass flow variations decrease which is to be anticipated according to the physical laws governing a forced damped oscillation. The pattern of the pressure variation shortly before inception of burnout is shown in Fig. 97. Here, the curve 1 describes the variation of the pressure differential across the throttling device, curve 2 the system pressure whereas curve 3 shows the temperature measured at the test channel wall. The "plus" direction indicated in the trace of the system pressure means an increase and, correspondingly, the "minus" direction a decrease. It can be seen from this trace that the maximum amplitude of the pressure variations occurred directly after inception of film boiling, i.e., during the increase of the temperature in the test channel wall. In the evaluation of the test results which have been plotted in the preceding graphs in Figures 95 and 96 the last amplitude occurring before inception of film boiling was taken as a basis in each case.

./.

4.6 Reflections on Pulsating Burnout

As discussed in detail in the preceding chapters, pressure and mass flow fluctuations arise in pulsating burnout which lead to an excessive increase in the temperature of the heating surface. The question now arises: is this pulsating burnout a physically different phenomenon from inception of film boiling during burnout under steady state flow conditions or is a condition reached after all where in spite of the pressure and mass flow fluctuations and the resulting enthalpy changes of the coolant the criteria of film boiling exist in spite of the relatively low heat flux?

With the heat flux kept constant, fluctuations in the mass flow will cause periodic changes in the steam quality at the outlet of test channel and in the flow velocity. Assuming a sinusoidal pattern of the mass flow fluctuations, the inter-relationship between steam quality at the test section outlet, enthalpy of the flowing medium and mass flow can be represented by the following system of equations:

$$\frac{\delta i}{\delta t} + \frac{\delta i}{\delta z} \cdot \frac{M}{\rho \cdot F} - \frac{D}{\rho} \cdot \frac{\pi}{F} \cdot q = 0 \tag{15}$$

$$\frac{\delta \rho}{\delta t} + \frac{\delta M}{\delta z} \cdot \frac{1}{F} = 0 \tag{16}$$

$$M = A \cdot \cos(wt) + M_o - A \tag{17}$$

$$x = \frac{i - i'}{r} \tag{18}$$

where

i	=	enthalpy of flowing medium	kcal/kg
t	=	time coordinate	sec
z	=	path coordinate	m
m	=	mass flow	kg/h
ρ	=	density	kg/m^3
F	=	cross sectional area	m^2
D	=	diameter	m

./.

q	=	heat flux	W/cm^2
A	=	constant	kg/h
M_o	=	mass flow before inception of pulsation	kg/h
w	=	constant	1/sec
x	=	steam quality	-
i'	=	saturation enthalpy	kcal/kg
r	=	evaporation heat	kcal/kg

The abovementioned system of equations presupposes the existence of a homogeneous steam/water mixture in the test section.

The differential equations 15 and 16 were transformed into difference equations and the system integrated stepwise by a computer. If the values computed for the steam quality on the basis of this system of equations are plotted against mass flow for any point of time within an oscillating period, the continuous curve shown in Fig. 98 will be obtained. In the same graph can be entered the boundary line for the hydrodynamically stable burnout, i.e. the film boiling, which is obtained if, for a constant heat flux, the steam quality at the test channel outlet is plotted against various mass flows. Below this boundary line there will be nucleate boiling under hydrodynamically stable conditions, above it the criterion of film boiling will have been exceeded. If then a continuous curve is entered for that heat flux at which dynamic burnout just occurs, and if this continuous curve touches the boundary line of the hydrodynamically stable burnout, this would suggest the conclusion that dynamic burnout and hydrodynamically stable burnout are identical in their physical nature and that, in the course of the periodic fluctuations, a state is reached in the test channel for a short period during which the criteria of film boiling apply.

./.

Accurate information on the pattern of the continuous curve
are conditional, above all, on a perfectly exact measurement
of the mass flow fluctuations in respect of amplitude and
frequency. Mass flow fluctuations in the course of our tests
were mostly made by means of a rotary vane Potter-type flow
meter located at a short distance upstream of the test channel.
As check measurements showed, this Pottermeter, while giving
very exact readings of the frequency of the mass flow
variations, was greatly affected by damping processes and
intermediate storage of the fluid so preventing any accurate
information being obtained on the amplitudes. The attempt was
therefore made, by measuring the pressure drop over the heated
length of the test channel, to measure the actual amplitude of
the mass flow fluctuations. Fig. 99 shows 3 examples for the
pattern of mass flow fluctuations briefly before and during
inception of dynamic burnout. As the frequency of these mass
flow fluctuations is very low and, since they have a rate of
propagation through the test channel of as low as about 0.5 m/s,
a value which is far below the velocity of sound in two-phase
mixtures, this method of determining mass flow fluctuations
from the pressure difference is not affected to any great
extent by the pressure waves occurring in the test channel.

Our tests have shown that the dynamic burnouts will occur
only when the mass flow fluctuations go below the zero line,
which means that a reverse flow occurs in the test channel,
in other words, the mixture of high steam quality which just
flowed through the test channel is returned into the channel
once more and undergoes considerable superheating.

This would suggest that in dynamic burnout we are concerned
more with a drying up of the heating surface and that, for
a moment, there was only superheated steam in the channel
which has relatively poor heat transfer coefficients.

./.

In individual cases, dynamic burnout was found to occur already when the mass flow was just dropping to zero and, consequently, complete stagnation of the flow occurred in the test channel. The pattern of steam quality variation at the outlet of the test channel has been plotted in Fig. 100 against the mass flow for a typical incidence of dynamic burnout. As can be seen from the graph this curve for the interrelationship between steam quality and mass flow intersects the above discussed boundary line for the hydrodynamically stable burnout instead of just touching it as one would have assumed. This corroborates the assumption that dynamic burnout is caused by the short-time production of superheated steam in some part of the test channel.

APPENDIX I

Summary of Analytical Correlations to prediet the Critical
Heat Flux

A Further Compilation of Burnout Equations is given in [74]

In the following is a summary of the analytical correlations
available to us for the predietion of the critical heat flux
in first type burnout. The order of the list is alphabetical
by the names of the authors and does net constitute a valuation
of the individual correlations. Sinee the equations in most
cases contain empirically found constants a conversion into
the metric system of units has frequently been omitted.

1) **Correlation by Bernath [6]**

Burnout equation

$$q''_{DNB} = h_{DNB} \, (T_{w,DNB} - T_{DNB}) \qquad (1)$$

where:

$$T_{w,DNB} = 1.8 \left[57 \ln p - 54(\tfrac{P}{P+15}) - \tfrac{V}{4} \right] + 32 \qquad (2)$$

$$h_{DNB} = 10890 \, (\tfrac{D_e}{D_e + D_1}) + \tfrac{48}{D_e^{0.6}} \cdot V \qquad (3)$$

where $D_1 = \dfrac{P_h}{\pi}$

Notation:

D_e	in.	hydraulic diameter calculated from wetted circumference
P_h	in.	wetted circumference
$T_{w,DNB}$	$^\circ F$	tube wall temperature at burnout location

./.

T_{DNB} °F   temperature of coolant at burnout point

V   ft/sec   velocity

h_{DNB} BTU/hr-ft^2-°F   heat transfer coefficient at critical heat flux

P   psia   system pressure

q''_{DNB} BTU/hr-ft^2 critical heat flux

Range of validity:

Geometry: round tubes

500 psia $<$ P $<$ 3000 psia

4.5 ft/sec $< v_b <$ 54 ft/sec

$x_A < 0$ x_A = quality at test section outlet

0.5×10^6 BTU/hr-ft$^2 < \phi < 2.3 \cdot 10^6$ BTU/hr-ft^2

143" $< D_e <$ 0.66"

2) "Bettis" correlations [7]

Burnout equation

for round tubes $(0.2 \cdot 10^6 < G < 8.0 \cdot 10^6$ lb/hr-ft$^2)$

$$\frac{\phi_{B.O.}}{10^6} = C_1 \left(\frac{H_{B.O.}}{10^3}\right)^{-2.5} \left(1 + \frac{G}{10^7}\right)^2 \cdot e^{-0.0012 \, L/D} \quad (4)$$

original equation: C_1 = 0.28
design equation: C_1 = 0.182

for rectangular channels $(1.6 \cdot 10^6 < G < 5.0 \cdot 10^6$ lb/hr-ft$^2)$

$$\frac{\phi_{B.O.}}{10^6} = C_2 \left(\frac{H_{B.O.}}{10^3}\right)^{-2.5} \left(1 + \frac{G}{10^7}\right)^2 \cdot e^{-0.0012 \, L/S} \quad (5)$$

original equation: C_2 = 0.37
design equation: C_2 = 0.240

./.

for rectangular channels ($0.2 \cdot 10^6 \leqslant G \leqslant 1.6 \cdot 10^6$ lb/hr-ft^2)

$$\frac{\emptyset_{B.O.}}{10^6} = C_3 \left(\frac{H_{B.O.}}{10^3}\right)^{-2.5} \cdot e^{-0.0012 \, L/S} \qquad (6)$$

original equation: $C_3 = 0.50$
design equation: $C_3 = 0.325$

Notation:

D	ft		hydraulic diameter
G	lb/hr-ft^2		mass flow
H$_{B.O.}$	BTU/lb		enthalpy at burnout point
L	ft		heated channel length
$\emptyset_{B.O.}$	BTU/hr-ft^2		critical heat flux

Range of validity:

1850 psia $\leqslant$ P $\leqslant$ 2150 psia
500 BTU/lb $\leqslant$ H$_{B.O.}$ $\leqslant$ 1000 BTU/lb
21 $\leqslant$ L/D $\leqslant$ 365
59 $\leqslant$ L/S $\leqslant$ 468

3) **Correlation by Buchberg [1, 5]**

Burnout equation

$$\left(\frac{q}{A}\right)_{B.O.} = 520 \cdot G^{0.5} \left(T_{Sat} - T_{B.O.}\right)^{0.20} \qquad (7)$$

for $\left(T_{Sat} - T_{B.O.}\right) > 3 \, °F$

Notation:

G	lbm/ft^2-hr		mass flow
T$_{B.O.}$	°F		temperature of flowing medium at burnout point
T$_{Sat}$	°F		saturation temperature
$\left(\frac{q}{A}\right)_{B.O.}$	$\dfrac{BTU}{hr-ft^2}$		critical heat flux

./.

Range of validity:

250 psia $\leq$ P $\leq$ 2000 psia

$0.96 \cdot 10^6$ lbs/hf-ft^2 $\leq$ G $\leq$ $7.65 \cdot 10^6$ lbs/hr-ft^2

$0.92 \cdot 10^6$ BTU/hr-ft^2 $\leq$ $(\frac{q}{A})_{B.O.}$ $\leq$ $2.92 \cdot 10^6$ BTU/hr-ft^2

4) Correlation by Cicchitti [9, 10]

Burnout equation

$$q = 577 \cdot r \cdot K \cdot y \cdot \left(\frac{G}{135.6}\right)^{-n} \tag{8}$$

Definitions:

$$y = \frac{1 - x}{x + a} \tag{9}$$

$$a = v'/(v''-v') \tag{10}$$

$$K = K' \cdot (D/2.54)^{-1/4} \tag{11}$$

Notation:

D	cm		hydraulic diameter
G	g/cm^{2}s		mass flow
K'	-		pressure-dependent value
q	W/cm^2		critical heat flux
r	kcal/kg		heat of evaporation
v'	m^3/kg		specific volume of water in saturated state
v''	m^3/kg		specific volume of saturated steam
x	-		steam quality

./.

5) Correlation by "CISE" [11]

General burnout equation

$$\frac{\hat{W}_s}{r \cdot H_{gl}} = \frac{1 - \frac{P}{P_{cr}}}{(\frac{G}{100})^{1/3}} \cdot \frac{L_s}{L_s + 0.315 \cdot (\frac{P_{cr}}{P} - 1)^{0.4} \cdot D^{1.4} \cdot G} \qquad (12)$$

Burnout equation

for constant heat flux:

$$\frac{\hat{W}}{r \cdot H_{gl}} = (\frac{1 - \frac{P}{P_{cr}}}{(\frac{G}{100})^{1/3}} - x_{in}) \cdot \frac{L}{L + 0.315 (\frac{P_{cr}}{P} - 1)^{0.4} \cdot D^{1.4} \cdot G}$$

$$(13)$$

Notation:

D	cm	hydraulic diameter
G	g/cm²s	mass flow per unit area
H_{gl}	kcal/kg	heat of evaporation
L	cm	heated length
L_s	cm	heated length in quality range
$\hat{W}$	Watt	burnout heat flux for heated length
$\hat{W}_s$	Watt	burnout heat flux for heated length within quality range
P	kgf/cm²	system pressure
P_{cr}	kgf/cm²	critical pressure
r	g/sec	mass flow
x_{in}	-	quality at test section inlet

./.

Range of validity:

$45 \text{ kgf/cm}^2 \leqslant p \leqslant 150 \text{ kgf/cm}^2$

$100 (1 - P/P_{cr})^3 \text{ g/cm}^2\text{s} < G < 400 \text{ g/cm}^2\text{s}$

$x_{in} < 20\%$

$x_A > 0$ (quality at test section outlet)

$D > 0.7 \text{ cm}$

6) Correlation by Gambill [12]

Burnout equation

$$q"_{DNB} = (q"_{DNB})_{PB} + (q"_{DNB})_{FC} \tag{14}$$

Definitions for sub-cooled range:

$$(q"_{DNB})_{PB} = K \cdot H_{fg} \cdot \frac{P_g}{g} \cdot \left[\frac{\sigma \cdot g_c \cdot g\, (\rho_f - \rho_g)}{\rho_g^2} \right]^{1/4} \cdot \left[1 + \right.$$

$$\left. + (\frac{\rho_f}{\rho_g})^{0.923} (\frac{c_p}{25} \frac{\Delta T_{sc}}{H_{fg}}) \right] \tag{15}$$

$$K = 0.12 \to 0.17$$

c_p is referred to $0.5\, (T_{Sat} + T_{DNB})$

$$(q"_{DNB})_{FC} = h_{FC} (T_{w,DNB} - T_{DNB}) \tag{16}$$

$$T_{w,DNB} = \left[T_G + T_{Sat} - 0.25 \text{ V} \right] 1.8 + 32 \tag{17}$$

./.

Values for T_G:

$T_{Sat}/705.4$	T_G ($^{\circ}$C)
.524	.0
.55	14.5
.6	33.5
.7	54.0
.775	61.4
.8	60.8
.9	51.7
1.0	33.5

Notation:

H_{fg}	BTU/lb	heat of evaporation
K	-	constant
T_{DNB}	$^{\circ}$F	temperature of coolant at burnout location
T_G	$^{\circ}$F	temperature according to Bernath curve
T_{Sat}	$^{\circ}$F	saturation temperature
$T_{w,DNB}$	$^{\circ}$F	tube wall temperature at burnout location
ΔT_{sc}	$^{\circ}$F	sub-cooling at burnout location
V	ft/sec	velocity
c_p	BTU/lb-$^{\circ}$F	specific heat
g	ft/hr^2	gravitational acceleration
g_c	lb_m-ft/lb_f-hr^2	constant

./.

h_{FC}	$BTU/hr\text{-}ft^2 hr$	heat transfer coefficient for forced convection
q''_{DNB}	$BTU/hr\text{-}ft^2$	critical heat flux
$(q''_{DNB})_{FC}$	$BTU/hr\text{-}ft^2$	heat flux under forced convection
$(q''_{DNB})_{PB}$	$BTU/hr\text{-}ft^2$	heat flux under free convection
σ	lb_f/ft	surface tension
ρ_f	lb/ft^3	density of liquid
ρ_g	lb/ft^3	density of steam

7) Boundary curves by General Electric [13]

Burnout equations:

$$\varnothing_{B.O.}/10^6 = 0.705 + 0.237 \ (G/10^6) \qquad x < x_1 \qquad (18)$$

$$\varnothing_{B.O.}/10^6 = 1.634 - 0.270(G/10^6) - 4.710 \ x \qquad x_1 < x < x_2 \qquad (19)$$

$$\varnothing_{B.O.}/10^6 = 0.605 - 0.164(G/10^6) - 0.653 \ x \qquad x_2 < x \qquad (20)$$

Definitions:

$$x_1 = 0.197 - 0.108 \ (G/10^6) \qquad\qquad (21)$$

$$x_2 = 0.254 - 0.026 \ (G/10^6) \qquad\qquad (22)$$

Range of validity for equations 18, 19, 20:

P = 1000 psia

$0.4 \cdot 10^6 < G < 6.0 \cdot 10^6 \ lb/hr\text{-}ft^2$

$0 < x < -0.45$

$0.245 \ ins < D_H < 1.25 \ ins$

$29 \ ins < L < 108 \ ins$

./.

Extended equations for other pressure ranges:

$$(\emptyset_{B.O.})_P = (\emptyset_{B.O.})_{1000 \text{ psia}} + 440 (1000 - P) \qquad (23)$$

Extended equation for $x > x_1$ and $D_H < 0.6$ ins:

$$(\emptyset_{B.O.})_{D_H} = \emptyset_{B.O.} - d (D_{\overline{H}}^2 - 0.36) (x-a) \qquad (24)$$

$$\text{with} \quad d = 2.19 \cdot 10^6$$

Notation:

D_H	ins	hydraulic diameter
G	$lb/hr\text{-}ft^2$	mass flow
L	ins	heated tube length
P	psia	system pressure
x	-	steam quality
$\emptyset_{B.O.}$	$BTU/hr\text{-}ft^2$	critical heat flux

8) Correlation by von Glahn [14, 15]

V. Glahn calculated the critical heat flux from the so-called critical degree of evaporation x_c.

$$x_c = f_1 = \frac{Q}{M \cdot \Delta h} \qquad (25)$$

$$f_1 = f \frac{Re_D \cdot Pr_D^{0.4}}{(1.3 \cdot L/D \cdot P^{1.5}/P^{4.5})} \cdot (\frac{\eta^{"}}{\eta^{'}})^{1.7} \cdot (\frac{\Delta\rho}{\rho^{"}})^{0.4} \cdot N_B \qquad (26)$$

N_B is designated the boiling number and attained from the equation

$$N_B = (\eta^{"2} \cdot (g \cdot \Delta\rho)^{1/2})/(\rho^{"} \cdot \sigma^{1.5}) \qquad (27)$$

./.

The constant heat flux is given by:

$$x_c = f_1 = \frac{4 \cdot q \cdot L/D}{G \cdot \Delta h} \cdot F^{0.5} \qquad (28)$$

$F = 1$ for cylindrical channels

$F = 0$ for rectangular channels

$$F = \left[D_i/(D_a + D_i) \right] (D_i/D_a)^{0.4}$$ for annuli heated at the inner tube circumference D_i

$$F = (0.5)^{(D_i/D_a)^{0.4}}$$ for annuli heated at both sides

x_c is to be taken from the charts given. From this, the critical heat flux can be predicted in turn.

Notation:

D	m	hydraulic diameter
D_a	m	diameter of outer tube of annuli
D_i	m	diameter of inner tube of annuli
F	-	characteristic value for shape of test channel
G	kg/m²h	mass flow
L	m	heated length
M	kg/h	mass flow
Q	kcal/h	total power supplied
Pr_D	-	Prandtl number, referred to D
Re_D	-	Reynolds number, referred to D
$x_c = f_1$	-	critical degree of evaporation
g	m/s²	gravitational acceleration
q	kcal/m²h	critical heat flux
Δh	kcal/kg	enthalpy difference
σ	kp/m	surface tension

./.

η''	kg s/m^2	dynamic viscosity of saturated steam
η'	kg s/m^2	dynamic viscosity of water in saturated state
ρ''	kg/m^3	density of saturated steam
ρ'	kg/m^3	density of water in saturated state

$$\Delta\rho = \rho' - \rho''$$

9) Correlation by Griffith [16]

Burnout equation

$$\varnothing_{B.O.} = f\left[P/P_c\right] \cdot (F) \; \rho_g(H_g-H_b)\left[\frac{g(\rho_1 - \rho_g)}{/u_1}(\frac{k_1}{\rho_1 \cdot \bar{c}_1})^2\right]^{1/3} \quad (29)$$

Definition:

$$(F) = 1+10^{-6}(\frac{u_b \cdot D \cdot \rho_1}{/u_1})+0.014\left[\frac{\rho_1 \cdot \bar{c}_1 (T_s-T_b)}{\rho_g \cdot H_{fg}}\right] \quad (32)$$

$$+ 0.5\cdot10^{-3}\left\{(\frac{u_b \cdot D \rho_1}{/u_1})\left[\frac{\rho_1 \cdot \bar{c}_1(T_s-T_b)}{\rho_g \cdot H_{fg}}\right]\right\}^{1/2} \quad (31)$$

The function f (P/P_c) is given in the form of graphs same as various physical factors.

Values for f (P/P_c) according to Griffith:

P/P_c	$f(P/P_c)$
0.005	125
0.01	96
0.05	41
0.1	24
0.5	6.3
1.0	1.4

./.

Notation:

D	ft		hydraulic diameter
H_b	BTU/lb		mean enthalpy
H_{fg}	BTU/lb		heat of evaporation
H_g	BTU/lb		enthalpy of saturated steam
P	psia		system pressure
P_c	psia		critical pressure
T_b	^{o}F		mean temperature of coolant
T_s	^{o}F		saturation temperature
$\bar{c}_1$	BTU/lb-^{o}F		specific heat of liquid
g	32.2 ft/sec^2		gravitational acceleration
k_1	BTU-ft/ft^2-hr-^{o}F		heat conductivity of liquid
u_6	ft/sec		mean velocity of flowing medium
$\emptyset_{B.O.}$	BTU/hr-ft^2		critical heat flux
$/^{u}_1$	lb/ft-hr		viscosity of liquid
ρ_g	lb/ft^3		density of saturated steam
ρ_1	lb/ft^3		density of liquid

Range of validity:

$$0.0045 < \frac{P}{P_{cr}} < 0.97$$

$$0 \text{ ft/sec} < u_b < 110 \text{ ft/sec}$$

$$0 \ ^{o}F < T_1 < 280 \ ^{o}F \qquad \text{(sub-cooling)}$$

$$0.075 \cdot 10^6 \text{ BTU/hr-ft}^2 < \emptyset < 11.4 \cdot 10^6 \text{ BTU/hr-ft}^2$$

$$0 < x_A < 0.7 \qquad \text{(quality at test section outlet)}$$

./.

10) Correlation by Iwaschkewic [17]

Burnout equation

$$K_{Kr} = q_{Kr}/r^+ \ (g \cdot \gamma \ '')^{0.5} \ (\sigma \cdot \Delta\gamma)^{0.25} \tag{32}$$

$$K_{Kr} = 1.9 \cdot 10^{-5} \cdot Re \left[1 + 1.8 \cdot 10^{-6} \cdot v_q \left(\frac{K_3}{(1+K_2)^2} + K_4 \right) \cdot Re \right]^{-1} \tag{33}$$

Definitions:

$$K_2 = (h - h)/r \qquad \text{with } K_2 = 0 \quad \text{for } T = T' \tag{34}$$

$$K_3 = l_1 (\Delta\gamma/\sigma)^{1/2} \ \text{with } K_3 = 50 \ \text{for } K_3 \geqslant 50 \tag{35}$$

$$K_4 = L_s/d_h \qquad \text{with } K_4 = 125 \ \text{for } K_4 \geqslant 125 \tag{36}$$

$$Re = w(\sigma/\Delta\gamma)^{1/2}/\gamma' \qquad \text{for } D(\Delta\gamma/\sigma)^{1/2} \geqslant 1 \tag{37}$$

$$Re = w \cdot D/\gamma' \qquad \text{for } D(\Delta\gamma/\sigma)^{1/2} \leqslant 1 \tag{38}$$

$$r^+ = r(1 - x_A) \qquad \text{for } T = T'; \ x \geqslant 0 \tag{39}$$

$$r^+ = r \left\{ 1 + K_2 \cdot \left[1 + 0.065(\rho'/\rho'')^{0.8} \right] \right\} \text{for } T < T' \tag{40}$$

$$v_q = \bar{q}/q \ \text{with } q = \frac{1}{U} \int_u q \cdot dU \tag{41}$$

Definition of characteristic dimensional parameter D:

for tubes:	D = half tube radius
for rectangular channels with one-sided heating:	D = channel width
with both sides heated:	D = half channel width

./.

Notation:

K_{Kr}	-	characteristic value for critical heat flux
L_s	m	boiling length
d_h	m	hydraulic diameter
g	m/s^2	gravitational acceleration
h	kcal/kg	enthalpy of coolant
h'	kcal/kg	enthalpy of water in saturated state
l_1	m	length over which sub-cooled boiling prevails
q_{Kr}	kcal/s m^2	critical heat flux
r	kcal/kg	heat of evaporation
w	m/s	velocity
x_A	-	quality at test section outlet
σ	kp/m	surface tension
γ'	kp/m^3	specific gravity of water in saturated state
γ''	kp/m^3	specific gravity of saturated steam
$\Delta\gamma = \gamma' - \gamma''$		
ρ'	kg/m^3	density of water in saturated state
ρ''	kg/m^3	density of steam in saturated state

./.

Range of validity:

$0.02 \text{ cm} < d_h < 3.0 \text{ cm}$

$0 \, ^oC < \Delta T_2 < 160 \, ^oC$

$0 < x_A < 0.7$

$0.3 \text{ m/s} < w < 34 \text{ m/s}$

$3.5 \text{ cm} < L < 180 \text{ cm} \qquad L = \text{channel length}$

$2 \cdot 10^3 < Re < 3 \cdot 10^6$

$0 < K_2 < 0.8$

$15 < K_3 < 2000$

$0 < K_4 < 220$

$0.11 < K_5 < 48$

11) Correlation by Janssen, Levy and Kervinen [18]

Burnout equation for annuli heated at inner circumference:

$$0.3685 \cdot 10^{-6} \cdot q = \left[\frac{1 + 0.16 \cdot P^+ - 0.04 \cdot P^{+2}}{1 - 0.008 \cdot E \cdot g^{+0.8}} \right] \cdot$$

$$\cdot \left\{ 0.0172 \cdot E \cdot g^{+0.8} - \left[0.3175 \, g^{+-2} - 1.8534 \cdot g^{+-1} \right] \right.$$

$$- \left[2.4 + 3.2 \cdot D_h + 0.83 \cdot D_h \cdot g^+ \right] \cdot$$

$$\left. \cdot \left[x - 0.629 \cdot g^{+-2} + 0.3429 \cdot g^{+-1} - 0.2494 + 0.0020 \cdot g^{+2} \right] \right\}$$

$$\tag{42}$$

Definitions:

$$P^+ = \frac{1}{400} (1000 - 14.2 \cdot p) \tag{43}$$

$$g^+ = 0.2045 \cdot 10^{-6} \cdot q \tag{44}$$

$$E = \sqrt{\frac{D_2}{D_1}} \, (D_2 - D_1)^{-0.2} \tag{45}$$

./.

12) Correlation by Jens and Lottes [19]

Burnout equation

$$\frac{q_{B.O.}}{10^6} = C_1 \cdot (\frac{G/F}{10^6})^n \cdot (\vartheta_s - \vartheta_m)^{0.22} \tag{46}$$

Notation:

C_1, n	-	constant
G/F	lb/h-ft^2	mass flow
ϑ_m	°F	mean water temperature
ϑ_s	°F	saturation temperature
$q_{B.O.}$	BTU/h-ft^2	critical heat flux

The constant C_1 and the exponent n in the above equation were determined according to empirical values by the Purdue University and the University of California.

C_1 and n for equation (46)

Pressure psia	UCLA		Purdue	
	C_1	n	C_1	n
500	0.817	0.16		
1000	0.626	0.275	0.915	0.275
1500	0.445	0.50	0.545	0.500
2000			0.300	0.725

./.

Range of validity:

	UCLA	Purdue
P (psia)	500, 1000, 2000	1000, 2000, 3000
G/F (lb/hr-ft^2)	$0.96 \cdot 10^6 < G/F < 7.79 \cdot 10^6$	$0.9 \cdot 10^6 < G/F < 7.48 \cdot 10^6$
q (BTU/hr-ft^2)	$0.94 \cdot 10^6 < q < 3.76 \cdot 10^6$	$1.08 \cdot 10^6 < q < 4.21 \cdot 10^6$
L/D (-)	109	$22 < L/D < 168$
$(\vartheta_s - \vartheta_m)$ (°F)	$1 < (\vartheta_s - \vartheta_m) < 163$	$1 < (\vartheta_s - \vartheta_m) < 149$

13) Correlation by Konkow and Modnikowa [20]

For a quality range of a two-phase flow in vertical channels their equation defines at what quality the water film in the boundary layer disappears and consequently the poorer heat transfer to steam commences.

Burnout equation

$$x = \left[q \cdot (\sigma / \Delta\gamma)^{1/2} / (r \cdot \gamma'' \cdot \gamma') \right]^{-0.125} \cdot (\eta'/\eta'')^{-0.2} \cdot Pr_F^{-0.5}$$
$$\cdot \left[D / (\sigma / \Delta\gamma)^{1/2} \right]^{+0.2} \cdot \left[0.35 + 500 / (Re_F \cdot v'/v'' + 350) \right]$$

$$(47)$$

Notation:
D	m	tube diameter
Pr_F	-	Prandtl number for film flow
Re_F	-	Reynolds number for film flow

./.

q	kcal/m^{2}h	heat flux
r	kcal/kg	heat of evaporation
v", v'	m^3/kg	specific volume in saturated state
x	-	quality
σ	kp/m	surface tension
γ",γ'	kp/m^3	specific gravities in saturated state
$\Delta\gamma = \gamma' - \gamma$"		
γ'	m^2/sec	kinematic viscosity of liquid phase in saturated state
η", η'	kp s/cm^2	dynamic viscosities in saturated state

Range of validity:

$$20 \text{ kgf/cm}^2 < p < 200 \text{ kgf/cm}^2$$

$$10 \text{ g/cm}^2\text{s} < G < 1320 \text{ g/cm}^2\text{s}$$

$$8 \cdot 10^3 \text{ kcal/m}^2\text{h} < q < 3.34 \cdot 10^6 \text{ kcal/m}^2\text{h}$$

$$0.004 \text{ m} < D < 0.0322 \text{ m}$$

14) Correlation by Labuntsow [21]

Burnout equation

$$q = 1.25 \cdot 10^6 \cdot f(p) \left\{ 1 + \left[2.5/f(p) \right] \cdot w^2 \right\}^{1/4} \cdot f(\Delta T) \quad (48)$$

./.

Definition:

$$f(p) = p^{1/3} (1 - p/p_{Kr})^{4/3} \tag{49}$$

$$f(\Delta T) = 1 + (15/p) \cdot c_p \cdot \Delta T \tag{50}$$

Notation:

p	$kgf/cm^2 a$	system pressure
p_{Kr}	$kgf/cm^2 a$	critical pressure
w	m/s	velocity .
ΔT	$^\circ C$	sub-cooling

The equation (44) applies only to sub-cooled flow.

15) Correlation by Macbeth [22]

Burnout equation for round tubes:

$$\emptyset_o \cdot 10^{-6} = \emptyset_E \cdot 10^{-6} - 0.0605 \ (S/L)^{0.7} \cdot (G \cdot 10^{-6})^{0.75} \cdot \Delta h_i \tag{51}$$

Notation:

G	$lb/hr \ ft^2$	mass flow
L	ft	heated length
S	ft	hydraulic diameter
Δh_i	BTU/lb	sub-cooling
$\emptyset_o$	$BTU/hr \ ft^2$	critical heat flux for $x_E = 0$
$\emptyset_E$	$BTU/hr \ ft^2$	observed critical heat flux

.../.

16) Correlation by Menegus [23]

Burnout equation

$$q = \frac{\cdot(1 + \beta_o \cdot \Delta T_2 + \dfrac{\beta_1 \cdot \Delta T_2}{D})(1 + \gamma_o \cdot V + \dfrac{\gamma_1 \cdot V}{D})}{1 + \dfrac{\delta_1}{D}} \cdot \alpha \qquad (52)$$

Definitions:

$$\alpha = (\frac{3200 - P}{3200})(\frac{0.2036 \cdot P}{P + 19.63}) - 0.04126 + 0.08341 - \frac{(P - 1650)^2}{5814} \qquad (53)$$

$$\beta_o = (\frac{P + 811}{P + 38.40})(\frac{4.48}{3200 - P}) + 1.814 \cdot 10^{-6}(\frac{P}{100})(\frac{3200 - P}{3200}) \qquad (54)$$

$$\beta_1 = \left[1.234 \cdot 10^{-4} + 1.098 \cdot 10^{-5}(\frac{P}{100})\right](\frac{3200 - P}{3200}) \qquad (55)$$

$$\gamma_o = (\frac{0.01004 \cdot P}{P + 118.54} + 1.080 \cdot 10^{-5})(\frac{3200 - P}{3200}) + 1.814 \cdot 10^{-6}(\frac{P}{100}) \qquad (56)$$

$$\gamma_1 = 1.176 \cdot 10^{-6}(\frac{P}{100}) + 2.016 \cdot 10^{-4} + 2.576 \cdot 10^{-4}(\frac{100}{P}) \qquad (57)$$

$$\delta_1 = 3.888 \cdot 10^{7}(\frac{P}{100}) + 1.037 \cdot 10^{-6} + 1.8816 \cdot 10^{-3}(\frac{100}{P}) \qquad (58)$$

Notation:	D	ft	hydraulic diameter
	P	psia	system pressure
	V	ft/s	mean velocity of coolant
	ΔT_2	°C	sub-cooling

./.

Range of validity:

$1 \ kgf/cm^2 < p < 164 \ kgf/cm^2$

$0 \ m/s < V < 16 \ m/s$

$0 \ ^\circ C < \Delta T_2 < 146 \ ^\circ C$

$0.368 \ cm < D < 54 \ cm$

17) Correlation by Reynolds [7]

Burnout equation

$$\left(\frac{\delta}{r}\right)^{1.94} = 1.49 \cdot 10^{-23} \left(\frac{\emptyset \cdot D}{\sigma \cdot u_b}\right) \left(\frac{\rho_b}{\rho_f}\right) \left(\frac{G \cdot D}{\mu_f}\right)^{1.5} \left(\frac{H_{fg} \cdot g_c}{g \cdot D}\right) \qquad (59)$$

Notation:

$\dfrac{\delta}{r}$	–	relative boundary layer thickness
D	ft	hydraulic diameter
G	$lb/hr\text{-}ft^2$	mass flow
H_{fg}	BTU/lb	heat of evaporation
g	ft/sec^2	gravitational acceleration
g_c	$ft\text{-}lb_m/lb_f\text{-}sec^2$	constant
u_b	ft/sec	mean flow velocity
$\emptyset$	$BTU/hr\text{-}ft^2$	heat flux
σ	lb/ft	surface tension
ρ_b	lb/ft^3	mean density of liquid
ρ_f	lb/ft^3	density of liquid in saturated state
μ_f	lb/ft-hr	viscosity of liquid in saturated state

./.

Range of Validity:

0.18 ins $< D < 0.306$ ins

$50 < L/D < 80$

500 psia $< p < 2000$ psia

$0.66 \cdot 10^6$ lb/hr-ft$^2 < G < 3.6 \cdot 10^6$lb/hr-ft^2

$0.01 < x_A < 0.67$

$0 \, ^\circ F < \Delta T_1 < 313 \, ^\circ F$ (inlet sub-cooling)

$0.6 \cdot 10^6$ BTU/hr-ft$^2 < \emptyset < 2.8 \cdot 10^6$ BTU/hr-ft^2

18) Correlation by Smolin, Poliakov, Yesikov [24]

Burnout equations

$$q = 10^4 \, (1 - Rg)^{1.11} \cdot G^{0.7} \tag{60}$$

$$\text{for } K_{lim} \leqslant 0.345 \cdot 10^{-3} \, m^2 s/kg$$

$$q = 9.1 \cdot 10^8 \, (1 - x)^{3.2} \cdot G^{-0.8} \tag{61}$$

$$\text{for } K_{lim} \geqslant 0.345 \cdot 10^{-3} \, m^2 s/kg$$

Definition:

$$K_{lim} = \frac{1 - x}{G}$$

Notation:

G	kg/m^{2}s	mass flow
Rg	-	dimensionless volumetric steam quality
q	kcal/m^{2}h	critical heat flux
x	-	quality

./.

Range of validity:

$$p = 150 \text{ kgf/cm}^2$$

$$D = 0.8 \text{ cm}$$

$$0 < x < 0.5$$

19) <u>Correlation by Tippets [25]</u>

<u>Burnout equation</u>

$$q_c = c'' \; \phi^m/_\xi \qquad\qquad (62)$$

Definitions:

$$\phi = \frac{\sigma \cdot \rho_L \; (1 + \rho_L/\rho_g)}{\emptyset_{TPF} \cdot f_F \cdot G^2 \cdot b(1+\sqrt{\rho_L/\rho_g})^2} \qquad\qquad (63)$$

$$\xi = \frac{1 + (1+c' \frac{x_c}{1-x_c})\frac{\rho_L}{\rho_g}}{(\frac{\rho_L}{\rho_g} \cdot \emptyset_{TPF} \cdot f_F)^{1/2} \cdot G \cdot h_{fg}} \qquad\qquad (64)$$

$$c'' = K' \; (2K_3 K_4)^m/\sqrt{2} \qquad\qquad (65)$$

$$c' = K_5 \overline{U}_L/\overline{U}_g \qquad\qquad (66)$$

Notation:

c', c''	–	empirically determined constants
b	ft	hydraulic radius (e.g. tube radius)

./.

f_F	-	friction coefficient acc. to Fanning
G	lb_m/ft^2sec	mass flow
h_{fg}	BTU/lb_m	heat of evaporation
K^f, K_3, K_4, K_5	-	constants
m	-	empirically determined constant
q_c	$BTU/sec\text{-}ft^2$	critical heat flux
$\bar{U}_L$	ft/sec	mean velocity of liquid over free flow area
$\bar{U}_g$	ft/sec	mean velocity of steam over free flow area
x_c	-	steam quality at critical heat flux level
ρ_L	lb_m/ft^3	density of liquid
ρ_g	lb_m/ft^3	density of steam
$\emptyset_{TPF}$	-	multiplication factor for two-phase pressure drop

20) Correlation by Tong. Currin and Engel [26, 27]

Burnout equation for sub-cooled range:

$$q^{"}_{DNB} = (0.23 \cdot 10^6 + 0.094 \cdot G) \cdot (3.0 + 0.01 \cdot \Delta T_{sc})$$

$$\cdot (0.435 + 1.23 \cdot e^{-0.0093\ L/D_e}) \cdot (1.7 - 1.4 \cdot e^{-a}) \qquad (67)$$

Definition:

$$a = 0.532 \left[(H_f - H_{in})/H_{fg} \right]^{3/4} (\rho_g/\rho_f)^{-1/3} \qquad (68)$$

./.

Range of validity:

$0.2 \cdot 10^6$ lb/hr-ft^2 $< G < 8.0 \cdot 10^6$ lb/hr-ft^2

800 psia $< p < 2750$ psia

$21 < L/D_e < 365$

$H_{in} \gtrsim 300$ BTU/lb

$0 \, ^\circ F < \Delta T_{sc} < 228 \, ^\circ F$

$0.4 \cdot 10^6$ BTU/hr-ft$^2 < q < 4.0 \cdot 10^6$ BTU/hr-ft^2

0.1 in $< D_e < 0.54$ in

Burnout equation for quality range:

$$\Delta H_{DNB} = 0.529 \, (H_f - H_{in}) + (0.825 + 2.36 \, e^{-17 \, D_e}) \cdot H_{fg} e^{-1.5G/10^6}$$

$$- 0.41 \, H_{fg} \, e^{-0.0048 \, L/D_e} - 1.12 \, H_{fg} \, \rho_g / \rho_f$$

$$+ 0.548 \cdot H_{fg} \tag{69}$$

Range of validity:

$0.4 \cdot 10^6$ lb/hr-ft^2 $< G < 2.5 \cdot 10^6$ lb/hr-ft^2

800 psia $< p < 2750$ psia

$9 \; " < L \lesssim 76 \; "$

$H_{in} \gtrsim 400$ BTU/lb

$0.1 \cdot 10^6$ BTU/hr-ft$^2 < q < 1.8 \cdot 10^6$ BTU/hr-ft^2

$0 < x_{exit} < 0.9$

0.1 in $< D_e < 0.54$ in

./.

Notation:

D_e	in	hydraulic diameter
G	$lb/hr\text{-}ft^2$	mass flow
H_f	BTU/lb	enthalpy of liquid in saturated state
H_{fg}	BTU/lb	heat of evaporation
H_{in}	BTU/lb	enthalpy at test section inlet
L	in	heated length
ΔT_{sc}	^oF	sub-cooling at burnout point
$q^{"}_{DNB}$	$BTU/hr\text{-}ft^2$	critical heat flux
x_{exit}	-	outlet quality
ρ_g	lb/ft^3	density of steam
ρ_f	lb/ft^3	density of water

2.1) Correlation of Weatherhead [28]

The correlations given by Weatherhead apply only to the sub-cooled boiling range.

Burnout equations for $p \geqslant 500$ psia, $G \geqslant 0.9 \cdot 10^6 lb/hr\text{-}ft^2$

$$D_h \geqslant 0.125"$$

for all ranges of sub-cooling:

$$\frac{q^{"}_{DNB}}{10^6} = \frac{2}{3} \cdot D_h^{-1/2} (\frac{H_{fg}}{10^3}) (\frac{G}{10^6})^m (1+ \tanh \frac{H_f - H_{DNB}}{100}) \qquad (70)$$

$$m = 0.175 \cdot 10^{-3} \frac{H_{fg}}{v_{fg}}$$

./.

for $(H_f-H_{DNB}) > 50$ BTU/lb:

$$\frac{q''_{DNB}}{10^6} = \frac{2}{3} D_h^{-1/2} (\frac{H_{fg}}{10^3}) (1+\frac{G}{10^6})^{1/2} (1+\tanh \frac{H_f-H_{DNB}}{100}) \qquad (71)$$

for $p < 500$ psia or $D_h < 0.125$:

$$\frac{q''_{DNB}}{10^6} = 1.75 \cdot D_h^{-1/2} (\frac{H_{fg}}{10^3}) (1+ \frac{G}{10^6})^{1/2} (\frac{H_f-H_{DNB}}{100}) \qquad (72)$$

for $G < 0.9 \cdot 10^6$ lb/hr ft^2

$$\frac{q''_{DNB}}{10^6} = \frac{H_{fg}}{1000} (1.75 + \frac{2}{3} \frac{H_f-H_{DNB}}{100}) \qquad (73)$$

Notation:

D_h	in	hydraulic diameter
G	lb/hr-ft^2	mass flow
H_{DNB}	BTU/lb	enthalpy at burnout point
H_f	BTU/lb	enthalpy of liquid in saturated state
H_{fg}	BTU/lb	heat of evaporation
q''_{DNB}	BTU/hr-ft^2	critical heat flux
v_{fg}	ft^3/lb	difference between specific volume of water and specific volume of steam in saturated state

./.

22) Correlation by Wilson and Ferrel [29]

Burnout equations

$$q = C_1 \cdot f(p) \left[C_2 \cdot G(S/L)^n \right]^a \tag{74}$$

Definitions:

$$a = A_1 + A_2 + \Delta T_1 + A_3 \cdot \Delta T_1^2 \tag{75}$$

$$f(p) = 1.83 - 59 \cdot 10^{-3} \cdot p \tag{76}$$

Constants	Rectangular Channel	Tube
C_1	47.4	27.4
C_2	$2.273 \cdot 10^{-3}$	$0.853 \cdot 10^{-3}$
A_1	0.44	0.3987
A_2	$7.3 \cdot 10^{-4}$	$10.36 \cdot 10^{-4}$
A_3	0	$-1.027 \cdot 10^{-6}$

Notation:

G	lb/hr-ft^2	mass flow
L	ft	heated channel length
S	ft	hydraulic diameter (width for rectangular channels, inside dia. for tubes)
ΔT_1	°C	sub-cooling
p	kgf/cm^2	system pressure
q	BTU/hr-ft^2	critical heat flux

./.

23) Correlation by Zenkewic [30]

Burnout equation

$$\frac{q_{DNB}''}{10^6} = H_{fg} \sqrt{\frac{\sigma \cdot \rho_f \cdot G \cdot g_c}{\mu}} \cdot \left(\frac{\rho_g}{\rho_1}\right)^{0.65} \left[95 + 420 \, (-x) \right]$$

$$\cdot \left[1.0 + \frac{320\,000}{\left(\frac{G}{\mu} \sqrt{\frac{\sigma}{\rho_f - \rho_g}}\right)^{1.1+2.6\, \rho_g/\rho_1 + 0.9(-x)}} \right] 0.0036 \qquad (77)$$

Notation:

G	lb/hr-ft^2	mass flow
H_{fg}	BTU/lb	heat of evaporation
g_c	lb$_m$-ft/lb$_f$-hr^2	constant
q_{DNB}''	BTU/hr-ft^2	critical heat flux
x	-	steam quality
σ	lb$_f$/ft	surface tension
ρ_f	lb/ft^3	density of liquid in saturated state
ρ_g	lb/ft^3	density of saturated steam
1	lb/ft^3	density of sub-cooled liquid
μ	lb/hr-ft	viscosity

Range of validity:

1400 psia $<$ p $<$ 3000 psia

$0.3 \cdot 10^6$ lb/hr-ft$^2 <$ G $< 5.2 \cdot 10^6$ lb/hr-ft^2

$0.157" <$ D$_e$ $< 0.473"$

$7.3" <$ L $< 63"$

$3.6 \, ^oF <$ (T$_{Sat}$-T$_{DNB}$) $< 180 \, ^oF$

./.

APPENDIX II

Prediction of Cooling-Down in the Wall of the
Test Channel after Cutting-Off the Heat Supply

1. Problem Outline

From the characteristic traces of the temperature and mass
flow in pulsating burnout shown in Fig. 62 is to be seen
that, on interrupting the heat supply after occurrence of
burnout, the temperature of the tube wall decreases very
slowly initially, and only 0.1 to 0.2 seconds after shut-down
does the expected cooling-down process begin to follow an
exponential curve. The temperature variation referred to is
shown schematically in Fig.101. At point A the transition
takes place from nucleate to film boiling, at point B the
electric heating power is shut off, then there is gradual
cooling-down from B to C, until eventually the anticipated
cooling-down process starts at C.

With a view to proving that the section B-C, i.e. the range
of slow temperature decrease, is only due to the steam
cushion existing in the test channel and the associated low
heat transfer, the calculations described in the following
were made, starting from two different assumptions.

In Case 1, it was assumed that the heat transfer coefficient
after shutting off the heating power will instantly assume a
value which corresponds to that with water cooling. For the
Case 2, a low heat transfer coefficient corresponding to
cooling by steam was assumed in the range B-C which then,
at Point C, suddenly increases to the heat transfer coefficient
of Case 1.

In detail, the following values were taken as a basis in
the calculation.

Assumption for Case 1:

Heat transfer coefficient:	α =	5000 kcal/m^2h degree
Wall thickness of channel:	s =	0.5 mm
Heat conductivity of channel:	λ =	14.5 kcal/mh degree
Specific heat of channel:	c =	0.12 kcal/kg degree
Density of channel:	ρ =	7800 kg/m^3

Modified assumption for Case 2:

Heat transfer coefficient:

Range B-C:	α =	1000 kcal/m^2h degree
Range C-D:	α =	5000 kcal/m^2h degree

s, λ, c and ρ correspond to the conditions in Case 1.

For the range B-C, a time period of t = 0.2 second was determined on the basis of the temperature/time trace (Fig. 62).

2. Calculation Procedure

To simplify the calculation be it assumed that the tube wall is a flat plate, completely insulated at one side. Be it, furthermore, assumed that there is no heat conduction in the longitudinal direction of the channel.

The heat conduction in the plane plate is defined by the formula

$$\frac{\delta\vartheta}{\delta t} = a \frac{\delta^2\vartheta}{\delta x^2}$$

Furthermore, the surface of the tube at the cooled side is governed by the condition

$$\lambda \frac{\delta\vartheta}{\delta x} = \alpha(\vartheta_o - \vartheta_F)$$

./.

The symbols in these expressions have the following
meaning:

ϑ = temperature

t = time

x = coordinate in the direction of the tube wall thickness

a = λ / c · γ the temperature conductivity

λ = the heat transfer coefficient

c = the specific heat

γ = specific gravity

For the Case 1, the method indicated by U. Grigull [72] for
the prediction of the temperature equalization in simple
bodies by means of the abbreviated Fourier analysis was
used. In Case 2, the same method was applied up to Point C,
and from Point C onwards the „ Differenzenverfahren " by
E. Schmidt [73] was used.

3. Results

The results of the calculation are shown in Fig.102. It is
found that in the assumed Case 1, i.e. with constant α,
the curve of the temperature variation follows steadily an
exponential function. In Case 2, however, with a sudden
change of the α-coefficient at Point C, the result of the
calculation agrees very well with the temperature variation
measured in the test (Fig. 62), in other words, at the
beginning of the cooling-down process, there is a very slow
decrease of the temperature due to the low heat transfer
coefficient of the steam and, from Point C onwards, intensive
cooling starts by the following water.

./.

Literature

1   H. Buchberg et al.
        Final Report Coo-24, March 1951, USAEC
        Department of Engineering, Los Angeles, Calif.

2   D. Henkel
        Technical Detail Report No. 1 of Euratom Research
        Contract No. 057-61-RDD between Euratom and M.A.N.
        M.A.N. Report No. 09.32.01, November 1963

3   VDI-Durchflussmessregeln DIN 1952
        6th Edition November 1948

4   G.P. Nassos
        Argonne National Lab. ANL 6738

5   Grigull, Gröber Erk
        Die Grundgesetze der Wärmeübertragung, 2. Edition
        Springer-Verlag 1961, Page 116 et. seg.

6   L. Bernath
        Chem. Eng. Progr. Symp. Ser. 56, No. 30, 1960

7   R.A. DeBortoli, S.J. Green, B.W. LeTourneau, M. Troy
        A. Weiss
        Report WAPD-188, October 1958
        Westinghouse Elctr. Corp., Bettis Plant, Pittsburgh,
        Pa., U.S.A.

8   H. Buchberg et al.
        Reprint of Heat Transfer and Fluid Mech. Inst.,
        Stanford University Press Calif., U.S.A., 1951,
        Pages 177-191

9   A. Cicchitti et al.
        Energia Nucleare, Vol. 6, No. 10, October 1959

10   A. Cicchitti et al.
        Energia Nucleare, Vol. 7, No. 6, June 1960

11   S. Bertoletti, G.P. Gaspari, C. Lombardi, G. Peterlongo,
        F.A. Tacconi
        Report: R-99, September 1964
        Cise, Segrate, Milan, Italy

12   W.R. Gambill
        Chem. Eng. Progr. Symp. Ser. 41, Vol. 51, 1963

13   E.J. Janssen, S. Levy
        Report: APED-3892, April 1962
        General Electric, San José, Calif., U.S.A.

14   U.H. von Glahn
        Techn. Not. D-1285, September 1962
        NASA-Lewis Res. Centre, Cleveland, Ohio, U.S.A.

15   U.H. von Glahn
        Techn. Note D.-1656, June 1963
        NASA-Lewis Res. Centre, Cleveland, Ohio, U.S.A.

16   P. Griffith
        ASME-Paper No. 57-HT-21, ASME-AICHE Heat Transfer Conf.
        University Park, Pa., U.S.A., August 1957

17   A.A. Iwaschkewic
        Teploenergetika, Vol. 8, No. 10, October 1961

18   E.J. Janssen, S. Levy, Kervinen
        Paper No. 63-WA-149 November 1963
        Winter Annual Meeting ASME, Philadelphia, U.S.A.

19   W.H. Lens, P.A. Lottes
        Report ANL-4627, May 1951
        Argonne Nat. Lab. Argonne III., U.S.A.

20   A.S. Konkow, V.V. Modnikowa
        Teploenergetika, Vol. 8, 1962

21   D.A. Labuntsow
        Atomnaja Energia, Vol. 10, 1961, Page 523 (Ref. in ANL-
        6734, June 1963, Argonne Nat. Lab., Argonne, Ill.,
        U.S.A., English translation in the Soviet Journal of
        Atomic Energy, Vol. 10, Page 510 (1962)

22   R.V. Macbeth
        Report: AEEW-R167, Burnout Analysis Part 2: The Basic
        Burnout Curve
        UKAEA-Reactor Group, January 1963

23   R.L. Menegus
        Report: DP-363, March 1959
        Dupont de Nemours, Wilmington, Delaware, U.S.A.

24   V.N. Smolin, V.K. Poliakow, V.I. Yesikov
        Atomnaja Energia, Vol. 13, No. 4, Pages 360/4, 1962

25   F.E. Tippets
        Trans. ASME, Ser.C., Vol. 86, No. 1, February 1964

26   L.S. Tong. et al.
        Nucleonics, Vol. 21, No. 5, Mai 1963

27   L.S. Tong, H.B. Currin, F.C. Engel
        Report: WCAP-3736, Vol. I and II, August 1964
        Westinghouse Electric, Corp. APD, Pittsburgh, Pa. U.S.A.

28   R.J. Weatherhead,
        Report: ANL-6675, March 1963
        Argonne National Lab., Argonne, Ill., U.S.A.

29   R.H. Wilson, J.K. Ferrel
        Report: BAW - 168, June 1961
        Babcock and Wilcox, AED, Lynchburg, Virg., U.S.A.

./.

30   B.A. Zenkewic
Atomnaja Energia 4, 1, 1958 (Russian)
Kernenergie, 2. Edition, Vol. 2, 1959 (German)

31   E. Janssen, J.A. Kervinen
GEAP 3899, February 1963

32   E. Polimik, E.P. Quinn
GEAP 3940, September 1962

33   R.V. Macbeth
AEEW R 358, June 1964

34   E.D. Waters, G.M. Hesson, D.E. Fitzsimmons, J.M. Batch
HW-77303, August 1963

35   J.M. Batch, G.M. Hesson
HW-80391, REV I, January 1964

36   B. Matzner, J.S. Neil
DP 857, September 1963

37   G.M. Hesson, D.E. Fitzsimmons, J.M. Batch
HW - 80523 REV I, March 1964

38   B. Alvensleben, C. Casper, K.H. Lochmann
AEG-Report E.A.E.S. Studsvik Symposium (Sweden)
October 1963

39   S.J. Green, G.W. Maurer, A. Weiss
ASME Paper 62-HT-43, August 1962

40   A.W. Bennett, J.G. Collier, P.M.C. Lacey
AERE R 3804, August 1961

41   S. Bertoletti, G.P. Gaspari, C. Lombardi, G. Peterlongo
M. Silvestri, F.A. Tacconi
Energia Nucleare, Vol. 12, No. 3, March 1965

42   L. Cravarolo et al.
Report: R-93, September 1964
Cise, Segrate, Milan, Italy

43   Snecma, ECOULE Ments Giratoires Dans L'eau Bouillante
(Rapport final) Rapport Euratom 26

44   D.H. Lee, J.D. Obertelli
AEEW R-213, August 1963

45   E.A. Kozakova
Eng. Digst. 12(1951)
Translation by: Izvest. Akad. Nauk SSSR
Otdel. Techn. Nauk (1950) No. 9

46   M.T. Cichelli, C.F. Bonilla
Trans. Amer. Inst. Chem. Eng. 41 (1945)

47   A.E. Bergles, W.M. Rohsenow
        Report No. 8767-21
        Mass. Inst. of Techn.

48   S. Bertoletti, G.P. Gaspari, C. Lombardi, G. Soldaini
        R. Zavattarelli
        Cise Report R-90, June 1964
        Cise, Segrate, Milan, Italy

49   J.M. Reynolds
        Technical Report n.10. Heat Transfer Laboratory
        Mechanical Engineering Department. MIT, July 1957

50   R.V. Macbeth
        AEEW-R 222, April 1963

51   H. Firstenberg, K. Goldmann, L.Lo Bianco, S. Preiser,
        G. Rabiowitz
        NDA 2131-16, June 1960

52   V.E. Doroshtschuk, F.P. Frid (V.T.I.)
        Teploenergetika, September 1959

53   M.A. Styrikovitch, L.E. Faktorovitch
        Teploenergetika, February 1959

54   Z.L. Miropolskii, M.E. Shitsman, I.L. Mostinskii
        A.A. Stavrovskii
        Teploenergetika, May 1960

55   V.N. Smolin, V.K. Poliakov, V.I. Yesikov
        Atomnaya Energija, May 1964

56   O. Baker
        Simultaneous Flow of an Oil and a Gas
        Oil and Gas Journal 53 (12)

57   J.G. Collier
        Nuclear Power, June 1961

58   Hewitt
        Two-Phase Flow Symposium, Grenoble, May 1965

59   Peter Griffith, John S. Maulpetsch
        A Study of System-Induced Instabilities in Forced-
        Convection Flow with Sub-cooled Boiling
        April 15, 1965
        Department of Mechanical Engineering
        Massachussetts Institute of Technology
        Report No. 5382-35

./.

60   Warren H. Lowdermilk, Chester D. Lansu and Byron
      L. Siegel
      Investigation of Boiling Burnout and Flow Stability
      for Water in Tubes
      September 1958
      NACA-TN-4382

61   Aladiev, Miropolski, Doroshtchuk, Styrikovitch
      Boiling Crisis in Tubes
      International Heat Transfer Conference
      Boulder (Colorado) August 1961

62   K.M. Becker, S. Jahnberg, I. Hagea, P.T. Hannsson
      and R.P. Mathisen
      Hydrodynamic Instability and Dynamic Burnout in Natural
      Circulation Two-Phase Flow
      AE-156
      September 1964

63   A.E. Bergles et al.
      Investigation of Boiling Flow Regimes and Critical
      Heat Flux
      March 1, 1965
      Dynatech. Report No. 517
      NYO-3304-3

64   R.J. Weatherhead
      Heat Transfer, Flow Instability and Critical
      Heat Flux for Water in a Small Tube at 200 psia
      September 1963
      ANL-6715

65   S. William Gouse, Jr. Carl D. Andrysiak
      Flow Oscillations in a Closed Loop
      with Transparent, Parallel, Vertical Heated Channels
      June 1963
      Department of Mechanical Engineering
      Massachussetts Institute of Technology
      Report No. 8973-2

66   Frank A. Jeglic and Thomas M. Grace
      Onset of Flow Oscillations in Forced-Flow
      Sub-cooled Boiling
      May 1965
      Lewis Research Center
      Cleveland, Ohio
      Nasa TND-2821

./.

- 134 -

67   J. Bourè
Instabilities Hydrodynamiques Limitant la
Puissanee des Reakteurs AEAU
Bouillante
Centre d'Etudes Nucleaires de'Grenoble
Rapport T.T. No. 55

68   J.E. Cesterline, D.M. Lee
Flow Instability and Critical Heat Flux
in Heated Parallel Channels
October 27, 1964
TID-21403

69   A.H. Stenning and T.N. Veziroglu
Instabilities in the Flow of Boiling Liquid
February 1965
University of Miami
Nasa CR-164

70   Transition Boiling Heat Transfer Program
Atomic Power Equipment Department
General Electric, San Jose, California
Contract AT (04-3)-189
U.S. Atomic Energy Commission

71   Yang, W.J. and Clark, J.A.
On the Application of the Source Theorie
to the Solution of Problems
Involving Phase Change
J. Heat Transf. (ASME-Trans.)
Ser. C., Vol. 86, No. 2, May 1964, P. 207

72   U. Grigull
Temperaturausgleich in einfachen Körpern
Springer-Verlag 1964

73   E. Schmidt
Einführung in die Thermodynamik
8. Edition, Springer-Verlag, 1960
Page 353 ff.

74   G.C. Clerici, S. Garriba, R. Sala, A. Tozzi
A Catalogue of the Commonest Burnout Correlations
forForced Convection in the Quality Region
Endbericht zum Euratom-Vertrag 073-65-11
TEEI von ARS

1 Test section	7 Electric heater
2 Steam separator	8 Pressurizer
3 Cooler	9 Power supply
4 Condenser	10 Cooler
5 Cooler	11 Regenerative heat exchangers
6 Pump	12 Mixed-bed filters
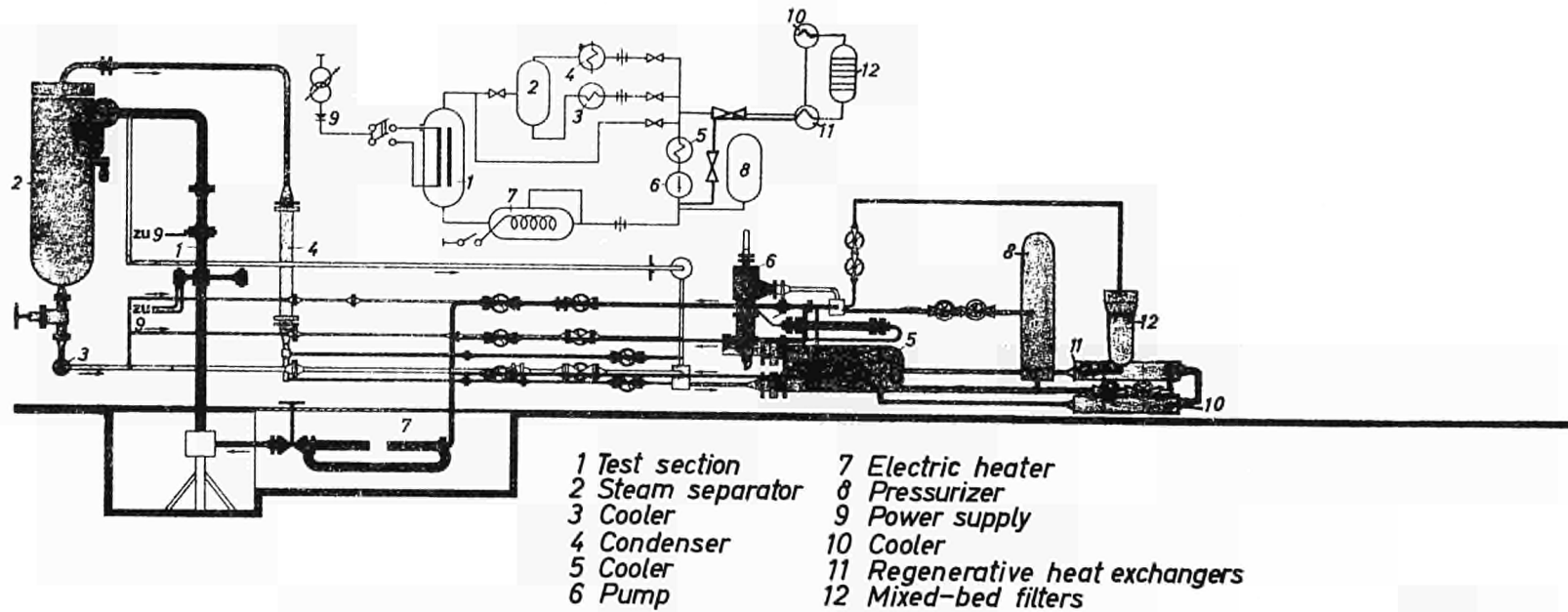
Schematic arrangement of test loop

Fig. 1

Test section

minus pole

2

test channel

pressure tube

1

plus pole

3

4

cooler

reducing valve

nitrogen reservoir

balance

h.p. hose

diaphragm

pressure equalizer

n.p. hose

Fig. 2

thermocouple leads

Araldit cast-resin cone

M 1:1
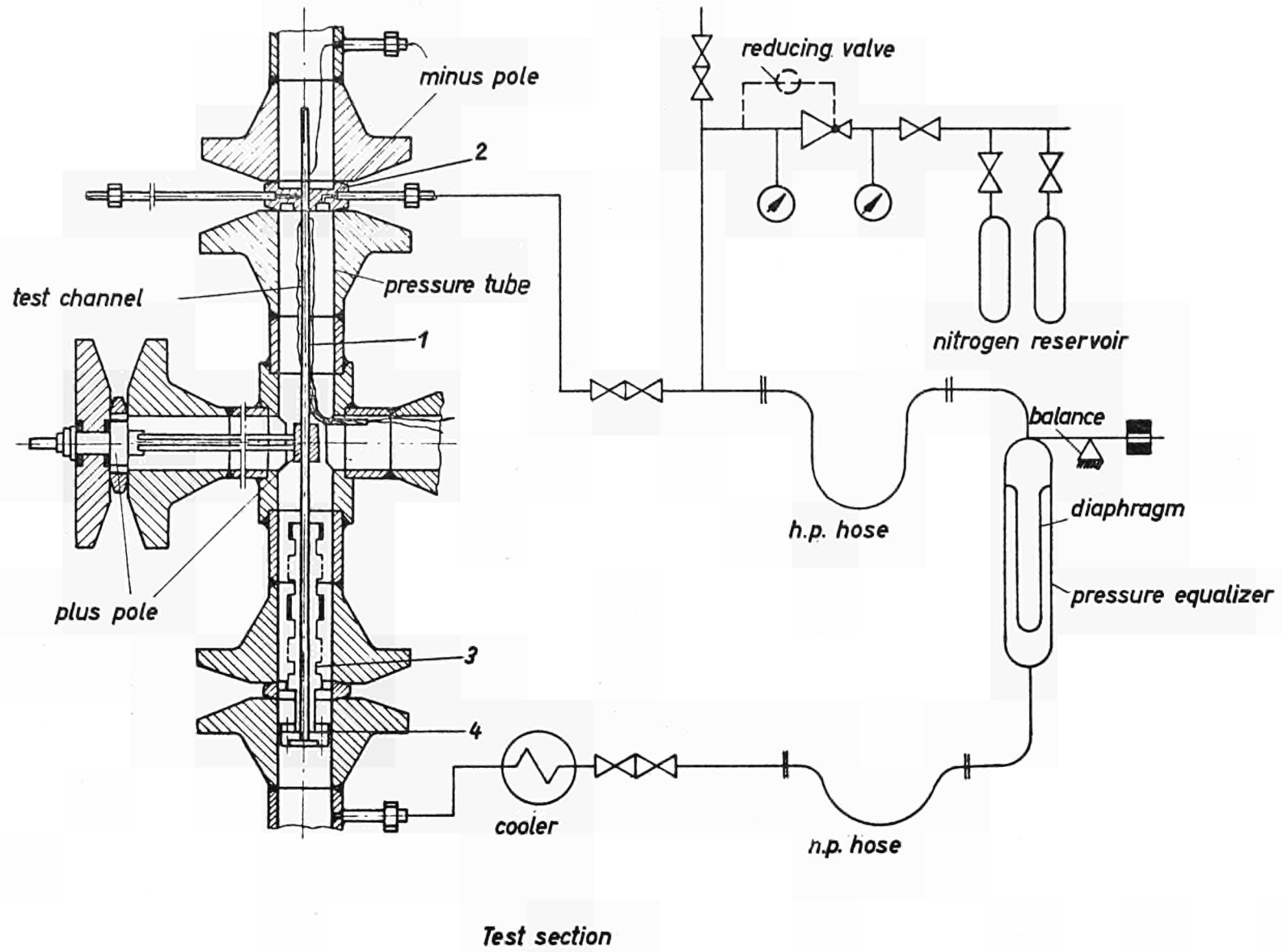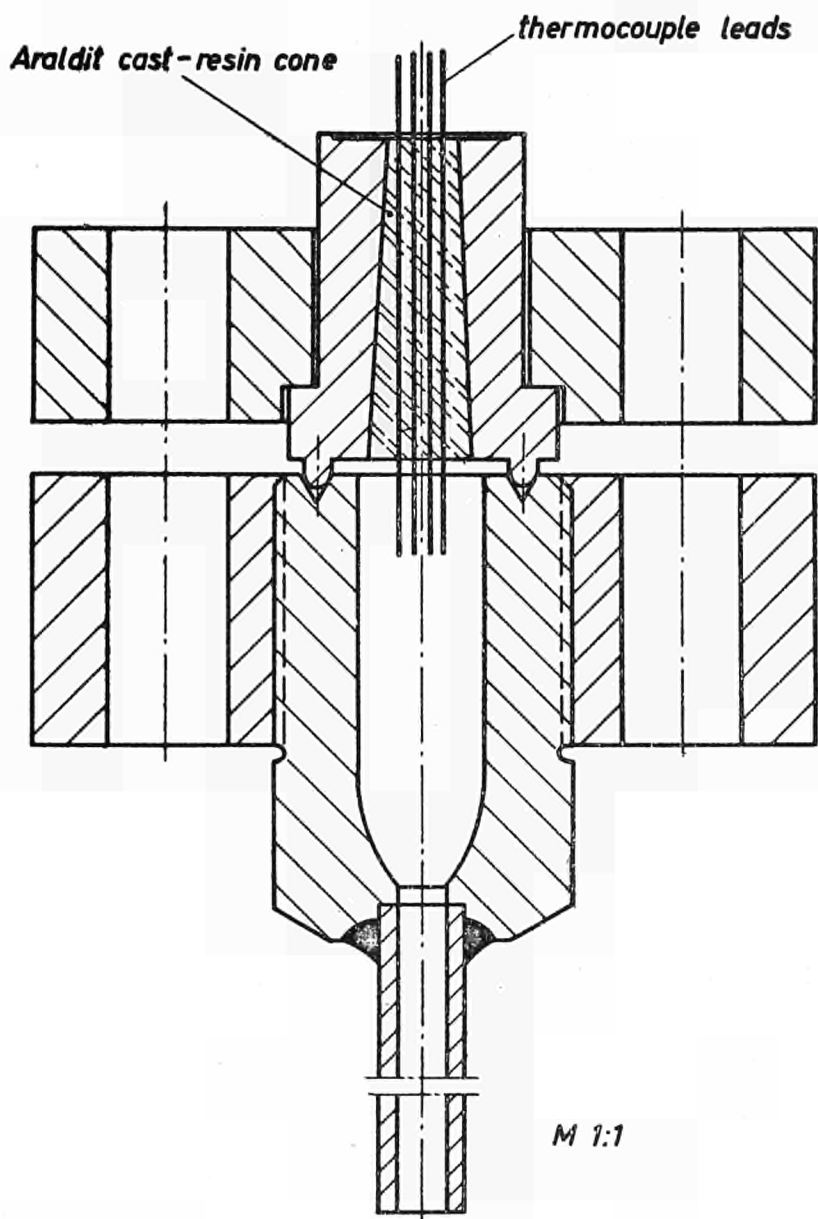
Thermocouple bushing

Fig. 3

M 1:2,5
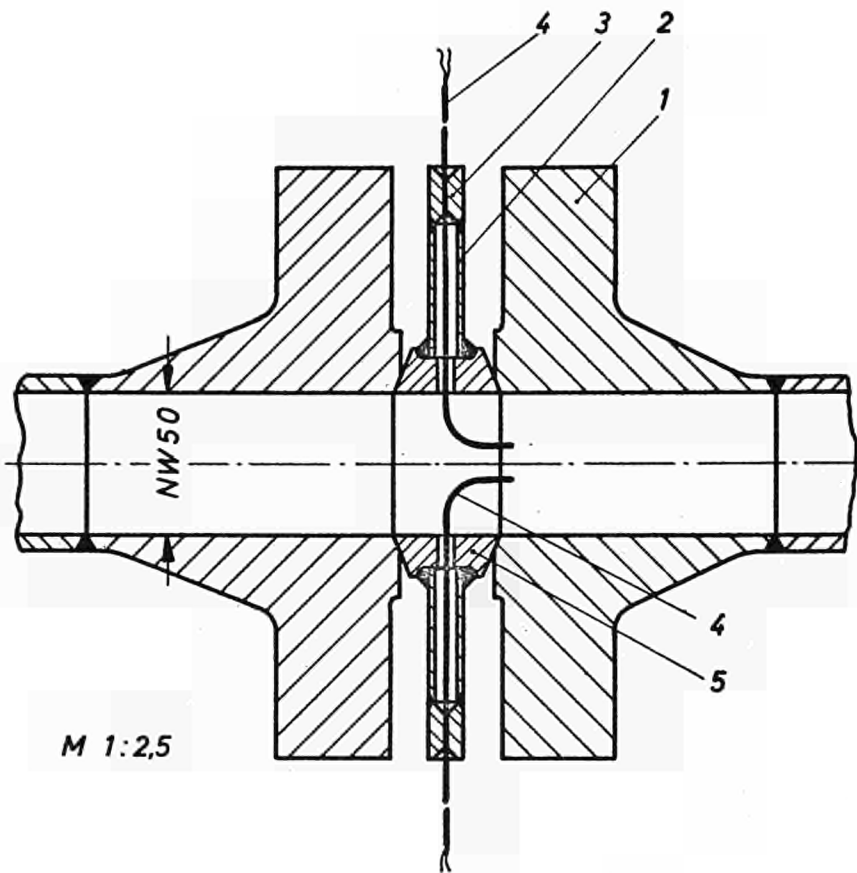
1 flange   4 thermocouple
2 branch-off 5 lenticular gasket
3 nipple

Temperature traverse for 50mm bore pipework

Fig. 4

1   Pipe 15 mm bore
2   Thermocouple
3   Union

M 1 : 2,5
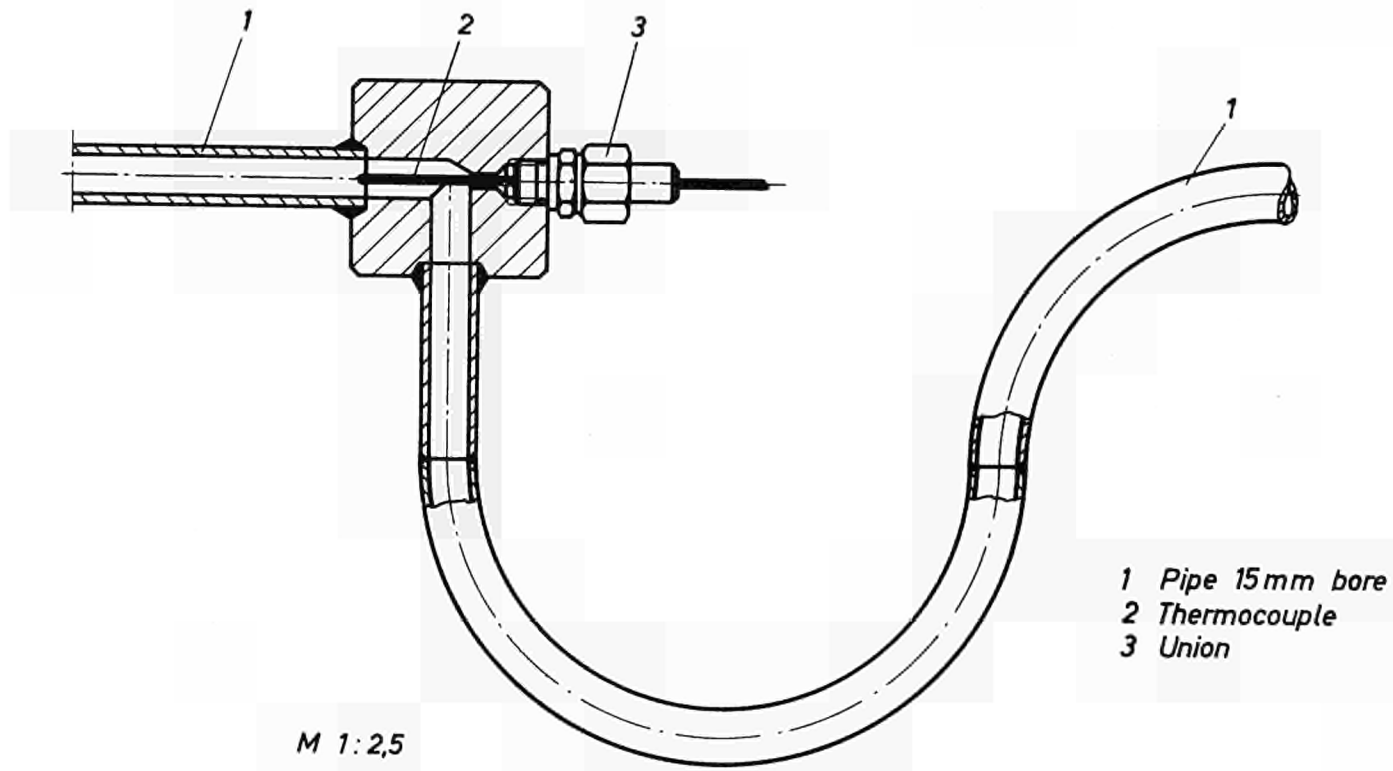
Temperature measuring loop for 15 mm bore pipe

Fig. 5

three-wire thermocouple

mica-insulated thermocouple

Layout of three-wire thermocouple
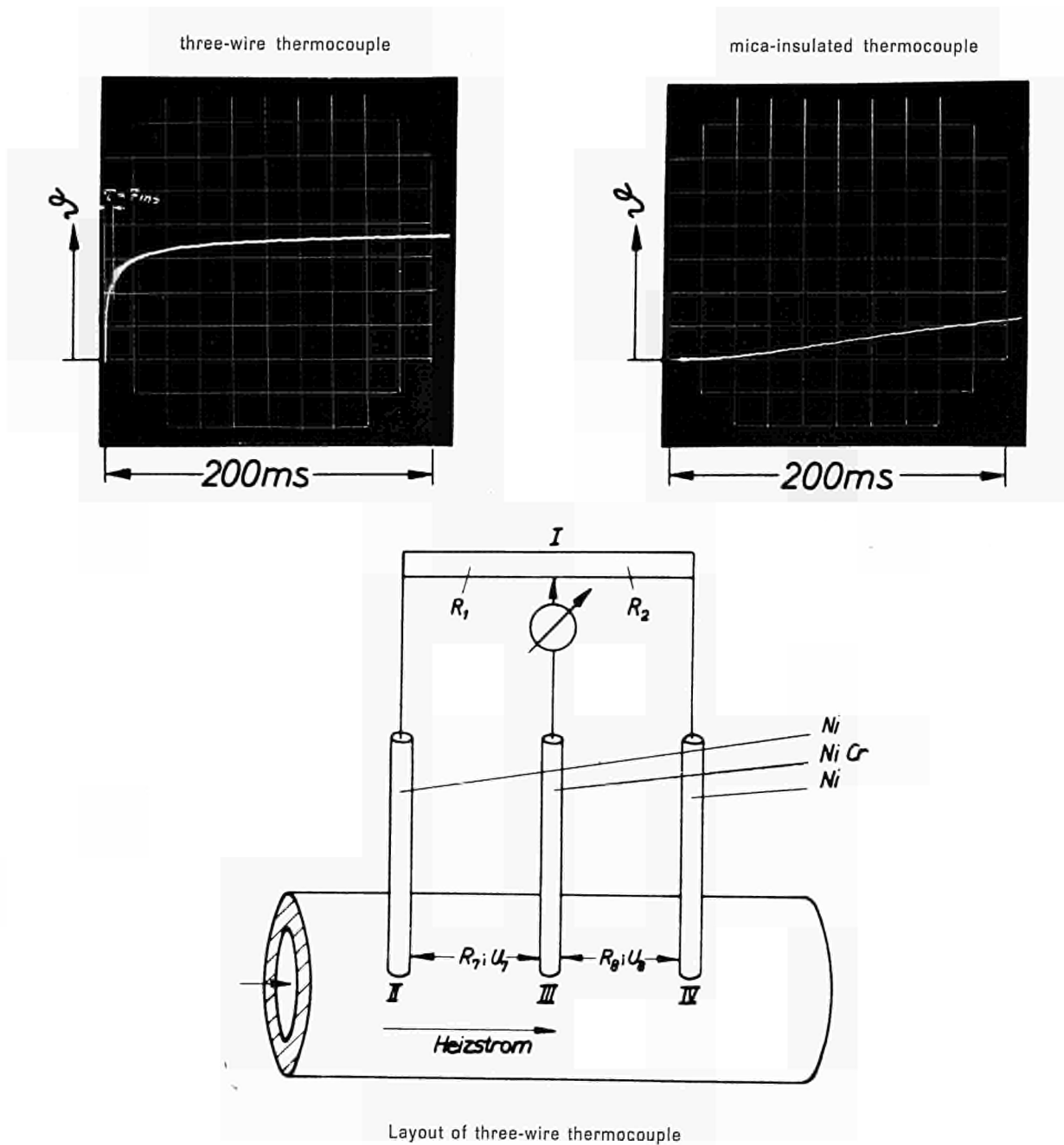
Figure 6
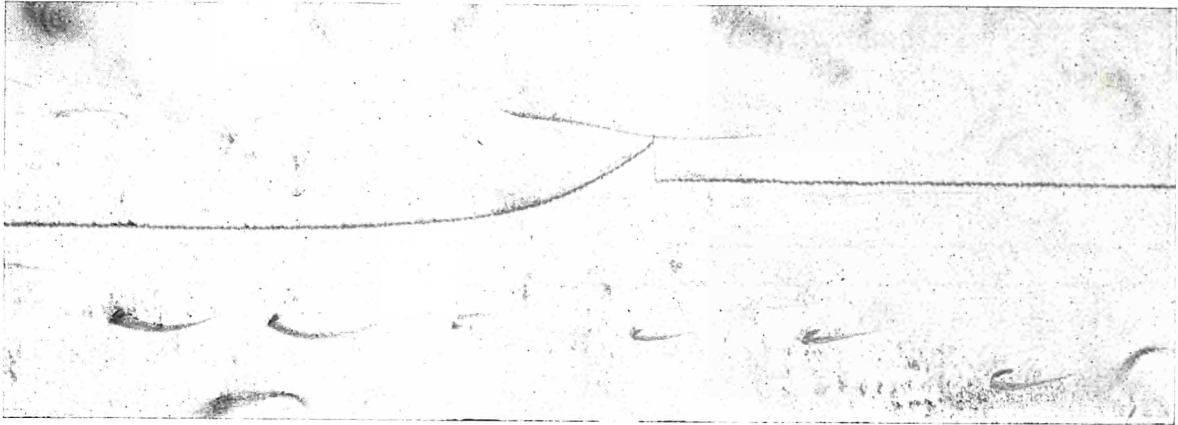
7 a : Thermocouple not balanced
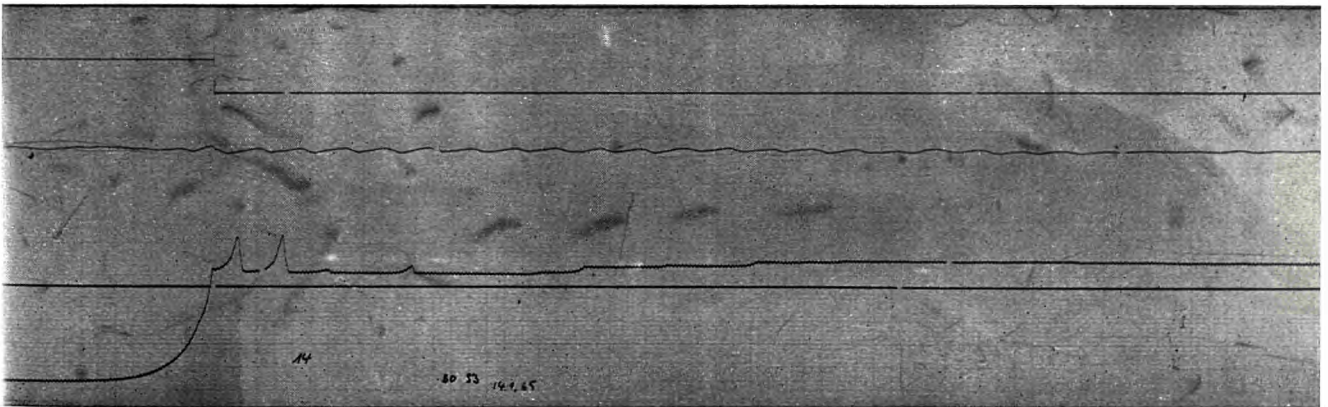
7 b : Thermocouple balanced

Fig. 7 : Balancing of three-wire thermocouple

test channel

platinum wire

insulation

platinum point

steam bubble

direction of flow

8 a

10 V

test tube

amplifier

R

galvanometer

I
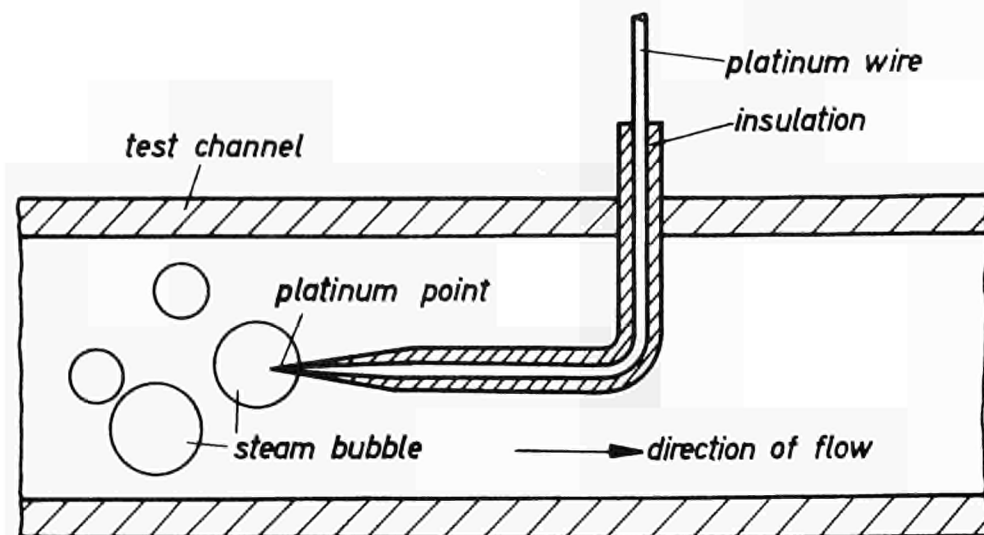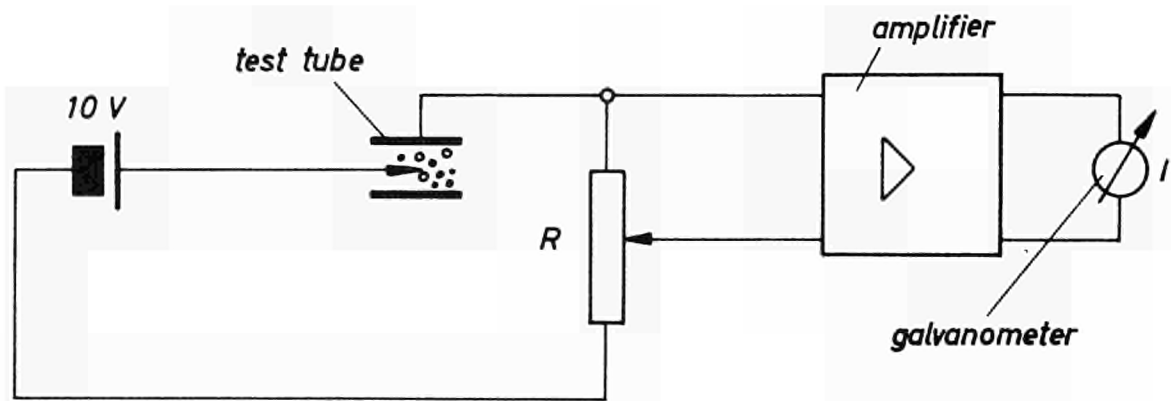
8 b

Schematic layout and connection diagram of
probe to determine steam bubble content

Fig. 8

d.c. circuit
breaker

heated channel

balancing potentiometer

differential amplifier

galvanometer to
check balance

filter

discriminator

control
amplifier
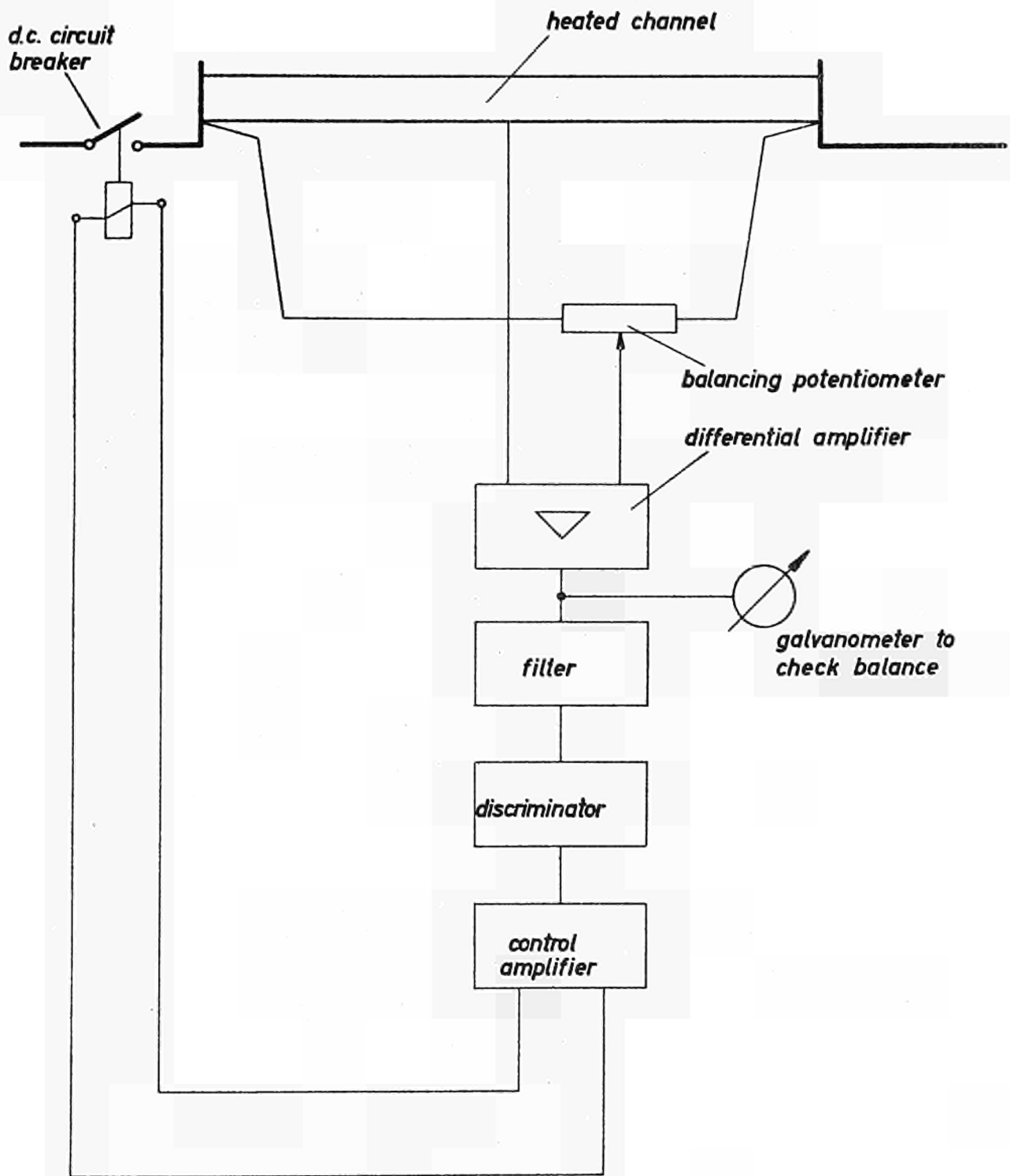
Fig. 9 : Block diagram of burnout detector
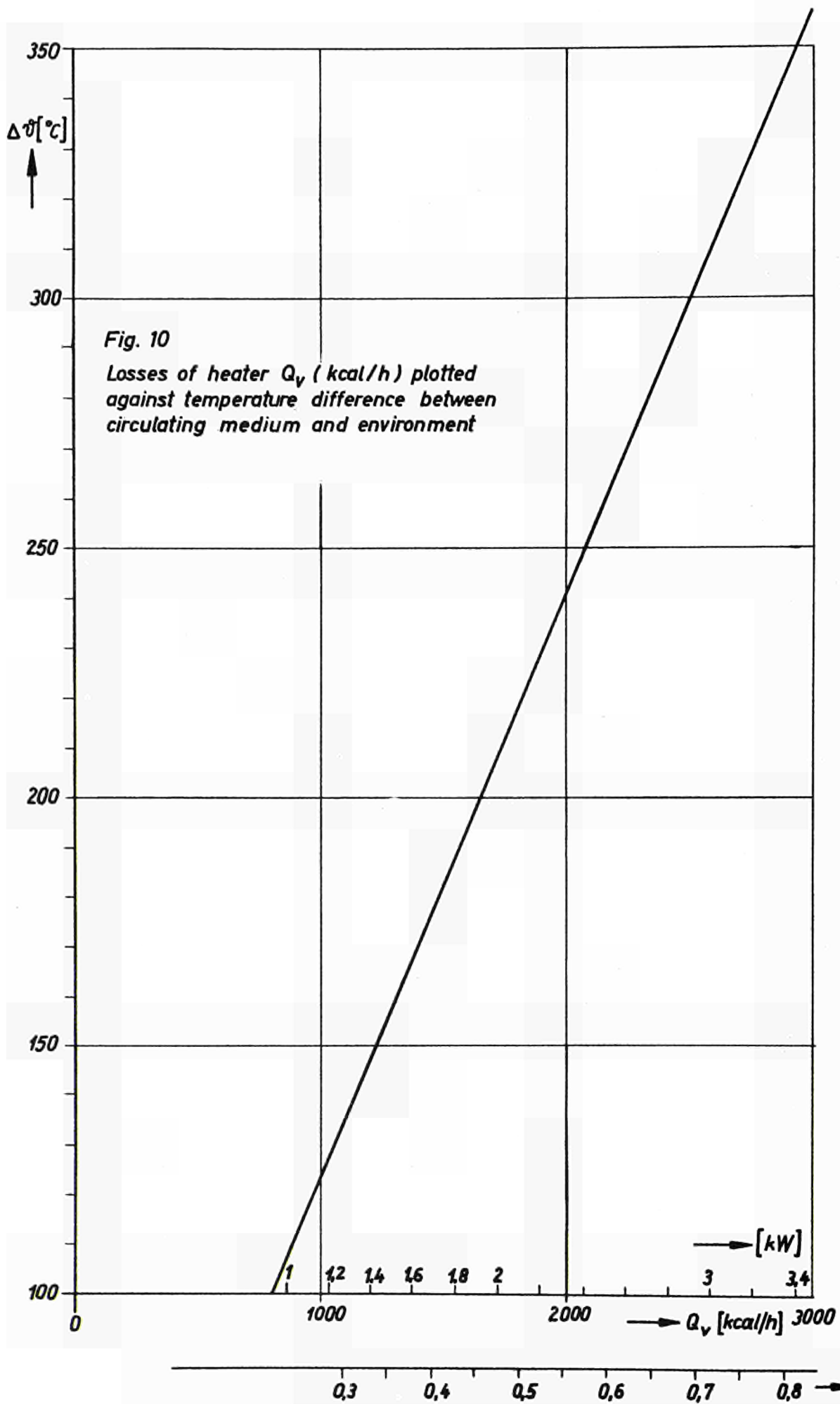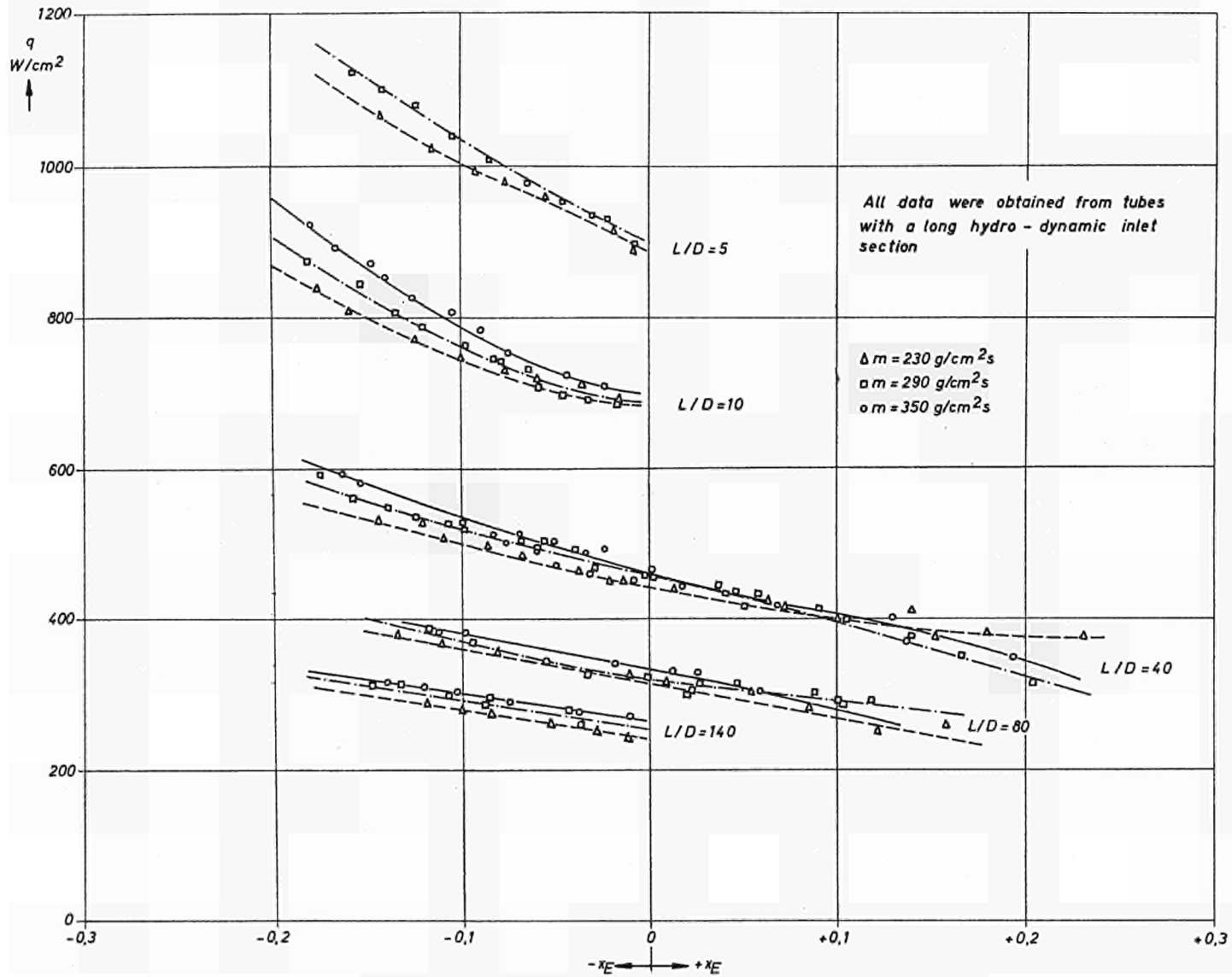
Fig. 10

Losses of heater Q_v (kcal/h) plotted against temperature difference between circulating medium and environment

Critical heat flux for internally - cooled tubes with an inside dia. of
D = 0.7 cm. at a pressure of p = 70 kg/cm²

Fig. 11
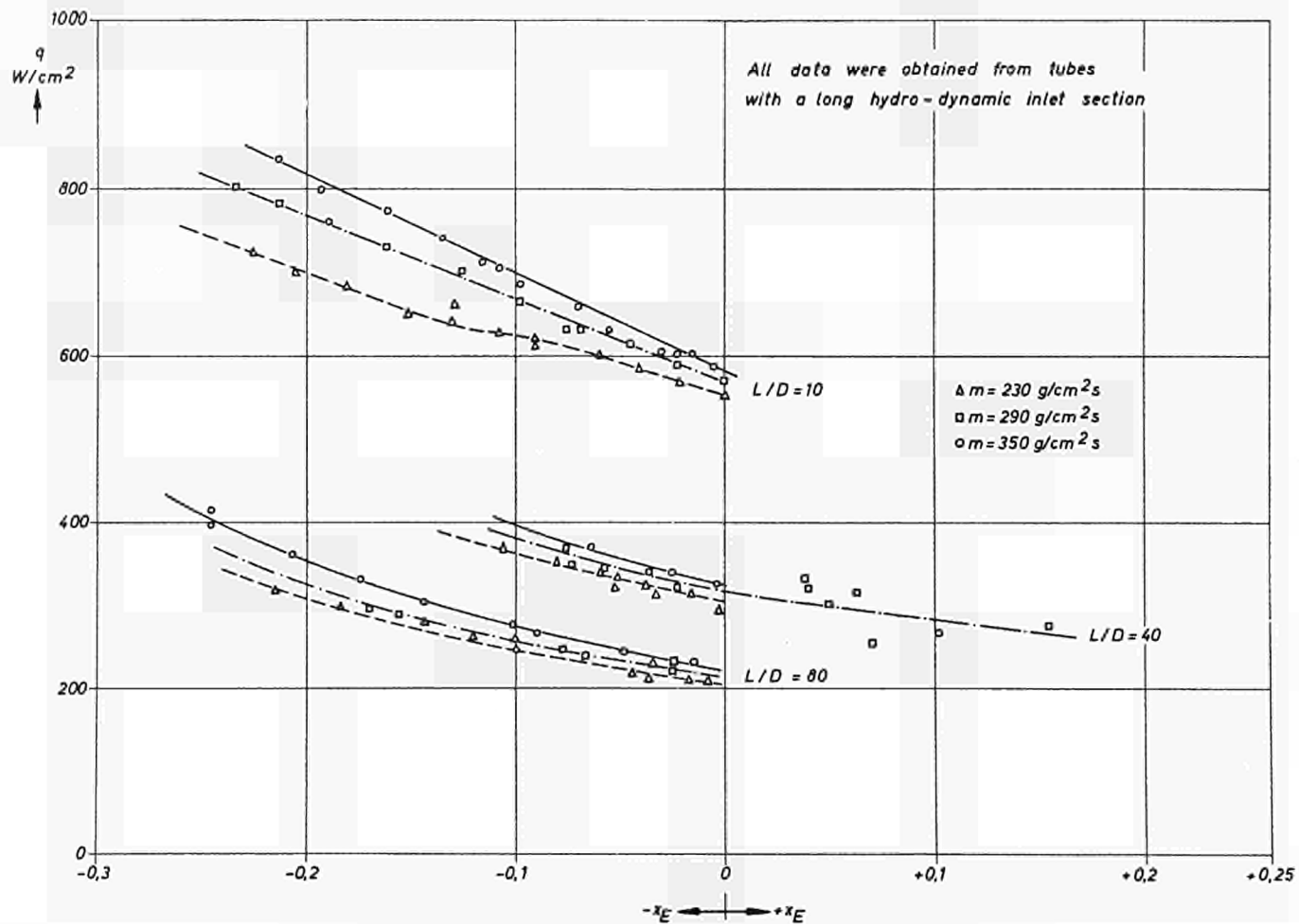
Critical heat flux for internally – cooled tubes with an inside dia. of
D = 0,7 cm. at a pressure of p = 100 kg/cm²

Fig. 12

- pole

S_1 0

5mm DB_1

DB_2 12mm   12mm   TC

S_2 100 mm

S_3 140 mm

280±0,5

S_4 270 mm

orifice 2

5

3⌀

+ pole

40

16⌀

5

40

16⌀

4⌀

orifice 1

S = voltage tap
DB = three-wire thermocouple
TC = thermo-coax thermocouple

dimensions in mm.
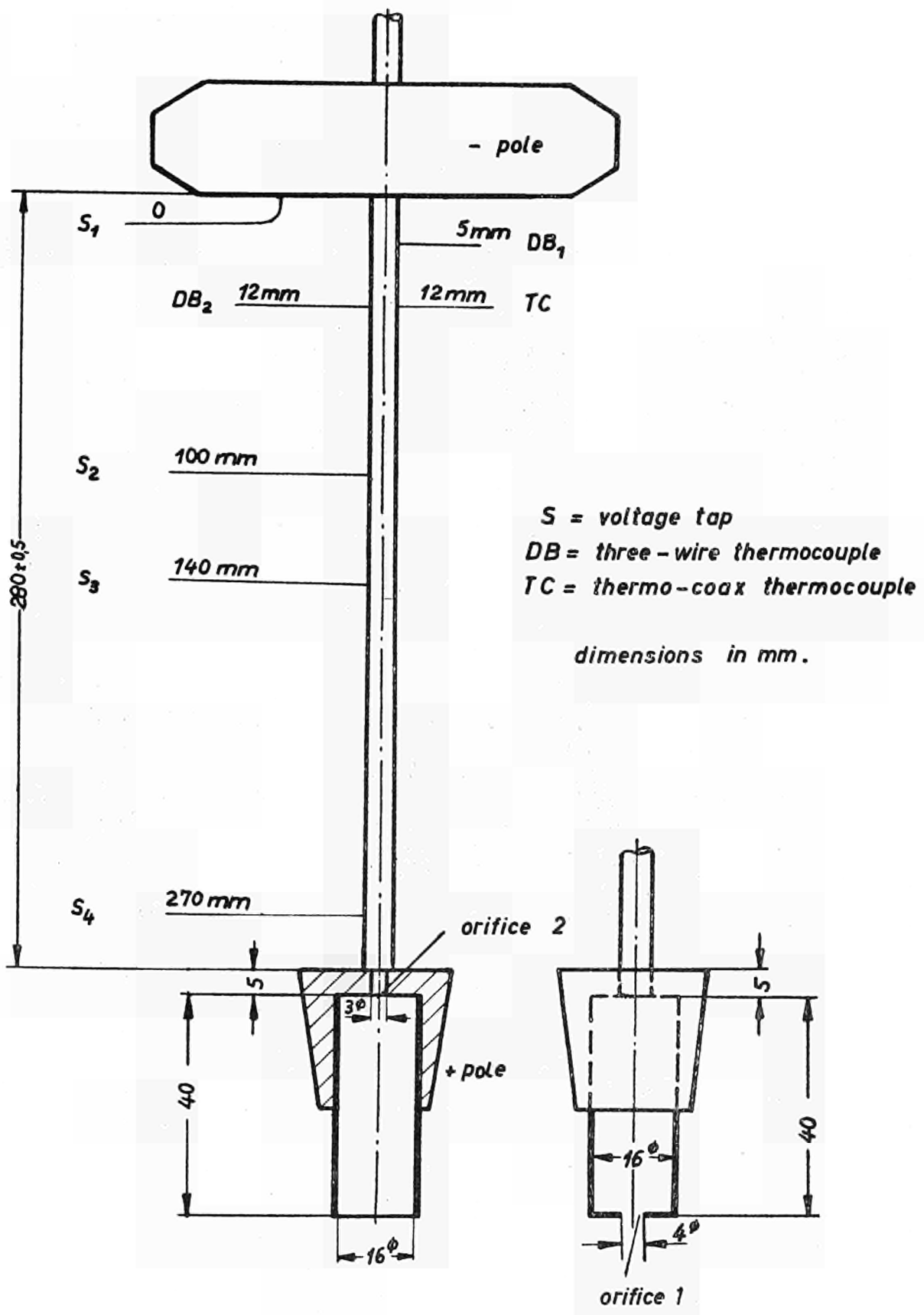
Schematic diagram of orificed test tubes

Fig. 13

Critical heat flux for tubes with orifices at the test section inlet with $D = 0.7$ cm. and $p = 70$ kg/cm^2

Fig. 14

Critical heat flux for tubes with orifices at the test section inlet with $D = 0.7$ cm. and $p = 100$ kg/cm^2

Fig. 15

- Pol

0
S_1
5 mm DB_1
12 mm   12 mm   TC

$S = voltage\ tap$
$DB = three-wire\ thermocouple$
$TC = thermo-coax\ thermocouple$

S_2 100 mm

$\psi = \dfrac{h}{\mathcal{T} \cdot D} = helix\ angle$

S_3 140 mm

dimensions in mm

280 ± 0,5

S_4 270 mm

+ Pol

h = 80

65

h

49

h

No. 1
twisted tape
$\psi = 75°$

No. 2
twisted tape
$\psi = 56°$

No. 3
twisted tape
$\psi = 48°$

Schematic diagram of test tubes with twisted tapes

Fig. 16

Critical heat flux for tubes with twisted tape No.1 at test section inlet
with $D = 0,7\,cm$ and $L/D = 40$
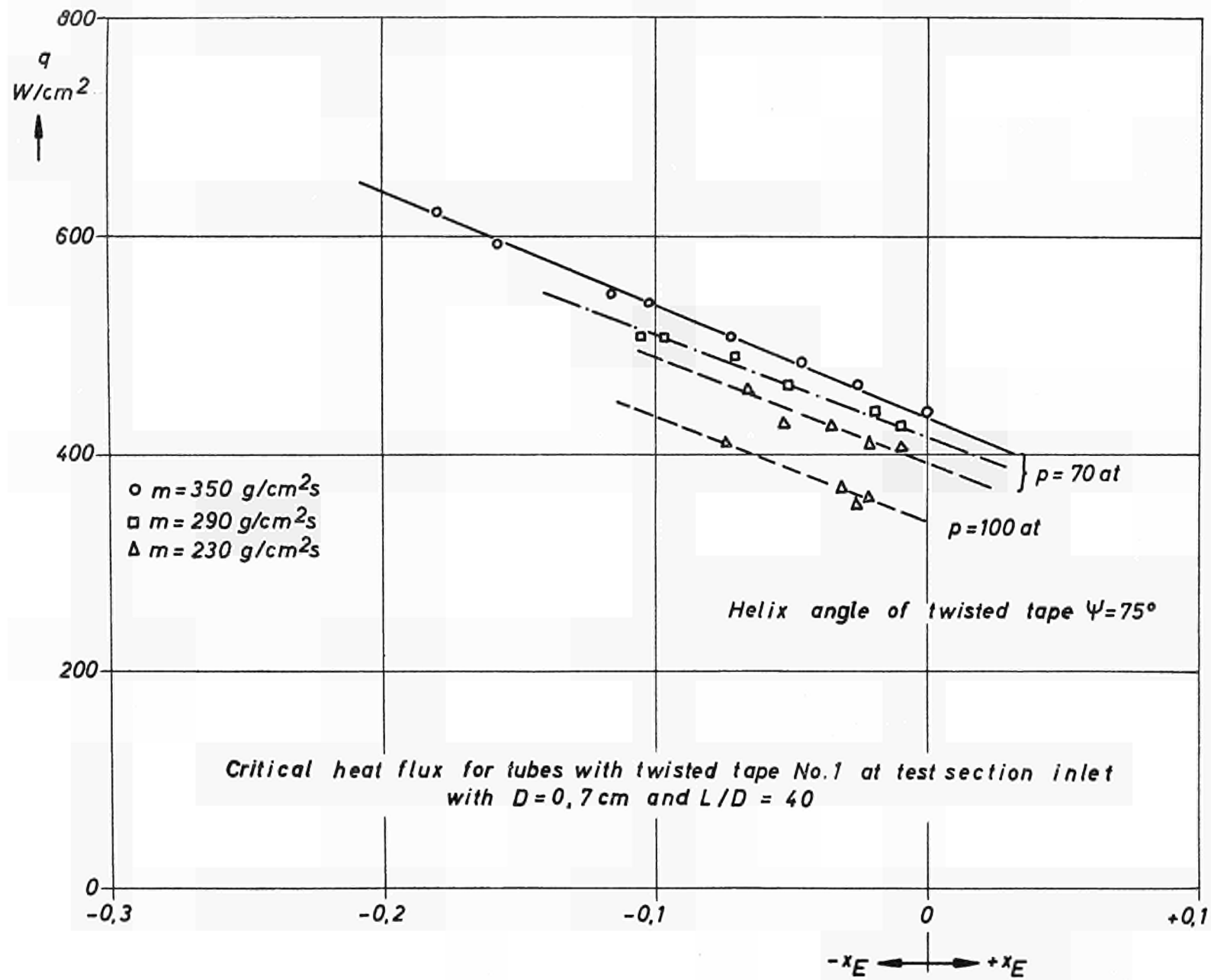
Fig. 17
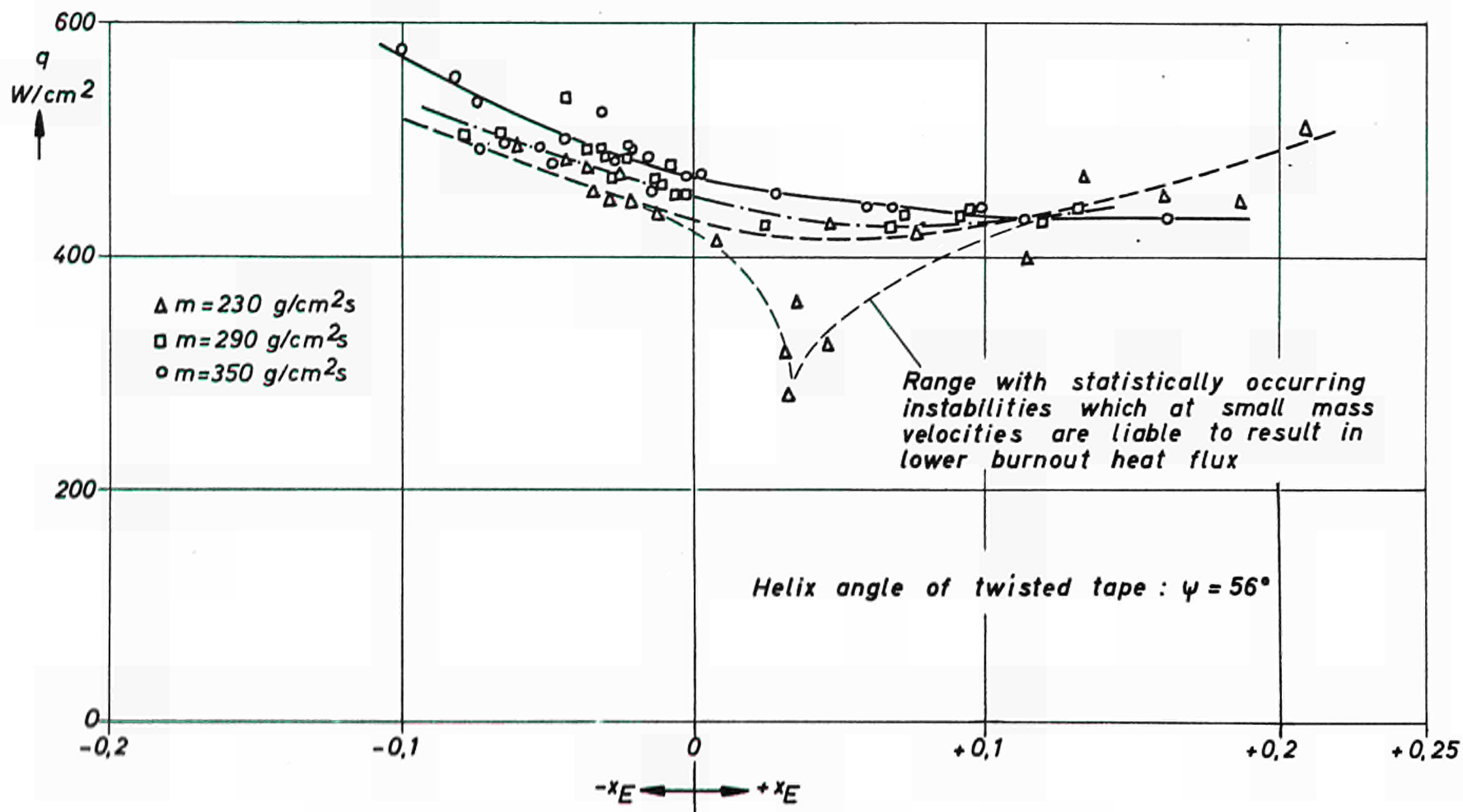
Critical heat flux for tubes with twisted tape No. 2 at test section inlet with D = 0.7cm., L/D = 40 and p = 100 kg/cm^2

Fig. 18
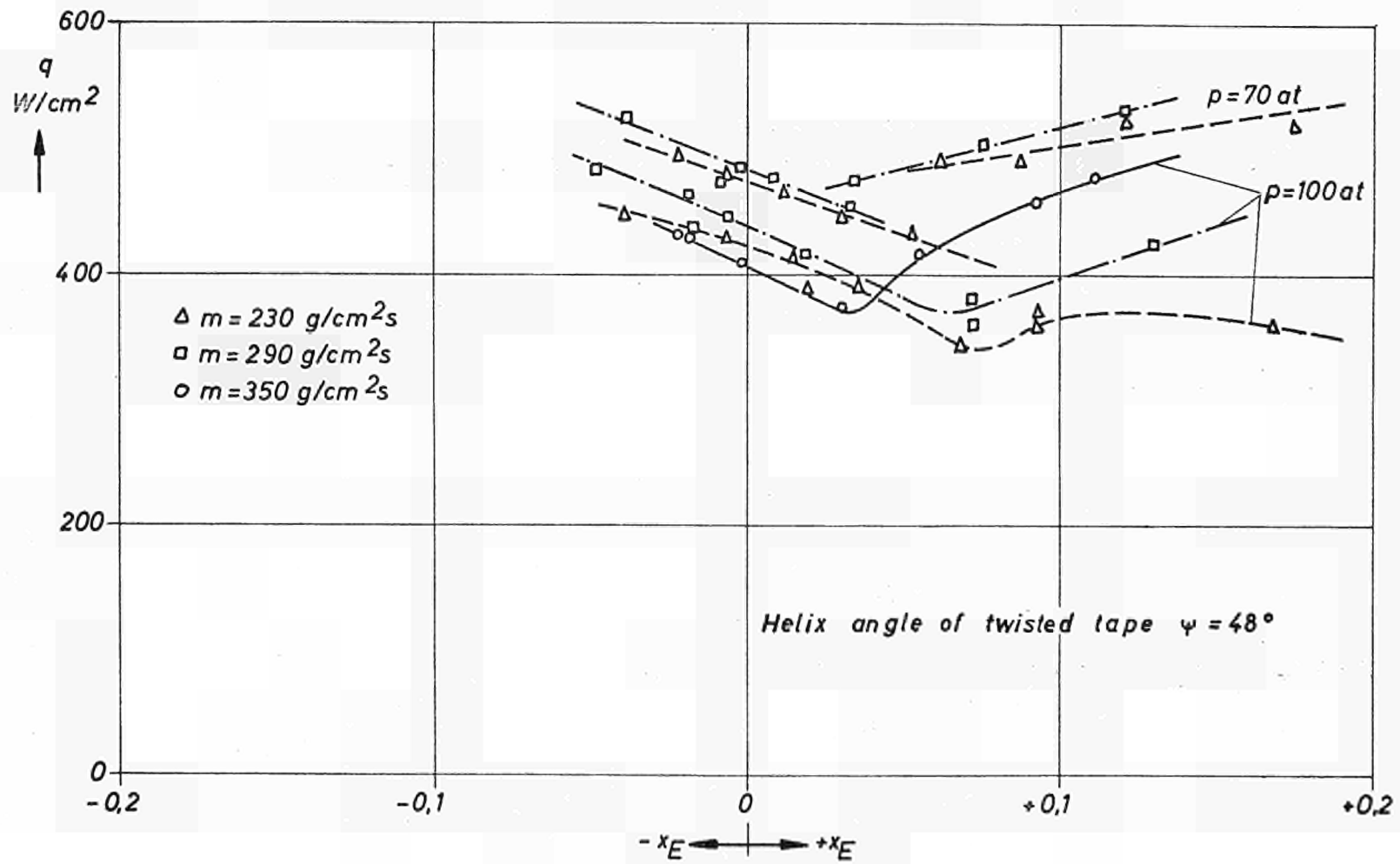
Critical heat flux for tubes with No. 3 twisted tape at test section inlet with D= 0,7cm and L /D = 40

Fig. 19

The effect of system pressure on the critical heat flux for
$m = 290 \ g/cm^2 s, \ D = 0.7 \ cm, \ L/D = 80$

Fig. 20
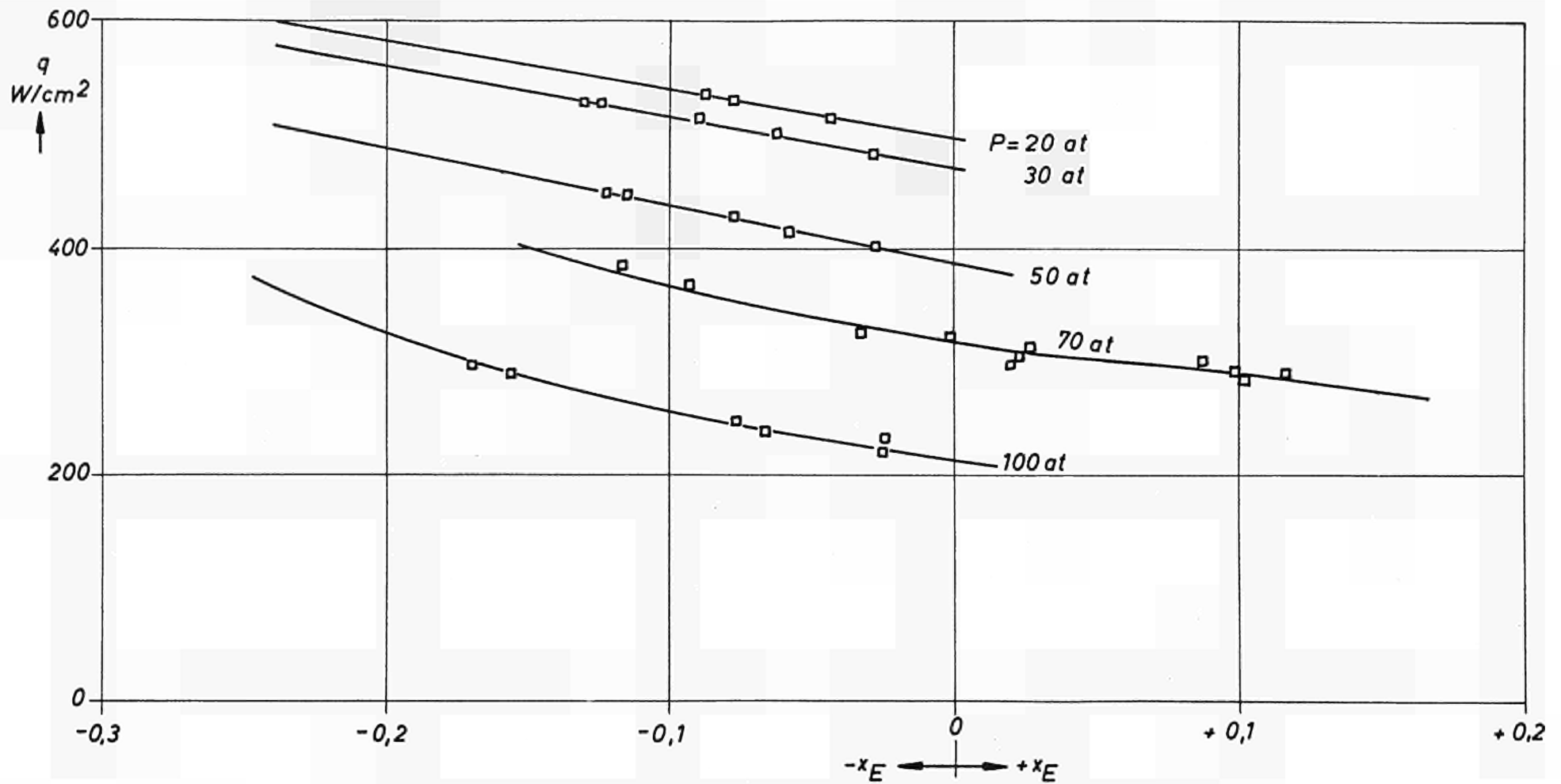
The effect of system pressure on the critical heat flux for
m = 350 g/cm²s , D = 0,7cm , L/D = 80
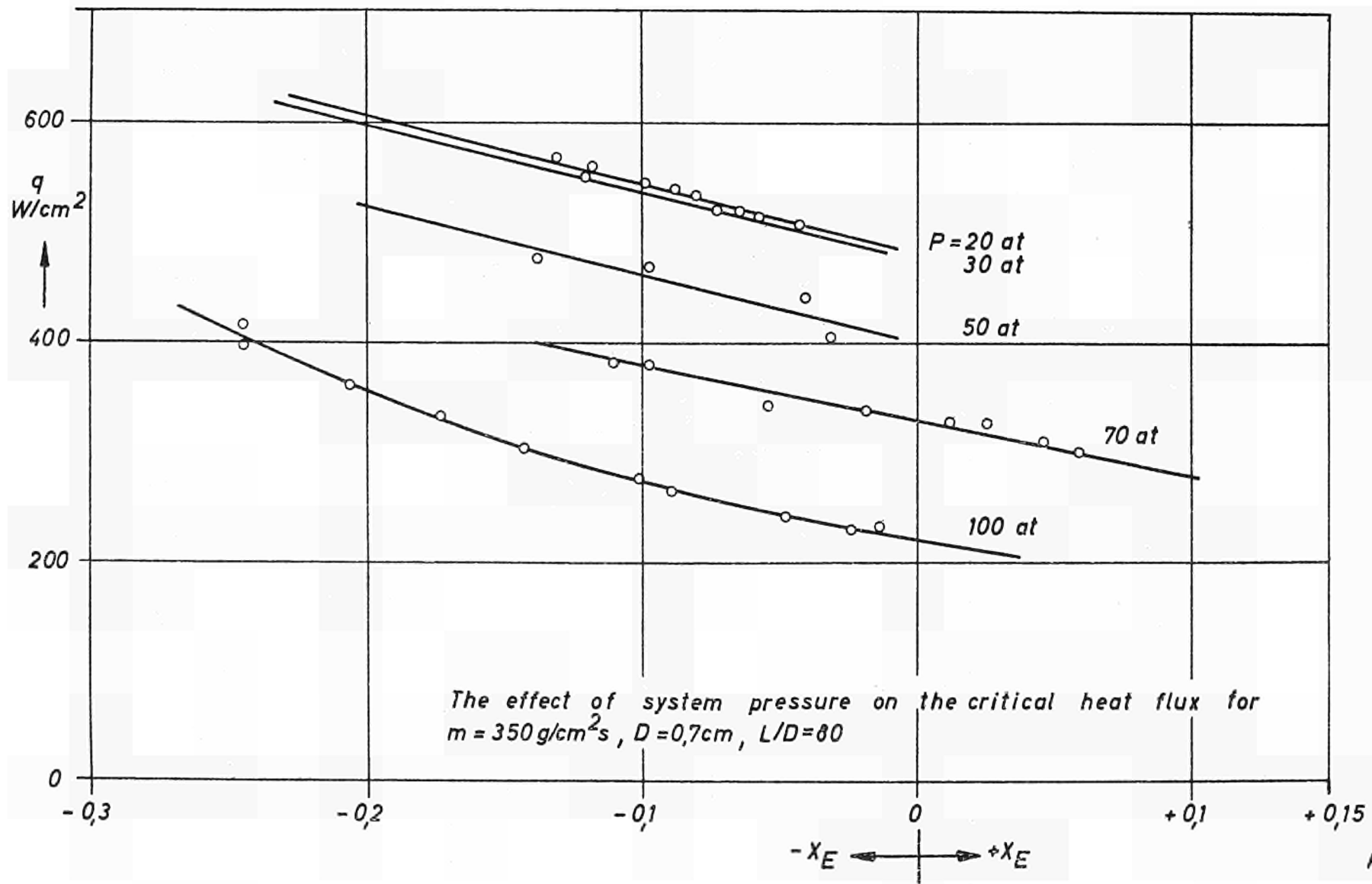
Fig. 21
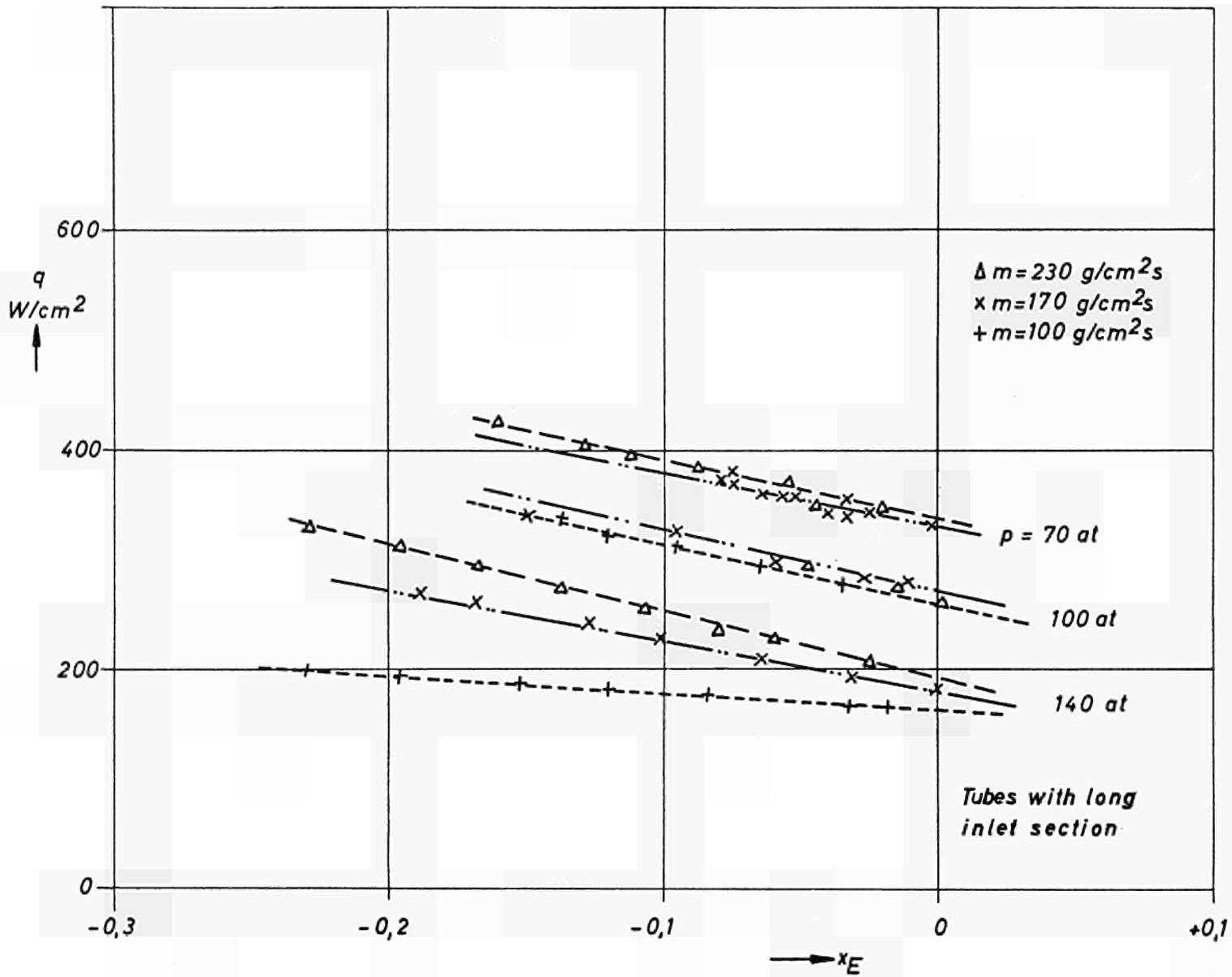
Critical heat flux for internally-cooled tubes with an internal dia. of
D = 1,1 cm and a L/D ratio of 40

Fig. 22
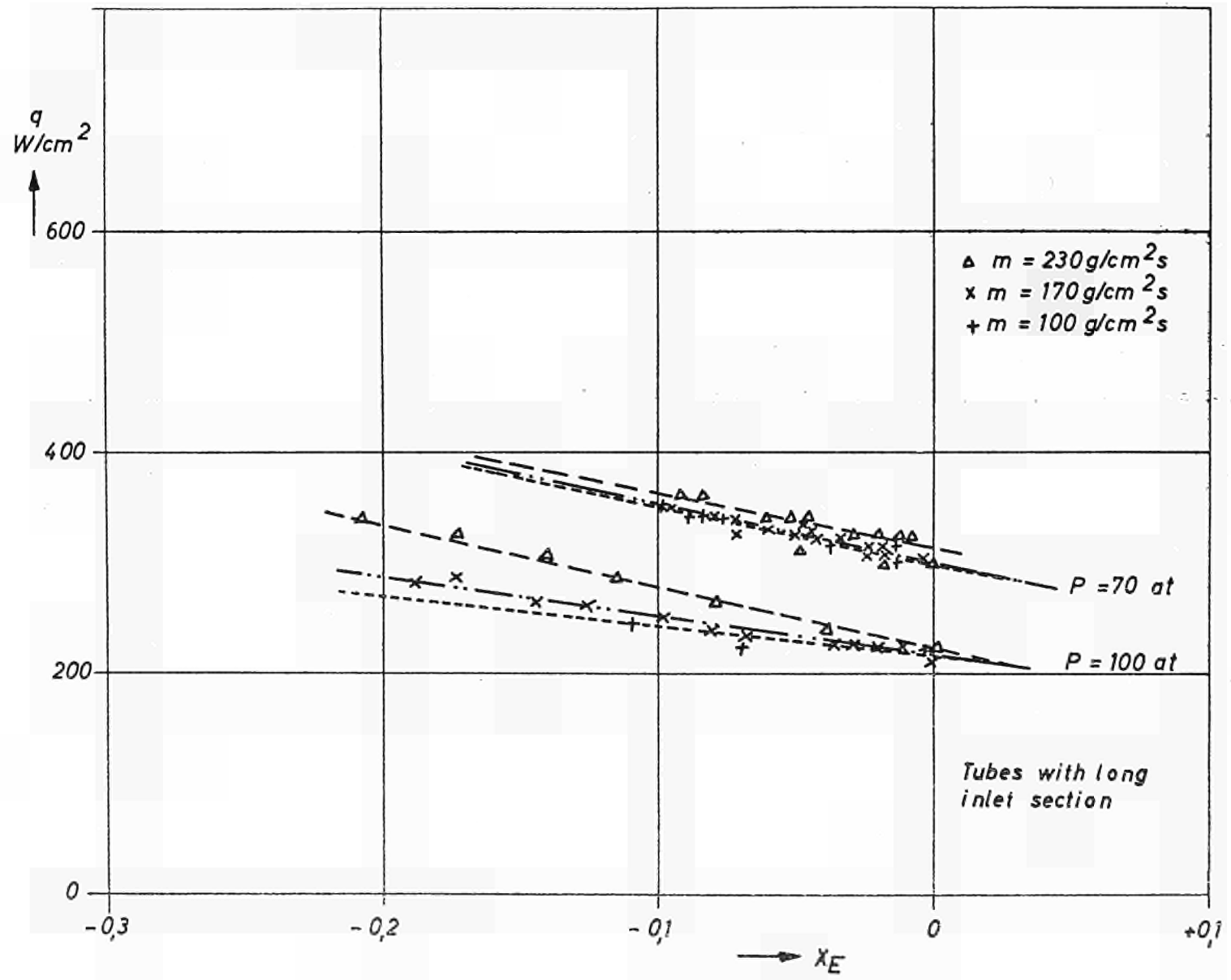
Critical heat flux for internally-cooled tubes with an internal dia. of
D=1,5 cm and a L/D ratio of 40

Fig. 23
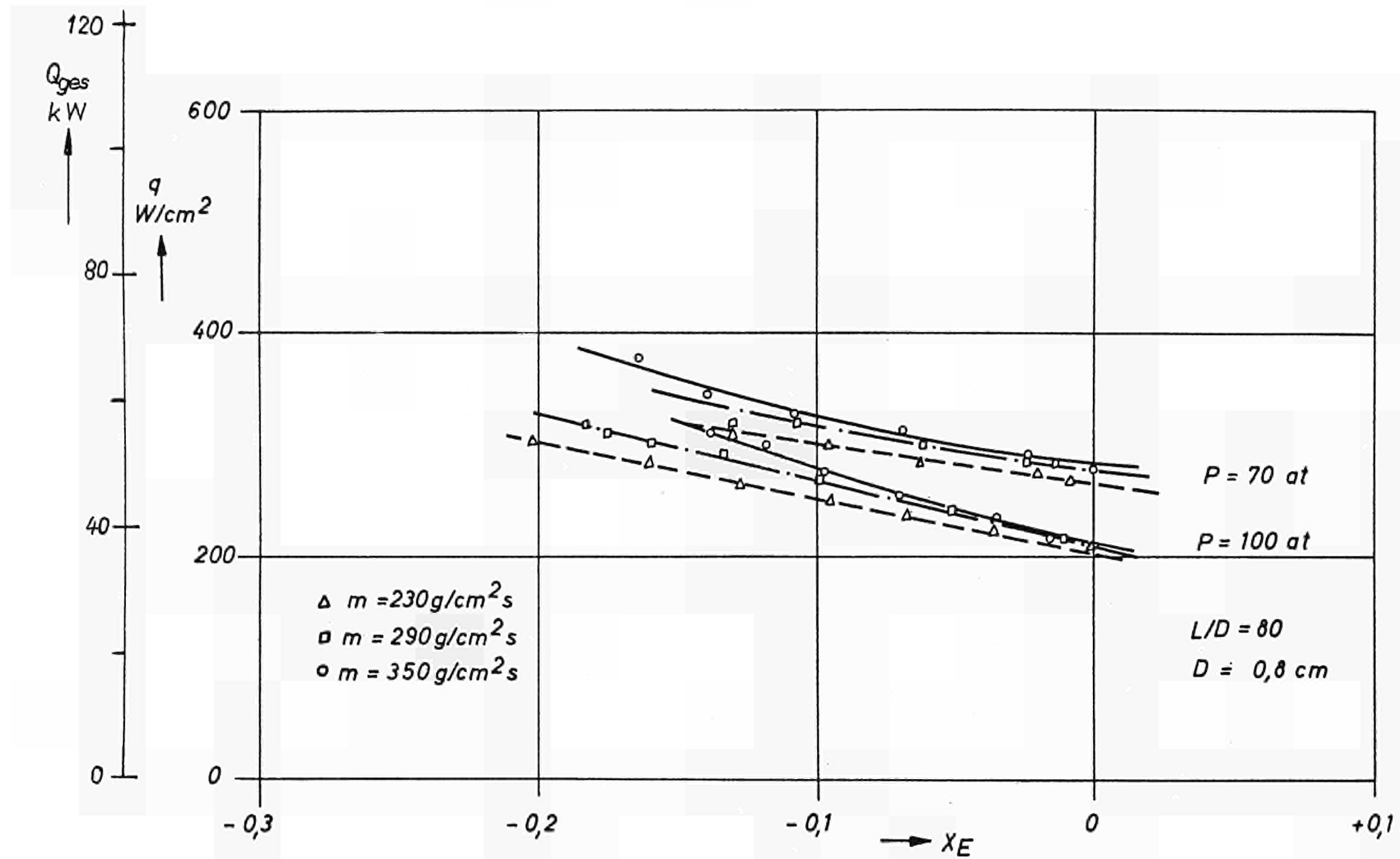
Critical heat flux for tubes with sinusoidal distribution of specific heat flux

Fig. 24
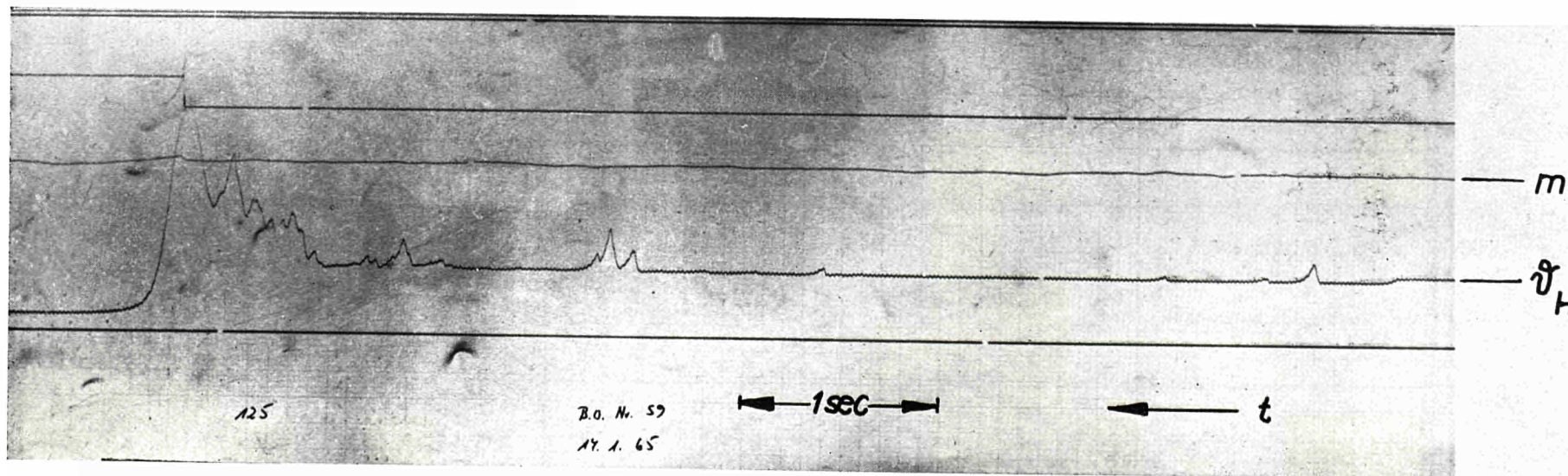
Fig. 25 : Variation of tube wall temperature and mass flow during transition from nucleate to film boiling
$m = 308.1$ g/cm²s, $p = 101$ kgf/cm², $X_E = -0.0014$, $X_A = 0.1153$, L/D = 40, $q_{BO} = 297.7$ W/cm²

Influence of hydro-dynamic inlet section on crictical heat flux for $D = o.7\ cm$. $L/D = 10$ and $p = 70\ kg/cm^2$

Fig. 26
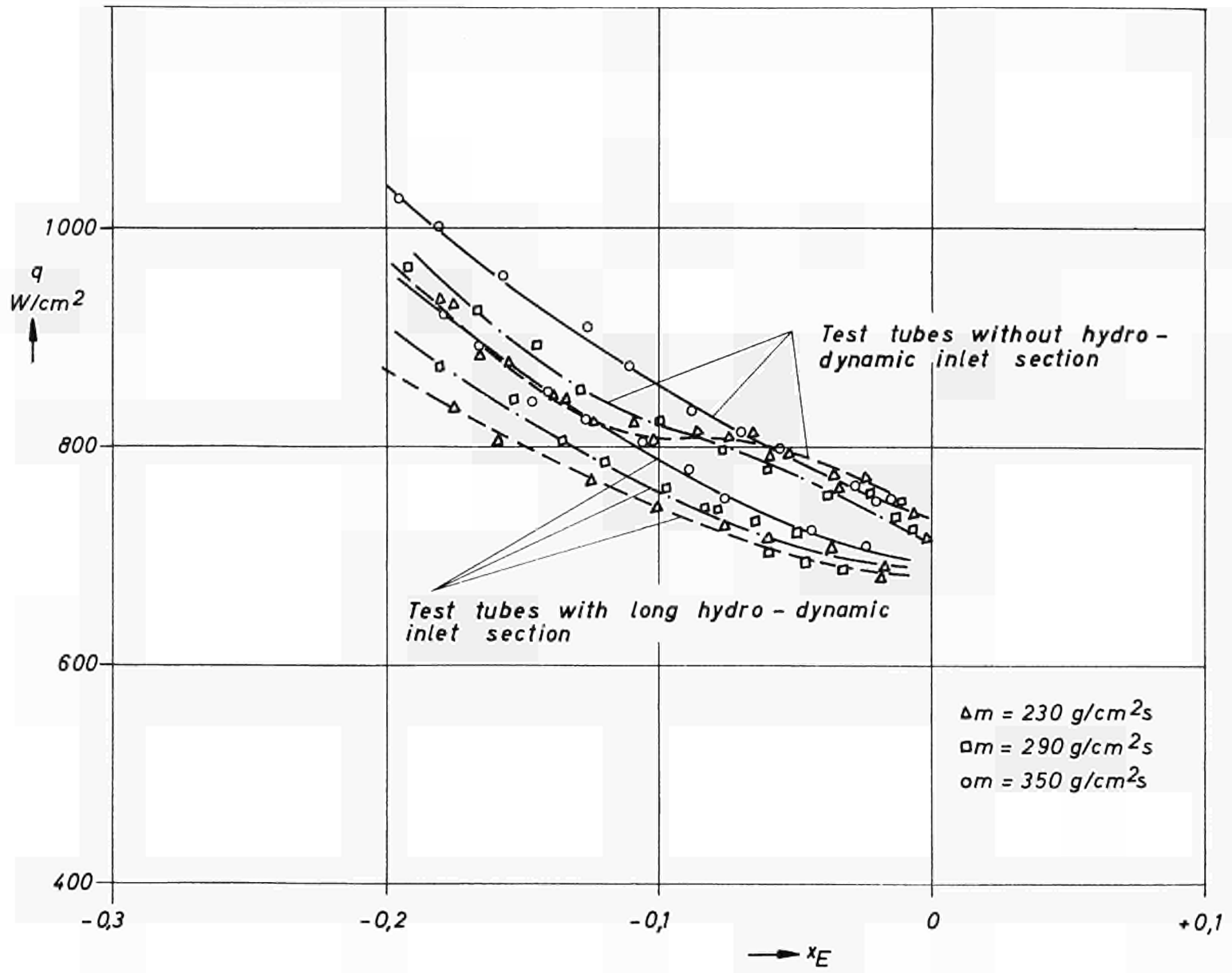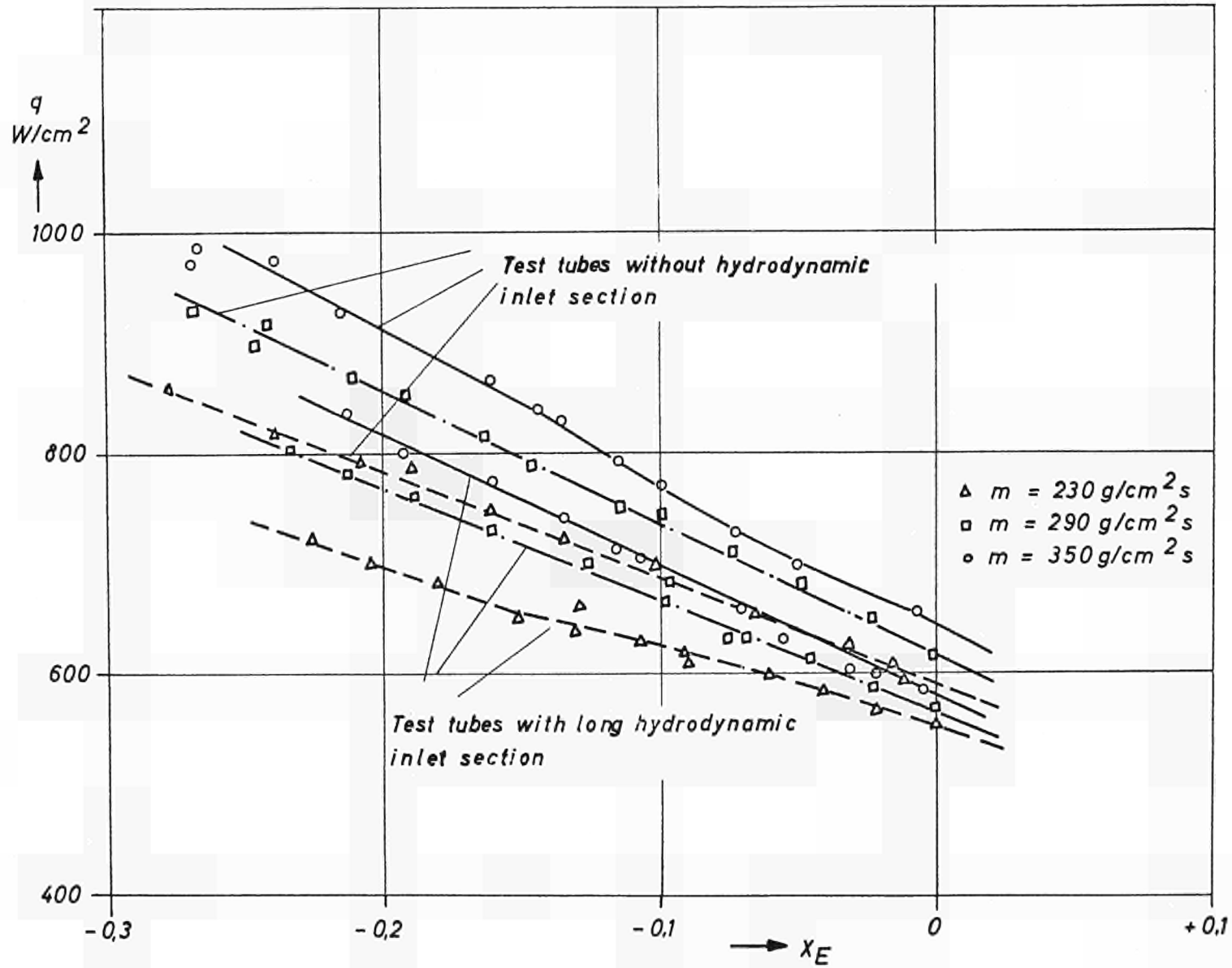
Influence of hydrodynamic inlet section on critical heat flux for

$D = 0,7 \, cm$, $L/D = 10$ and $p = 100 \, kg/cm^2$

Fig. 27
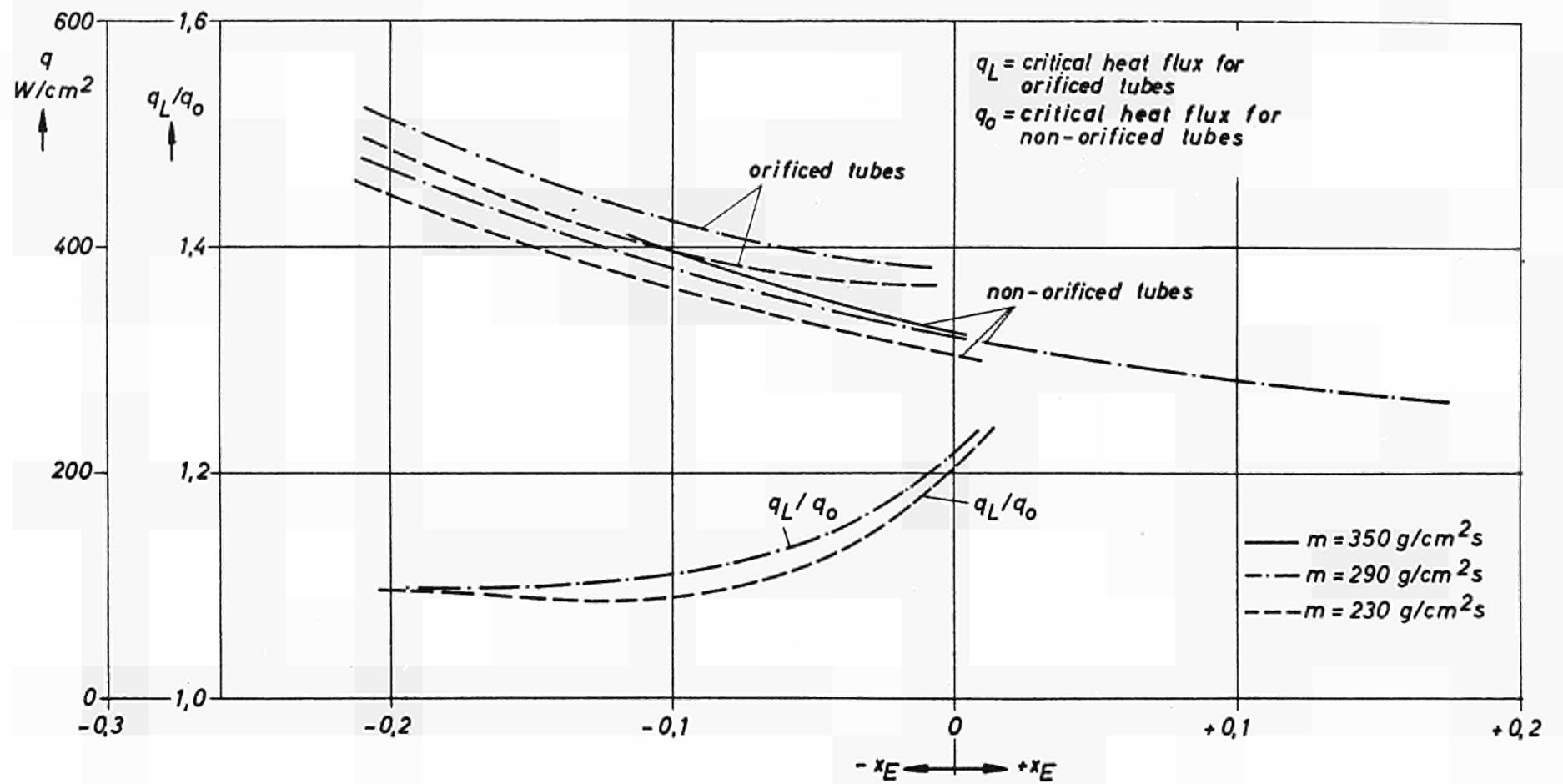
Influence of No.2 orifice at test section inlet on critical heat flux for $D = 0.7\,cm$, $L/D = 40$ and $p = 100\,kg/cm^2$

Fig. 28

Influence of No.2 and No.3 twisted tapes on the critical heat flux for $m= 230\ g/cm^2s$, $D=0.7\ cm$, $L/D =40$ and $p=70\ kg/cm^2$
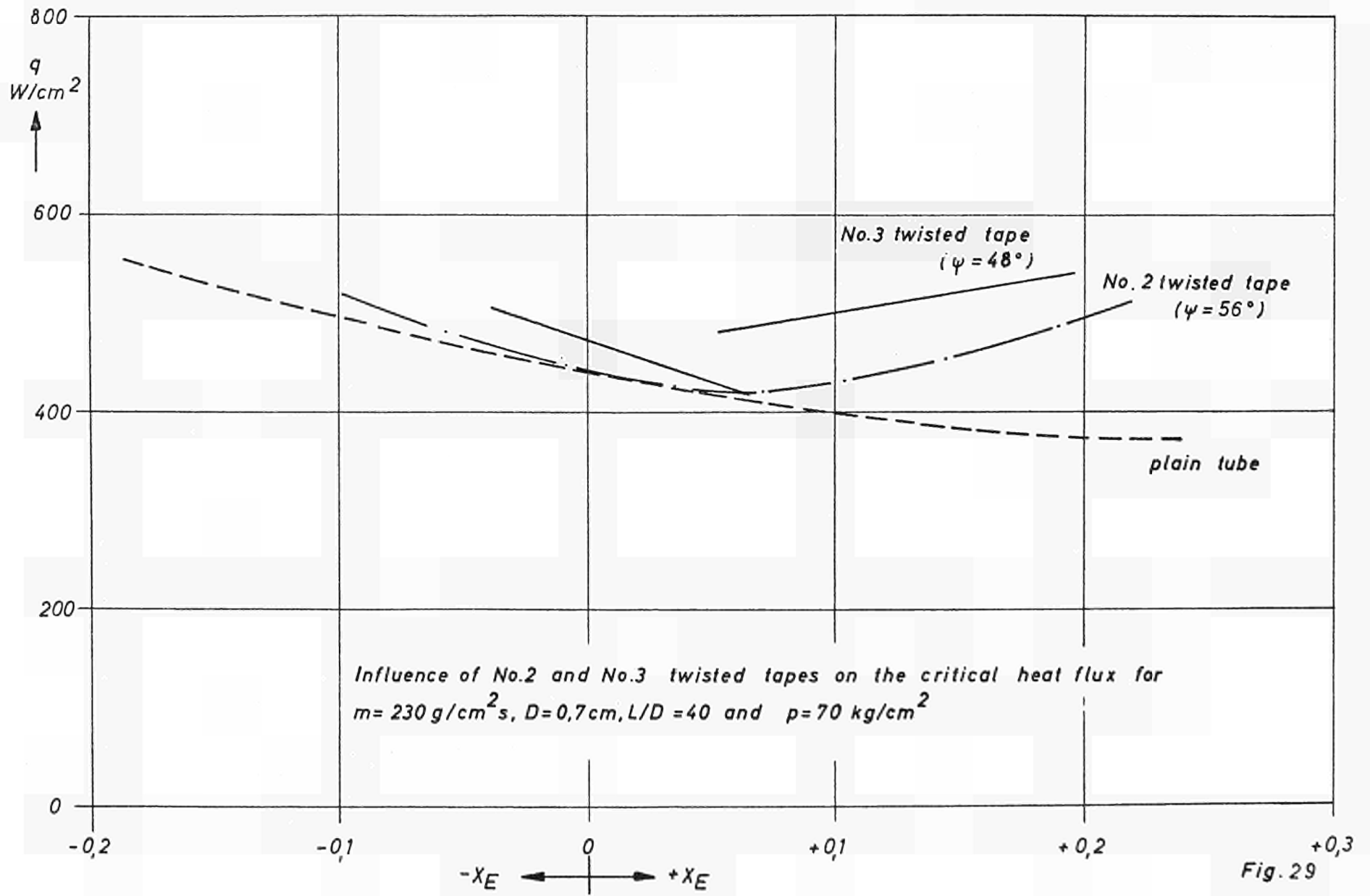
Fig. 29
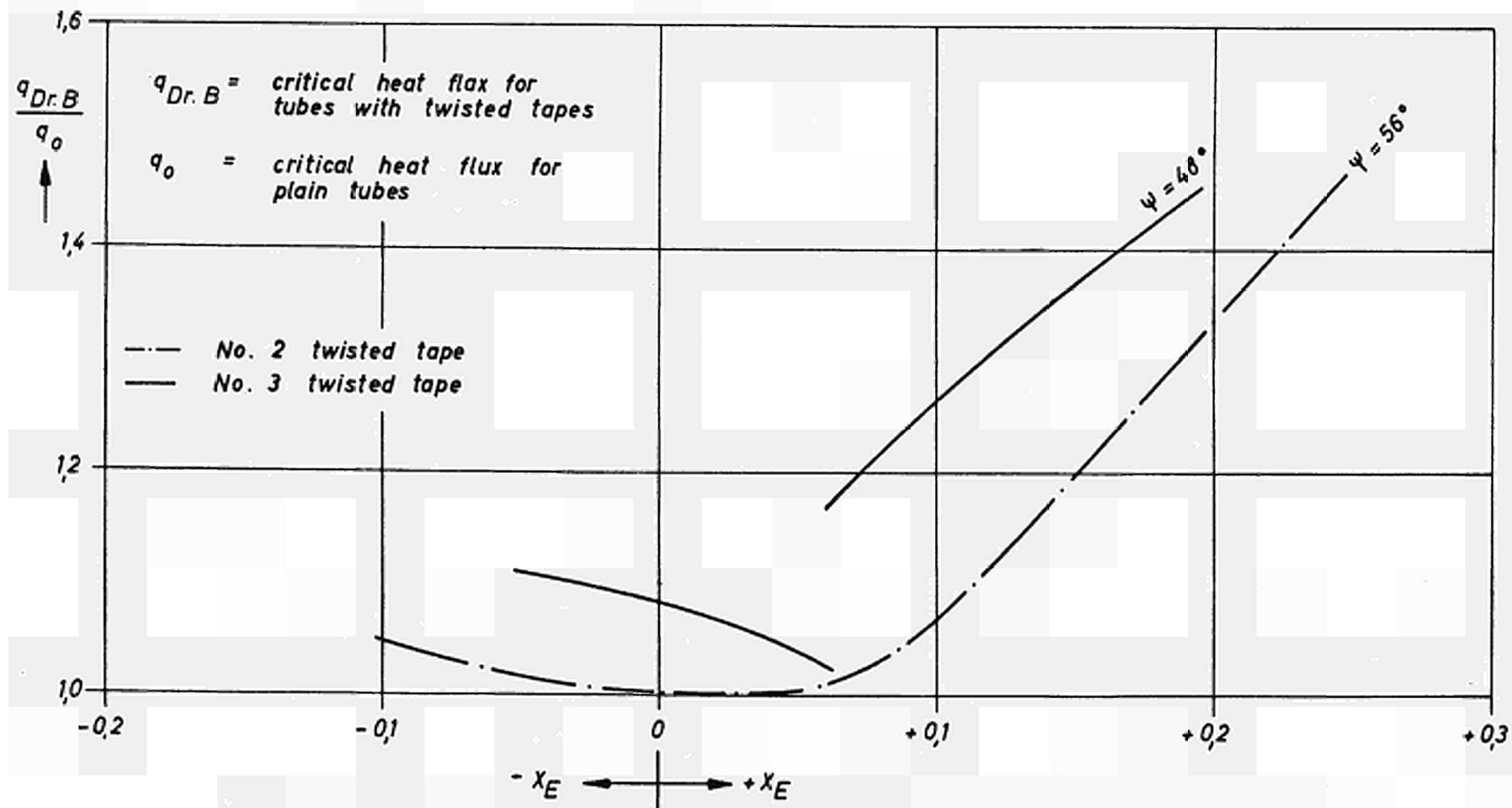
Relative change in critical heat flux due to No. 2 and No. 3 twisted tapes for
$m = 230$ g/cm^{2}s, $D = 0.7$ cm., $L/D = 40$ and $p = 70$ kg/cm^2

Fig. 30

Influence of No. 2 and No. 3 twisted tapes on the critical heat flux for $m = 290 \text{ g/cm}^2\text{s}$, $D = 0.7 \text{ cm}$, $L/D = 40$ and $p = 70 \text{ kg/cm}^2$

Fig. 31

$$\frac{q_{Dr.B.}}{q_0}$$

$q_{Dr.B.}$ = critical heat flux for tubes with twisted tapes

q_0 = critical heat flux for plain tubes

—·— No. 2 twisted tape
——— No. 3 twisted tape

$\psi = 48°$

$\psi = 56°$

$-x_E \longleftrightarrow +x_E$
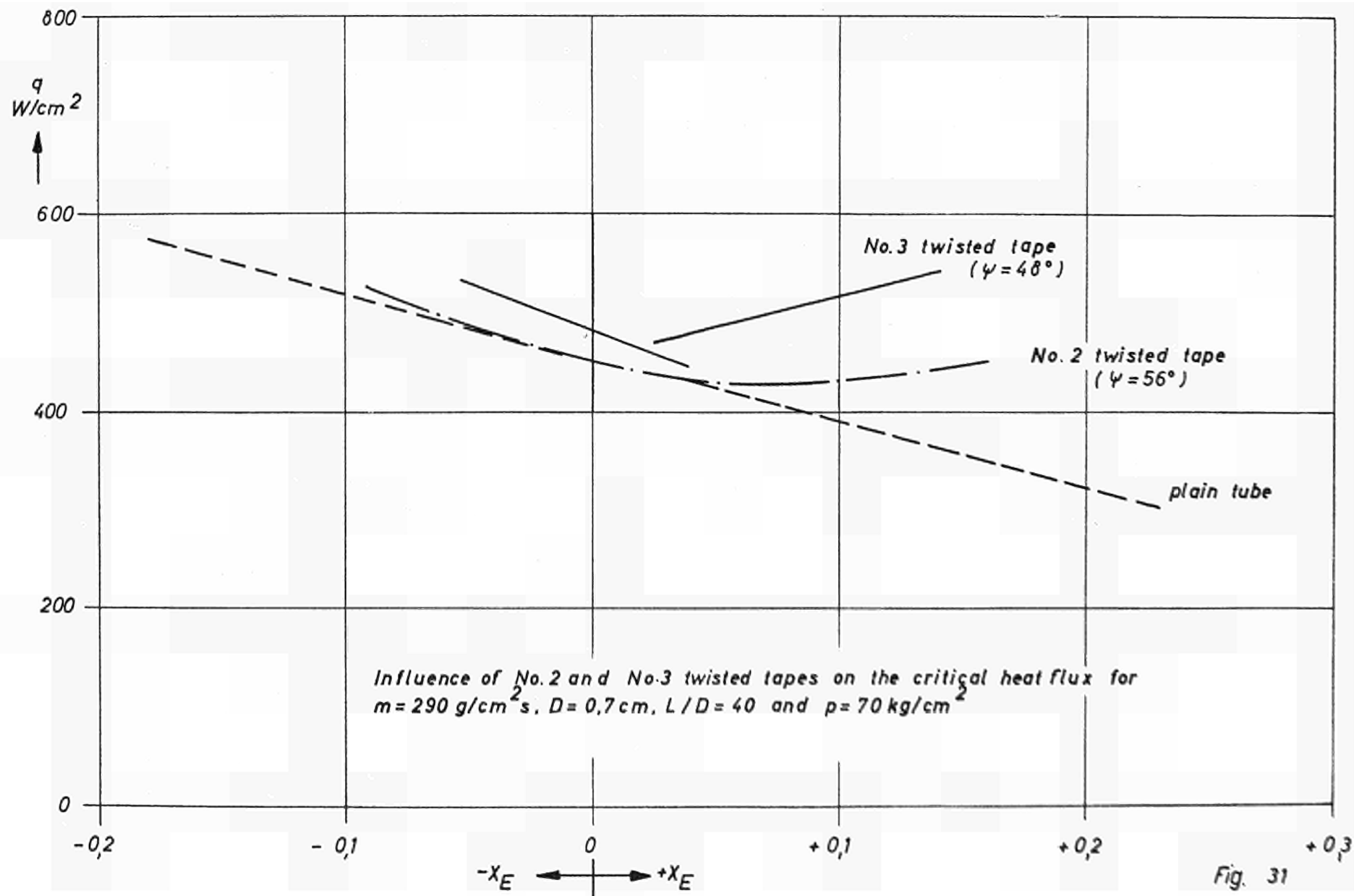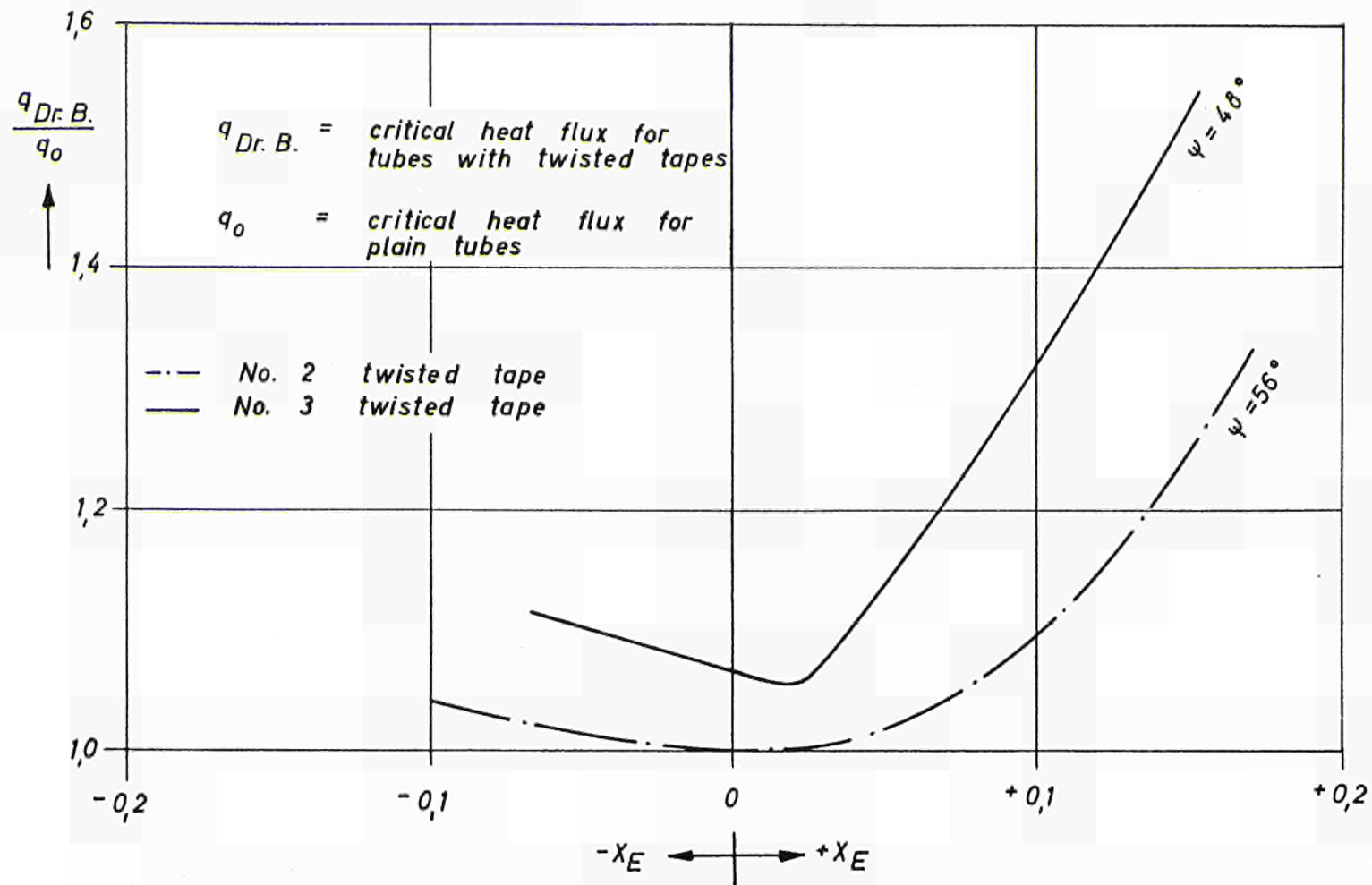
Relative change in critical heat flux due to No. 2 and No. 3 twisted tapes for $m = 290 \ g/cm^2 s$, $D = 0.7 \ cm.$, $L/D = 40$ and $p = 70 \ kg/cm^2$

Fig. 32
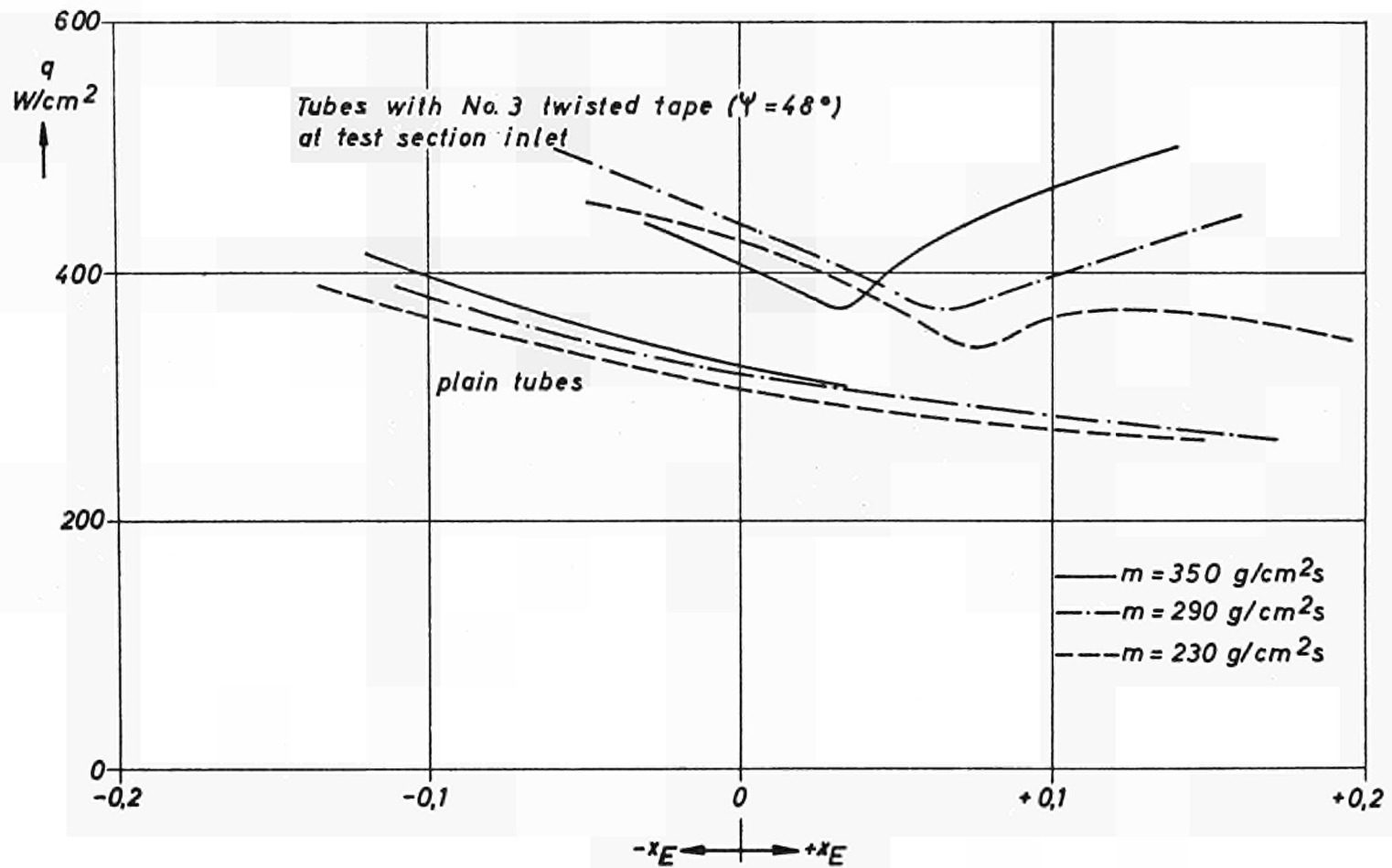
Influence of No. 3 twisted tape on the critical heat flux for
D = 0,7 cm, L/D = 40 and p = 100 kg/cm²

Fig. 33

Relative change in critical heat flux due to No. 3 twisted tape ($\psi = 48°$) at test section inlet for $D = 0.7$ cm., $L/D = 40$ and $p = 100$ kg/cm^2
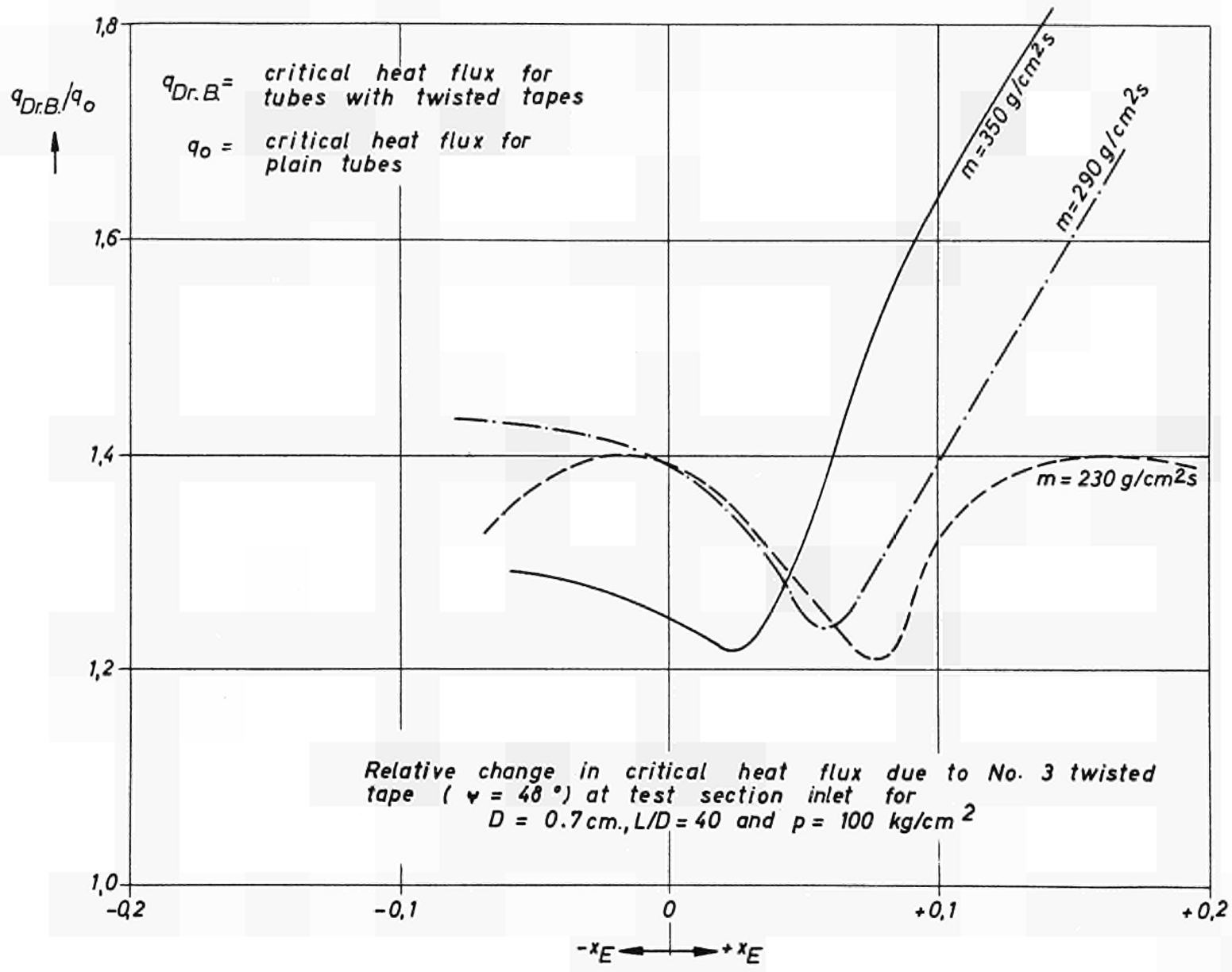
Fig. 34
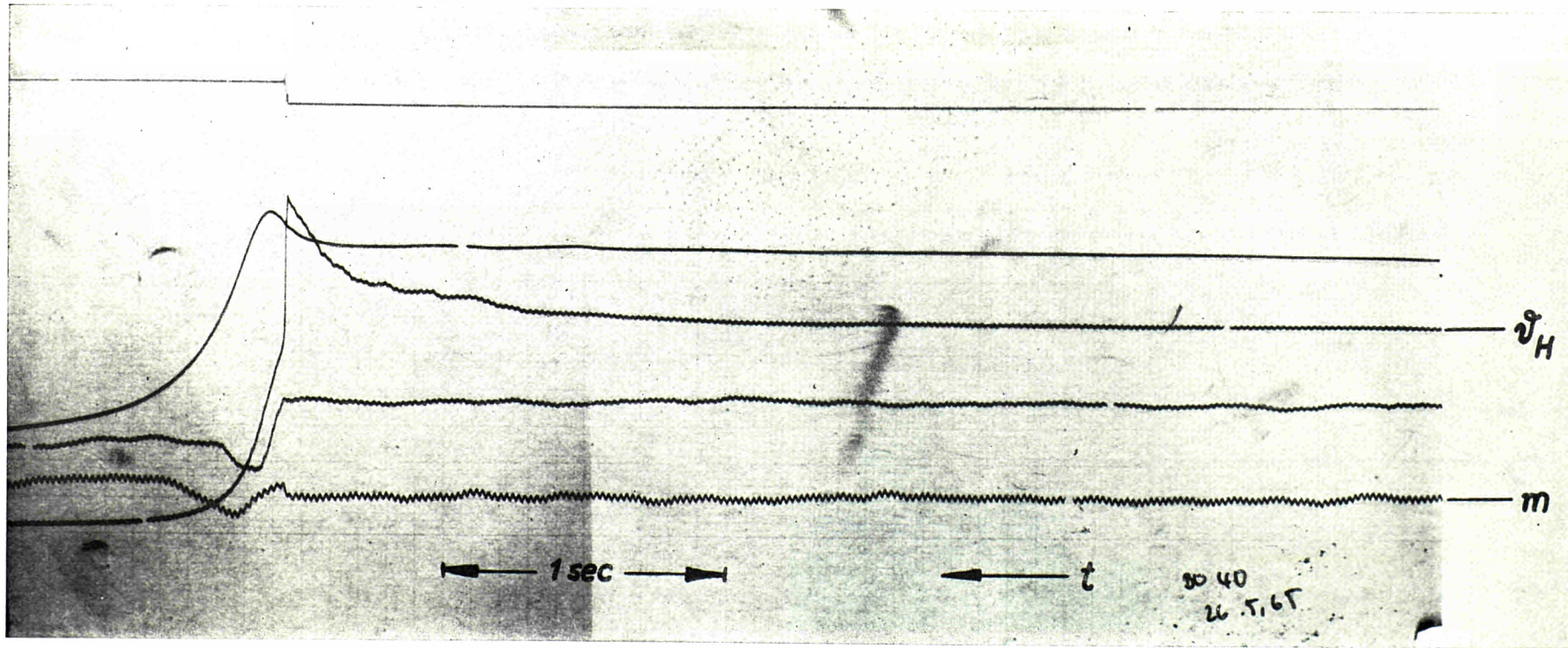
Fig. 35 : Variation of tube wall temperature and mass flow during transition from nucleate to film boiling for test channels with twisted tapes
m = 244.5 g/cm²s,   p = 70 kgf/cm², $X_E = -0.044$, $X_A = 0.163$, L/D = 40, $q_{BO} = 481.3$ W/cm²
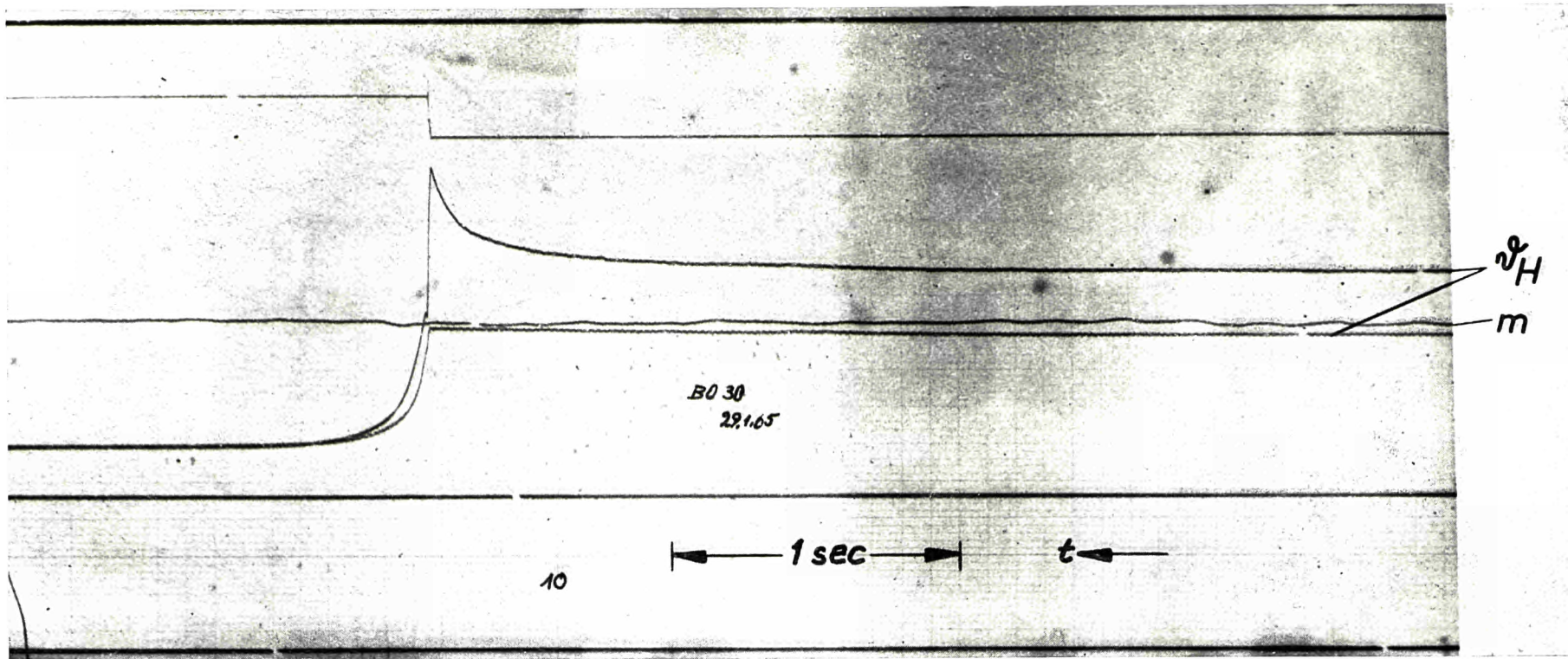
Fig. 36 : Variation of tube wall temperature and mass flow during transition from nucleate to fiim boiling for channels with small L/D ratio
$m = 231.8$ g/cm²s, $p = 70$ kgf/cm², $X_E = -0.0739$, $X_A = 0.0148$, $L/D = 10$, $q_{BO} = 800.6$, W/cm²
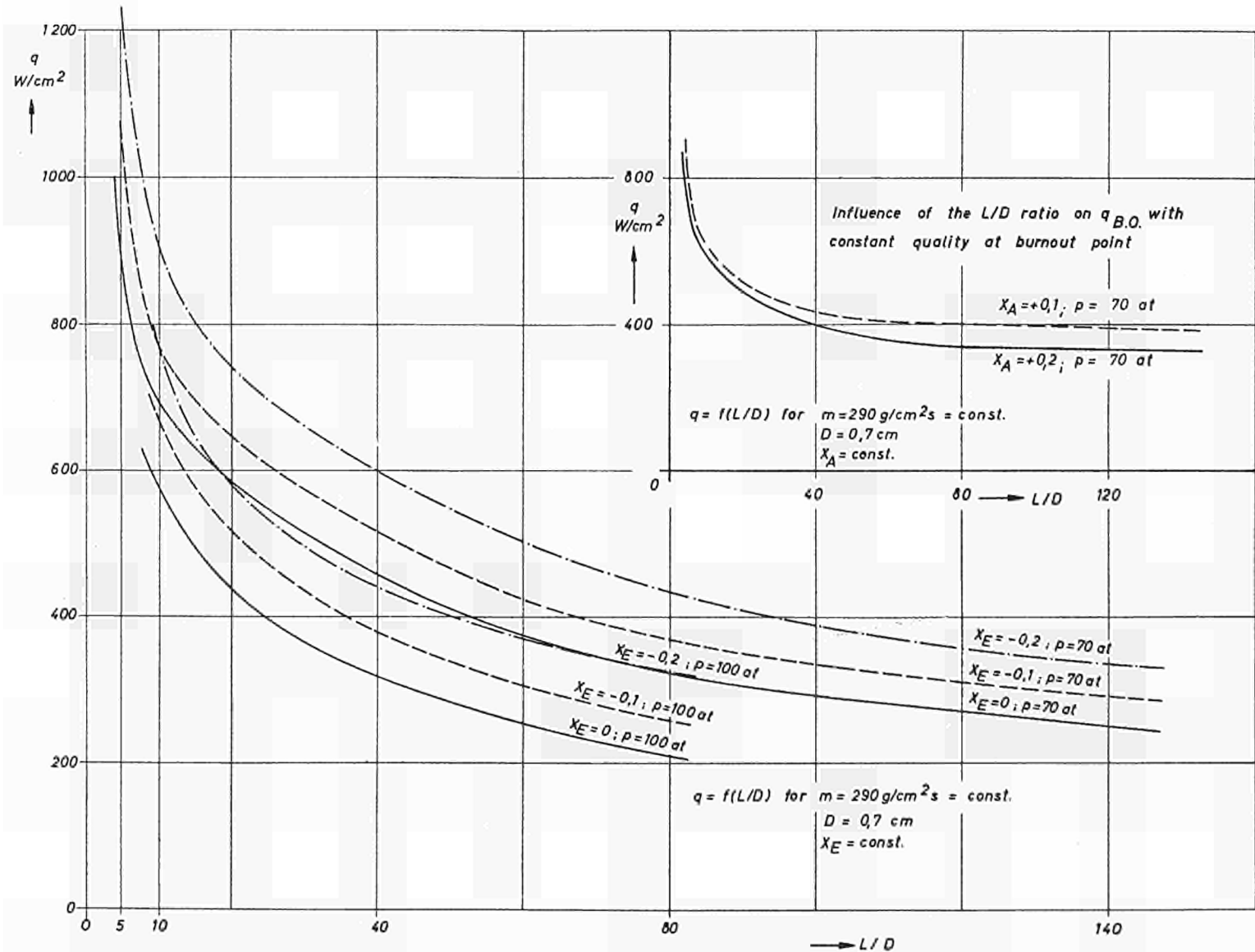
The critical heat flux versus L/D ratio with various qualitis for m = 290 g/cm²s and D = 0,7 cm.

Fig. 37
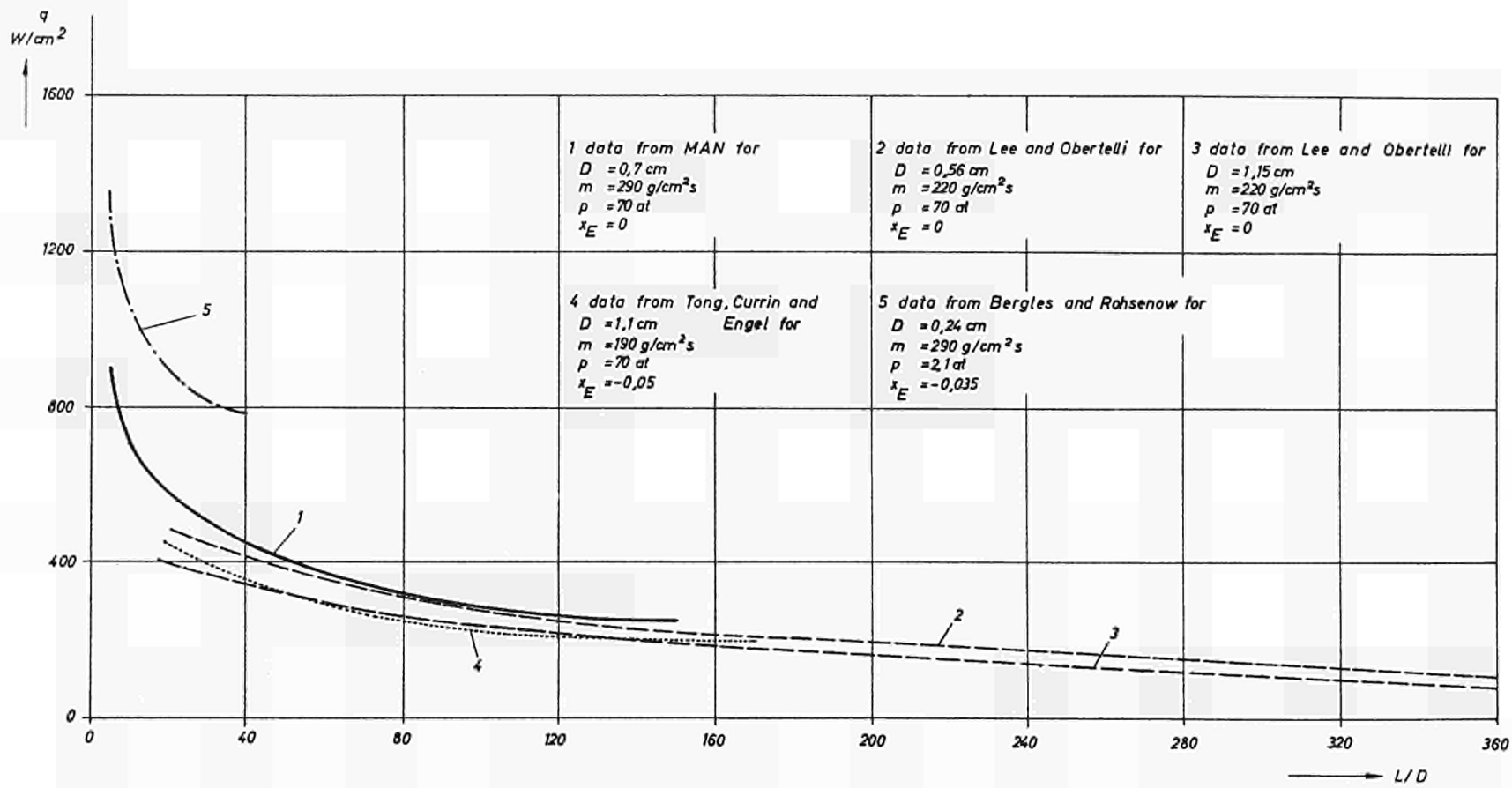
Influence of L/D ratio on critical heat flux. Summary of results of various publications

Fig. 38

0,5

0,41

0,33

power supply

h

i

k

l

tube wall

cooled side

14,5 15,5 16,5 17,5

a b c d e f g

0,08

0,16

0,25

m
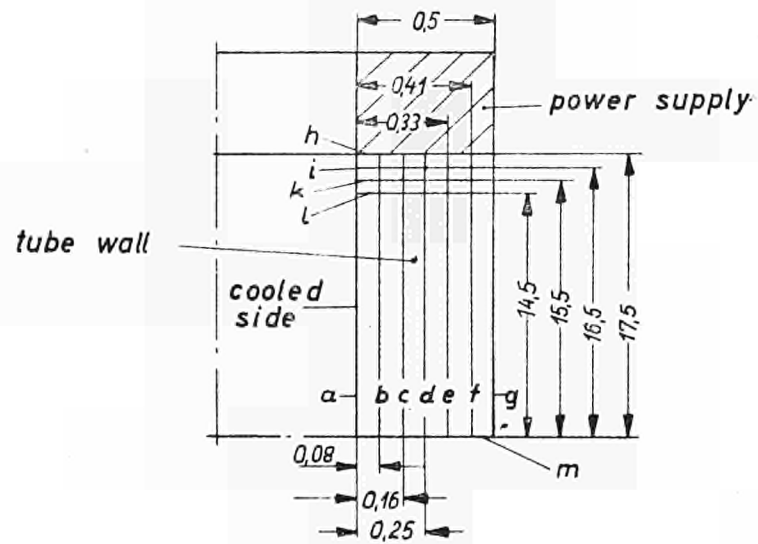
Temperature distribution in the wall of a test tube

Tube size: 7 mm. inside dia.
              35 mm. length
              0.5 mm. wall thickness
              940 w/cm^2 heat flux

°C

600

l ≙ m

k

i

400

h

200

wall thickness 0,5 mm

°C

600

f

g

400

a b c d e

270°C

200

0

half length = 17,5 mm
≙ L/D = 5

Fig. 39

All data were obtained with tubes having a
long hydro-dynamical inlet section

$\triangle\ m = 230\ g/cm^2 s$
$\square\ m = 290\ g/cm^2 s$
$\bigcirc\ m = 350\ g/cm^2 s$

$L/D = 5$

$L/D = 10$

$L/D = 40$

$L/D = 80$

$L/D = 140$

$-x_A \longleftarrow\ \longrightarrow +x_A$
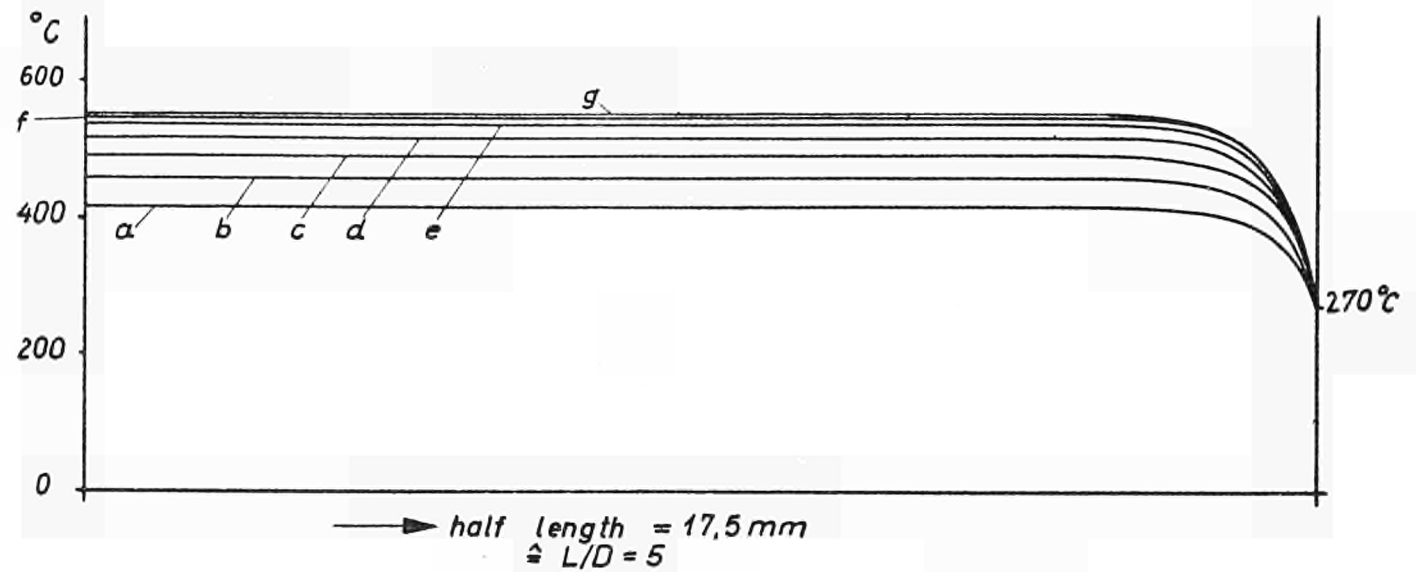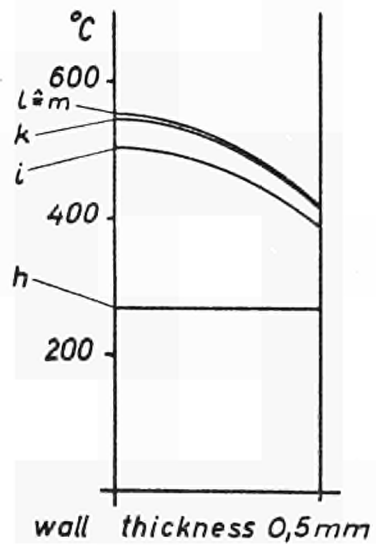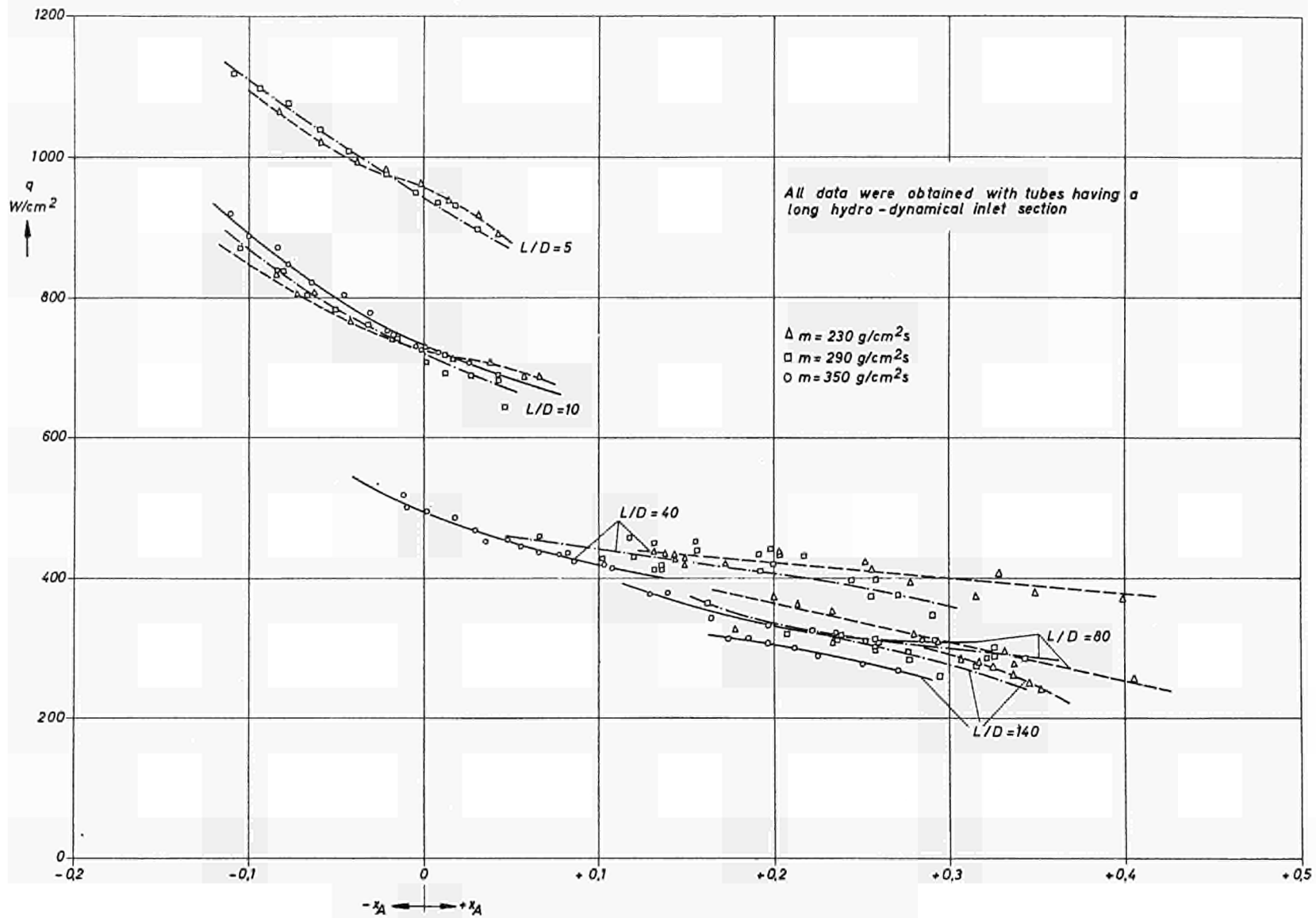
Critical heat flux for internally cooled tubes versus
steam quality at test section outlet $D = 0.7\ cm., p = 70\ kg/cm^2$

Fig. 40

q
W/cm^2

600

400

200

0

3

4

5

1

2

1   $m = 271 \ g/cm^2 s$
2   $m = 138 \ g/cm^2 s$
3   $m = 54 \ g/cm^2 s$
4   $m = 27 \ g/cm^2 s$
5   $m = 14 \ g/cm^2 s$

$L/D = 50$
$D = 0,305 \ cm$
$X_E = 0$

50   100   150   200   225,6

$\longrightarrow \quad p \quad at$
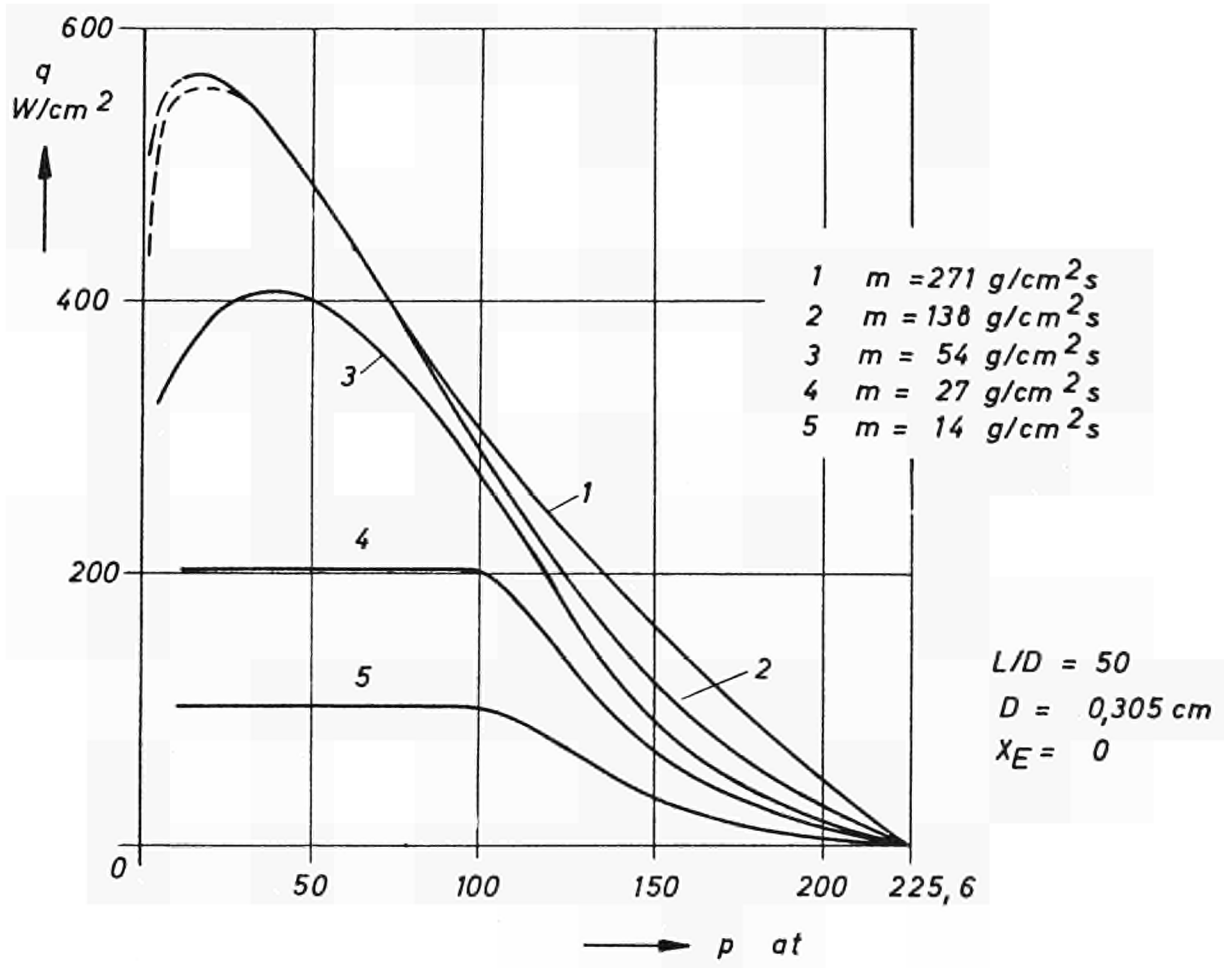
Influence of system pressure on
critical heat flux according to Macbeth

Fig. 41
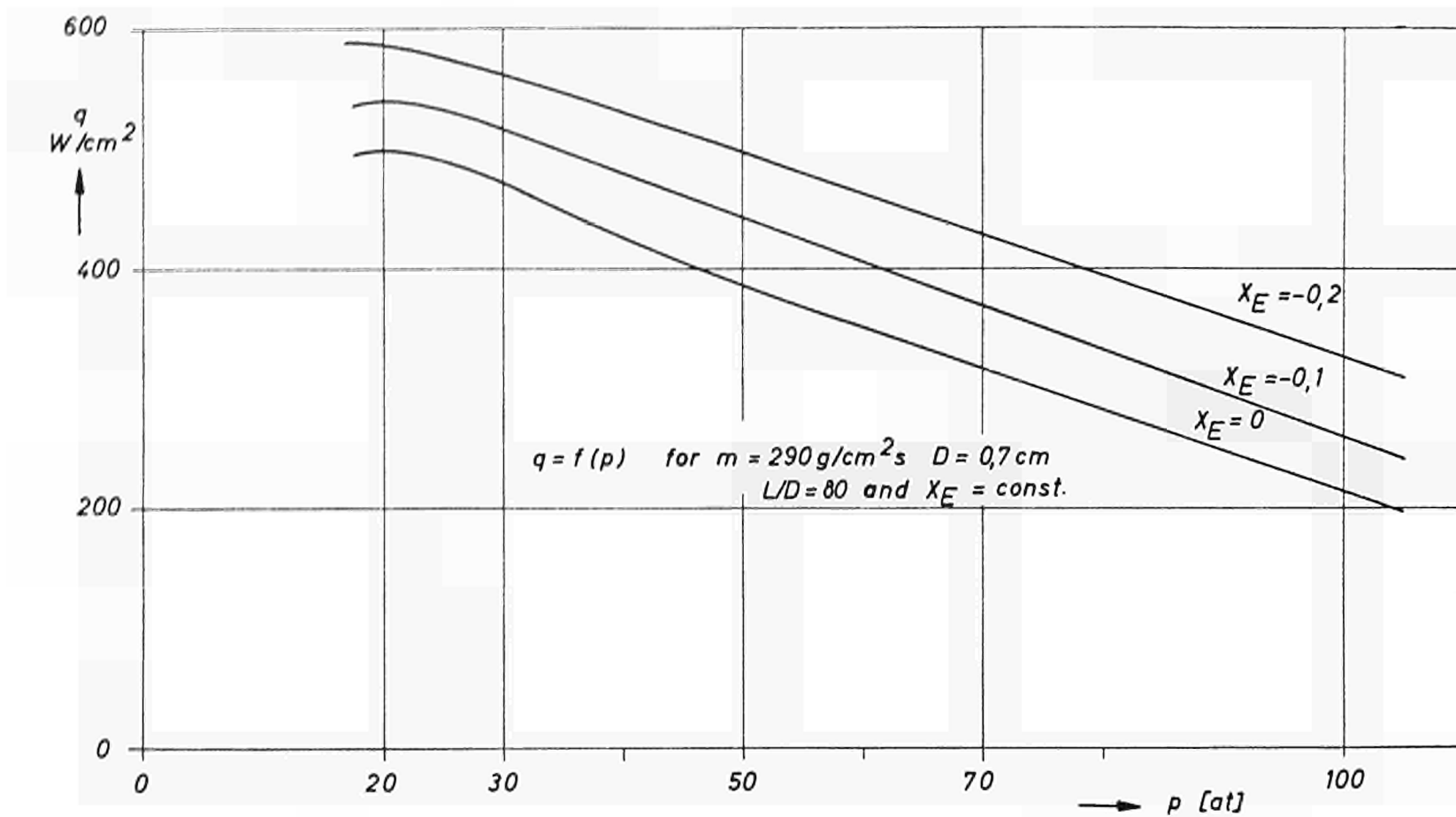
The critical heat flux versus system pressure for
$m = 290 \ g/cm^2s$, $D = 0.7 \ cm$, $L/D = 80$

Fig. 42

The critical heat flux versus system pressure for
$m = 350 \ g/cm^2 s$, $D = 0.7 cm$, $L/D = 80$
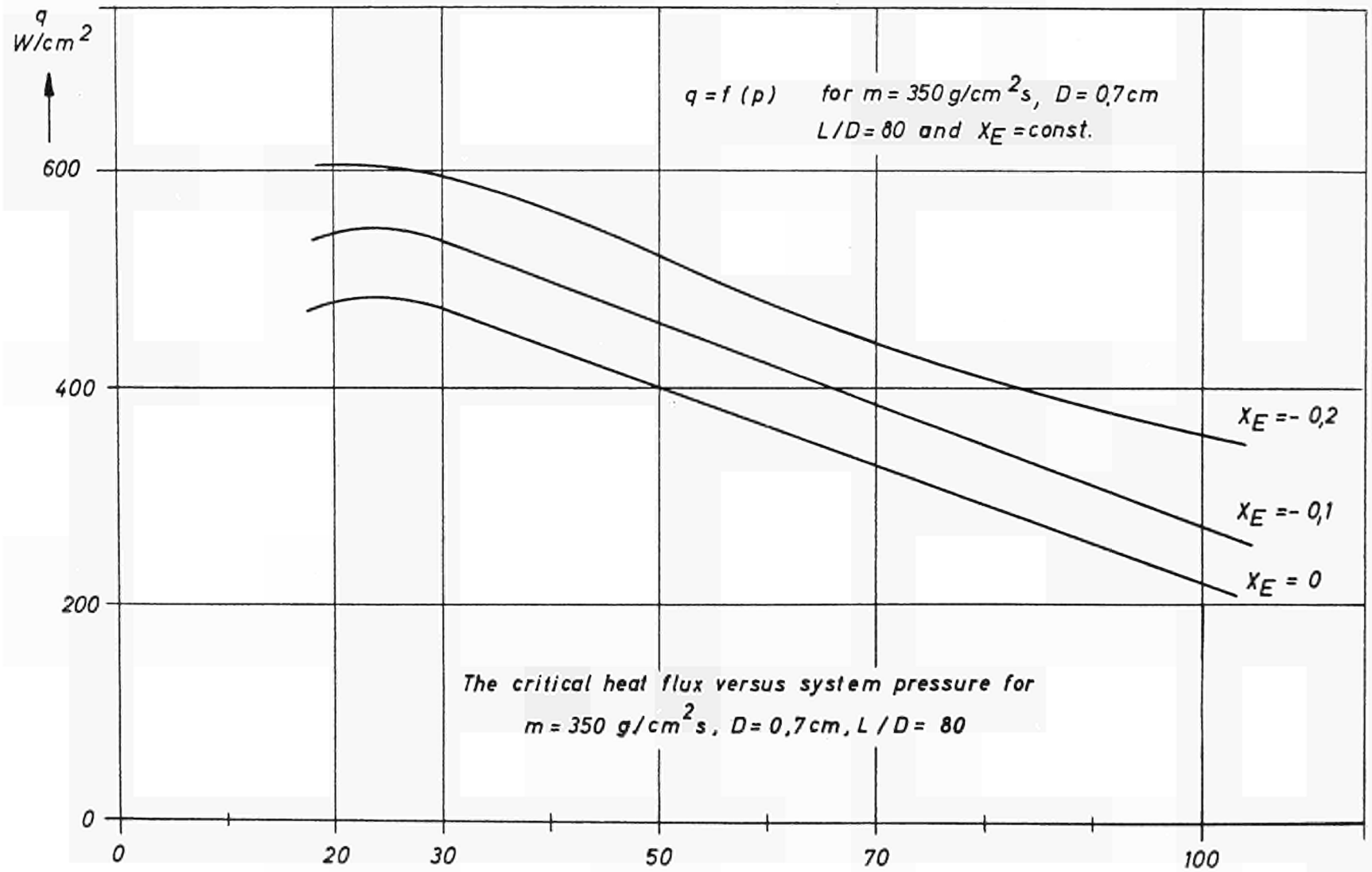
Fig. 43
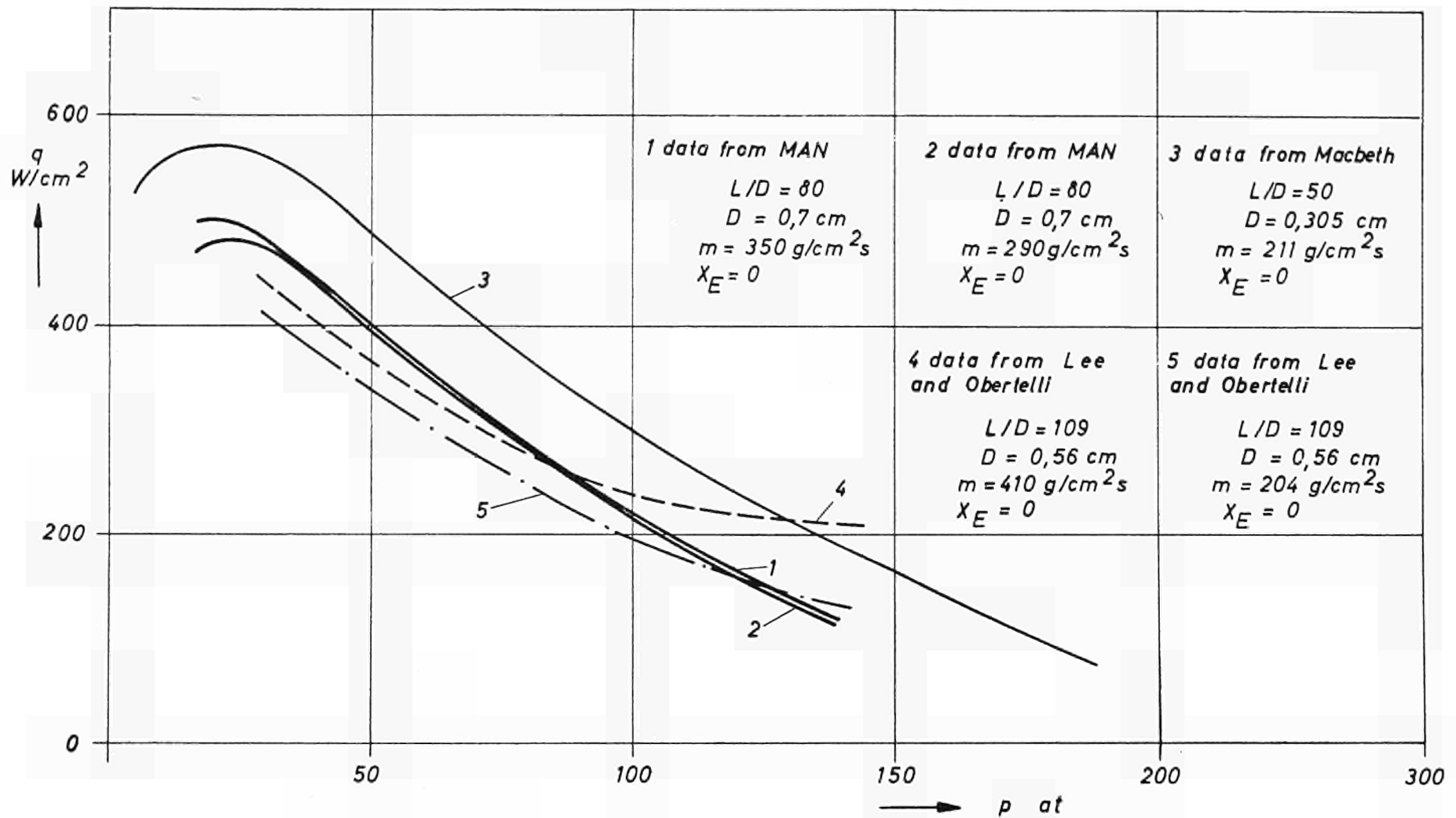
Comparison of influence of pressure on $q_{B.O.}$ based on data from MAN, Macbeth, Lee and Obertelli

Labels in the figure:

q W/cm² (vertical axis)

p at (horizontal axis)

1 data from MAN
L/D = 80
D = 0,7 cm
m = 350 g/cm²s
X_E = 0

2 data from MAN
L/D = 80
D = 0,7 cm
m = 290 g/cm²s
X_E = 0

3 data from Macbeth
L/D = 50
D = 0,305 cm
m = 211 g/cm²s
X_E = 0

4 data from Lee and Obertelli
L/D = 109
D = 0,56 cm
m = 410 g/cm²s
X_E = 0

5 data from Lee and Obertelli
L/D = 109
D = 0,56 cm
m = 204 g/cm²s
X_E = 0

Fig. 44
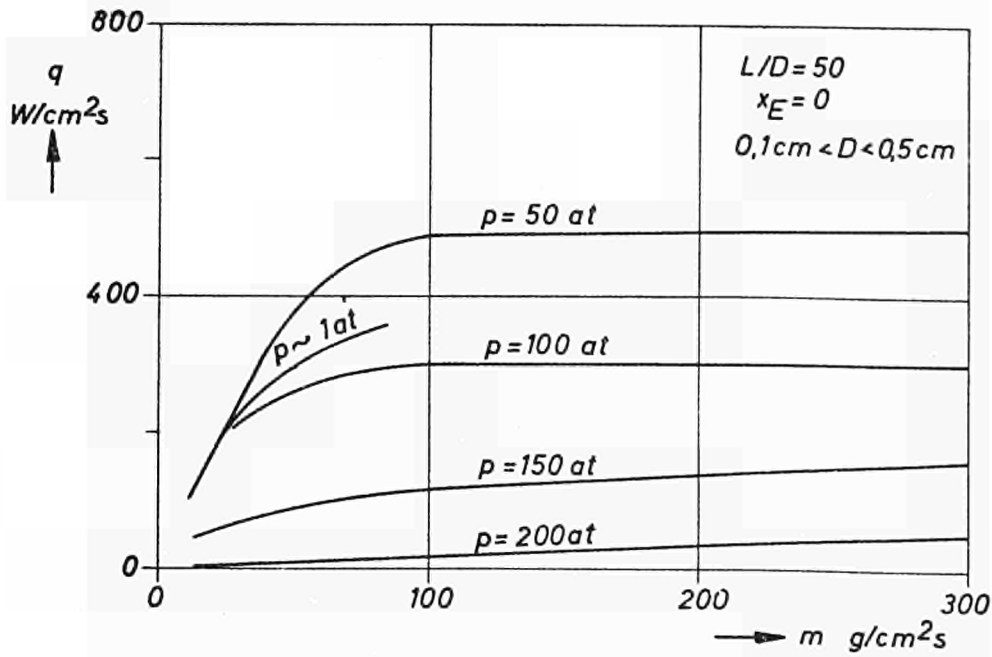
Influence of mass velocity on $q_{B.O.}$ according to Macbeth
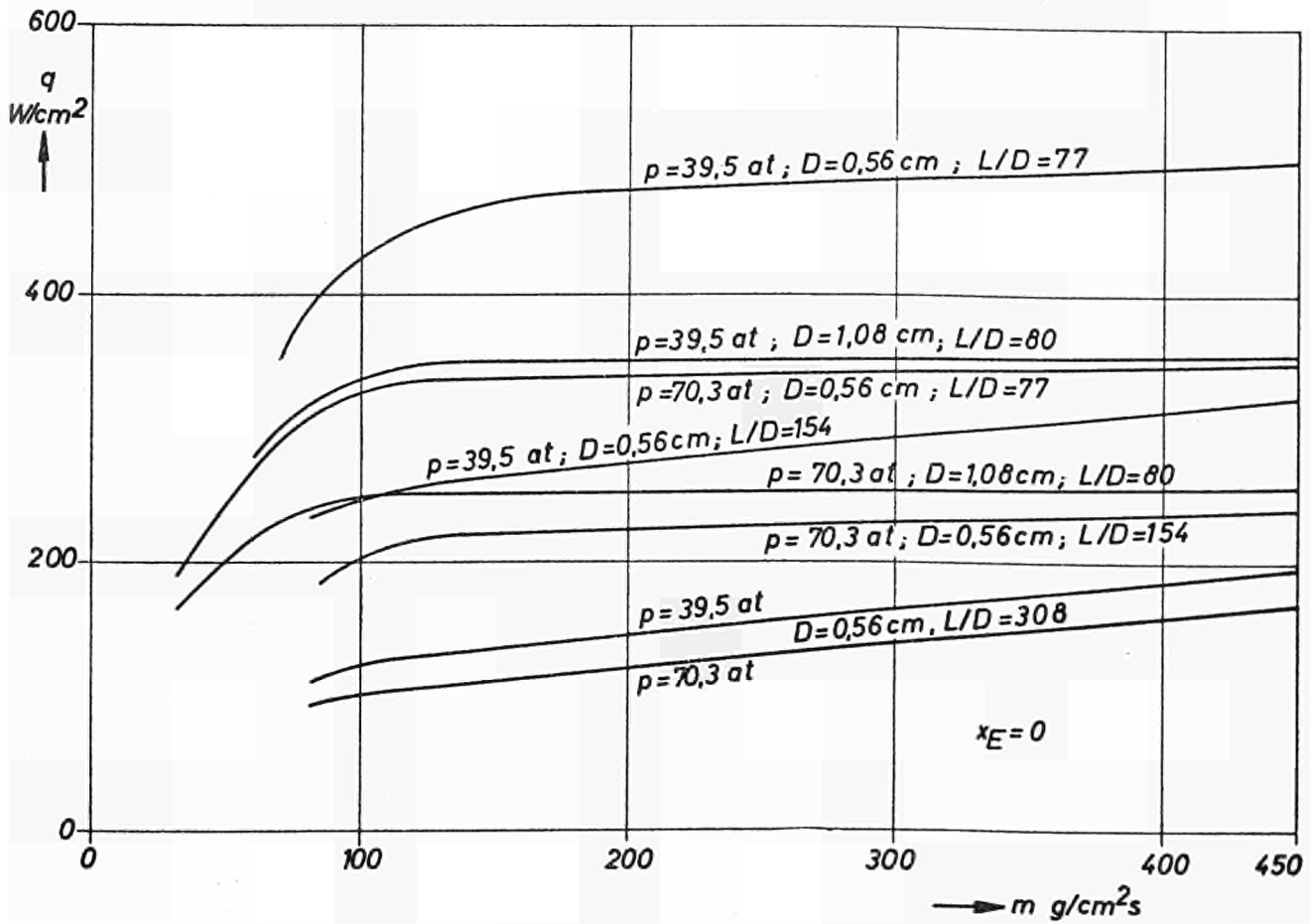
Influence of mass velocity on $q_{B.O.}$ according to Lee and Obertelli

Fig. 45
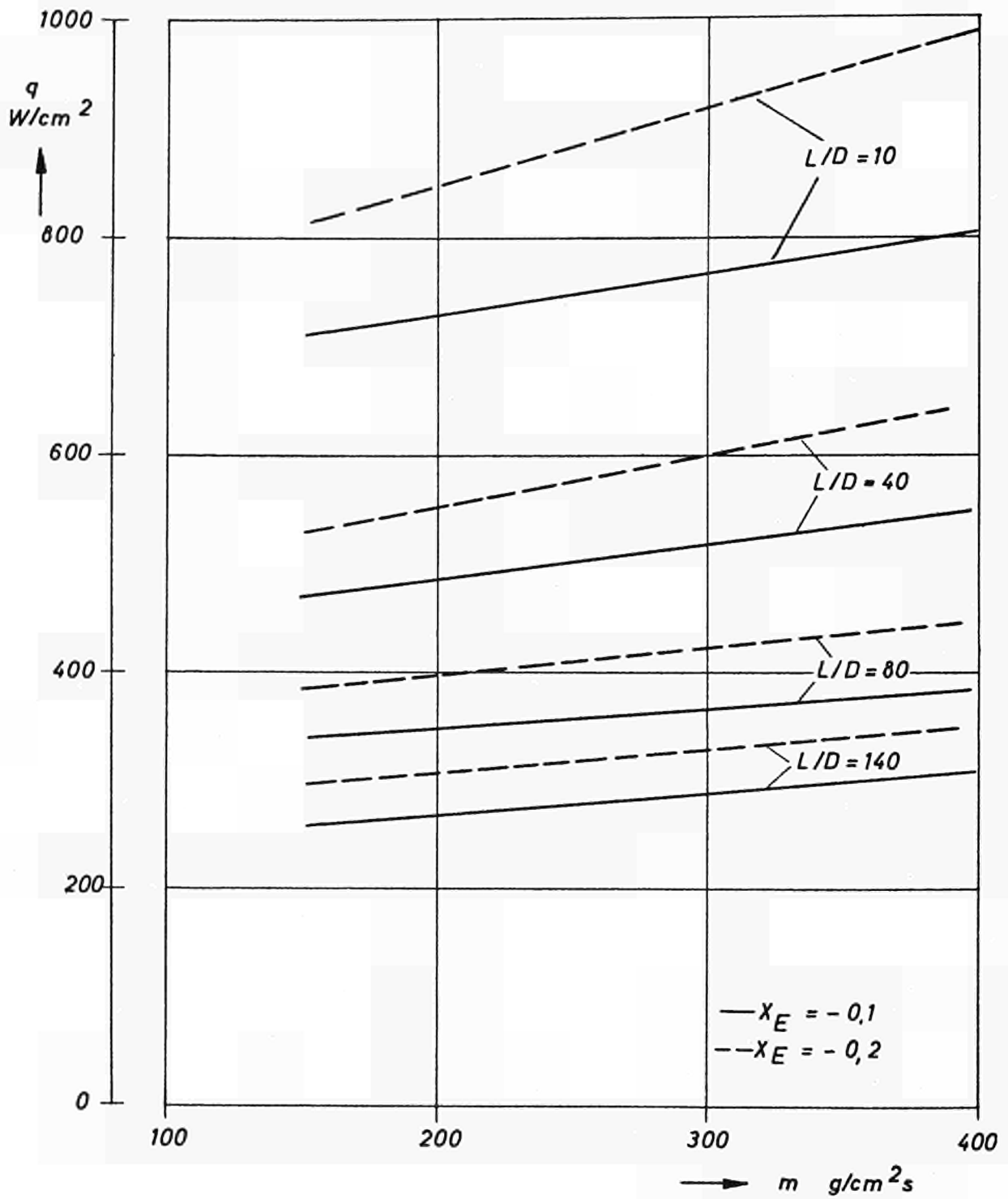
Influence of mass velocity on $q_{B.O.}$ for $p = 70$ kg/cm^2 and $D = 0.7$ cm.

Fig. 46
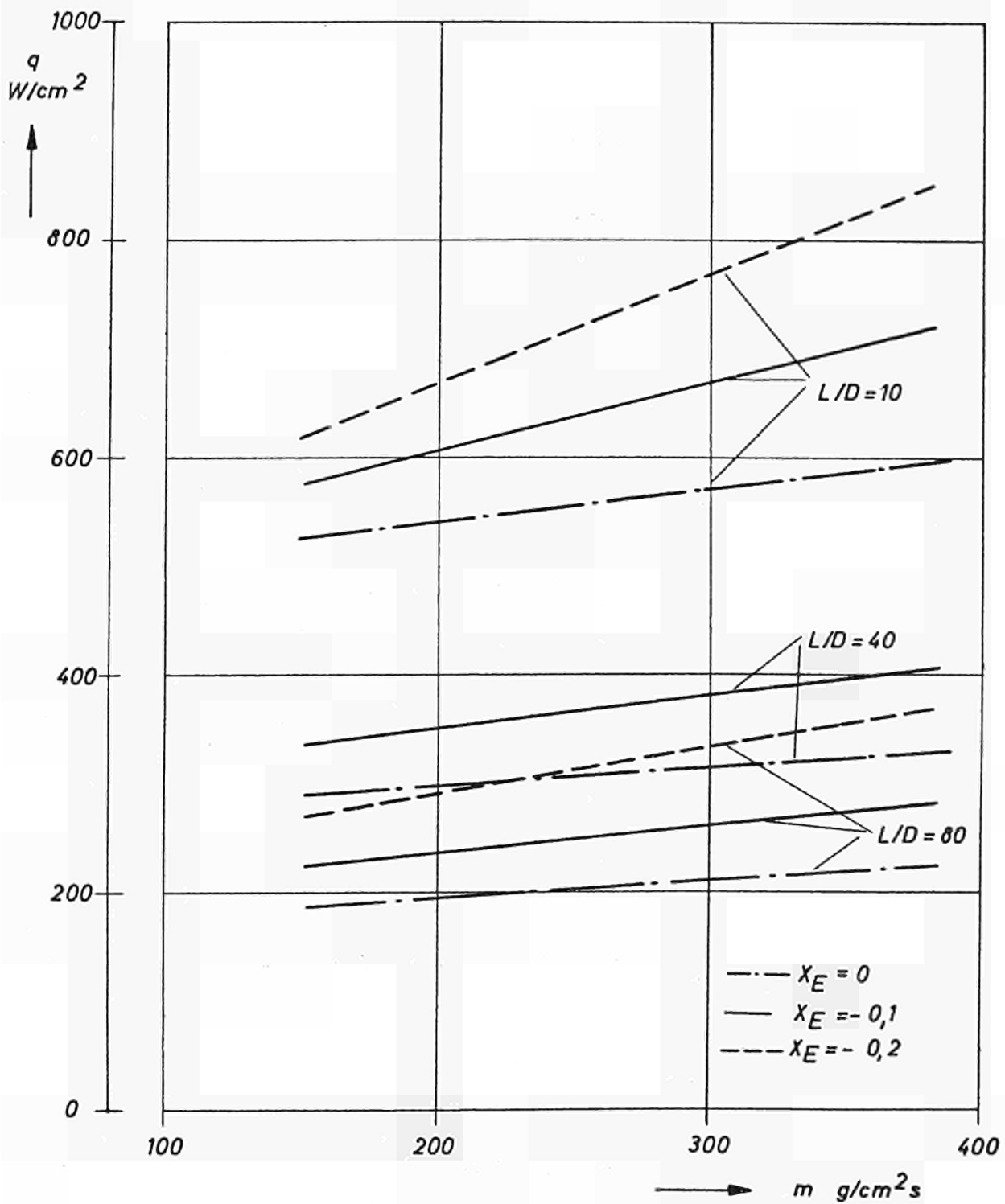
Influence of mass velocity on $q_{B.O.}$
for $p = 100$ kg/cm^2 and $D = 0.7$ cm.

Fig. 47

Weatherhead [18]

Menegus [11]

Lee and Obertelli [27]

q_0 = critical heat flux for D = 1.0 cm.

D [cm]
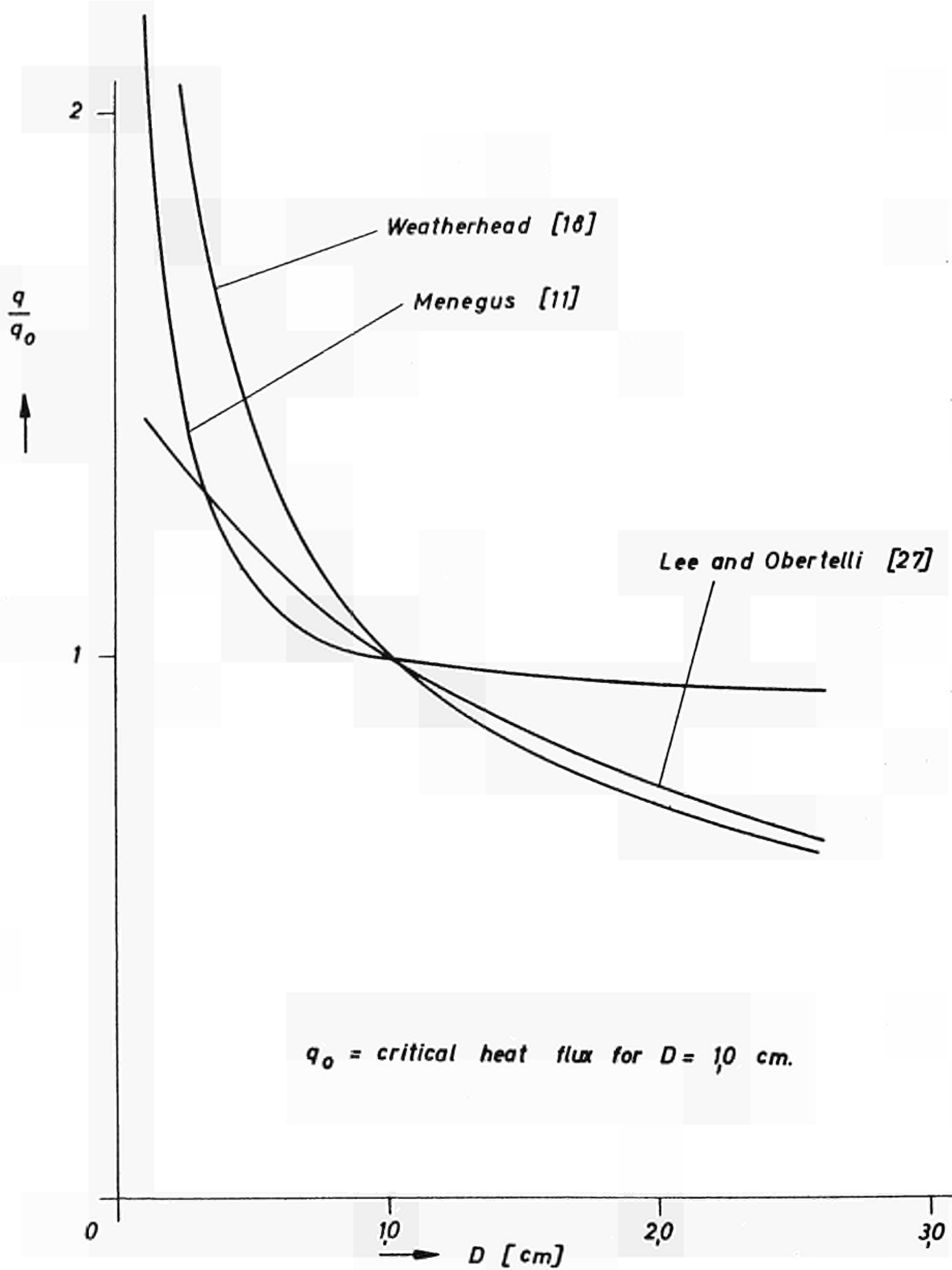
Relative change in critical heat flux as a function of tube diameter

Fig. 48

$q = f(D)$

for $m = 230\ g/cm^2\ s$, $L/D = 40$
and $X_E = const.$

$X_E = -0.2$, $p = 70\ at$

$X_E = -0.1$, $p = 70\ at$

$X_E = -0.2$, $p = 100\ at$

$X_E = 0$, $p = 70\ at$

$X_E = -0.1$, $p = 100\ at$

$X_E = 0$, $p = 100\ at$

The influence of the tube diameter on the critical heat flux for
$m = 230\ g/cm^2\ s$ and $L/D = 40$
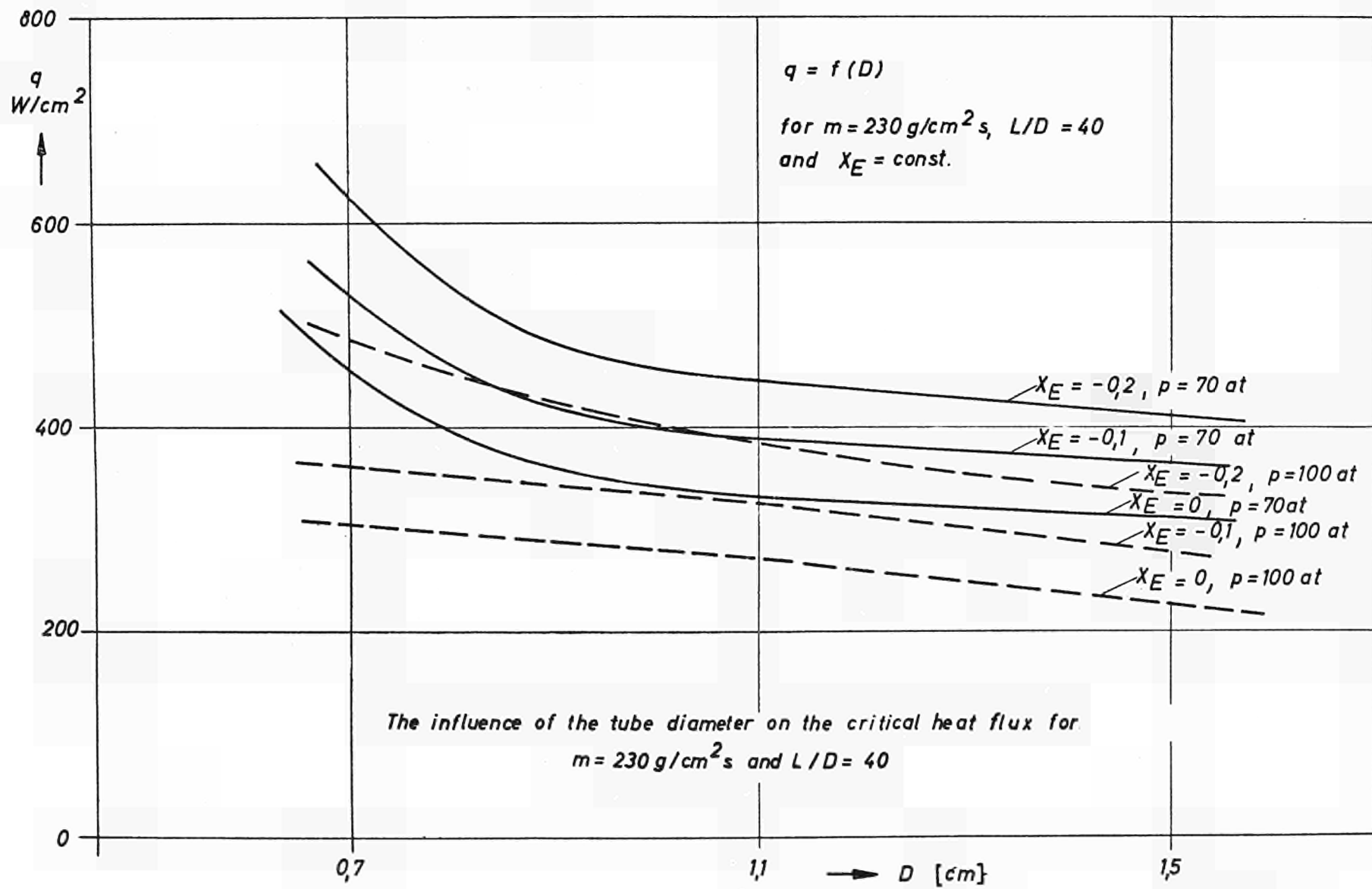
Fig. 49
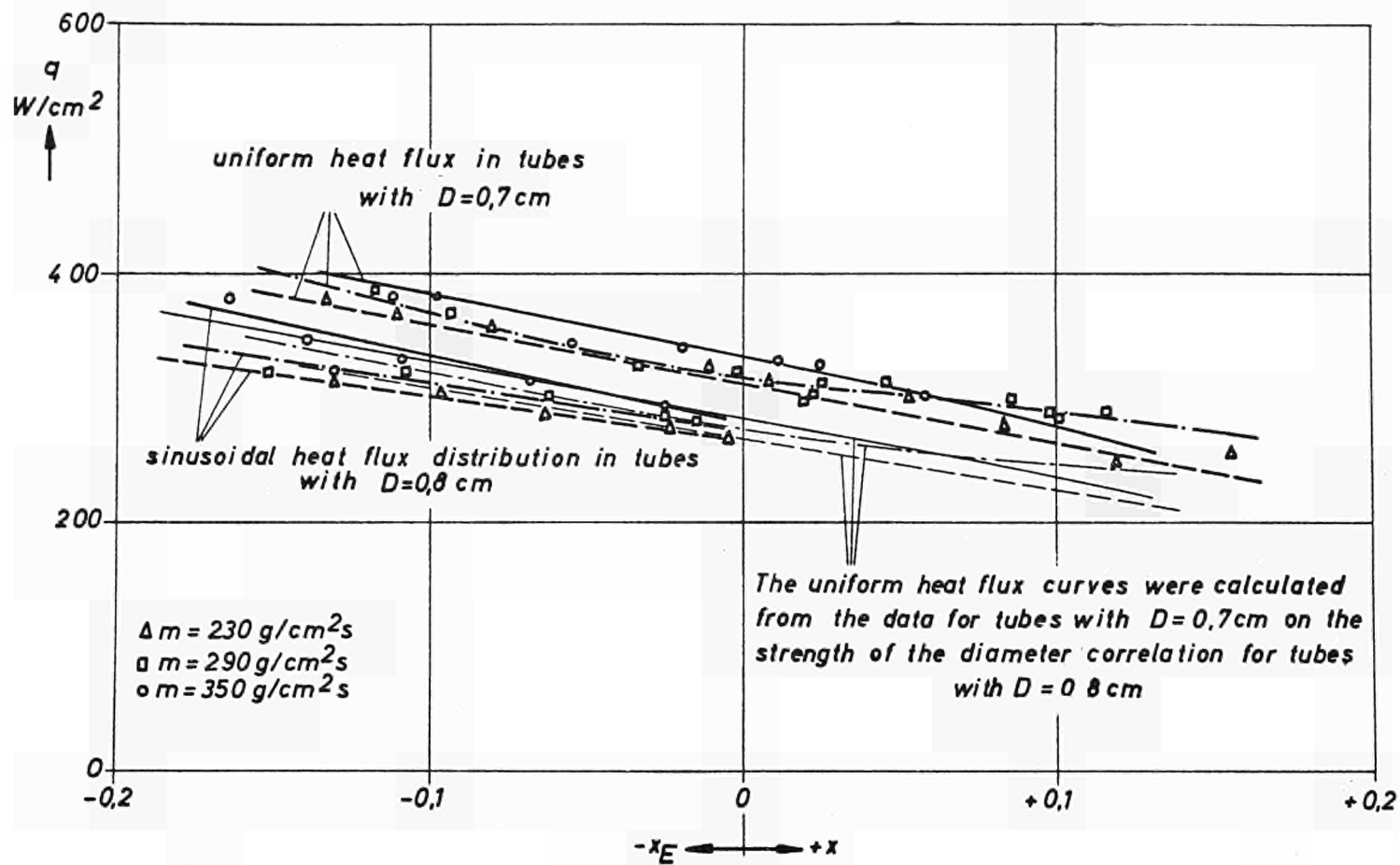
Comparison of critical heat fluxes between tubes with uniform and sinusoidal heat flux distribution with p= 70 kg/cm² and L/D = 80

Fig. 50
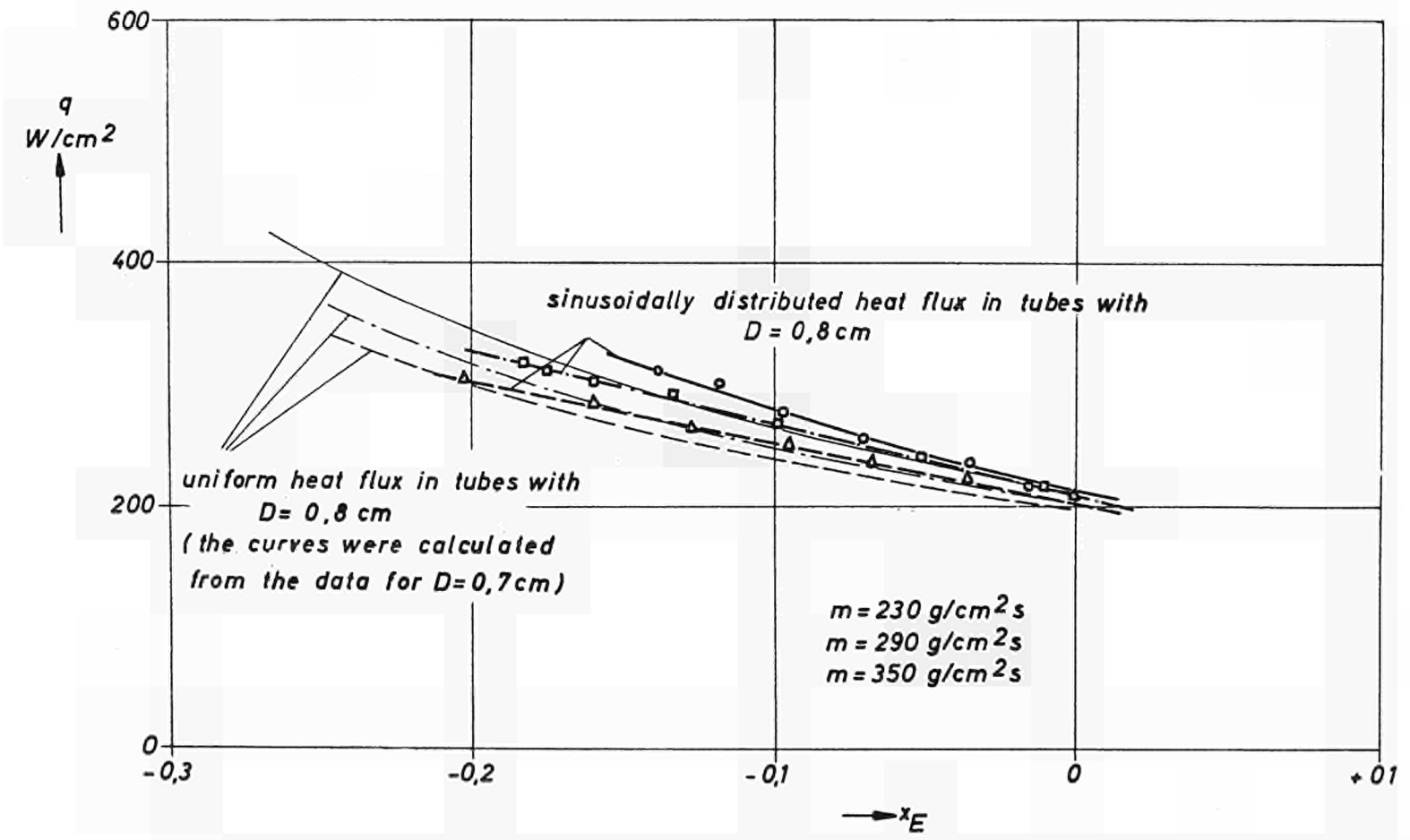
Comparison of the critical heat flux between tubes with uniform and sinusoidally distributed heat flux at p=100 kg/cm² and L/D = 80

Fig. 51
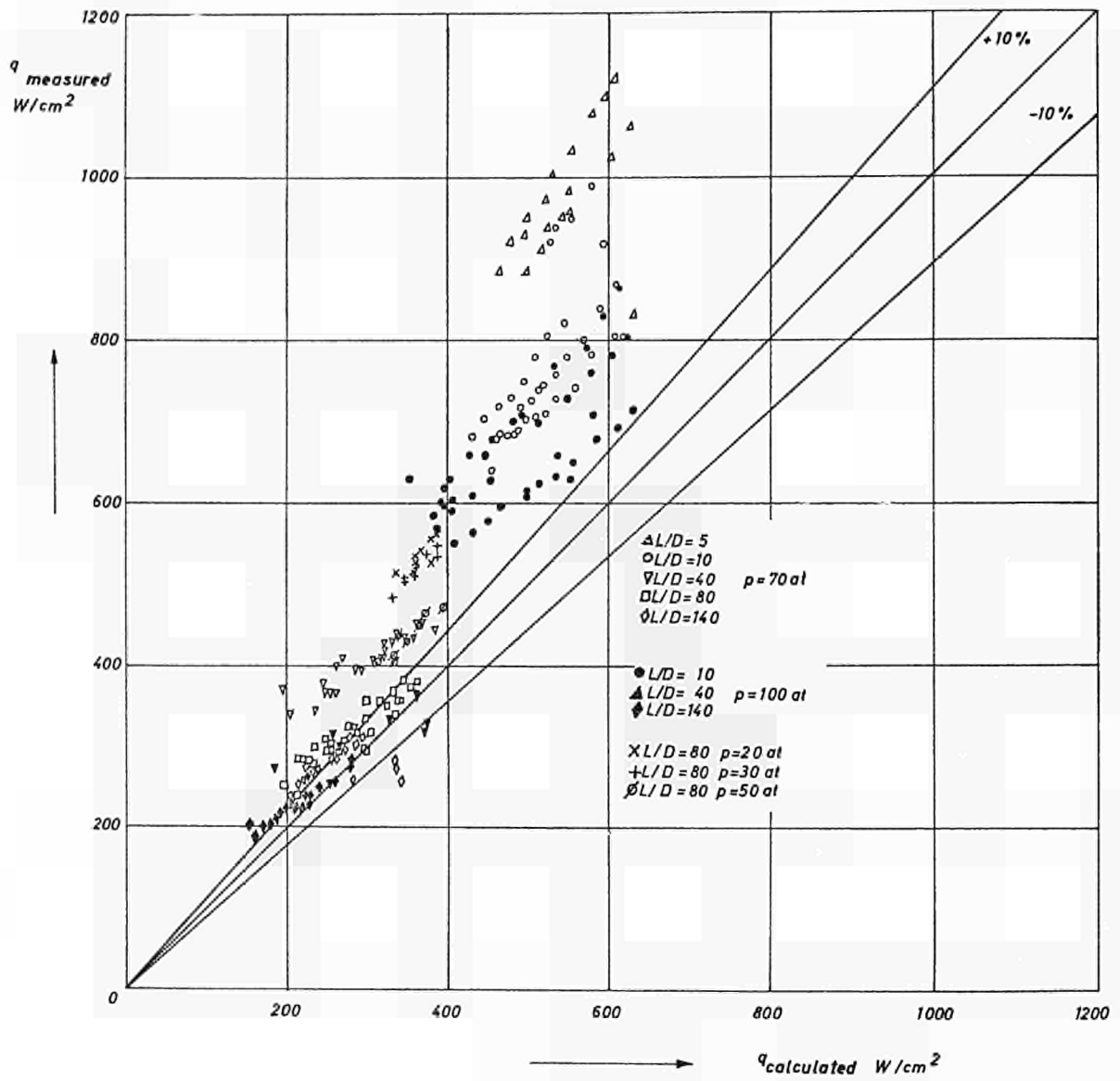
Comparison of MAN data for D = 0.7 cm. with original CISE correlation

Fig. 52
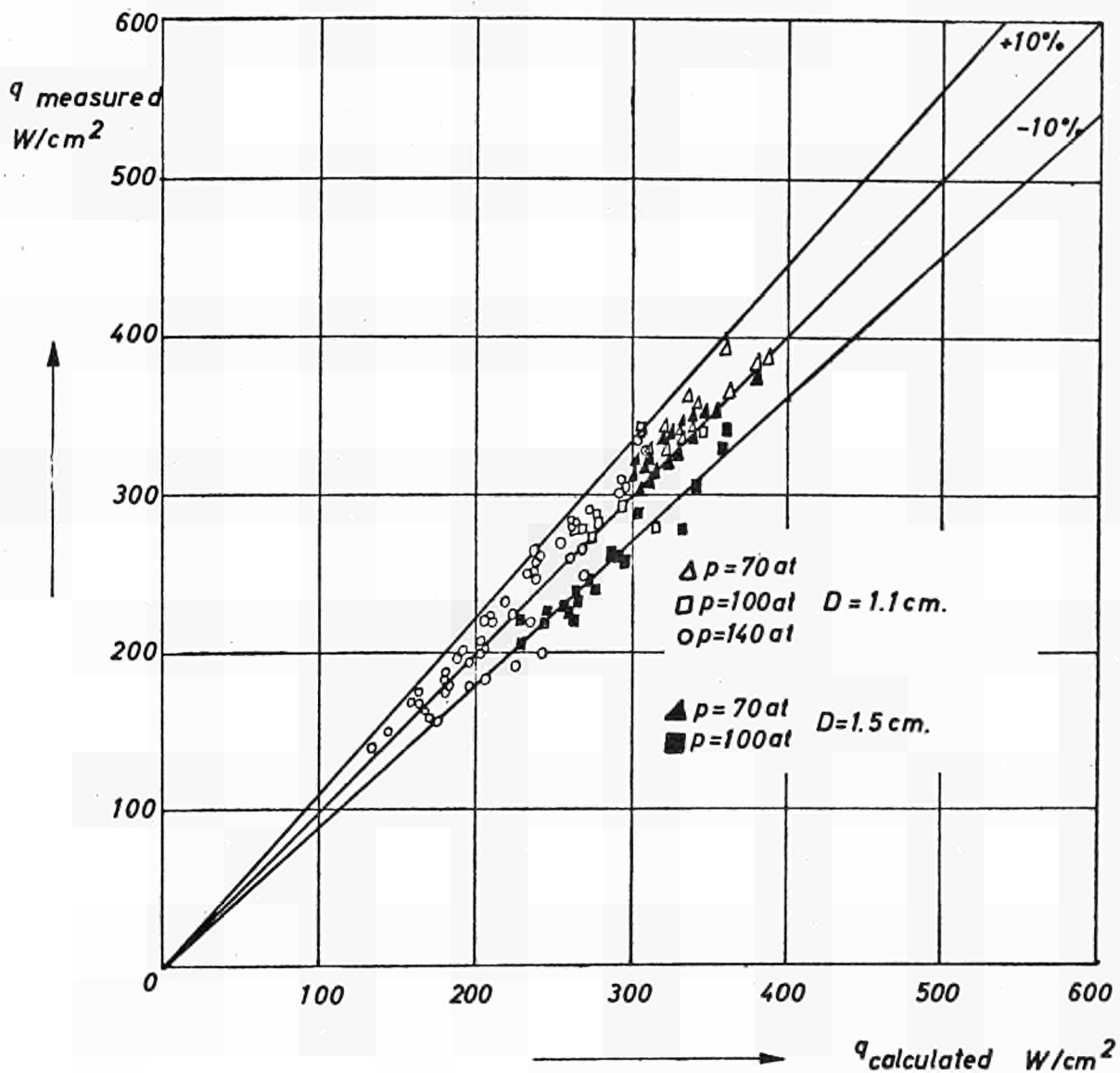
Comparison of MAN data for tubes with D = 1.1 cm. and 1.5 cm. with original CISE correlation

Fig. 53
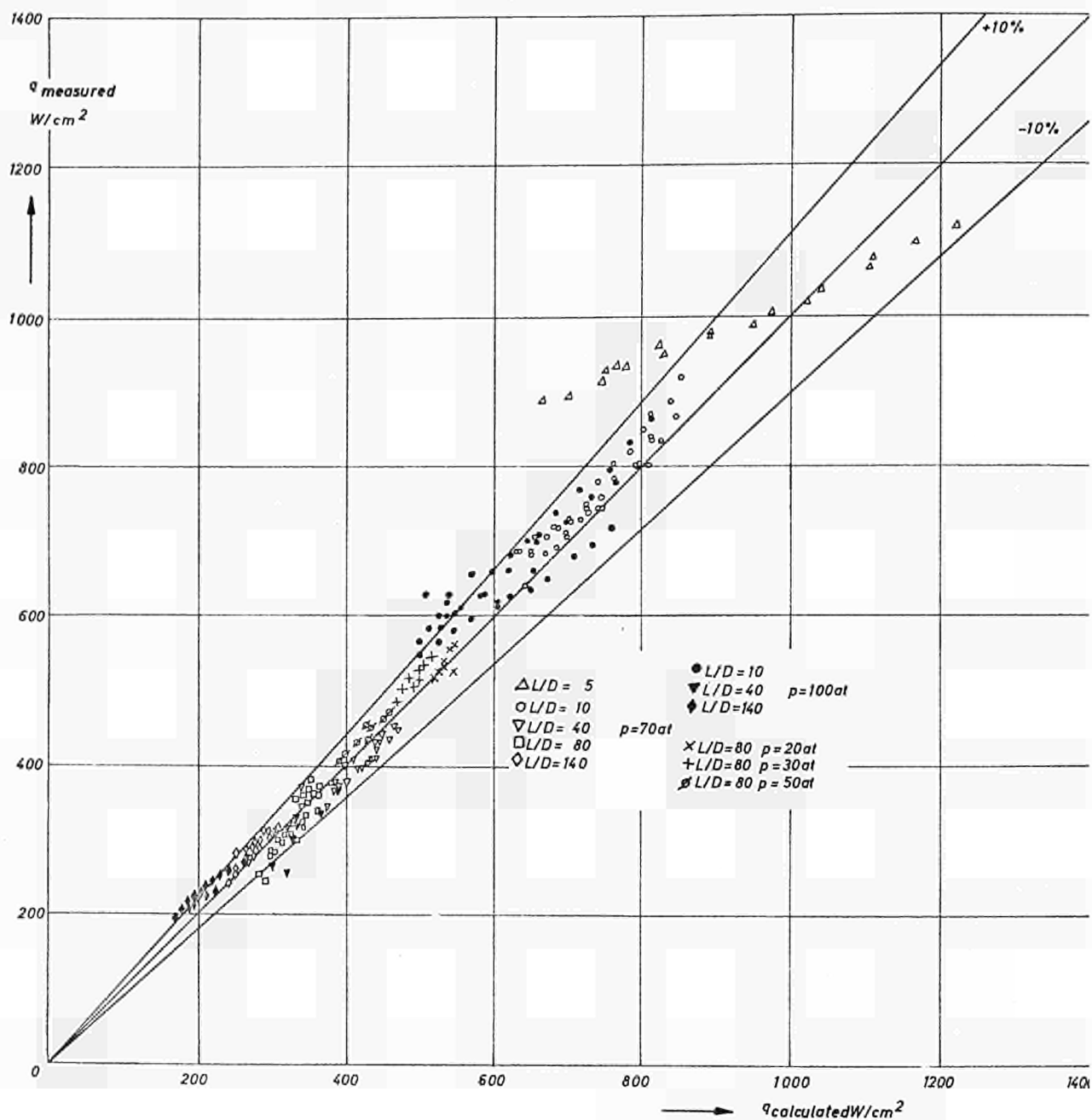
Comparison of MAN data for D = 0.7 cm. with the extended CISE correlation

Fig. 54

Data from MAN, Lee and Obertelli, CISE
with the extended CISE correlation

Fig. 55
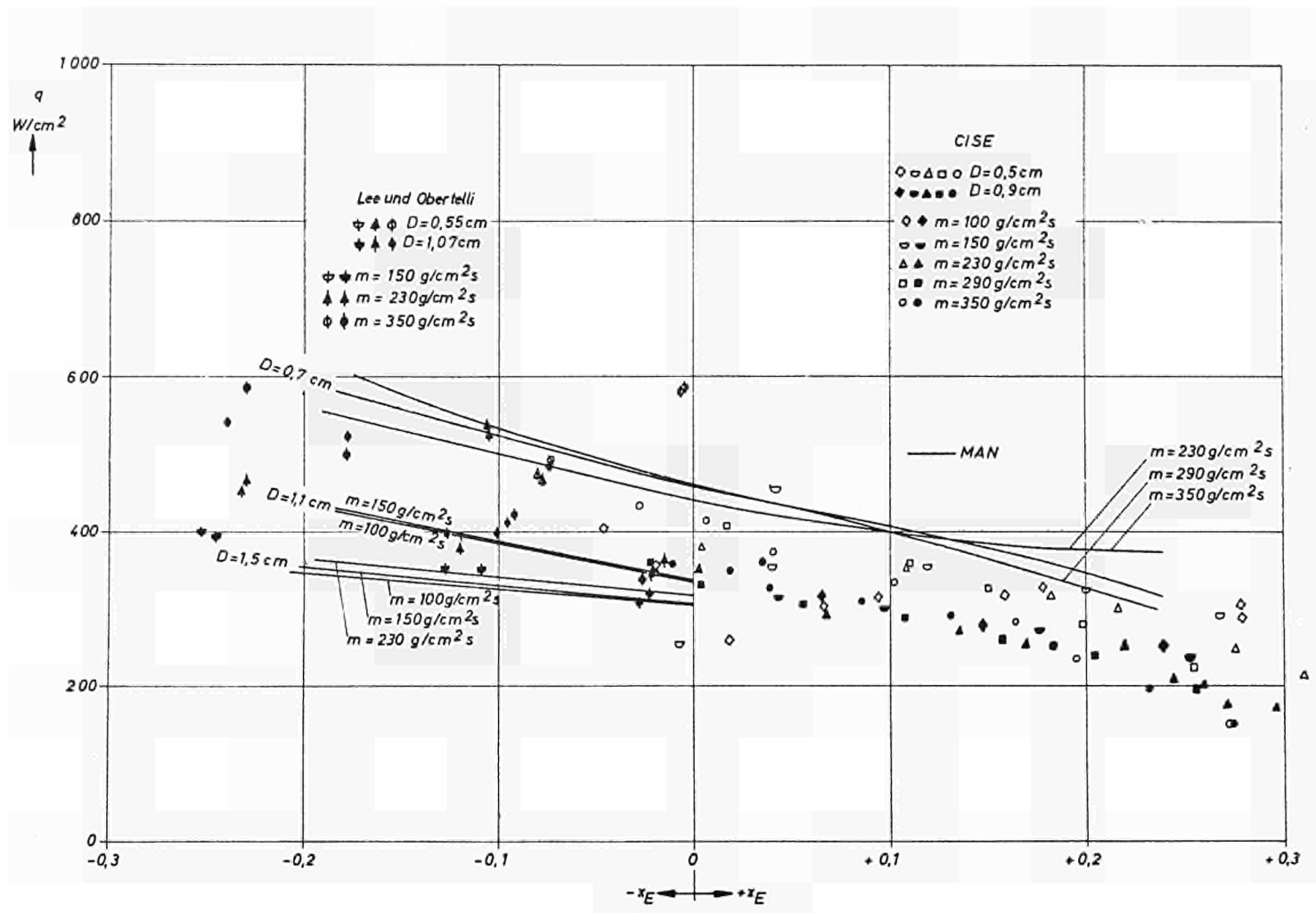
Comparison of data from MAN with data from Lee and Obertelli and CISE
at L/D = 40 and p = 70 kg/cm²

Fig. 56
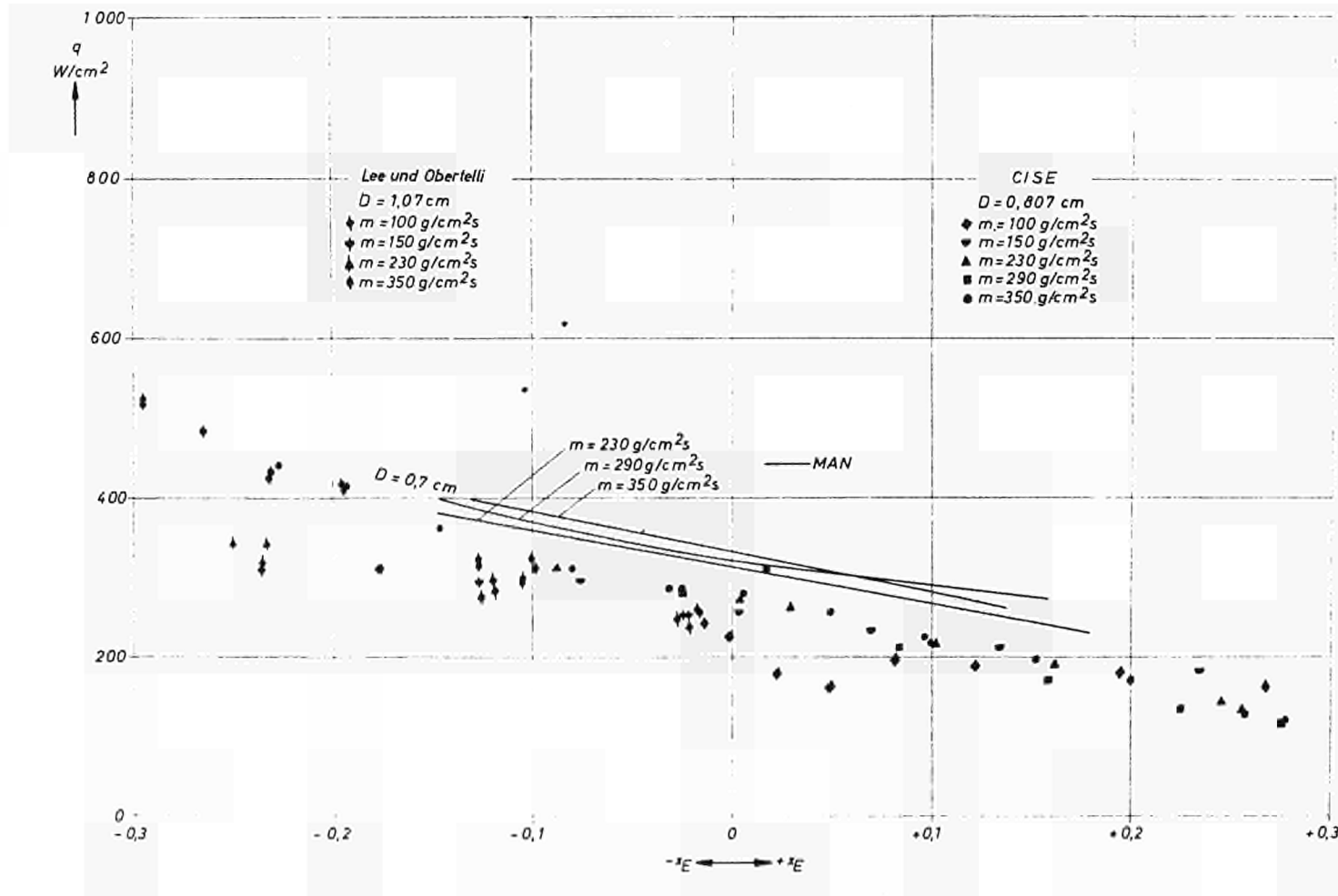
Comparison of data from MAN with data from Lee and Obertelli and CISE
at L/D = 80 and p = 70 kg/cm²

Fig. 57
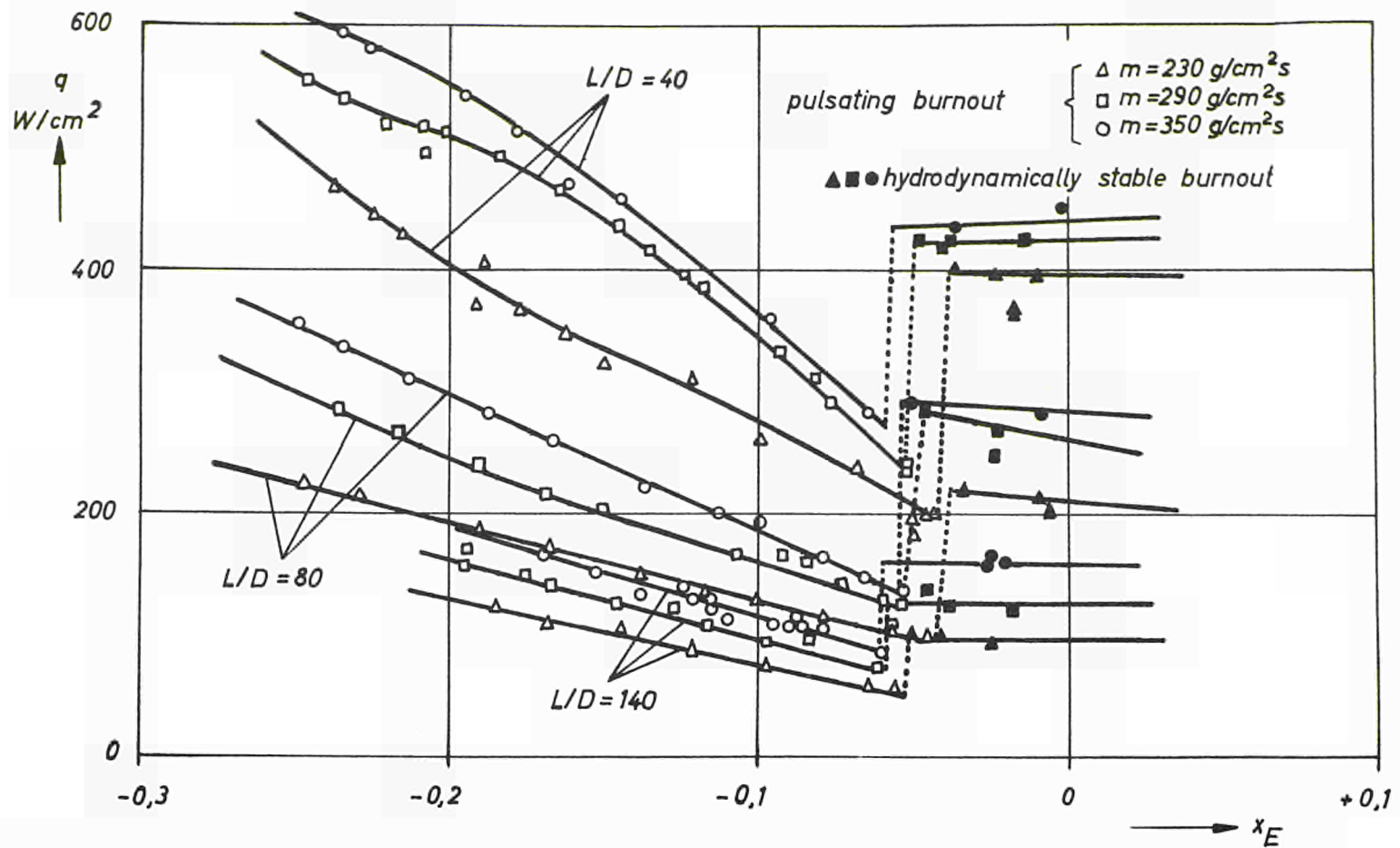
Fig. 58 : Critical heat flux plotted against inlet sub-cooling at 70 kgf/cm^2; D = 0,7cm
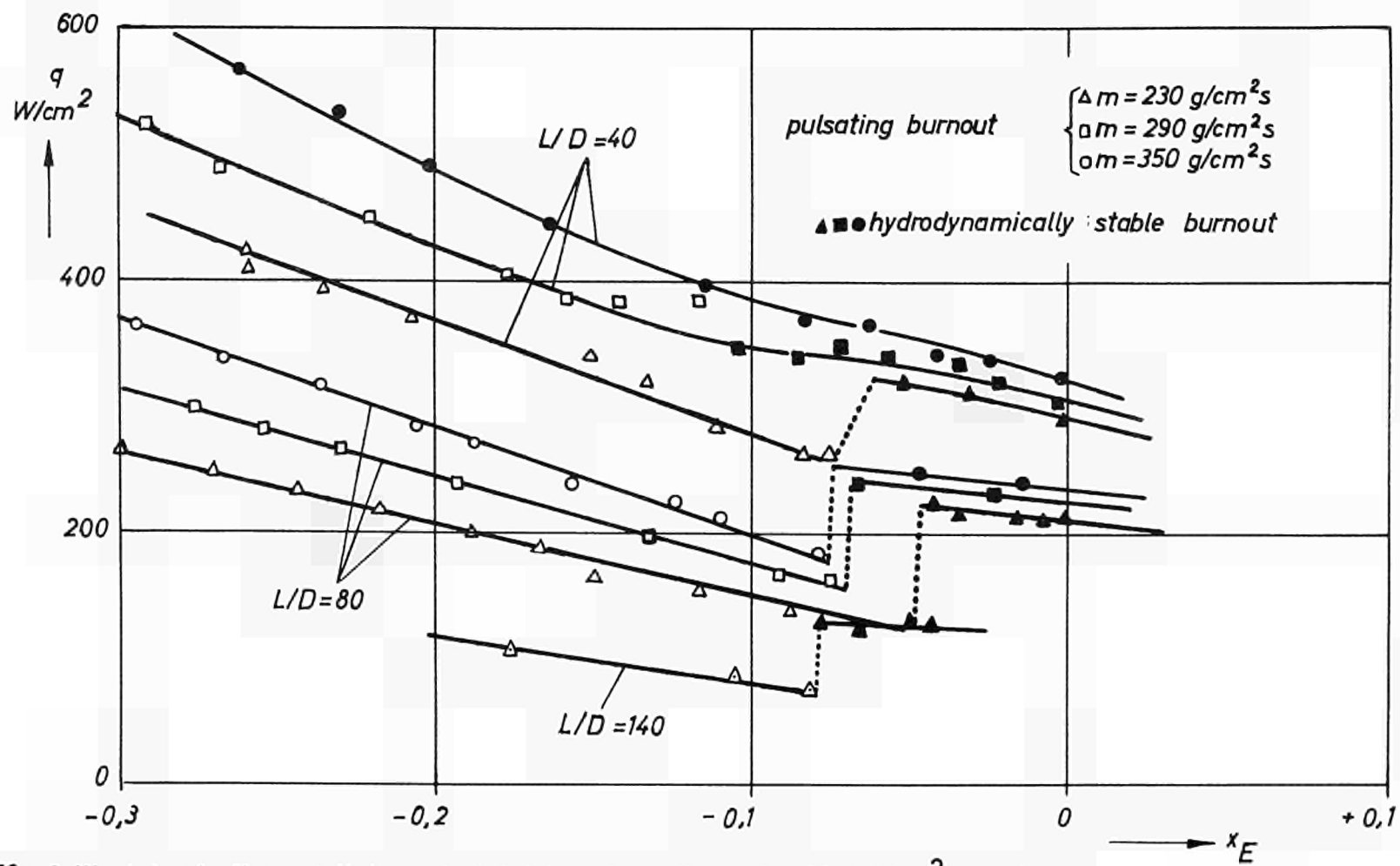
Fig. 59: Critical heat flux plottet against inlet sub-cooling at 100 kgf/cm^2; D= 0,7 cm
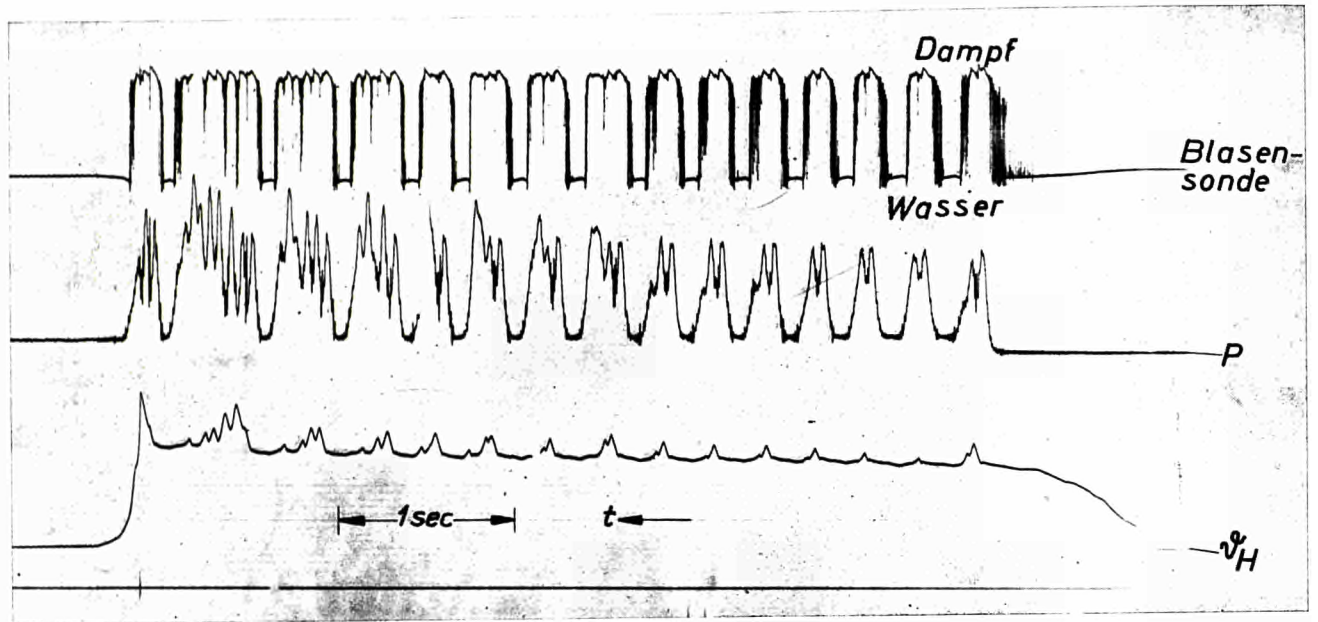
m = 40 g/cm²
L/D = 100

P = pressure
ϑ H = temperature
   three - wire thermocouple

Fig. 60 : Pulsating flow
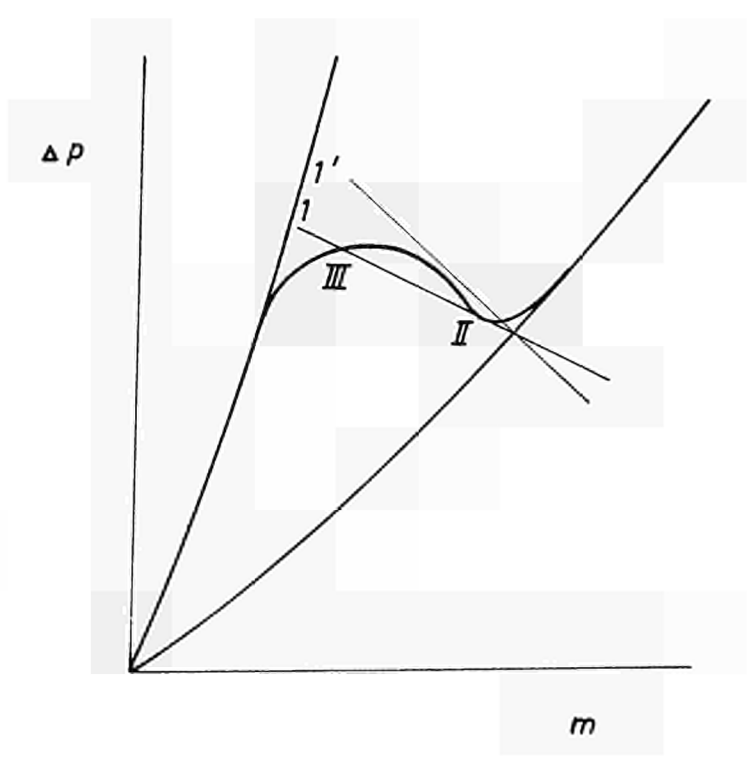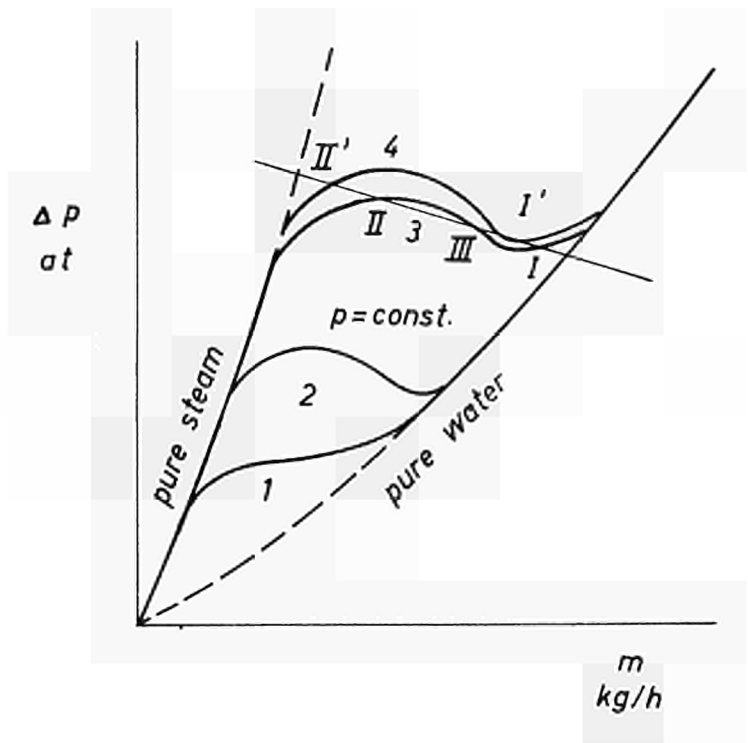
Delivery and resistance characteristics

Fig. 61
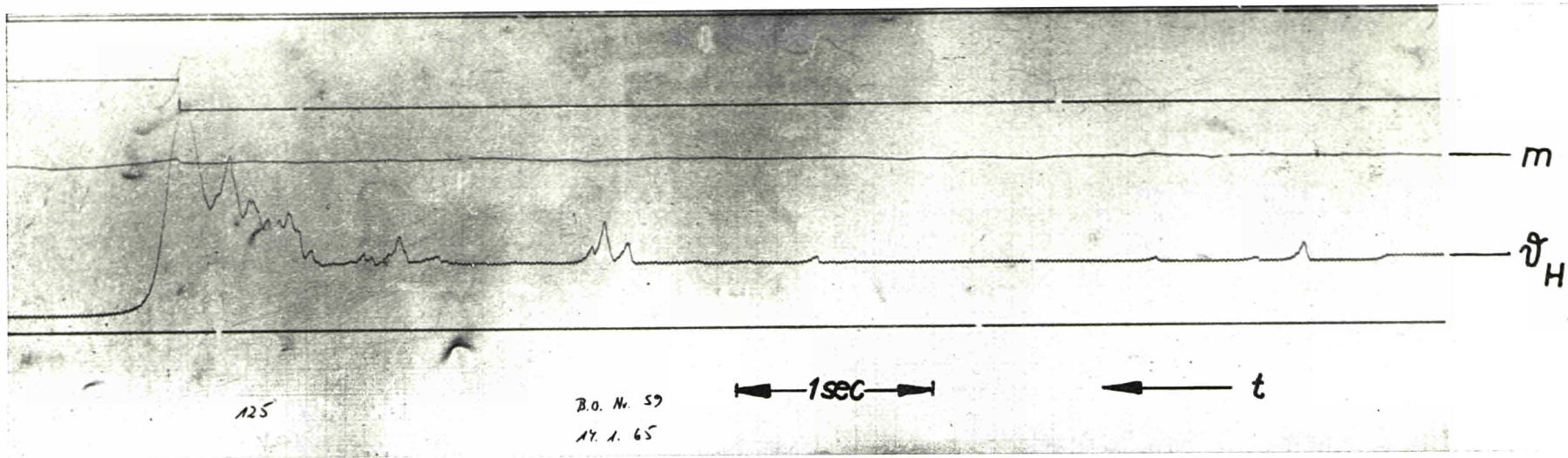
m = 308,1 g/cm²s
P = 101 at
X_E = — 0,0014
X_A = 0,1153
L/D = 40
q_{BO} = 297,7 W/cm²
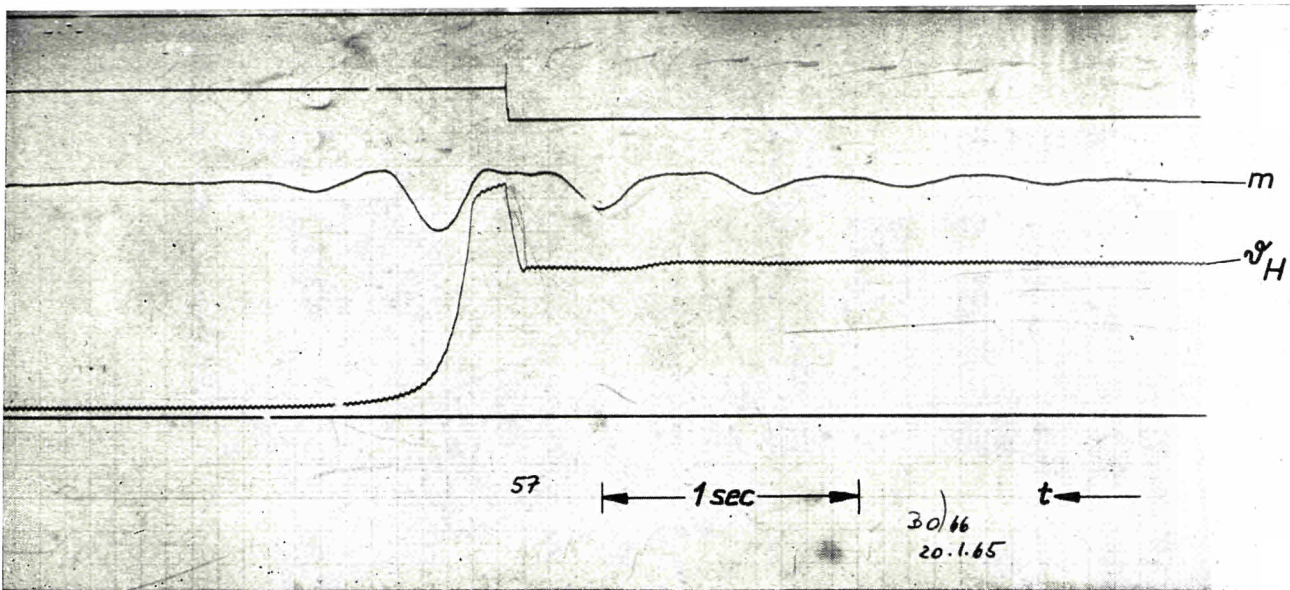
m = 350,4 g/cm²s
P = 100 at
X_E = — 0,2075
X_A = — 0,0057
L/D = 80
q_{BO} = 284,7 W/cm²

Fig. 62 : Variation of wall temperature and mass flow during inception of film boiling

Power

Mass flow

Temperature

Zero line
for mass
flow
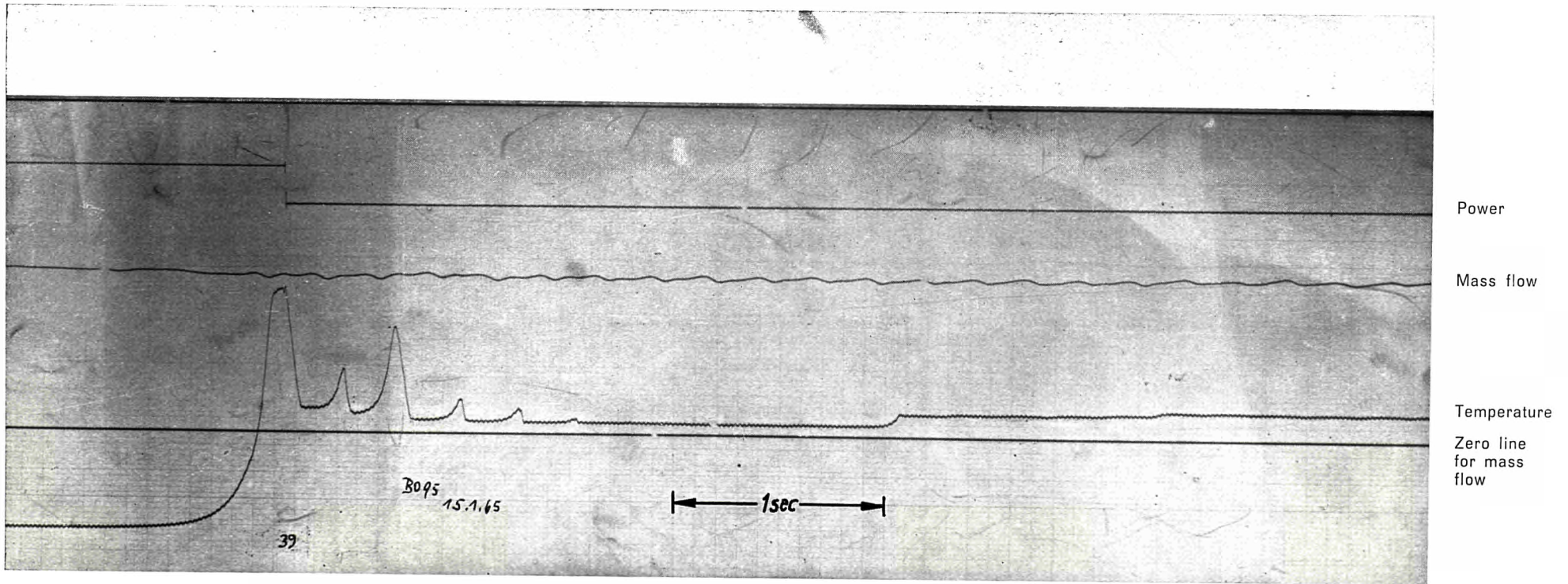
Fig. 63 : Variation of wall temperature and mass flow during inception of film boiling
m = 297 g/cm²s,   p = 86,9 kgf/cm², X_E = — 0.157, X_A = 0,002,   L/D = 40, q_{BO} = 414 W/cm²
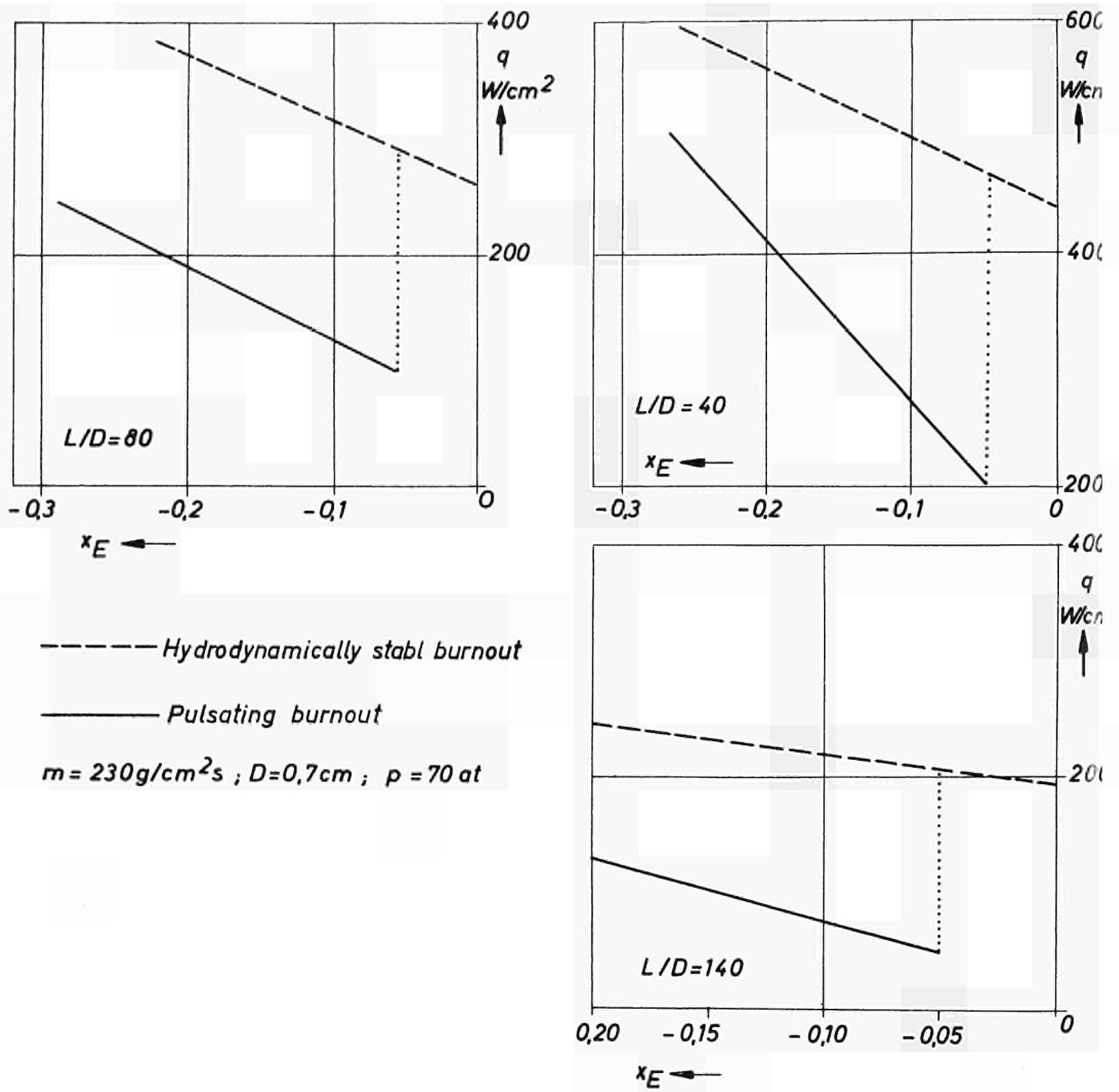
Comparison of pulsating and hydrodynamically stabl burnout with various L/D ratios

Fig. 64

m=230g/cm² s

m=170g/cm² s

m=100g/cm² s

D

P=70at

400

q
W/cm²

200

−0,3 ← x_E −0,2   −0,1   0

← $-x_E$ $+x_E$ →
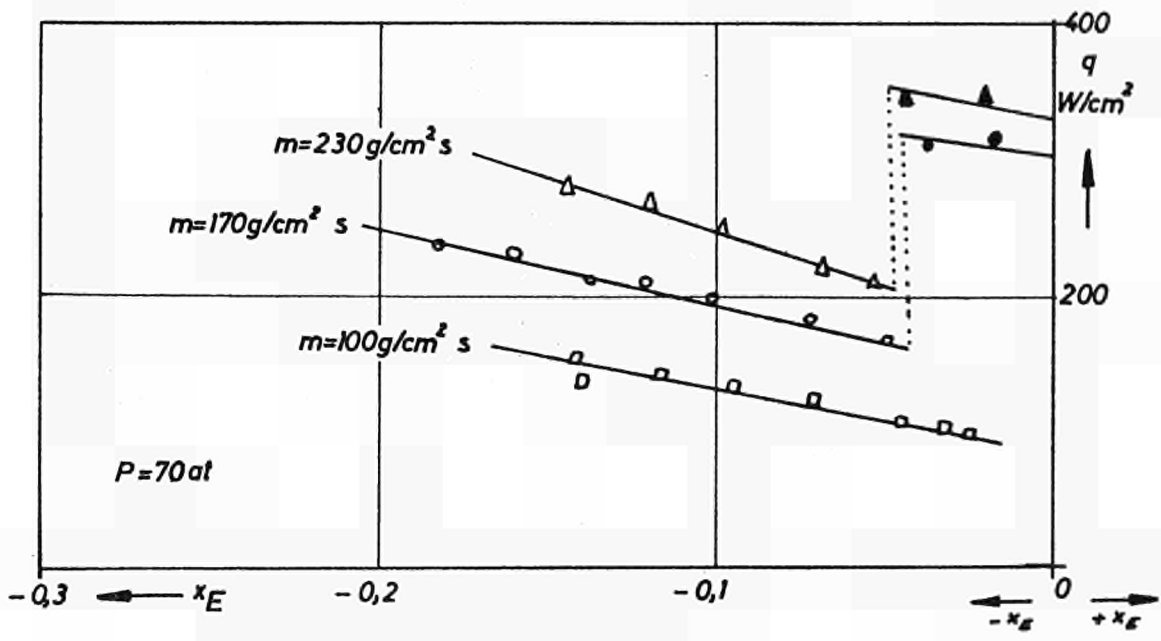
Pressurizer upstream of test section

□ ○ △ pulsating burnout   ▲ ● hydrodynamically stable burnout

m=230g/cm² s

m=170g/cm² s

m=100g/cm² s

P=100 at

400

q
W/cm²

200

−0,3 ← x_E −0,2   −0,1   0

$-x_E$ $+x_E$
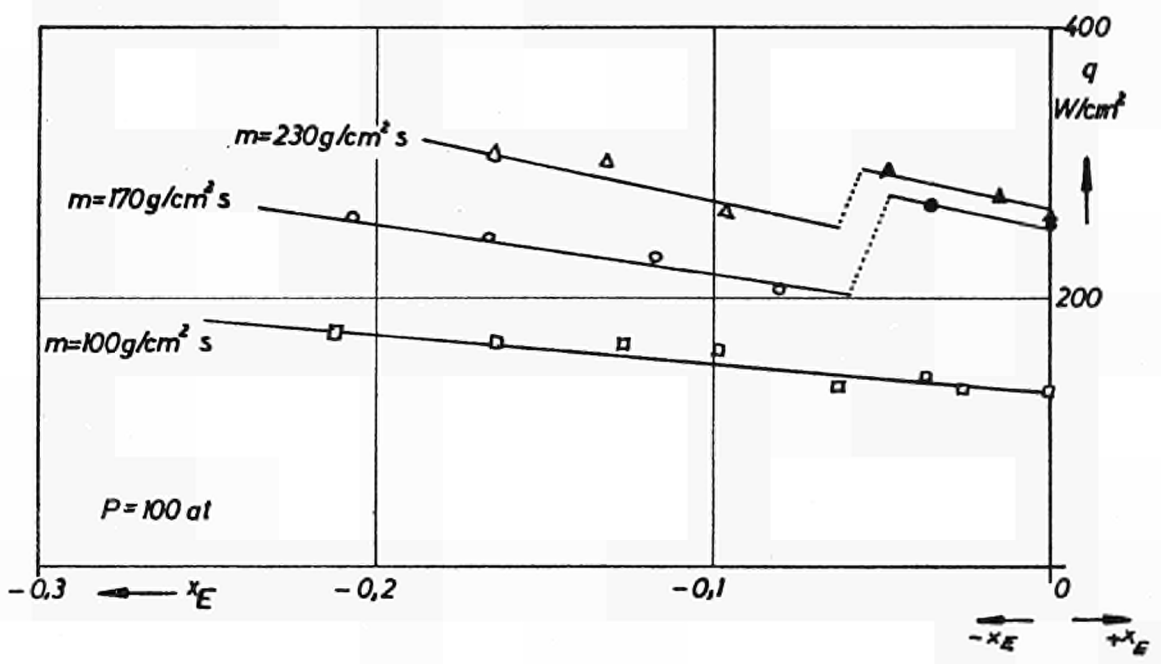
Fig. 65   Critical heat flux in test channels with 1.1 cm inside
dia and L/D ratio of 40

Pulsating burnout
$\square$ m = 100 g/cm² s
o m = 170 g/cm² s
▲ m = 230 g/cm² s

•Hydrodynamically stabl burnout

P = 70 at

P = 100 at
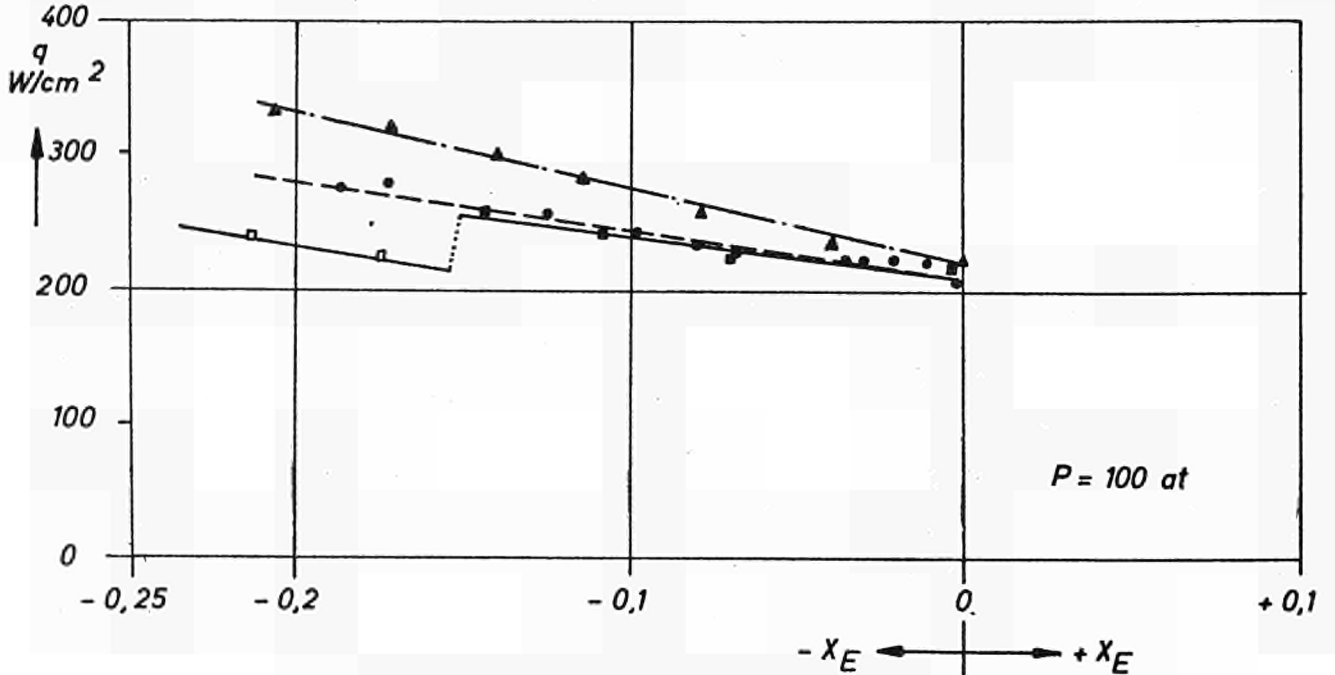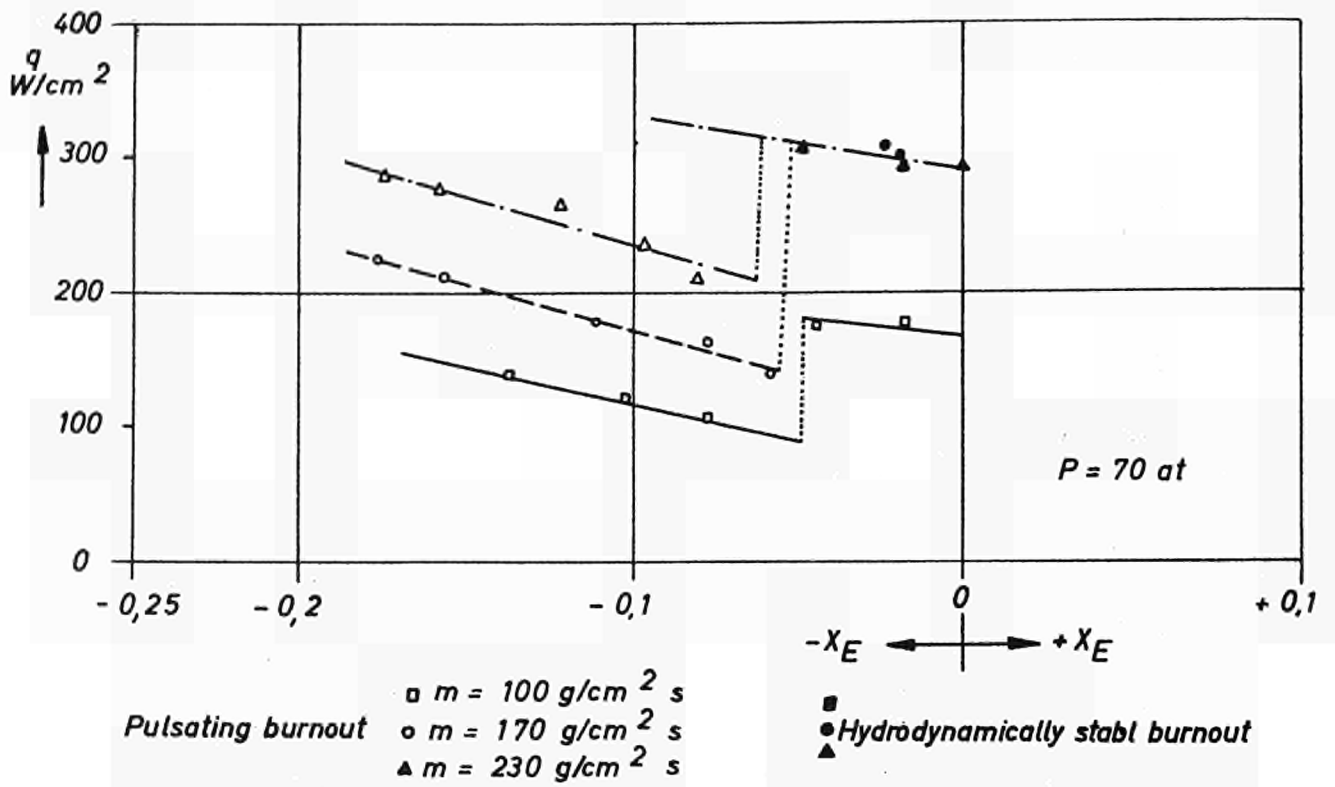
Pressurizer upstream of test section

Critical heat flux in test channels with an inside dia of 1.5 cm and an L/D ratio of 40 under pressures of 70 and 100 kgf/cm²

Fig. 66
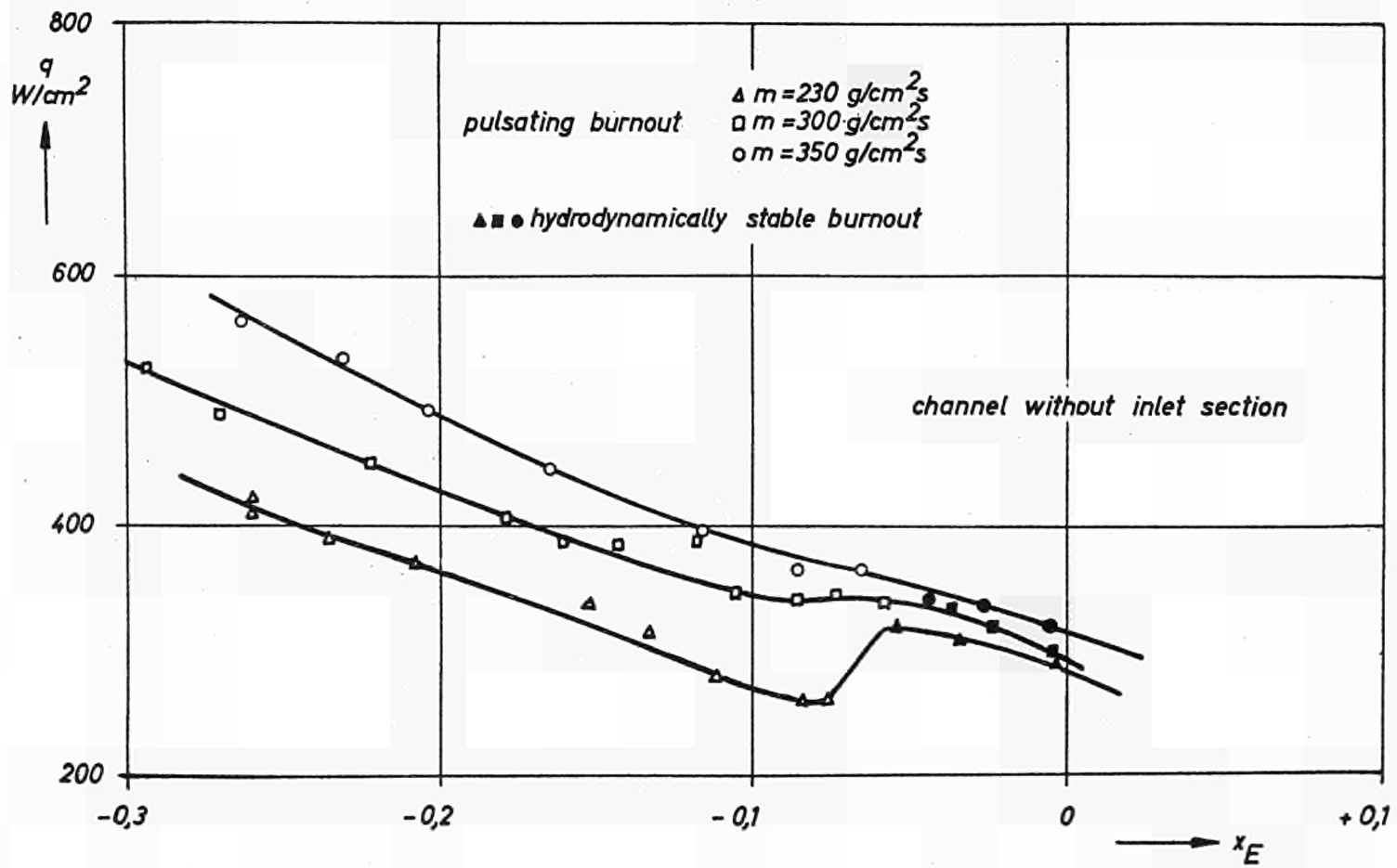
Fig. 67   Critical heat flux plotted against inlet sub-cooling at $100\,kgf/cm^2$, $L/D = 40$, $D = 0.7cm$
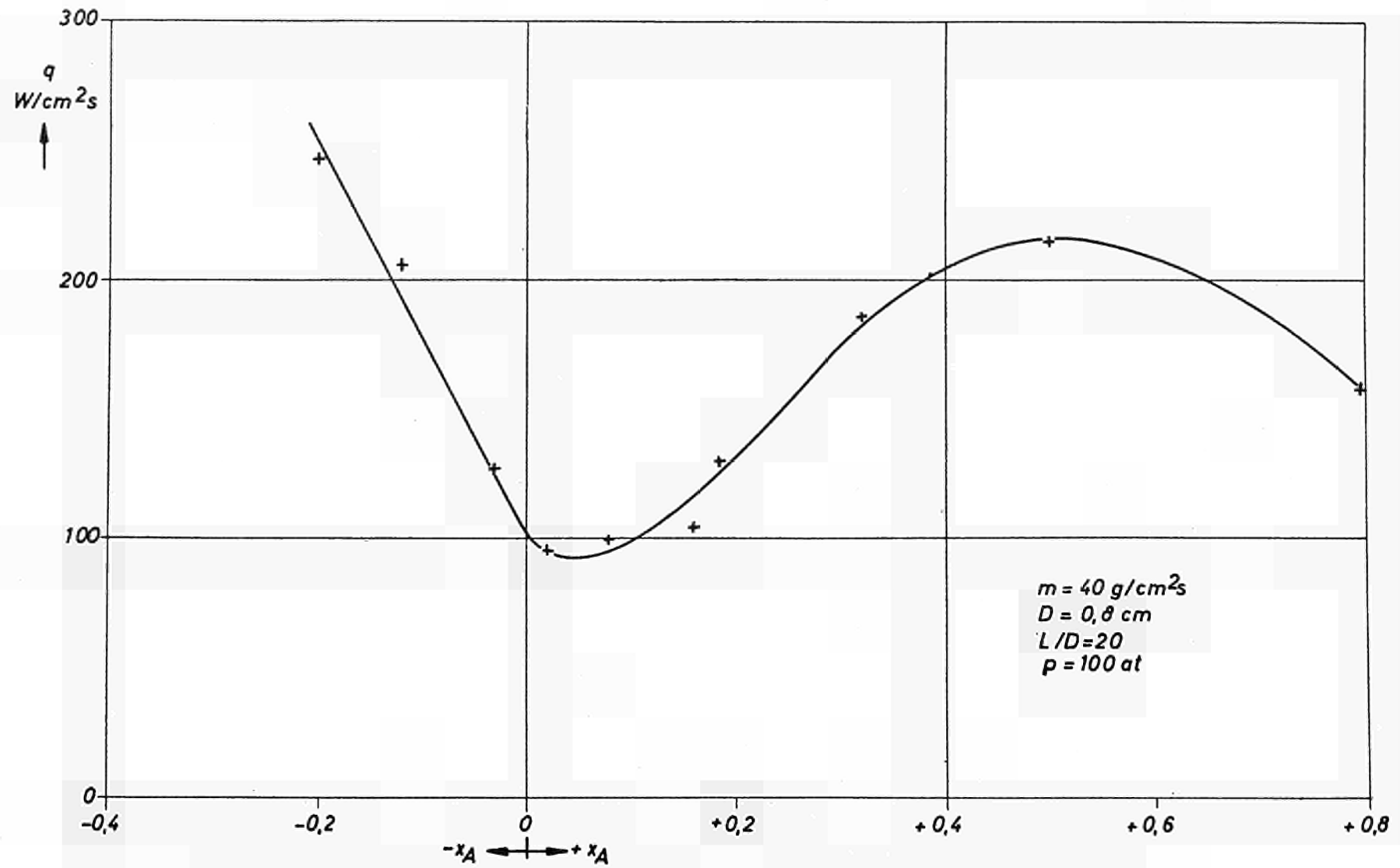
Fig. 68   Critical heat flux plotted against outlet quality according to measurements by Aladiev
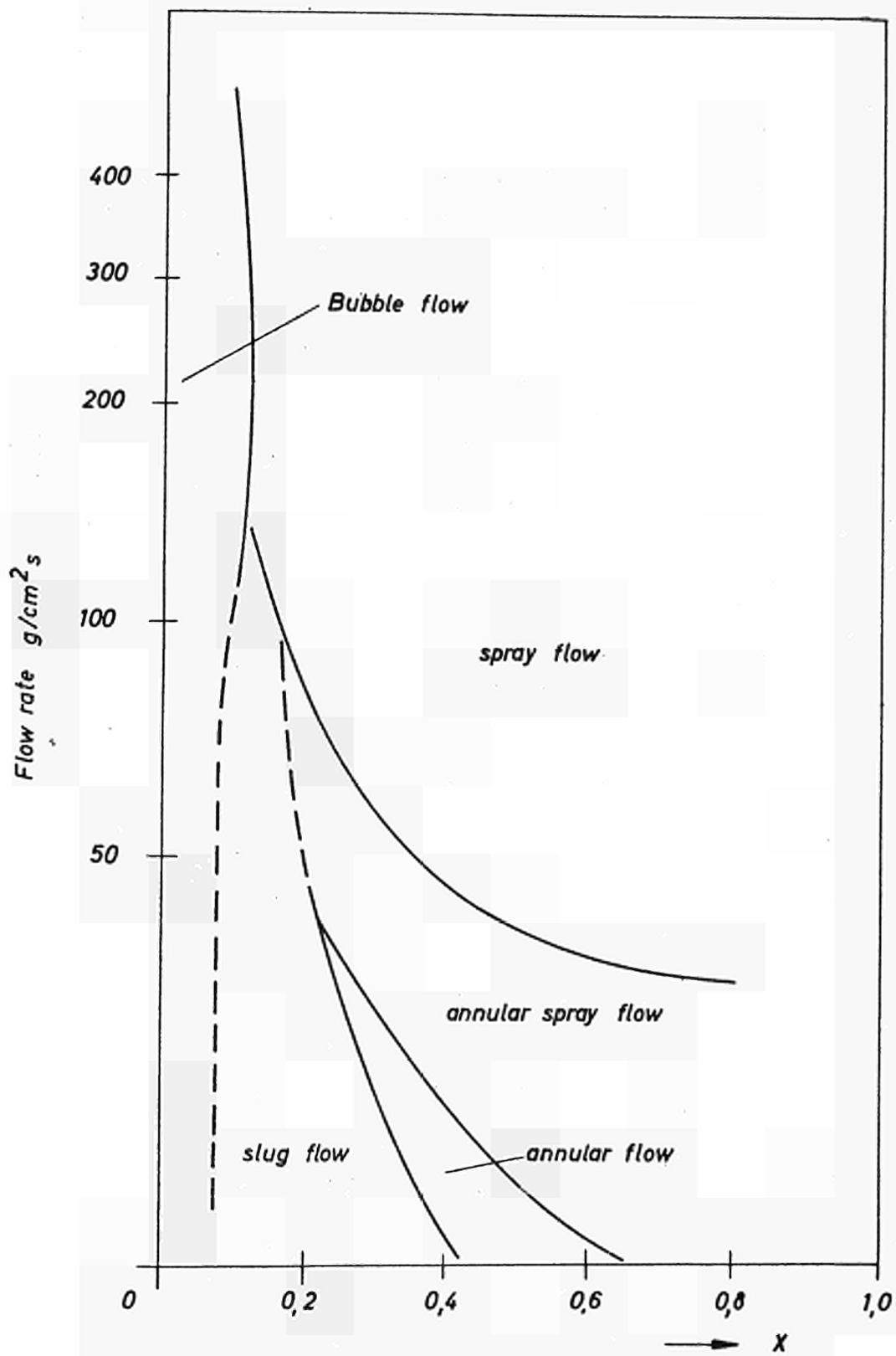
Two-phase flow regimes according to A.E. Bergles (63)

Fig. 69
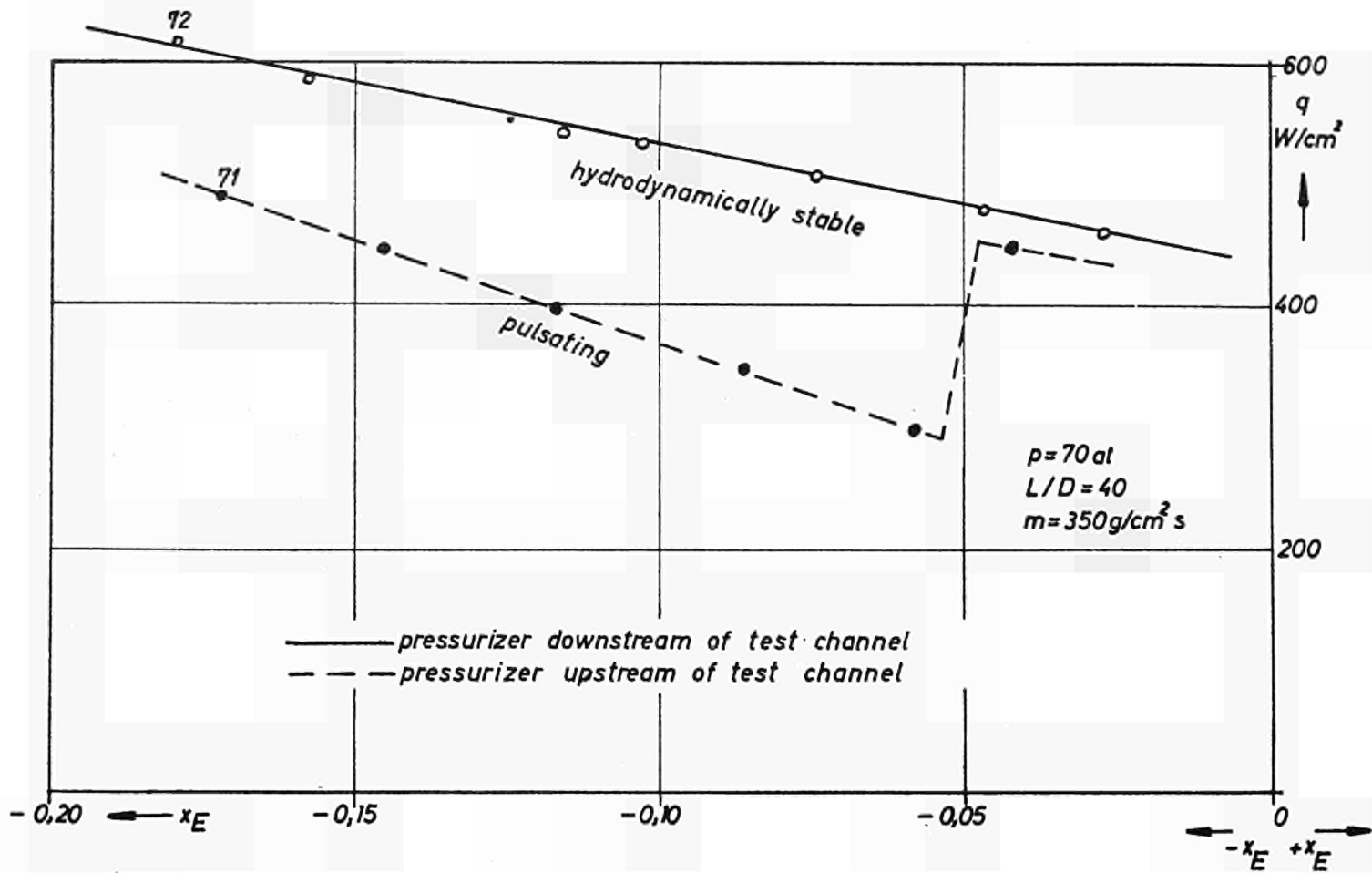
Fig. 70
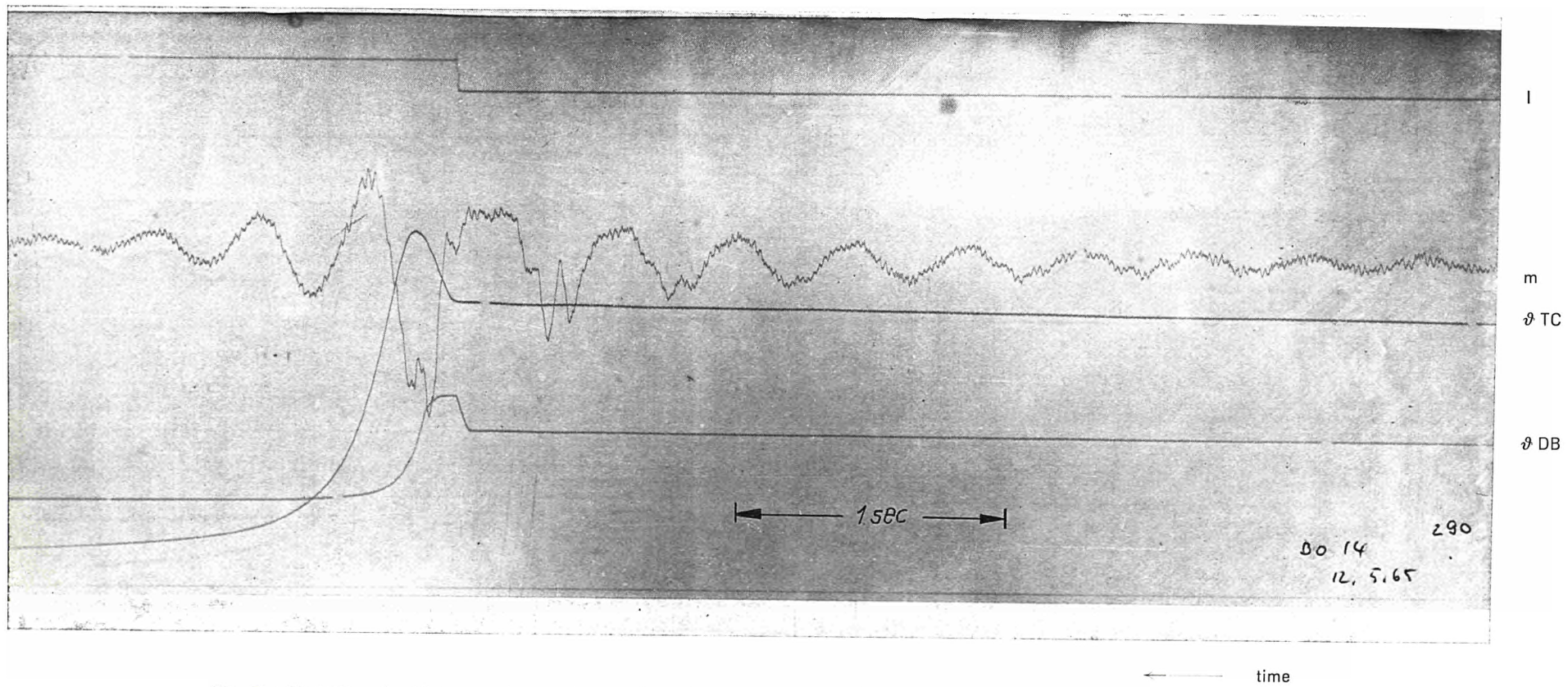
Fig. 71 : Variation of wall temperature and mass flow during inception of film boiling
m = 346,5 g/cm²s, p = 70 kgf/cm², X_E = — 0,172, X_A = — 0,023, L/D = 40, q_{BO} = 489,8

Pressurizer connected upstream of test channel

80 42
12.5.65   287

1sec

𝜗 DB

m
p

time
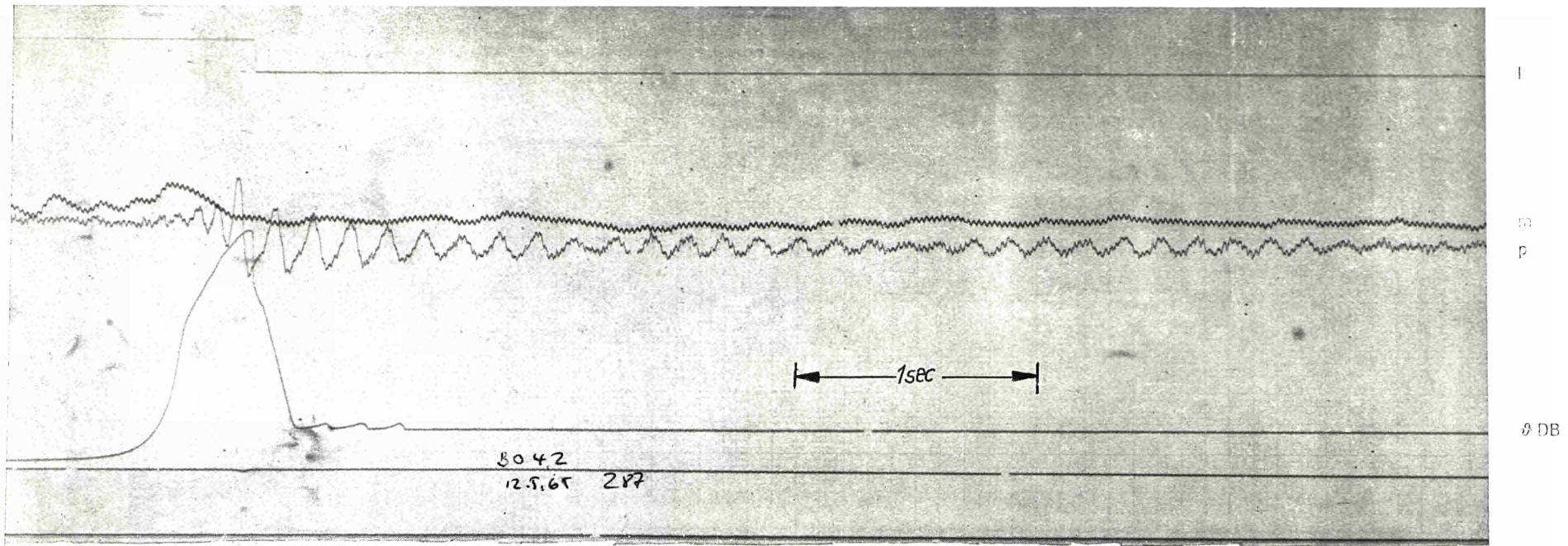
Fig. 72 : Variation of wall temperature, pressure and mass flow during inception film boiling
m = 358,7 g/cm²s,   p = 69 kgf/cm², X_E = — 0,181, X_A = 0,002,   L/D = 40, q_{BO} = 620,7

Pressurizer connected downsteam of test channel
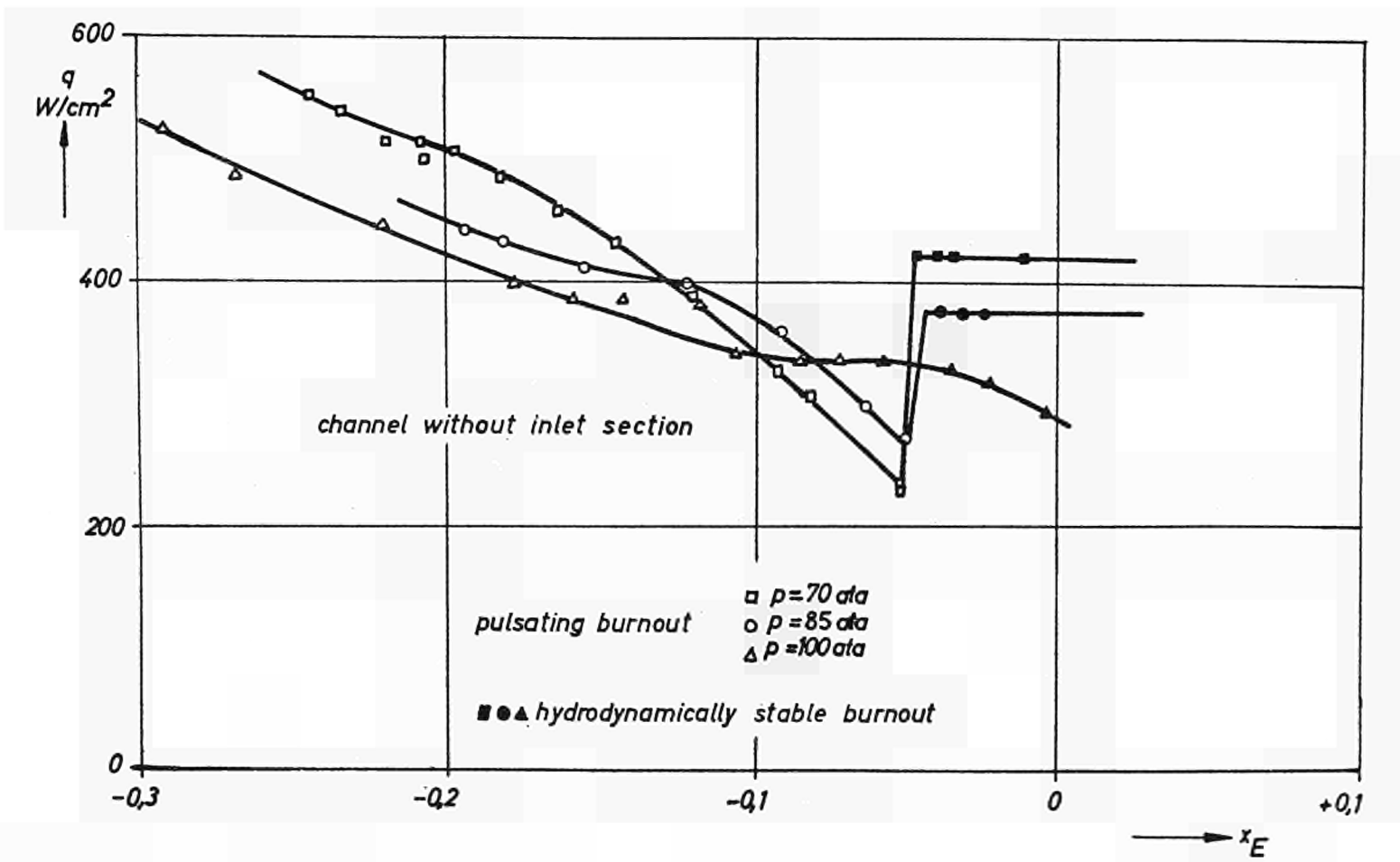
Fig. 73 Critical heat flux plotted against inlet sub-cooling at various pressures and $m = 300 g/cm^2 s =$ const. $L/D = 40$, $D = 0.7 cm$
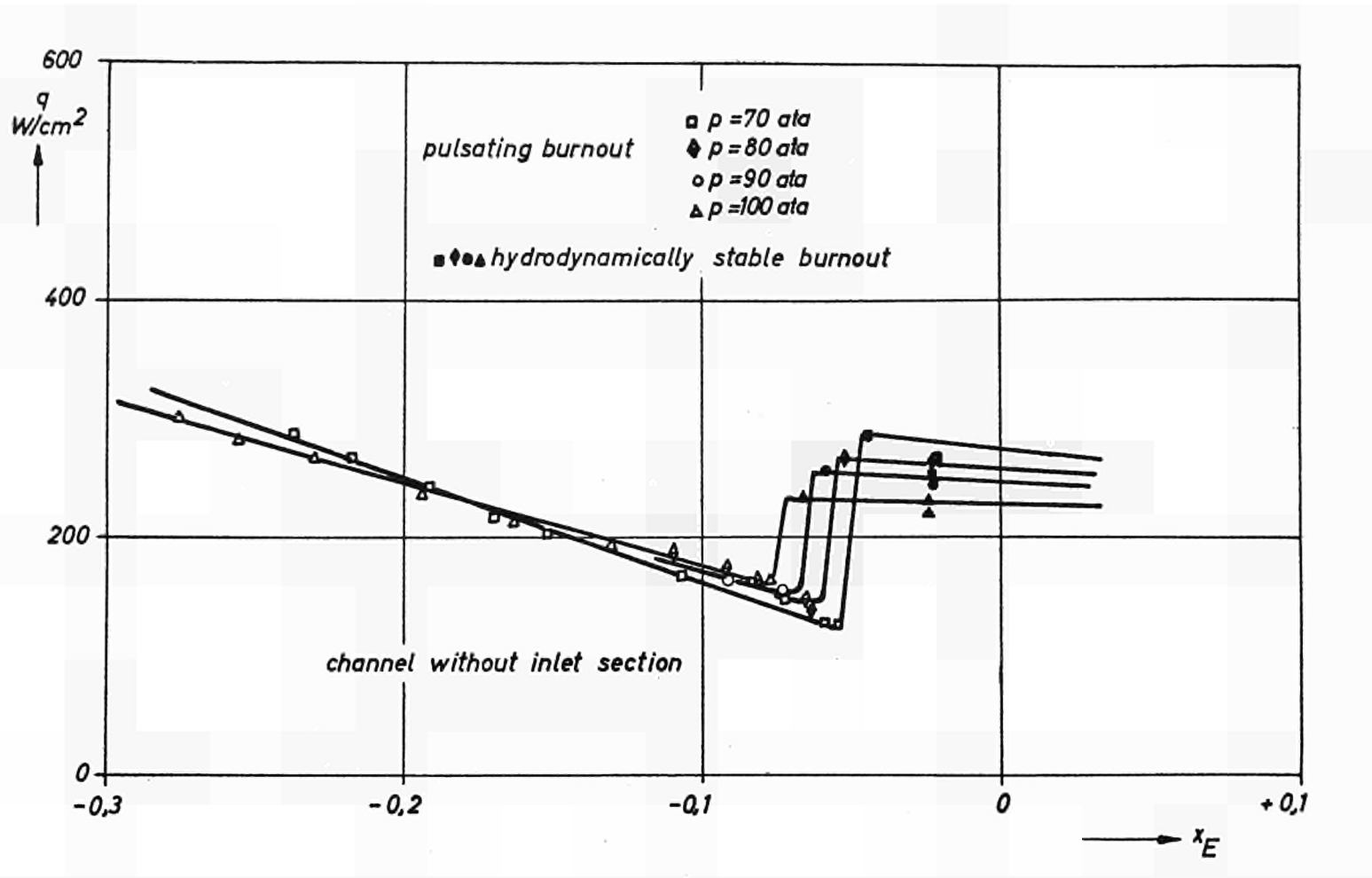
Fig. 74   Critical heat flux plotted against inlet sub–cooling at various pressures and $m = 300 \, g/cm^2 \, s = $ const. $L/D = 80$, $D = 0.7 \, cm$.
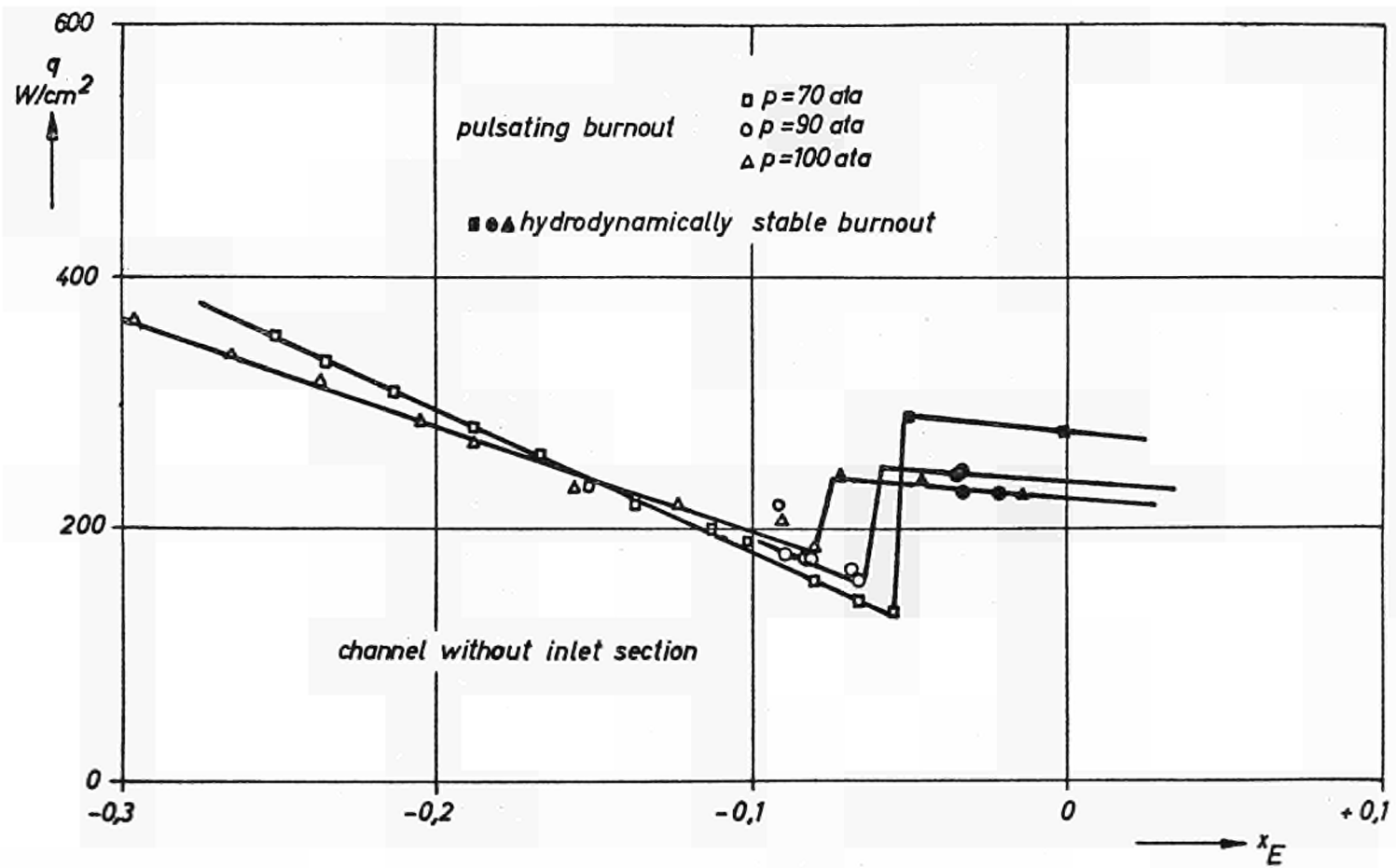
Fig.75   Critical   heat   flux   plotted   against   inlet   sub-cooling   at various   pressures   and   m = 350 g/cm^2 s = const. L/D = 80, D = 0,7 cm
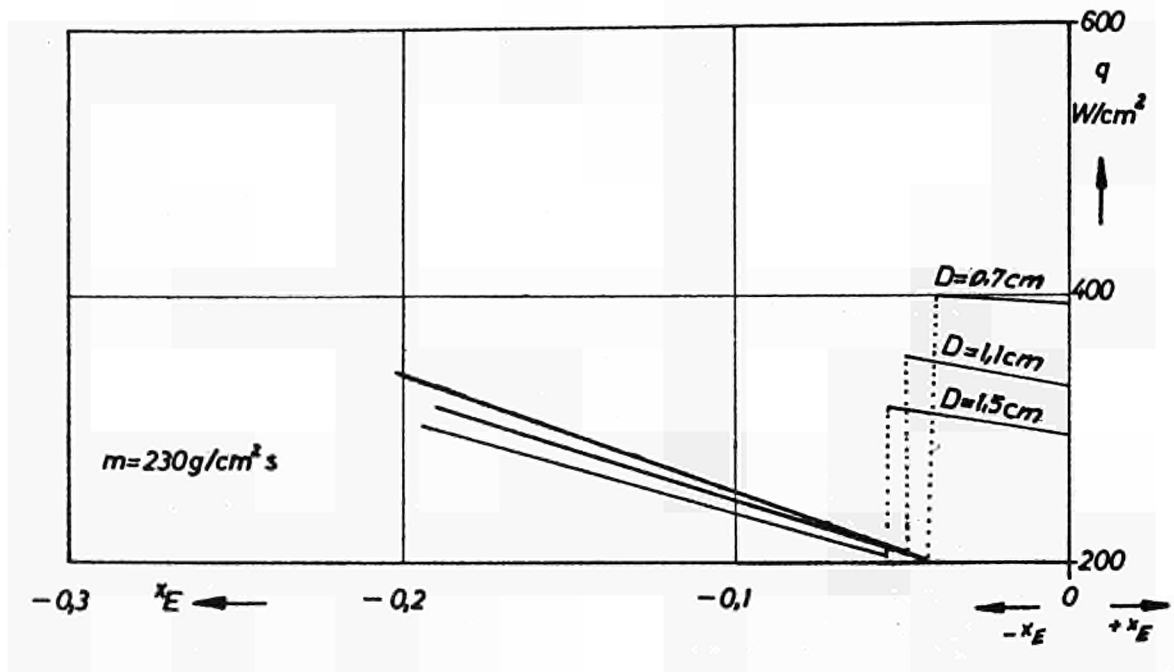
Critical heat flux in test channels with inside diameters of 0.7, 1.1 and 1.5 cm and an L/D ratio of 40 at $P = 70 \, kgf/cm^2$

Fig. 76

Top-left panel:
400
q W/cm²
↑
200
m=290g/cm s
P = 70 at
L/D = 80
-0,2 ←—xₑ   -0,1   0
Pressurizer influence without orifice plate

Top-right panel:
400
q W/cm²
↑
200
m=290g/cm s
P = 70 at
L/D = 80
-0,2   -0,1   0
←— -xₑ   +xₑ —→
orifice plate 1 at inlet
——— pressurizer upstream
----- pressurizer downstream

Bottom-left panel:
600
q W/cm²
↑
400
m=290g/cm s
P = 70 at
L/D = 80
200
-0,2 ←—xₑ   -0,1   0
——— without orifice plate
----- orifice plate at outlet
pressurizer upstream

Bottom-right panel:
400
q W/cm²
↑
200
m=290g/cm s
P = 70 at
L/D = 40
-0,2   -0,1   0
←— -xₑ   +xₑ —→
orifice plate 2 at inlet
× pressurizer upstream
• pressurizer downstream

Influence of pressurizer location and orifice plates on pulsating burnout

Fig. 77
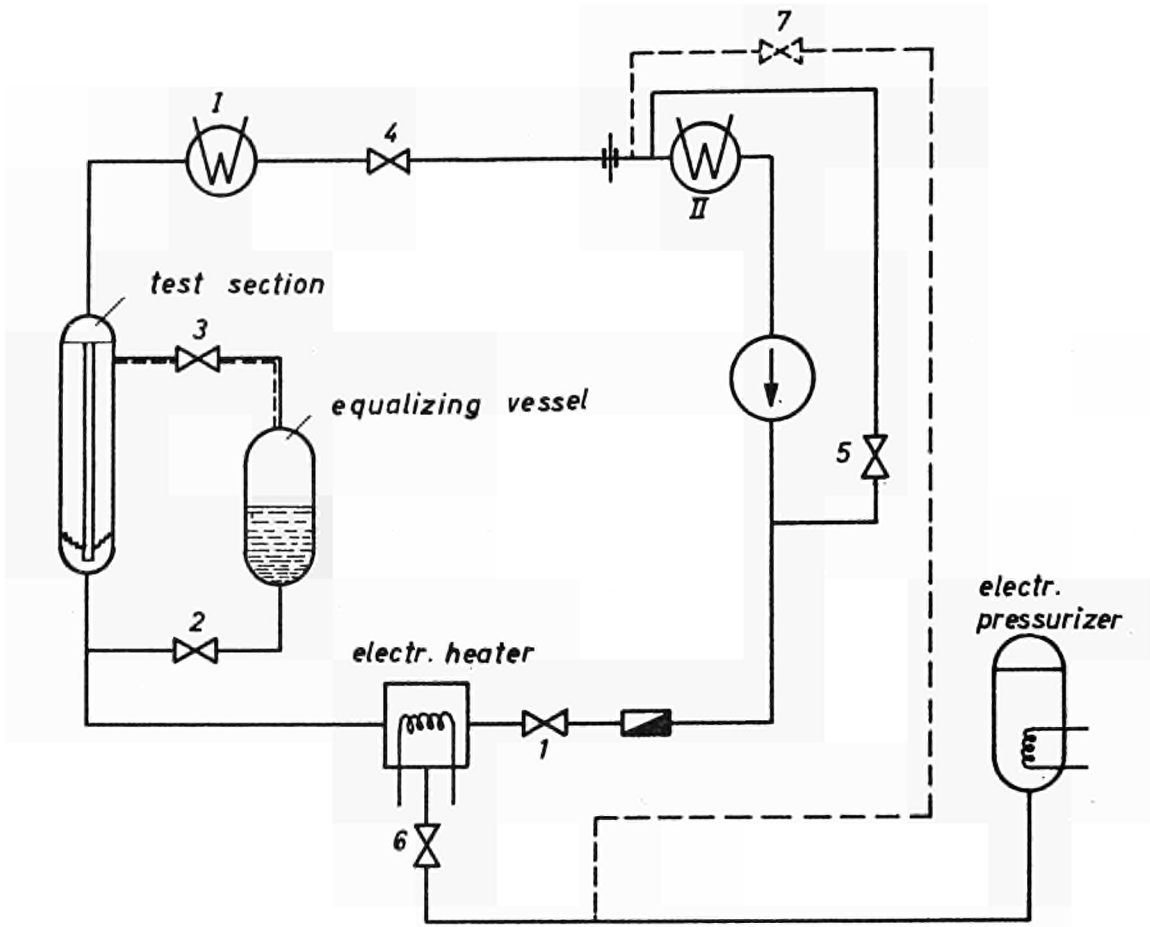
Layout	Valve No.						
No.	1	2	3	4	5	6	7
Normal position	x	o	o	o	x	o	△
2	x	o	o	o	x	△	o
3	o	o	o	x	x	△	o
4	o	o	o	x	x	o	△
5	o	△	o	x	x	o	△
6	o	△	o	x	x	△	o

Valve: o   open
        x   throttled
        △   closed

Fig. 78 :   Simplified   connection   diagram   of   Euratom   test   loop
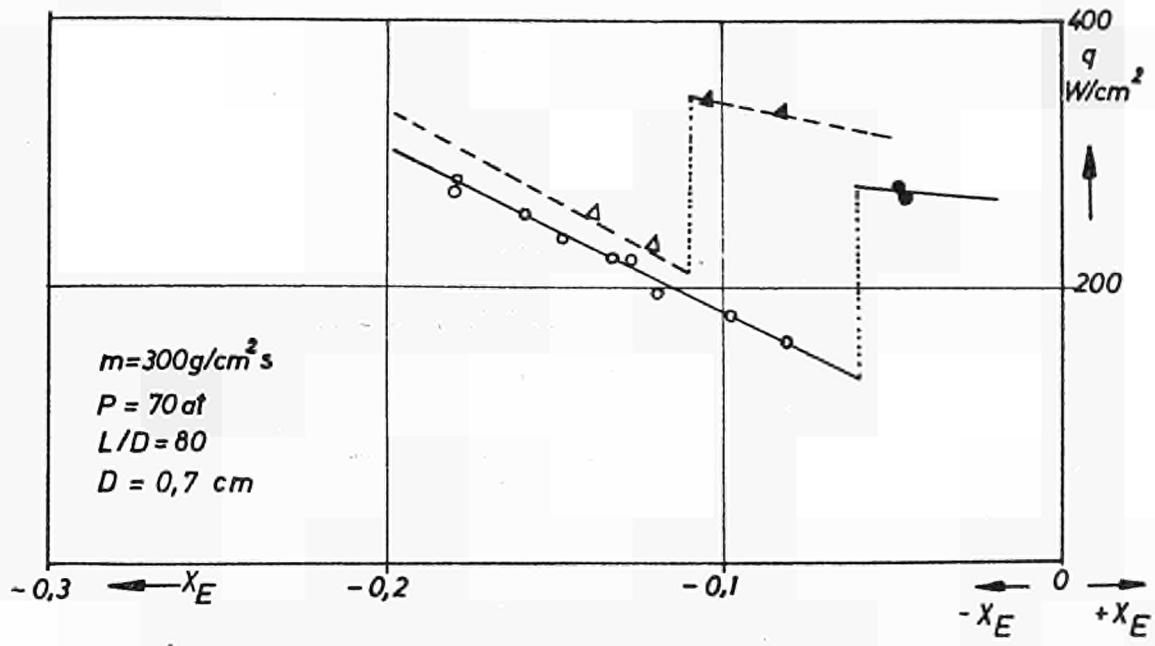
$m = 300 g/cm^2 s$
$P = 70 at$
$L/D = 80$
$D = 0,7 cm$

$- 0,3 \longleftarrow X_E$ $- 0,2$ $- 0,1$ 0
$- X_E$ $+ X_E$

$----^{\triangle}$ Pressurizer connected downstream of test channel

$\underline{\quad}^{o}$ Pressurizer connected upstream of test channel

$^{\triangle}_{o}$ pulsating burnout $^{\blacktriangle}_{\bullet}$ hydrodynamically stable burnout

$m = 230 g/cm^2 s$
$P = 100 at$
$L/D = 40$
$D = 0,7 cm$

$- 0,3 \longleftarrow X_E$ $- 0.2$ $- 0,1$ 0
$- X_E$ $+ X_E$
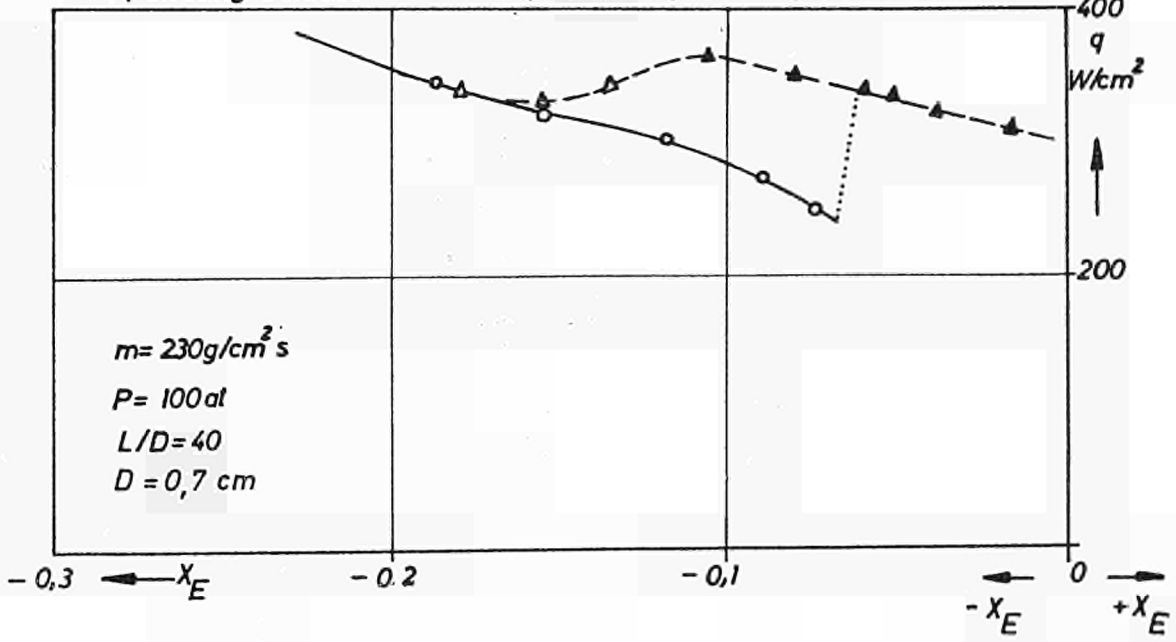
Critical heat flux plotted for various layouts of the test loop

Fig. 79

Detail X

3ϕ

7ϕ
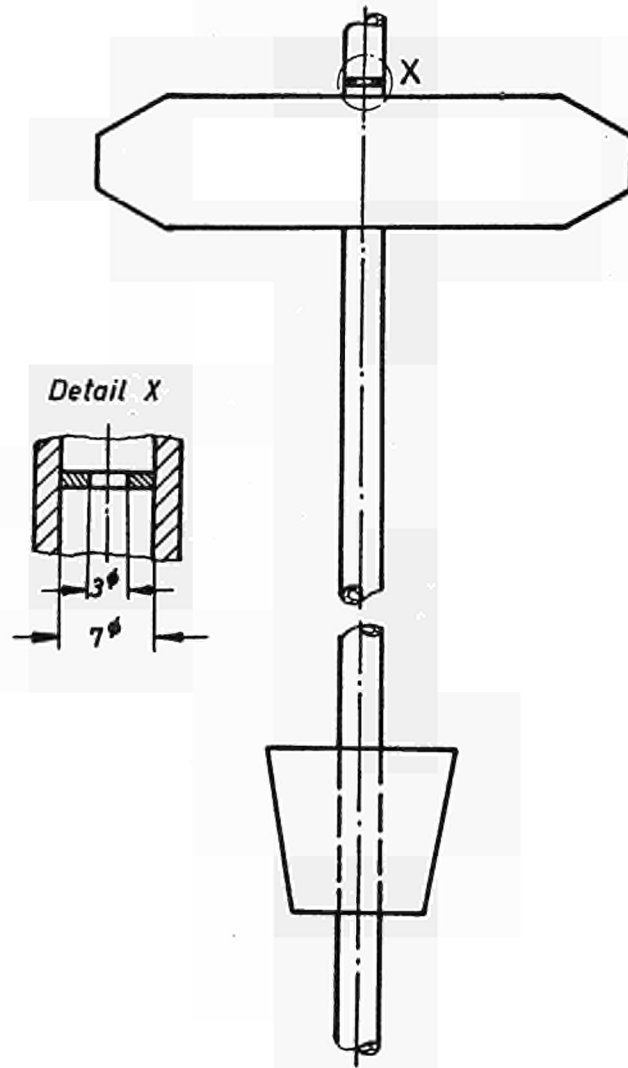
Fig. 80   Orifice plate at test section outlet
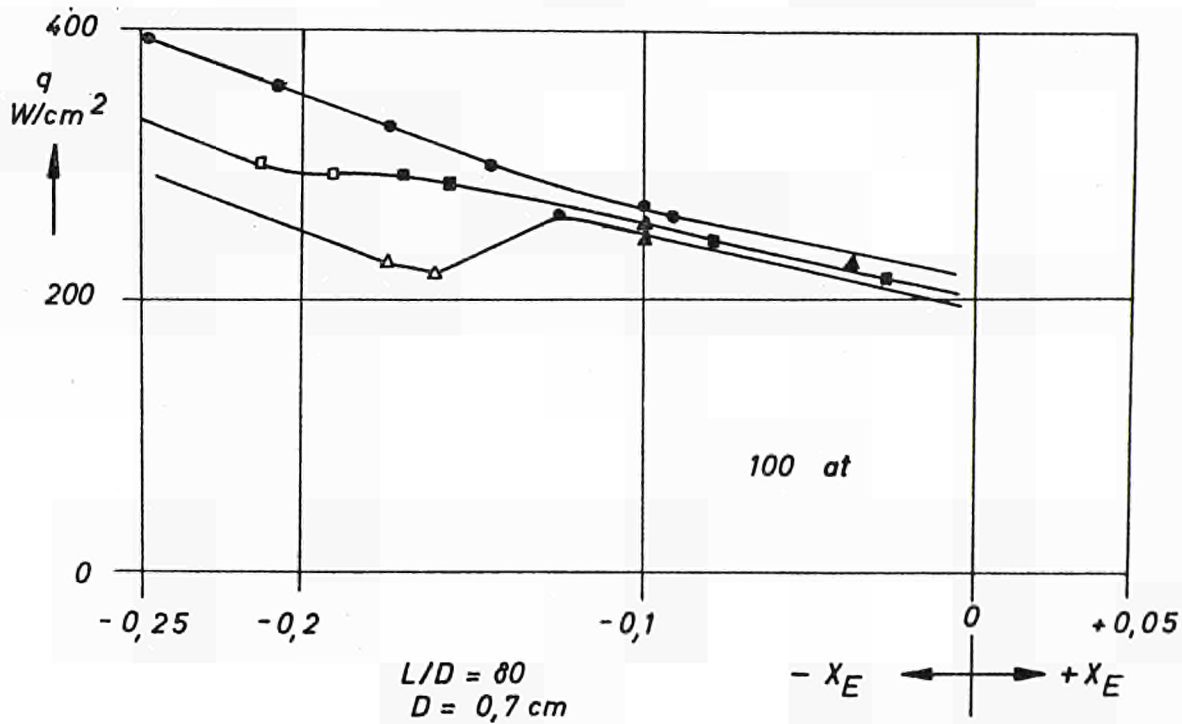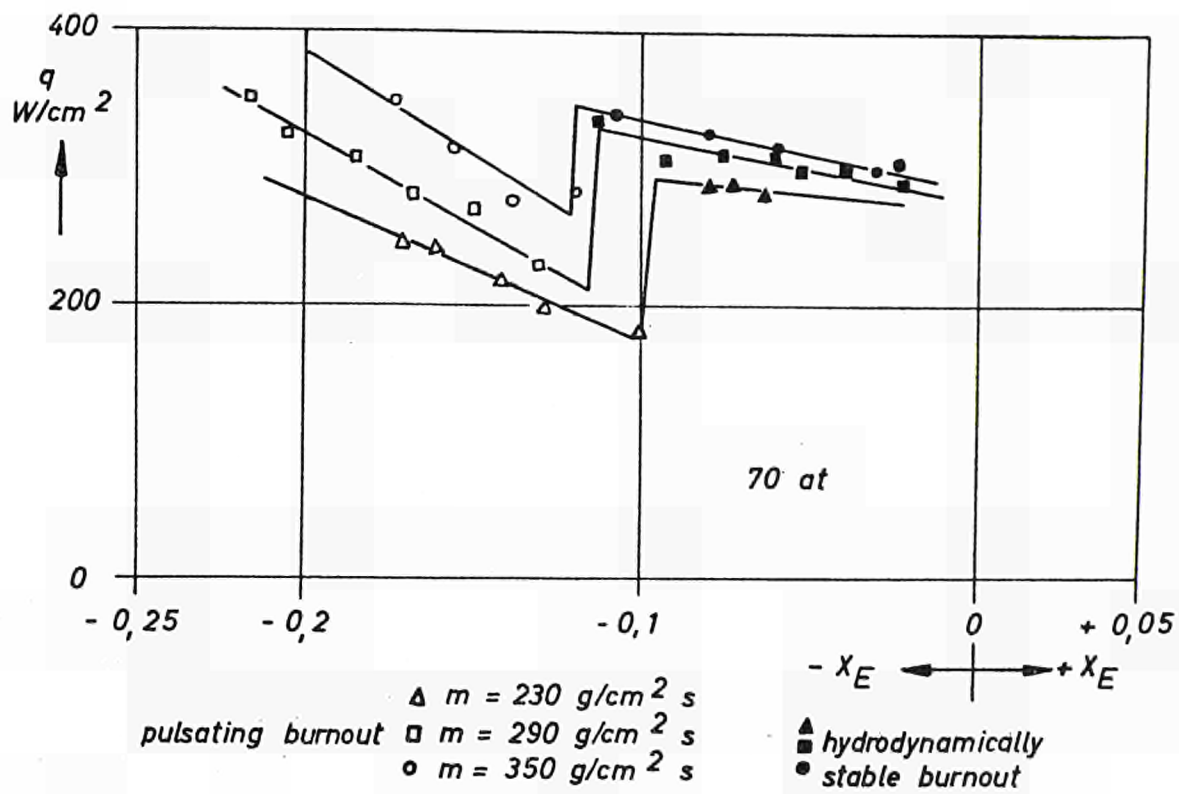
Critical heat flux in test channels with No.1 orifice plate at inlet

Fig. 81
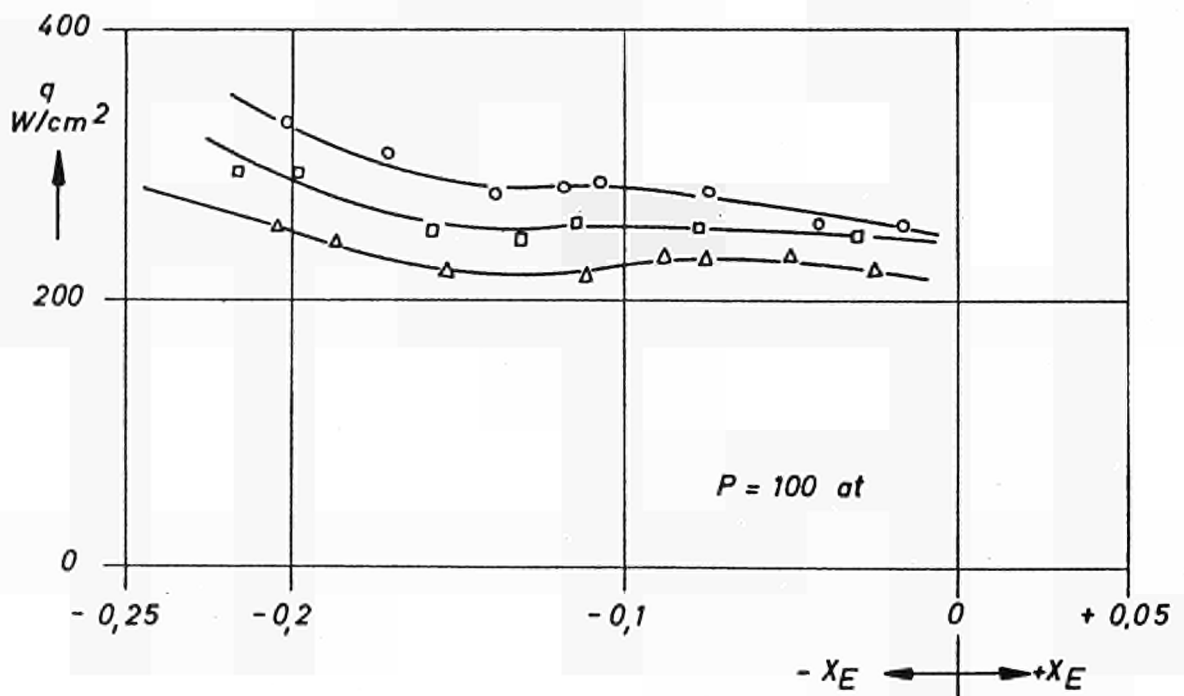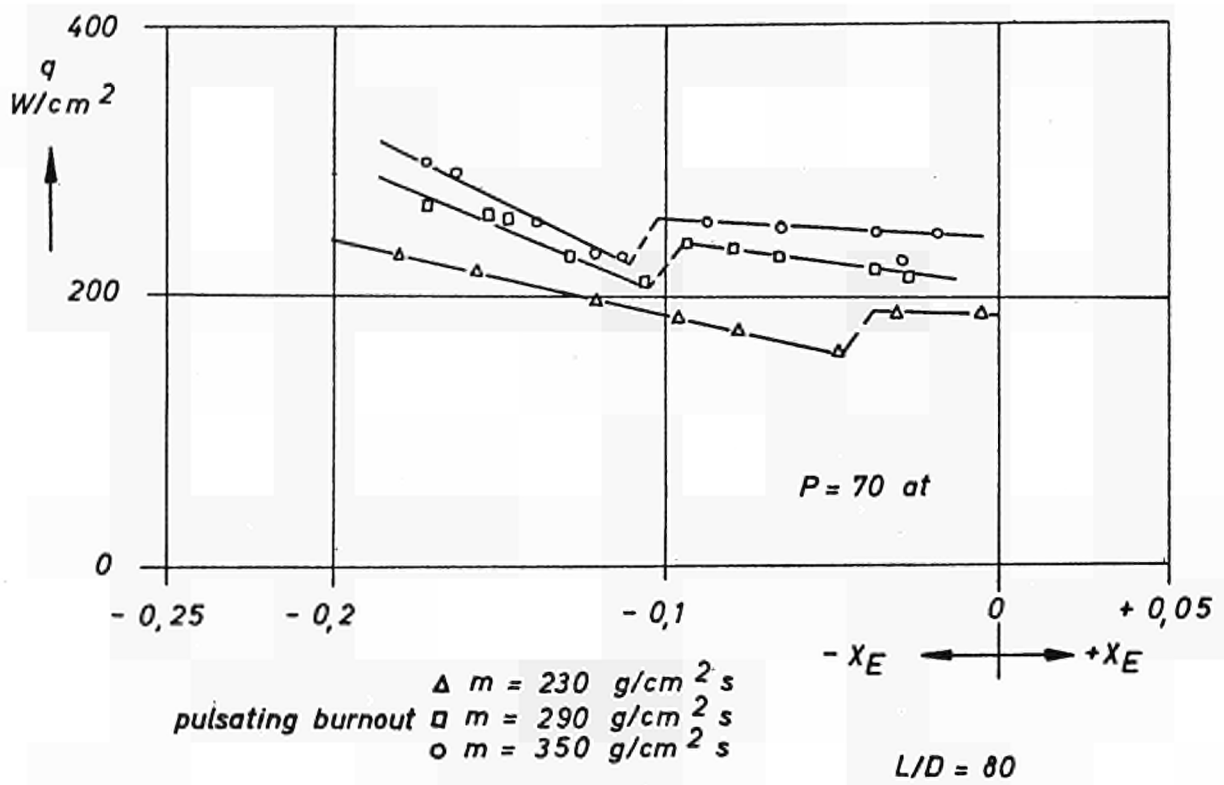
Critical heat flux plotted against inlet sub-cooling   D = 0.7 cm
Orifice plate at test section outlet

Fig. 82

Design of throttling device at test section inlet to determine the minimum pressure drop necessary to avoid pulsating burnout

Connection for differential pressure measurement

test channel

minus pole

pressure tube

connection for differential pressure measurement

throttling point

adjustable stem

flow direction
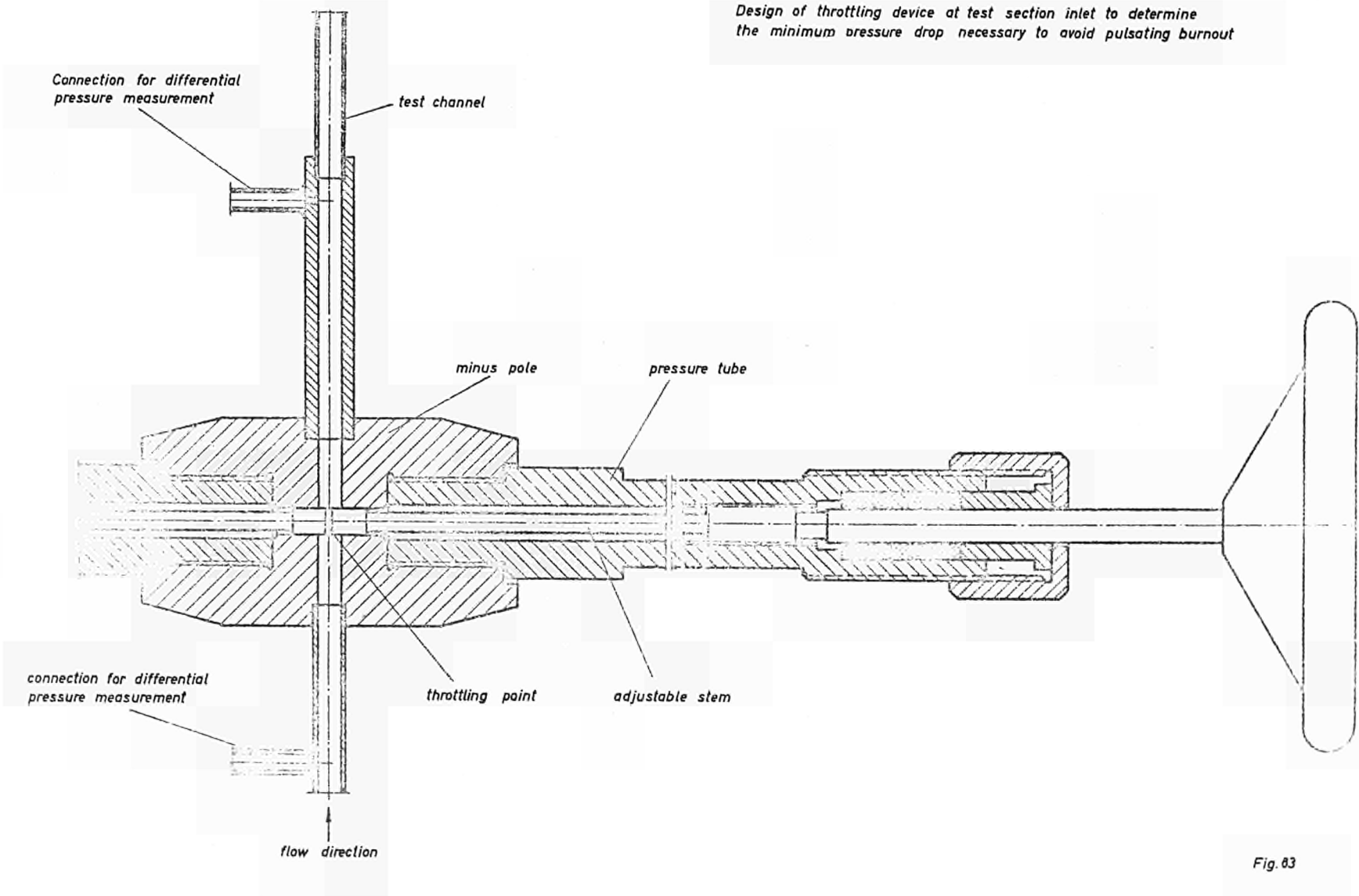
Fig. 83
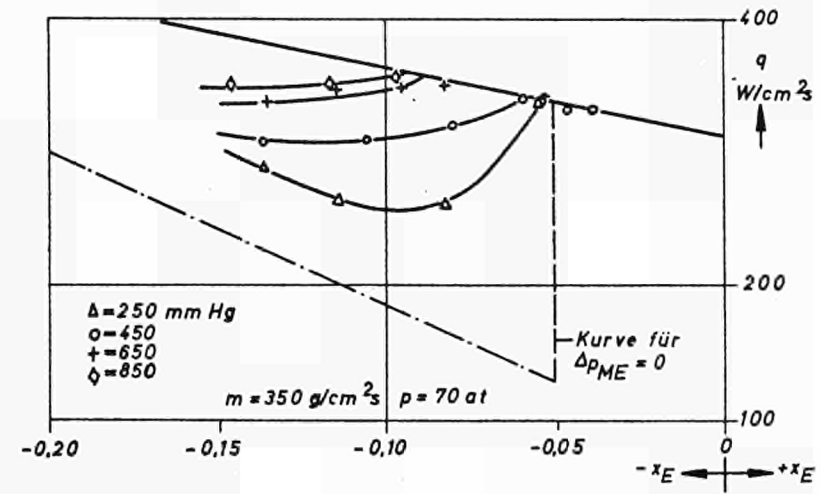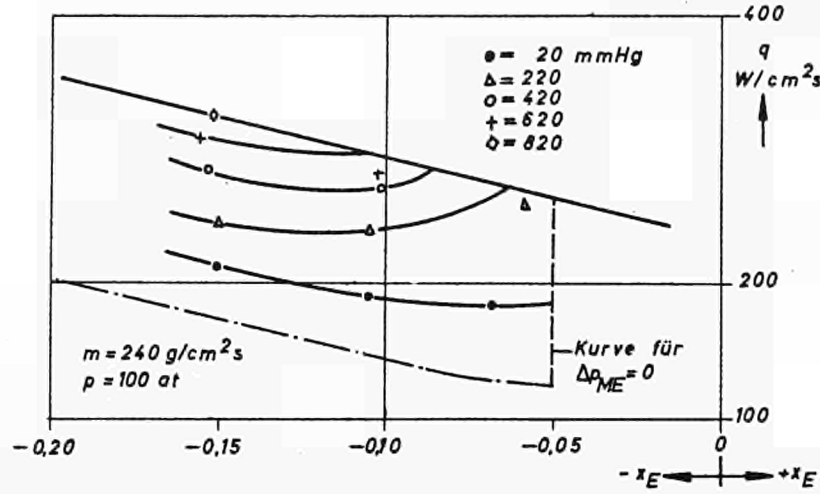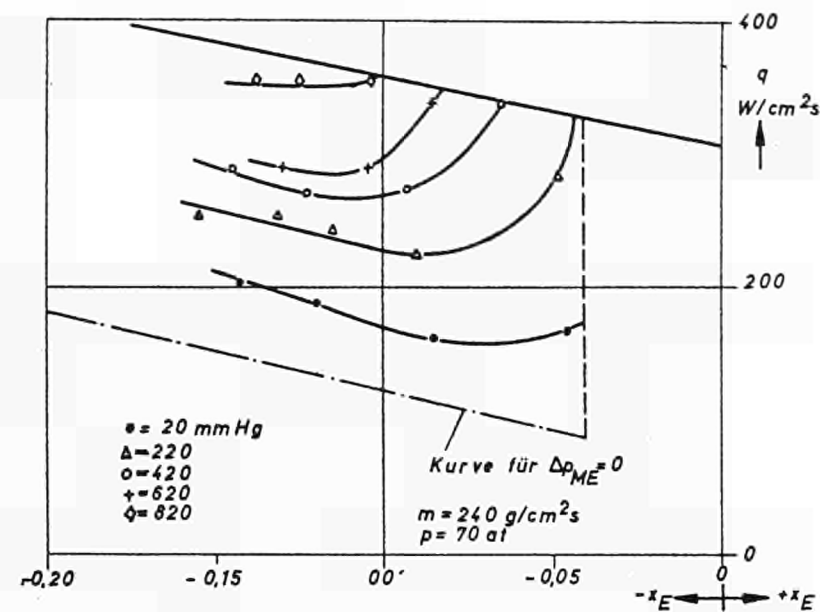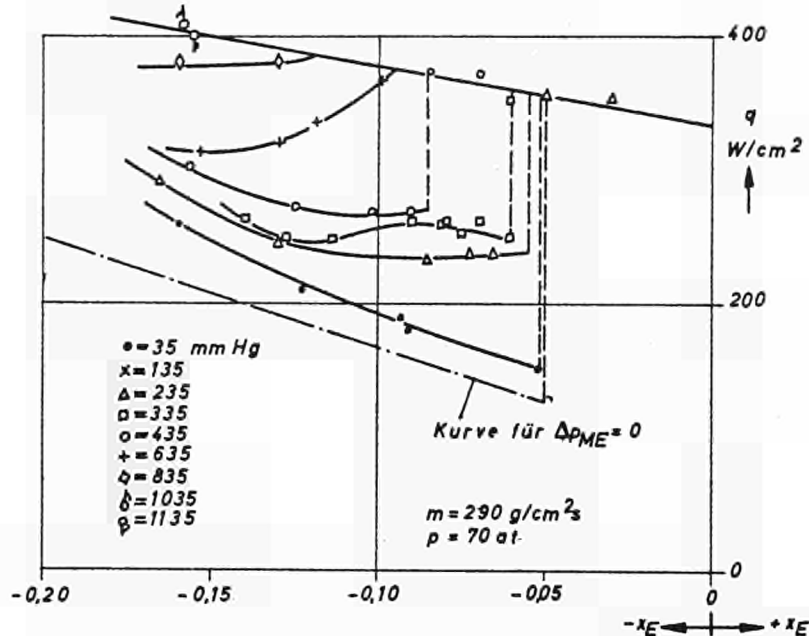
Influence of throttling at test section inlet on 2. type burnout L/D = 70, D = 0,7 cm
Pressurizer connected upstream of test section

Fig. 84

Top figure labels:
- q W/cm^{2}s
- Kurve für $\Delta p_{ME} = 0$
- $m = 290\,g/cm^2\,s$
- $p = 70\,at$
- $\bullet = 35\ mm\ Hg$
- $x = 135$
- $\triangle = 235$
- $\square = 335$
- $o = 435$
- $-x_E$ ←→ $+x_E$
- axis values: 600, 500, 400, 300, 200
- x-axis: −0,20 −0,15 −0,10 −0,05 0 +0,05

Bottom figure labels:
- q W/cm^{2}s
- Kurve für $p_{ME} = 0$
- $m = 350\,g/cm^2 s$
- $p = 70\,at$
- $\bullet = 50\ mm\ Hg$
- $x = 150$
- $\triangle = 250$
- $\square = 350$
- $o = 450$
- $-x_E$ ←→ $+x_E$
- axis values: 600, 500, 400, 300, 200
- x-axis: −0,20 −0,15 −0,10 −0,05 0 +0,05
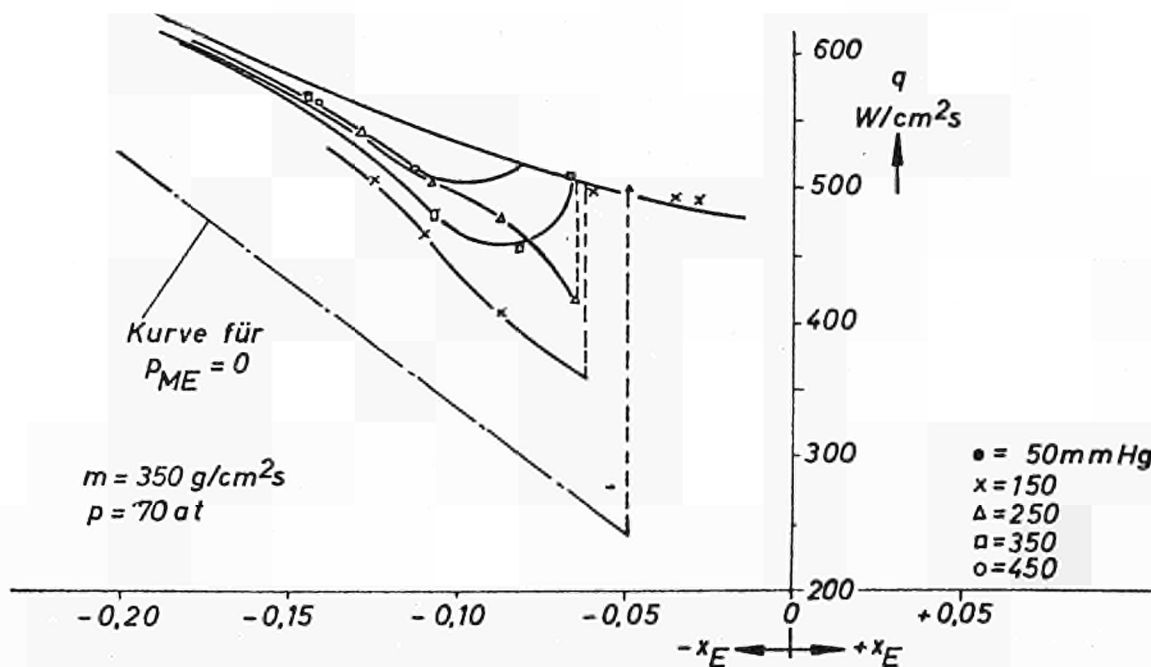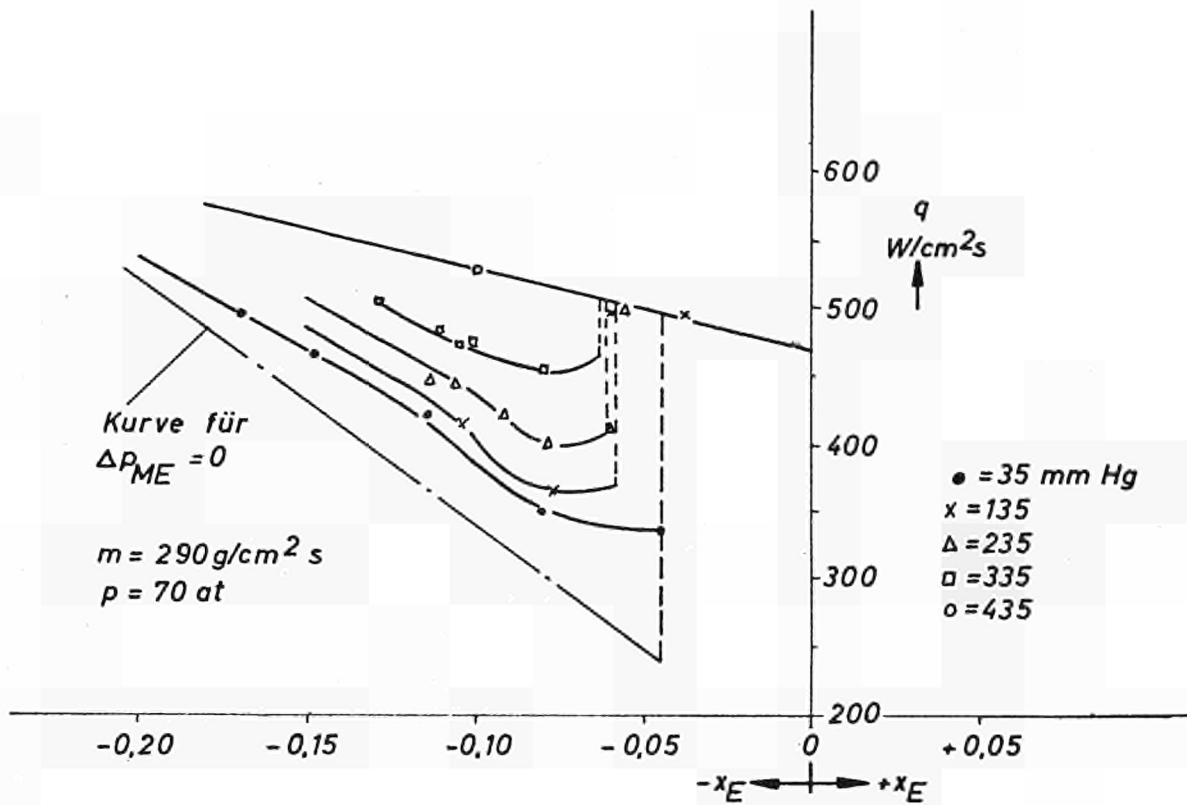
Influence of throttling at test section inlet on 2. type burnout $L/D = 40, D = 0,7cm$, $p = 70\ kgf/cm^2$

Pressurizer connected upstream of test section

Fig. 85
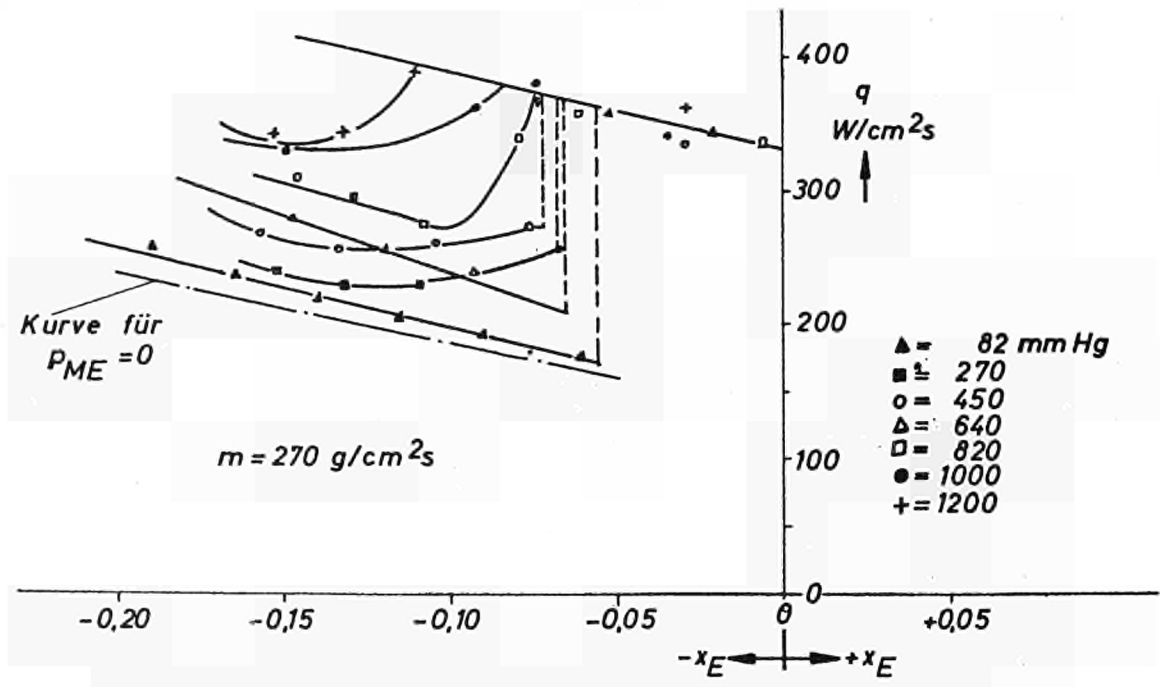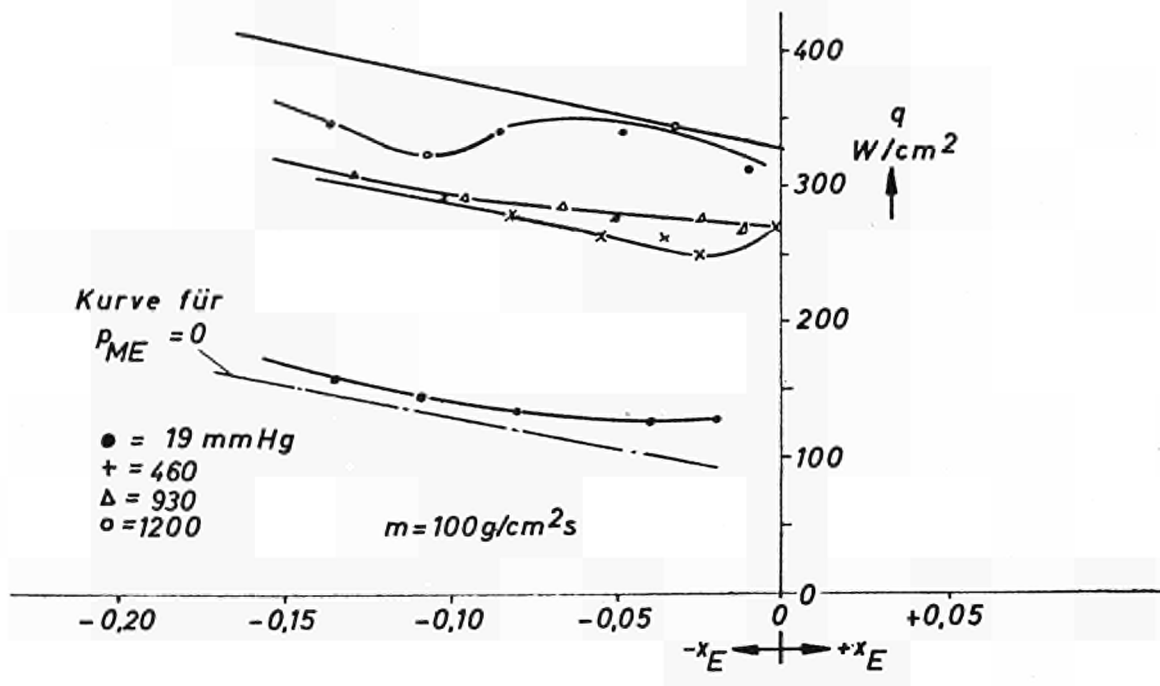
Influence of throttling at test section inlet on 2. type burnout
L/D = 40, D = 1.1 cm, p = 70 kgf/cm²

Pressurizer connected upstream of test section

Fig. 86

Top-left plot:
q W/cm²s
400
200
0
Kurve für Δp_ME = 0
o = 320 mm Hg
Δ = 510
▲ = 790
m = 220 g/cm²s
pressurizer connected upstream of test section
-0,20   -0,15   -0,10   -0,05   0
-x_E ←→ +x_E

Top-right plot:
Δp_ME = 650 mm Hg
▲ pressurizer connected downstream of test section
●Δo+∇ pressurizer connected upstream of test section
● = 65 mm Hg
Δ = 190
o = 380
+ = 640
∇ = 940
m = 100 g/cm²s
Kurve für Δp_ME = 0
q W/cm²s
400
200
0
-0,20   -0,15   -0,10   -0,05   0
-x_E ←→ +x_E
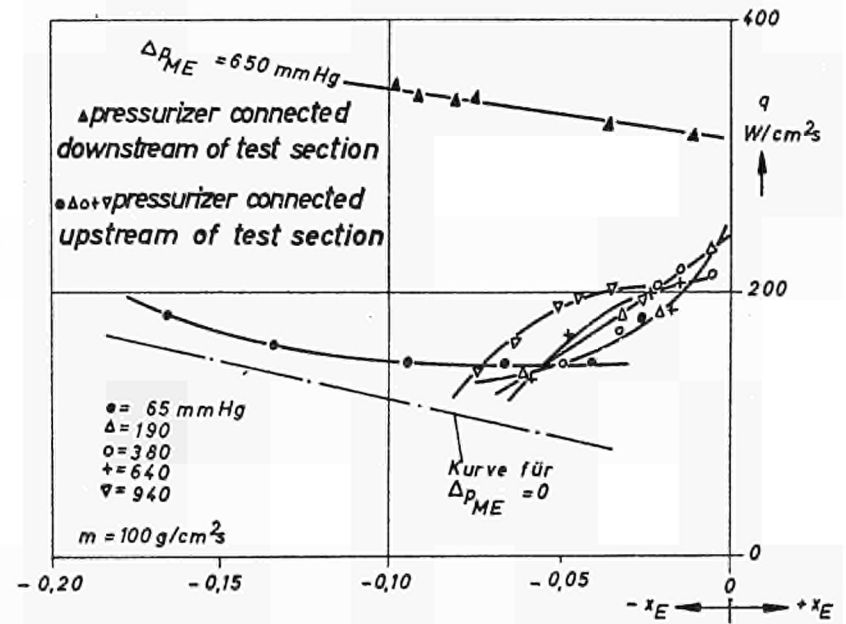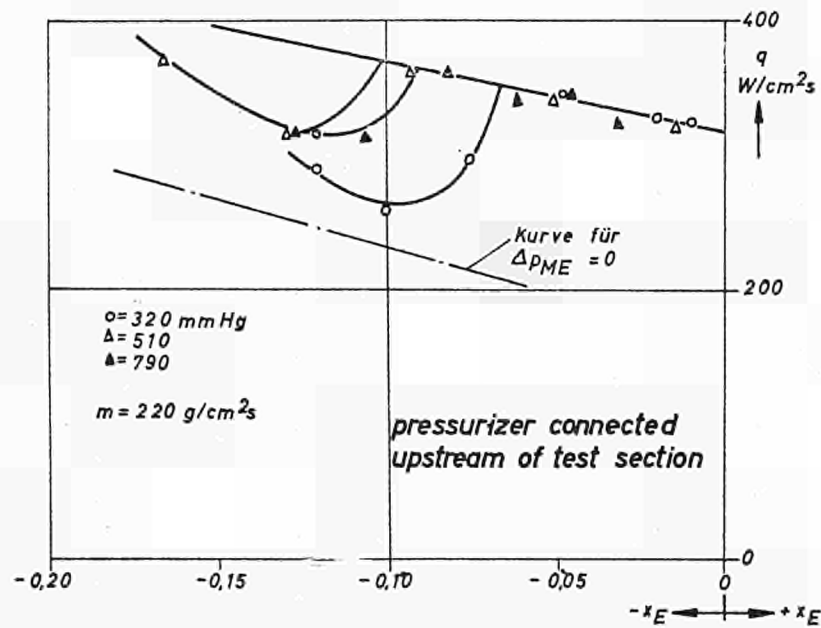
Bottom-left text:
Influence of throttling at test section inlet on 2. type burnout
L/D = 40, D = 1.5 cm, p = 70 kgf/cm²

Bottom-right plot:
▲ pressurizer connected downstream of test section
Δp_ME = 620 mm Hg
o Δ pressurizer connected upstream of test section
o = 630 mm Hg
Δ = 810 mm Hg
m = 160 g/cm²s
Kurve für Δp_ME = 0
q W/cm²s
400
200
0
0,20   0,15   0,10   0,05   0
-x_E ←→ +x_E
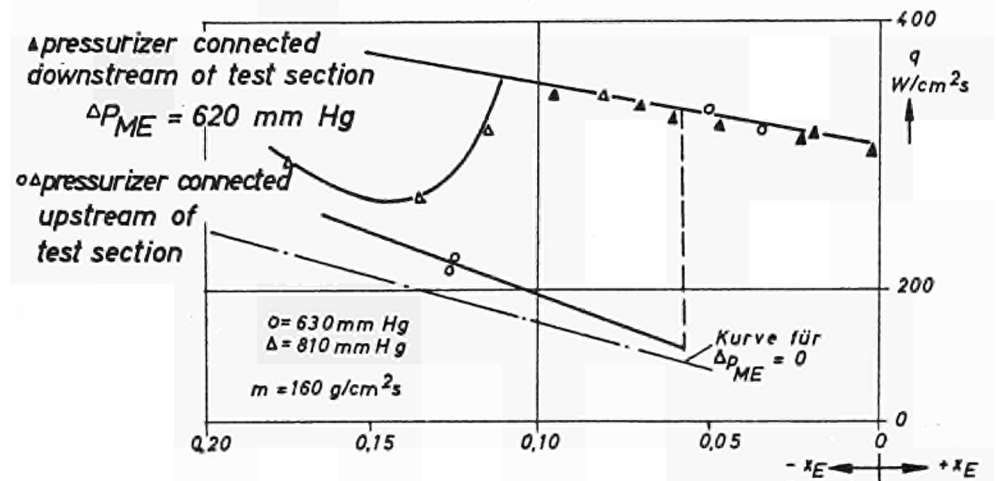
Fig. 87
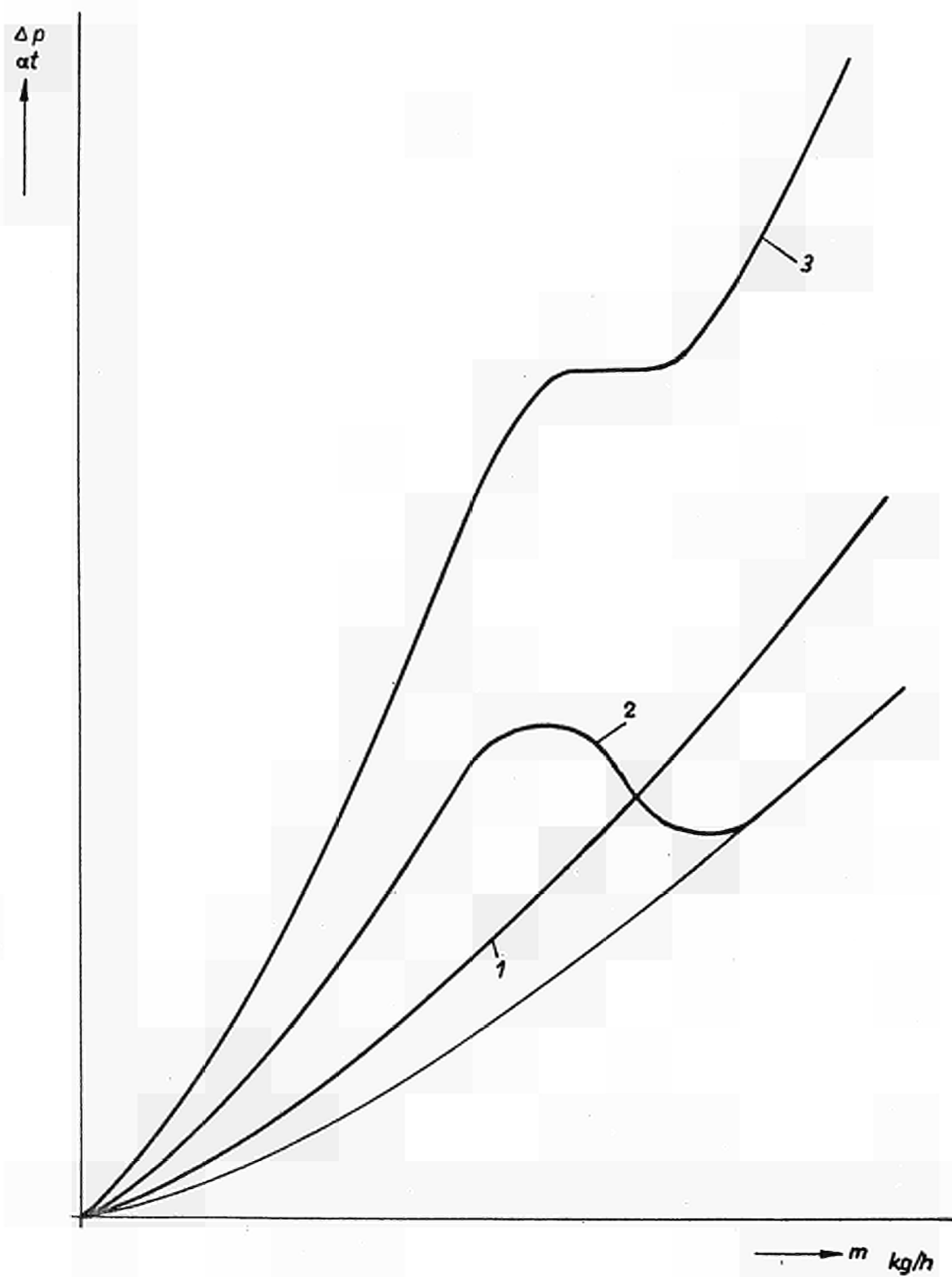
Fig. 88   Resistance charakteristics
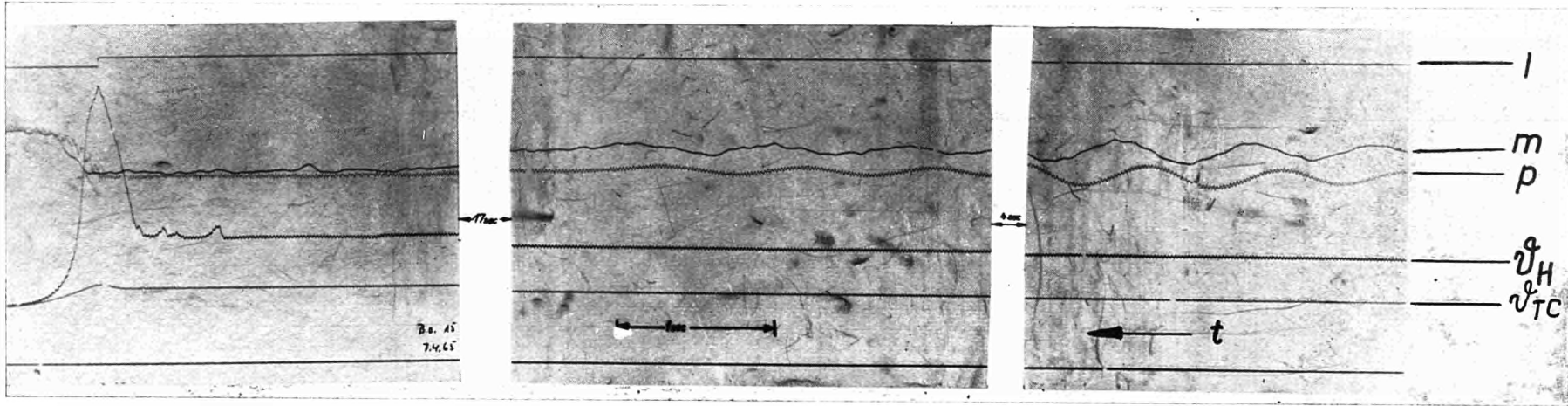
$m = 304{,}3 \ \mathrm{g/cm^2 s} \ ; \quad p = 70 \ \mathrm{at} \ ; \quad X_E = -\,0{,}1041$

$x_A = 0{,}1360 \ ; \quad L/D = 80 \ ; \quad q_{BO} = 334{,}7 \ \mathrm{W/cm^2}$

l =	Power	
m =	Mass flow	
ϑ H =	Temperature three-wire thermocouple	
ϑ TC =	Temperature thermocoax	

Fig. 89 : Hydrodynamically stable burnout
with preceding pulsations
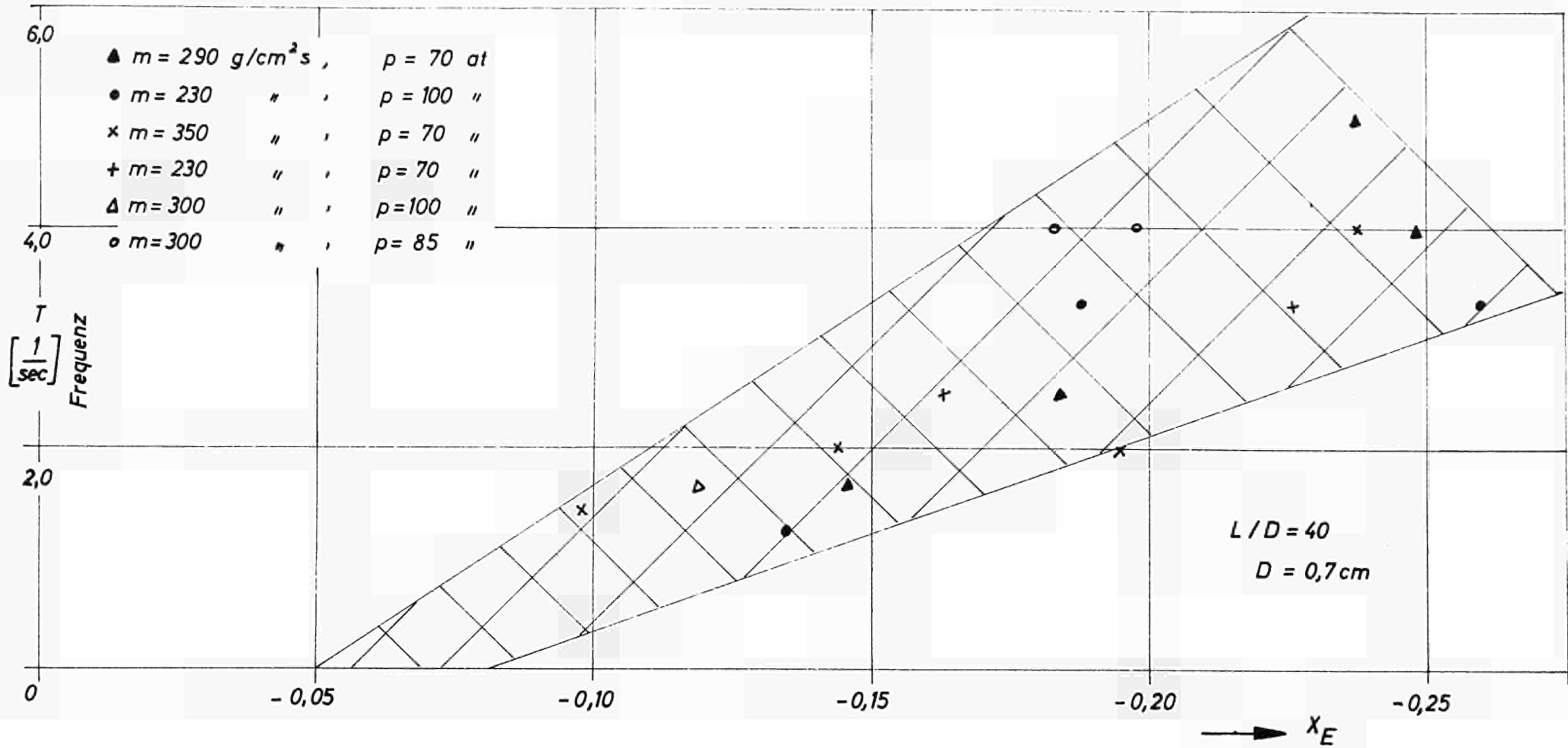
Fig. 90   Influence of inlet sub-cooling on frequency of pressure and mass flow pulsations during 2nd type burnout
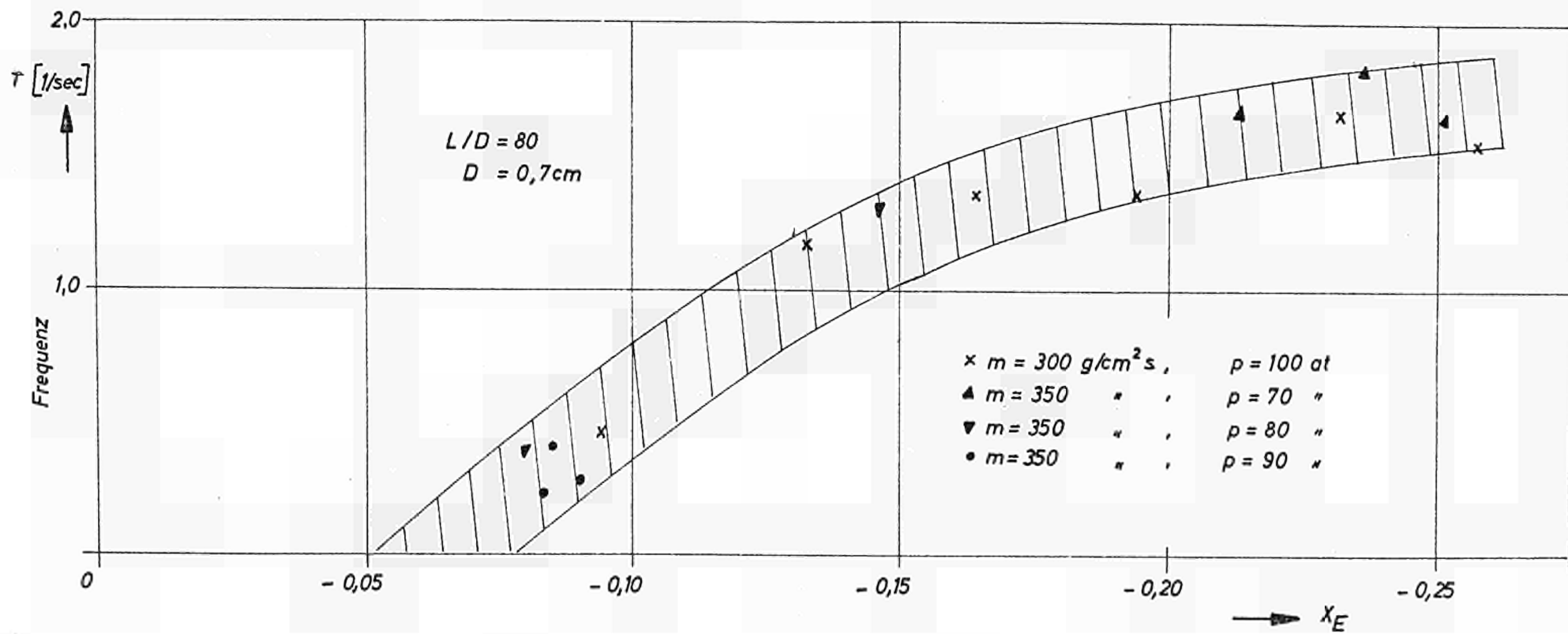
Influence of inlet sub-cooling on frequency of pressure and mass flow pulsations during 2nd type burnout

Fig. 91
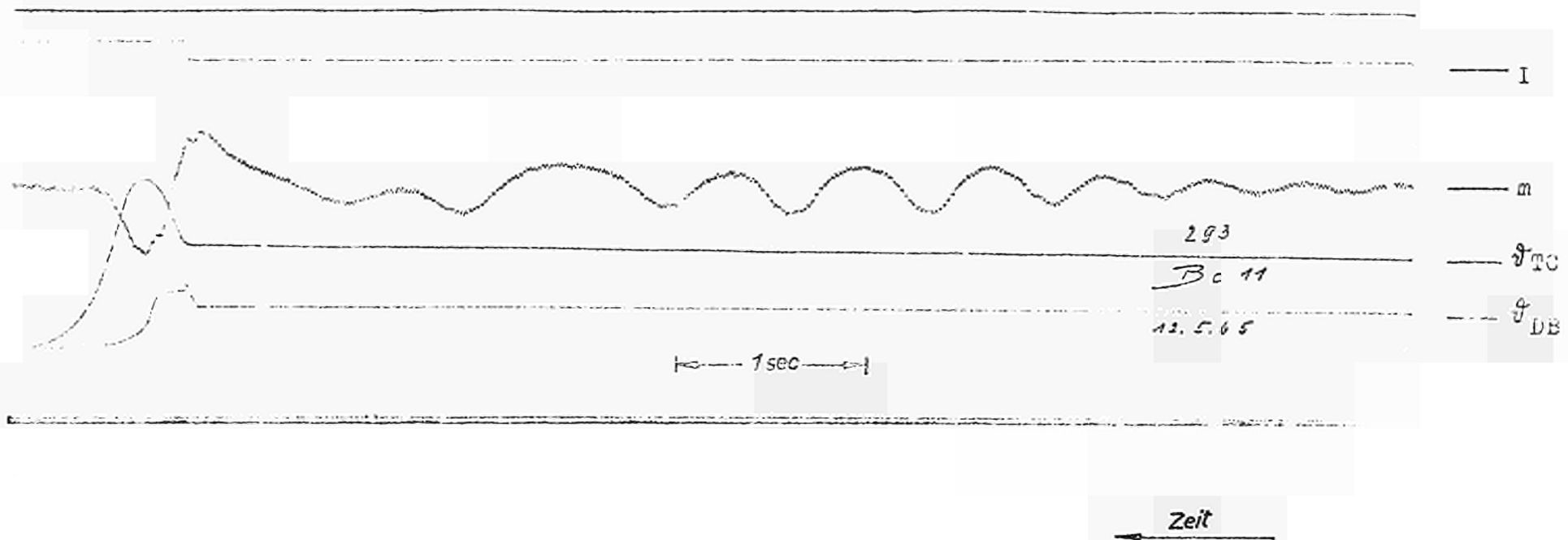
Fig. 92: Variation of wall temperature and mass flow during inception of film boiling

$m = 346,9 \text{ g/cm}^2\text{s}$, $p = 69,5 \text{ kgf/cm}^2$, $x_E = -0,087$, $x_A = 0,020$, $L/D = 40$, $q_{B.O.} = 350,1$

Pressurizer connected upstream of test channel
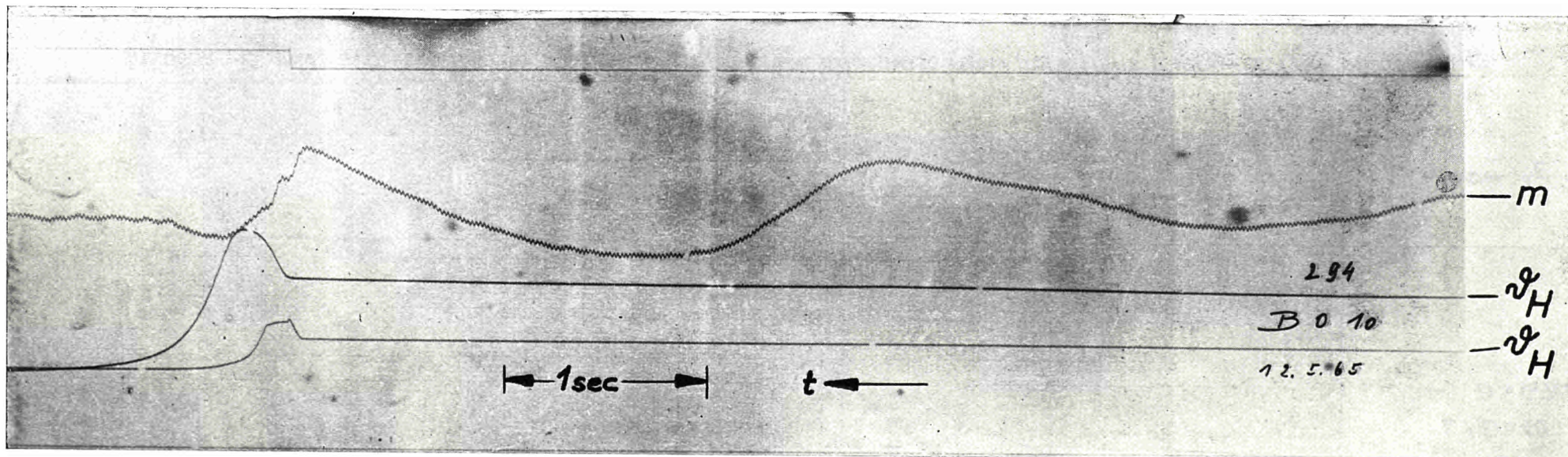
Fig. 93 : Variation of wall temperature and mass flow during inception of film boiling
$m = 346,3$ g/cm²s, $p = 70$ kgf/cm², $X_E = -0,058$, $X_A = 0,034$, L/D = 40, $q_{BO} = 303,0$

Pressurizer connected upstream of test channel
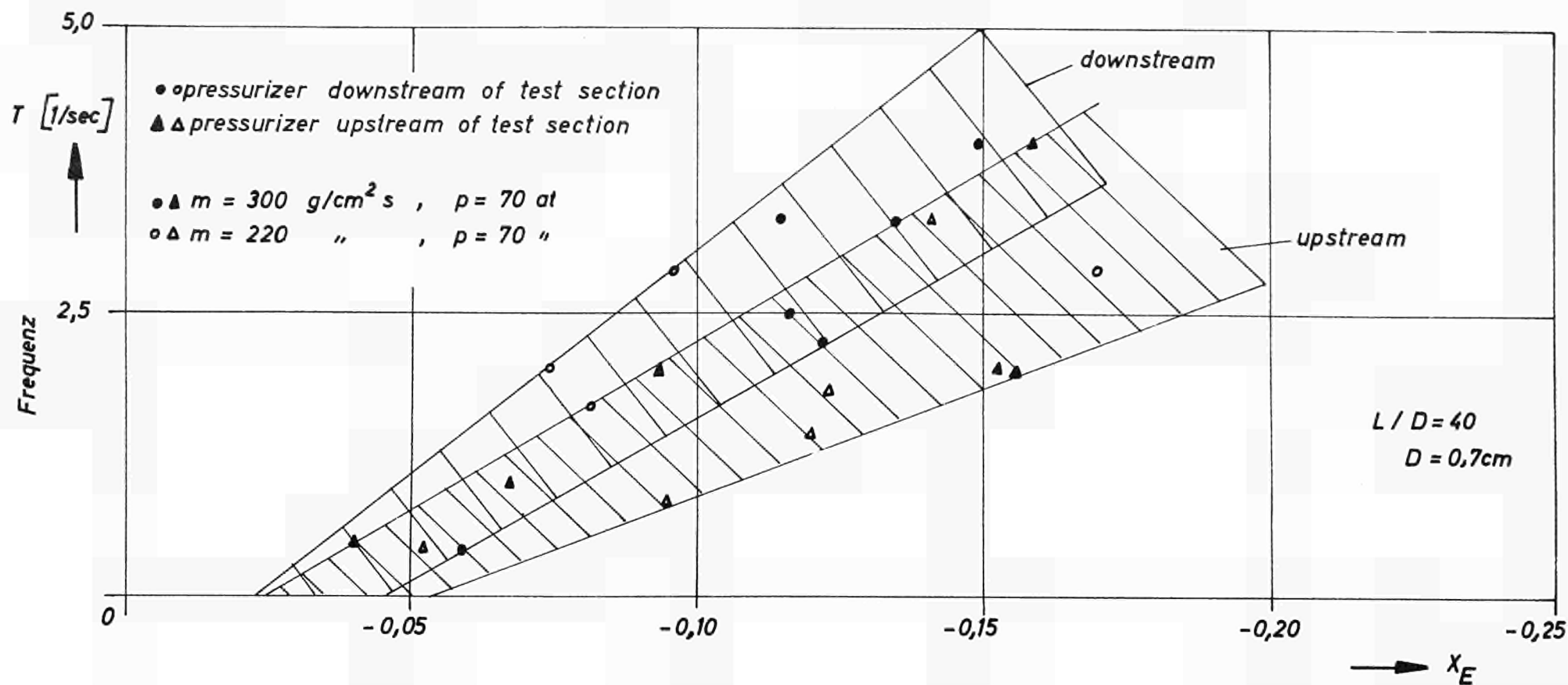
Influenz of inlet sub-cooling on frequency of pressure and mass flow pulsations during 2. type burnout

Fig. 94
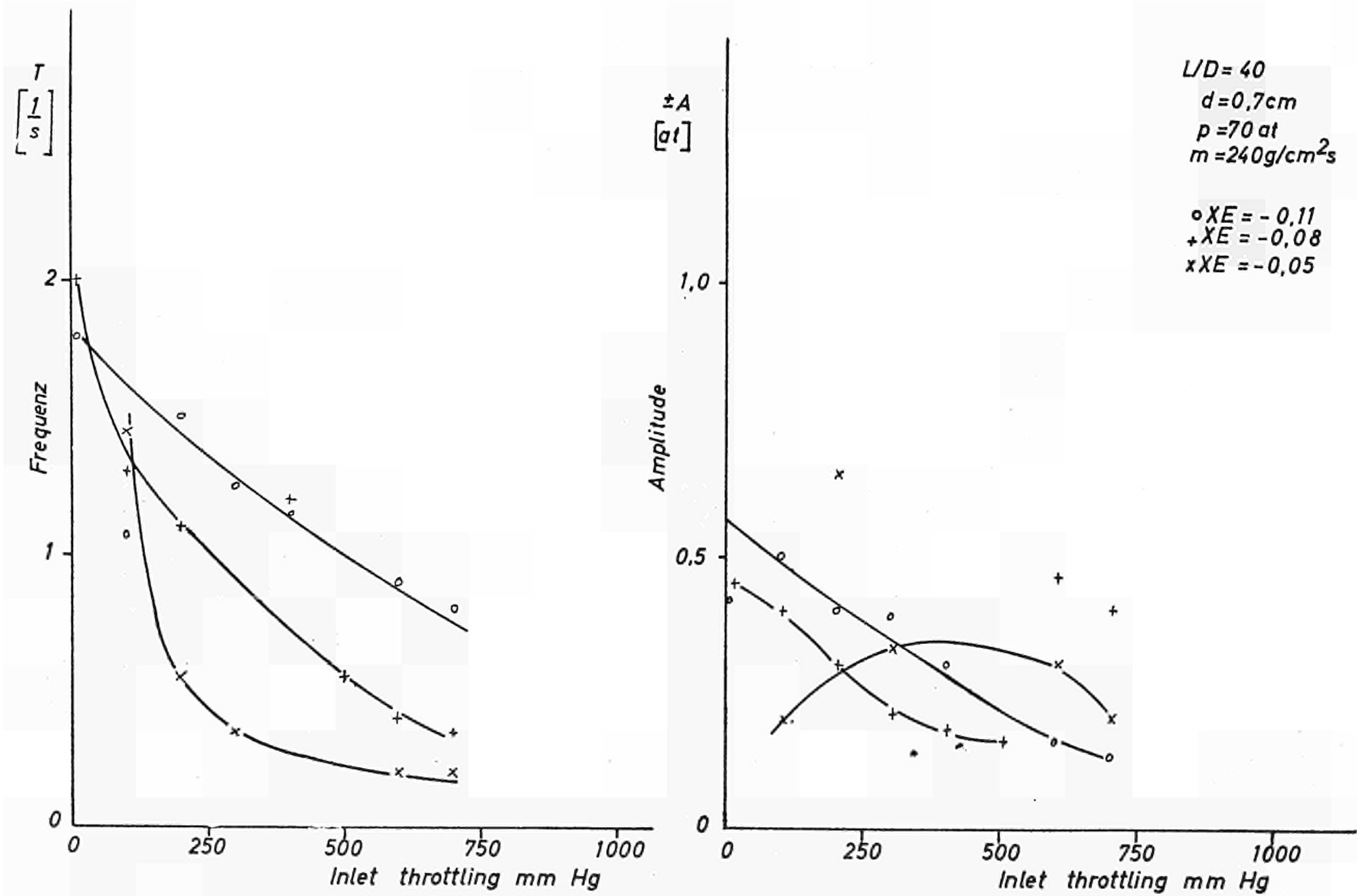
Fig. 95   Frequency and amplitude of pressure variations during pulsating burnout plotted against throttling at test section inlet
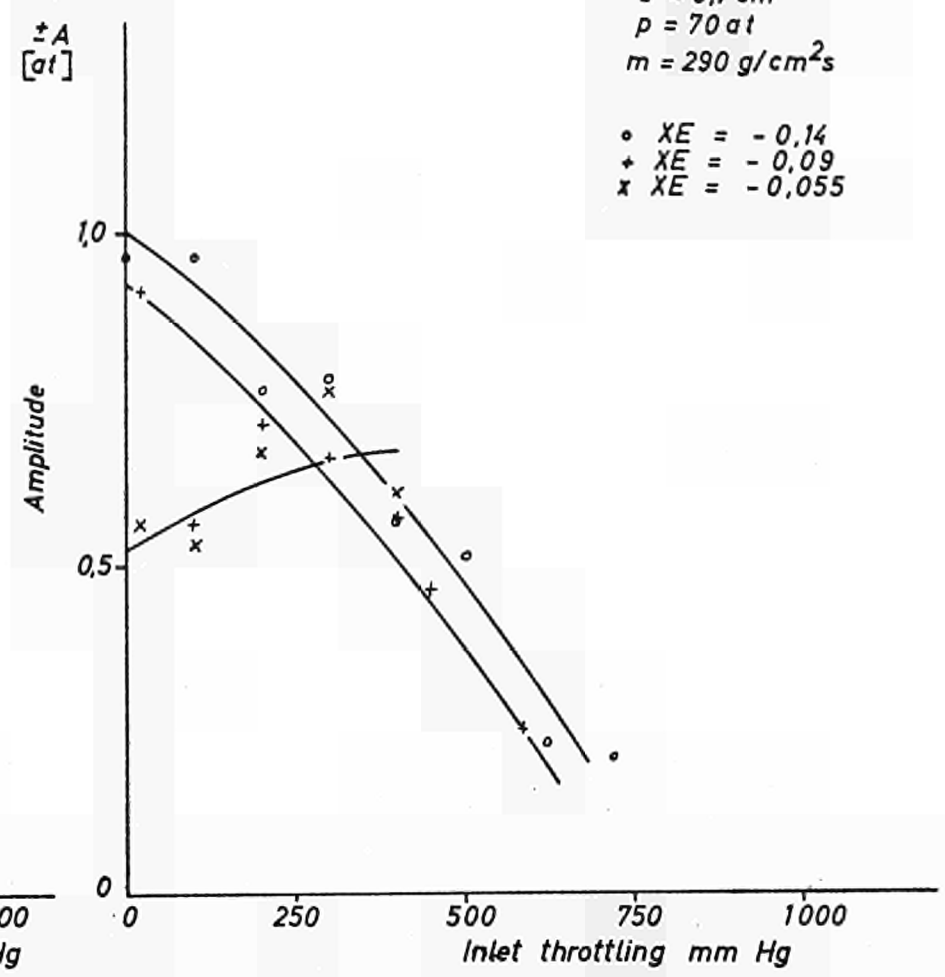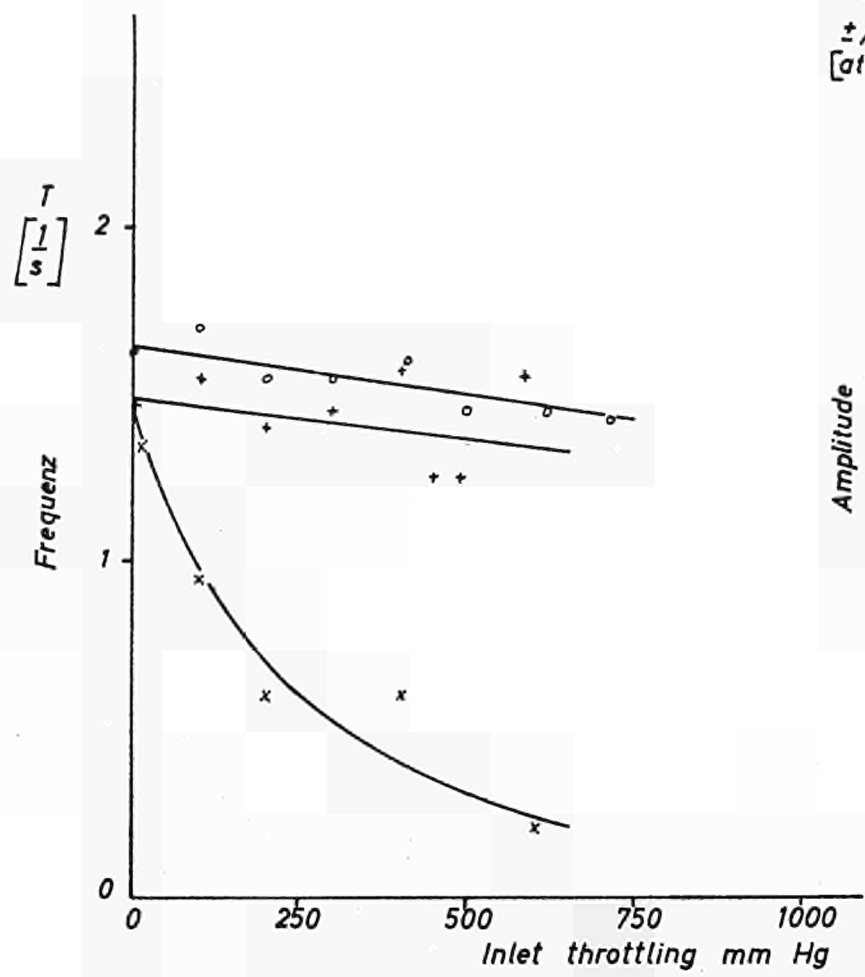
Frequency and amplitude of pressure variations in pulsating burnout plotted against throttling at test section inlet

Fig. 96

minus

plus
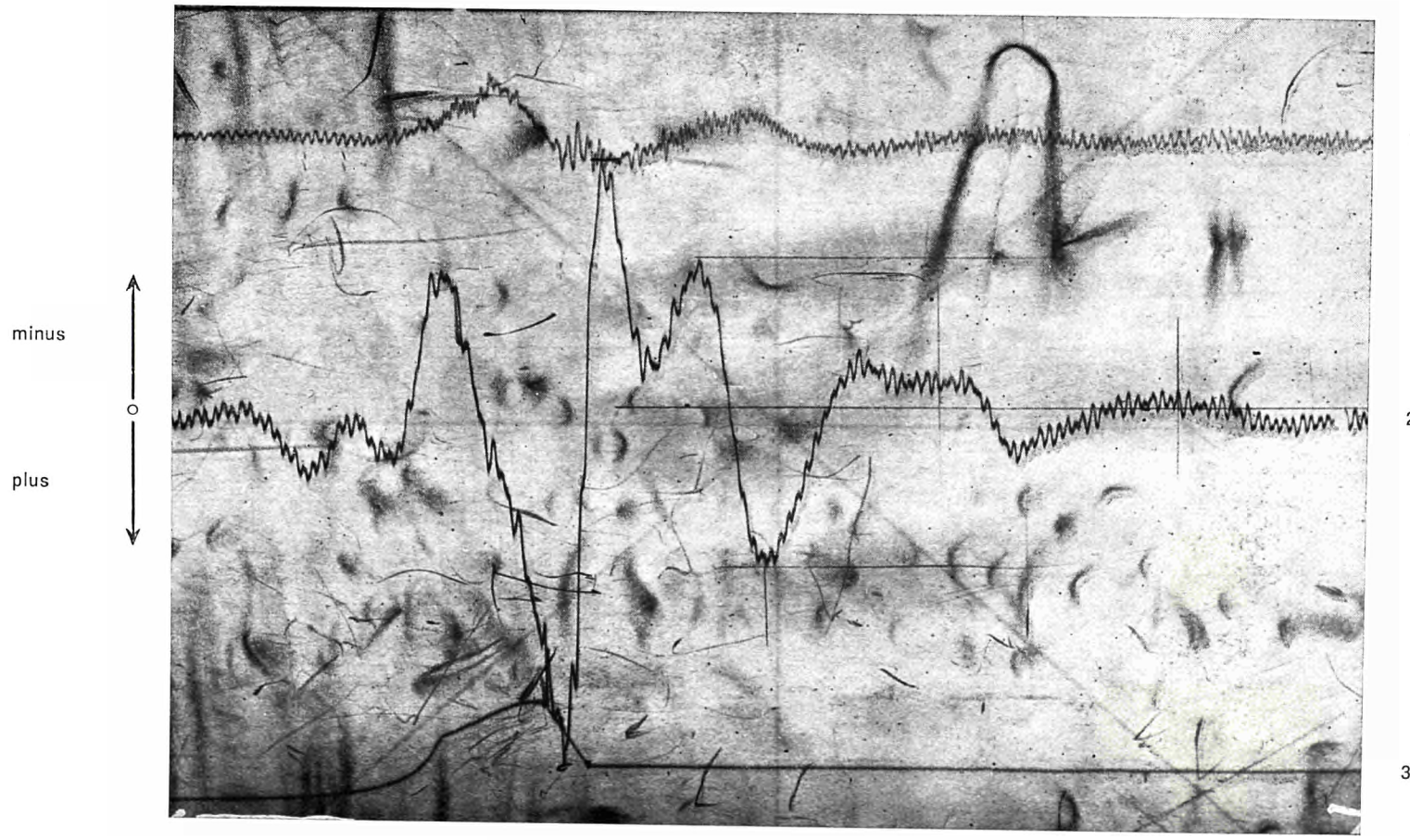
$L/D = 40$
$D = 0,7$ cm
$p = 68$ kgf/cm²
$m = 289,6$ g/cm²s
$q_{BO} = 534,9$ W/cm²
$X_E = -0,132$

Fig. 97 : Variation of pressure and mass flow during pulsating burnout
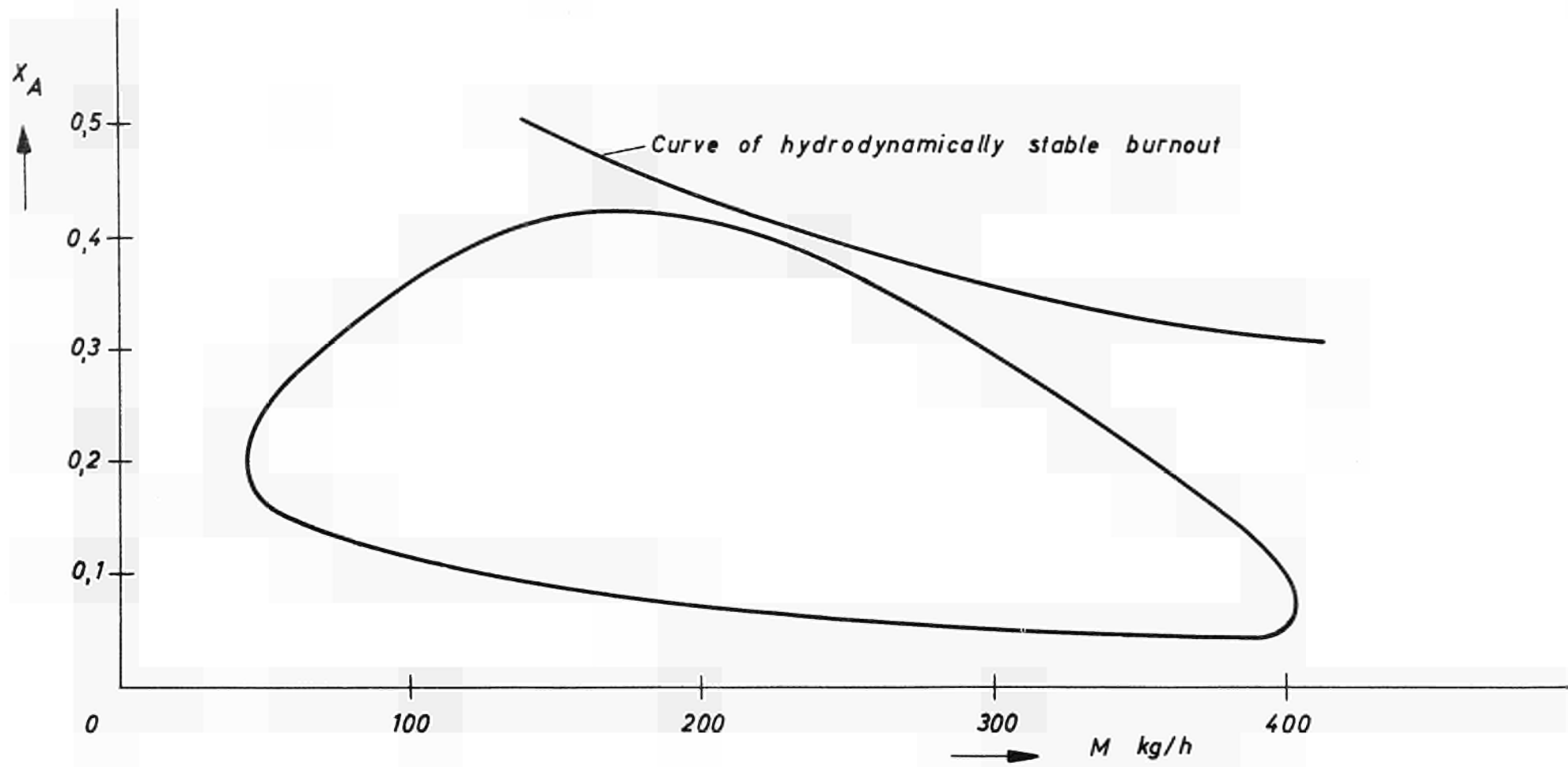
Curve of hydrodynamically stable burnout

Variation of steam quality at test section outlet under conditions of pulsating flow

Bild 98

m
zero
line
plus
↕
minus
ϑ DB
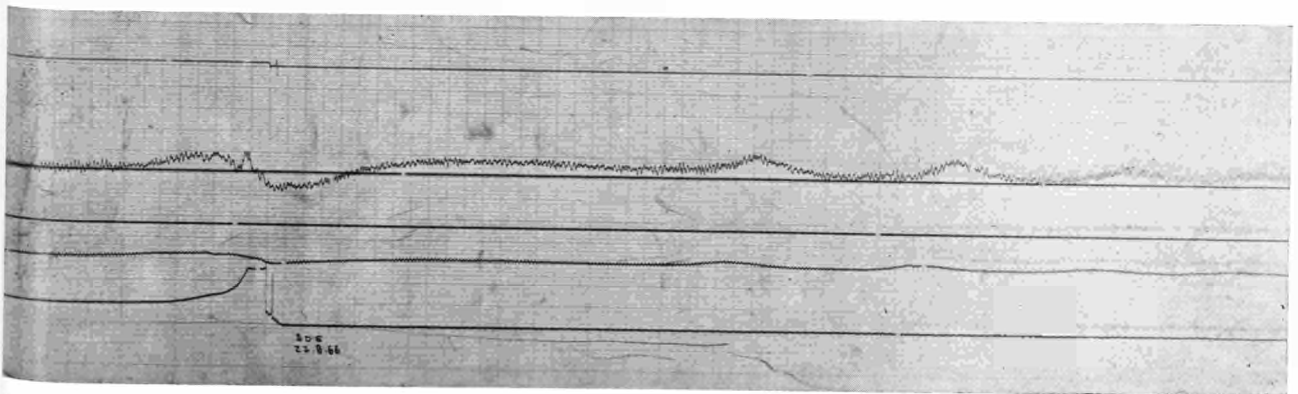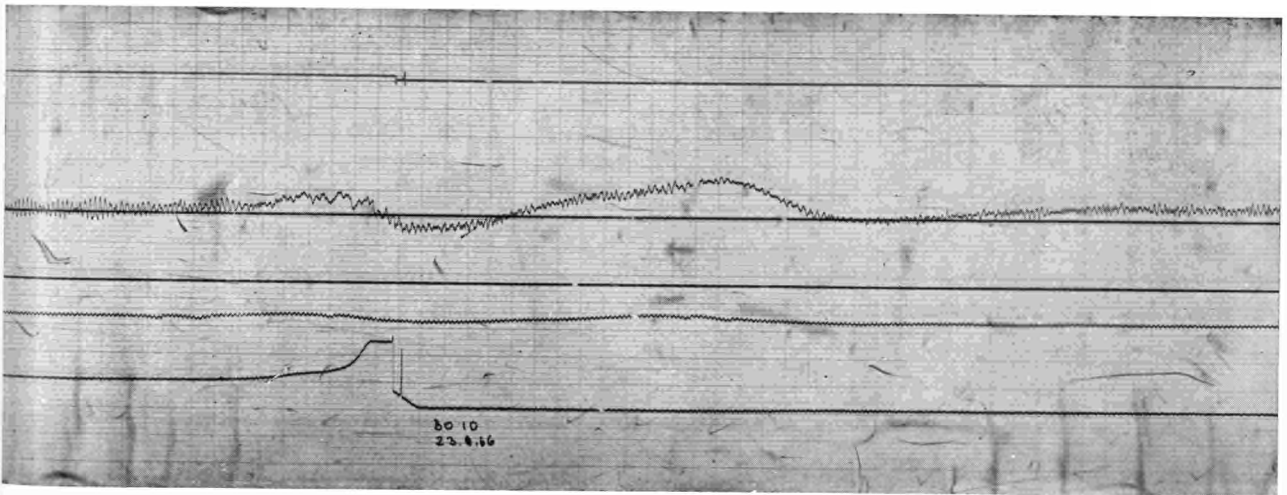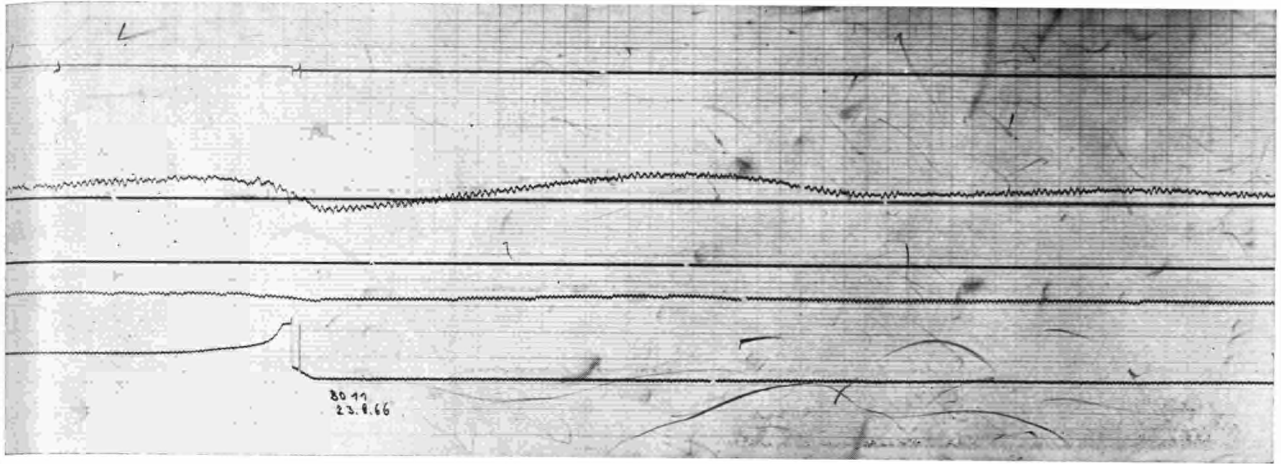
m = mass flow
ϑ = wall temperature of
test channel

Fig. 99 : Variation in time of mass flow during pulsating burnout
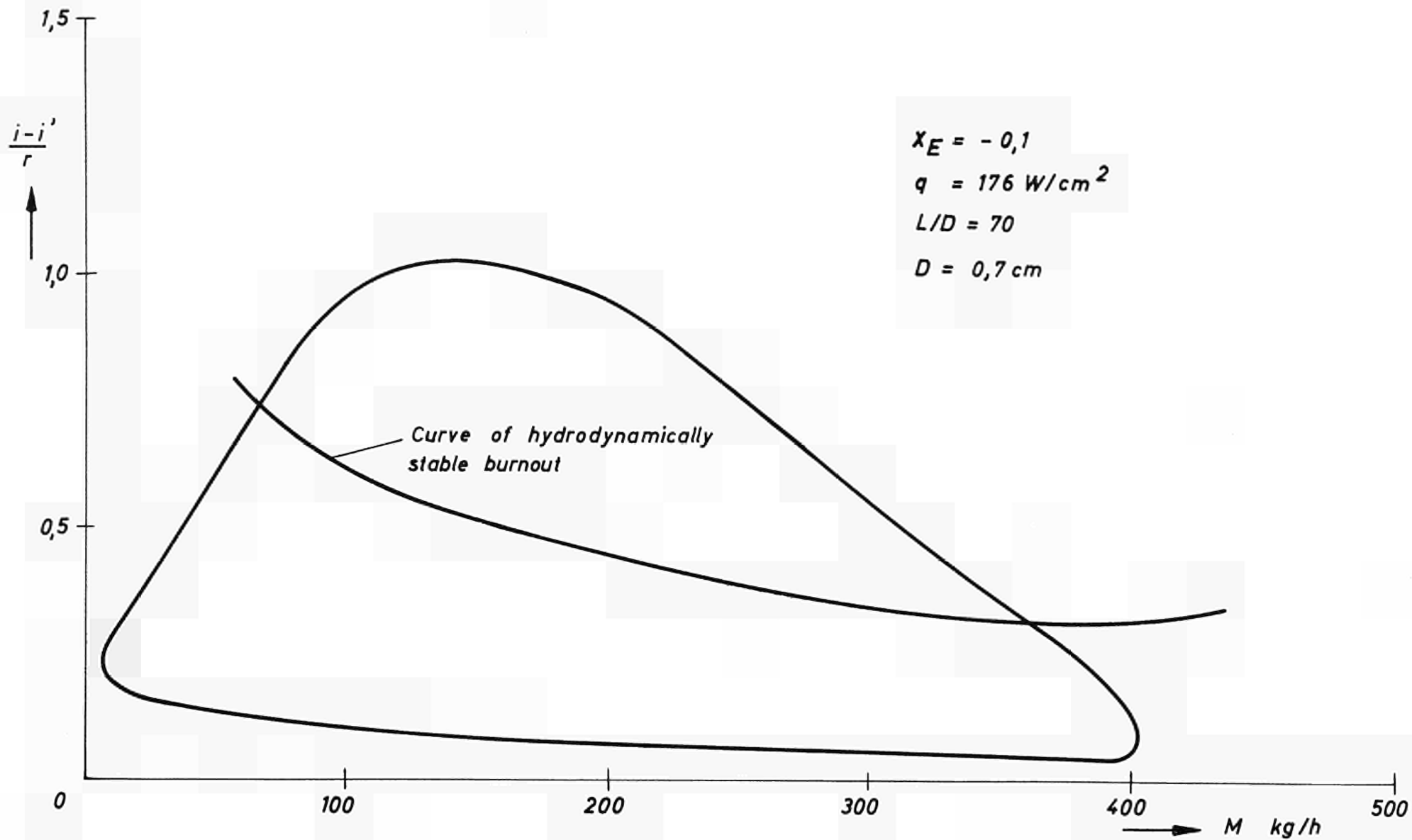
$$X_E = -0,1$$

$$q = 176 \; W/cm^2$$

$$L/D = 70$$

$$D = 0,7 \; cm$$

Curve of hydrodynamically stable burnout

$\dfrac{i-i'}{r}$

M   kg/h

Variation of steam quality at test section outlet under conditions of pulsating flow

Bild 100

Fig.101 : Temperature variation during burnout
(schematical)
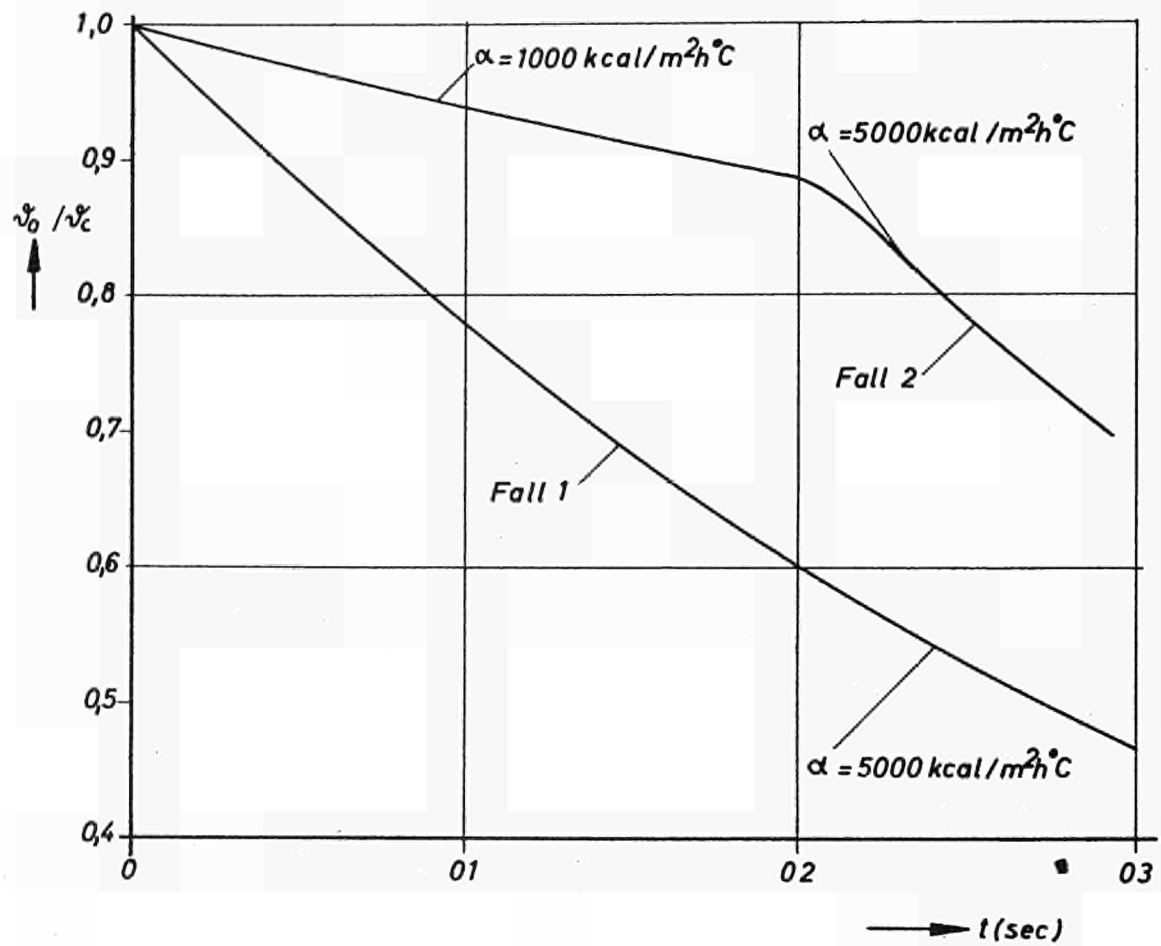
Fig. 102: Variation of temperature at tube wall with various heat transfer coefficients at cooled tube inside surface

TABLE I

SUMMARY OF IMPORTANT DATA FOR INVESTIGATIONS INTO FIRST TYPE BURNOUT

Ser. No.	Length/ diameter ratio L/D	Channel dia D cm	System pressure p at	Mass flow $\dfrac{m}{g/cm^2/s}$	Inlet quality x_E	Conditions	Remarks
1	140	0,7	70 u. 100	200 - 400	-0,3-0	long inlet section	L/D influence
2	80	0,7	70 u. 100	200 - 400	-0,5-+0,2	long inlet section	L/D influence
3	80	0,7	20 - 100	290 u.350	-0,3-0	long inlet section	p influence
4	80	0,7	70	200 - 400	-0,3-0	long inlet section	influence of loop arrangement on q_{BO}
5	80	0,7	70 - 100	200 - 400	-0,3-0	no inlet section	L/D influence
6	40	0,7	70 u. 100	200 - 400	-0,5-+0,2	long inlet section	L/D influence
7	40	0,7	70 u. 100	200 - 400	-0,3-0	long inlet section	influence of loop arrangement on q_{BO}
8	40	0,7	70 - 100	20C - 400	-0,3-0	no inlet section	L/D influence
9	40	1,1	70, 100, 140	100 - 250	-0,3-0	long inlet section	D influence
10	40	1,5	70 u. 100	100 - 250	-0,3-0	long inlet section	D influence
11	10	0,7	70 u. 100	200 - 400	-0,3-0	long inlet section	L/D influence
12	40	0,7	70 u. 100	200 - 400	-0,3-0	no inlet section	L/D influence
13	5	0,7	70	200 - 400	-0,2-0	long inlet section	L/D influence
14	40	0,7	70 u. 100	200 - 400	-0,2-0	twisted tape No.1 ($\psi = 75^\circ$)	
15	40	0,7	70 u. 100	200 - 400	-0,3-+0,2	twisted tape No.2 ($\psi = 56^\circ$)	
16	40	0,7	70 u. 100	200 - 400	-0,1-+0,2	twisted tape No.3 ($\psi = 48^\circ$)	
17	80	0,7	70 u. 100	200 - 400	-0,3-0	orifice plate No.1	
18	40	0,7	70 u. 100	200 - 400	-0,3-0	orifice plate No.2	
19	80	0,8	70 u. 100	200 - 400	-0,3-0	long inlet section	sinusoidal heat flux distribution

TABLE II

SUMMARY OF IMPORTANT DATA FOR INVESTIGATIONS INTO 2ND TYPE BURNOUT

Ser. No. –	Length/dia ratio L/D –	Channel diameter D cm	System pressure p at	Mass flow $\frac{m}{g/cm^2 s}$	Inlet quality x_E –	Flow conditions	Object of test
1	140	0,7	70 u. 100	200 - 400	-0,3-0	long inlet section	L/D influence
2	80	0,7	70 u. 100	200 - 400	-0,5-0	long inlet section	L/D influence
3	80	0,7	70, 80, 90 und 100	200 - 400	-0,31 - 0	no inlet section	p influence
4	80	0,7	70	200 - 400	-0,156 - 0	long inlet section	influence of loop arrangement
5	80	0,7	70 u. 100	200 - 400	-0,2-0,1	orifice plate No.1 at inlet	throttling at test section inlet
6	80	0,7	70 u. 100	200 - 400	-0,21-0	orifice plate at outlet	throttling at test section outlet
7	71,5	0,7	70 u. 100	200 - 400	-0,16-0	throttling valve at inlet	throttling at test section inlet
8	40	0,7	70 u. 100	200 - 400	-0,42-0,1	long inlet section	L/D influence
9	40	1,1	70, 100 und 140	100 - 250	-0,24-0	long inlet section	D influence
10	40	1,5	70 u. 100	100 - 250	-0,21-0	long inlet section	D influence
11	40	0,7	70 u. 100	200 - 400	-0,32-0	no inlet section	L/D influence
12	40	0,7	70 u. 100	200 - 300	-0,2-0,05	twisted tape No.1 at inlet	
13	40	0,7	70 u. 100	200 - 400	-0,2-0	twisted tape No.2 at inlet	
14	40	0,7	70	300 - 400	-0,17- -0,03	throttling valve at inlet	throttling at test section inlet
15	40	1,1	70	100 - 230	-0,3-0	throttling valve at inlet	throttling at test section inlet
16	40	1,5	70	100 - 230	-0,17-0	throttling valve at inlet	throttling at test section inlet
17	10	0,7	70	230	-0,18-0,1	without inlet section	L/D influence

m	$\Delta\vartheta_E$	$\Delta\vartheta_A$	x_E	x_A	q_{BO}	P
Massenfluß	Eintr.-Unter-kühlung	Austr.-Unter-kühlung	Eintr.-Qualität	Austr.-Qualität	max.Heizfl.-Belastung	Druck
Mass Flow Rate	Inlet Sub-cooling	Outlet Sub-cooling	Inlet-Quality	Outlet-Quality	Burn Out Heatflux	Pressure
g/cm² s	°C	°C	-	-	W/cm²	ata
248.1	35.4	0.0	-.117	.307	287.0	68.0
248.1	29.6	0.0	-.099	.317	280.5	69.0
247.0	24.6	0.0	-.083	.325	274.1	69.0
247.0	15.1	0.0	-.052	.337	261.1	69.0
246.9	7.8	0.0	-.027	.346	250.3	69.0
246.9	3.2	0.0	-.011	.353	242.7	71.0
304.3	64.3	0.0	-.213	.174	313.7	74.0
301.0	44.3	0.0	-.146	.236	311.6	70.0
300.8	39.6	0.0	-.131	.252	313.3	69.0
300.3	31.9	0.0	-.106	.259	297.7	69.5
301.1	25.1	0.0	-.085	.277	295.2	70.0
298.3	17.7	0.0	-.063	.221	225.1	75.0
298.3	16.0	0.0	-.057	.149	163.8	75.0
293.6	24.8	0.0	-.087	.276	285.0	74.0
293.6	10.0	0.0	-.036	.295	259.1	74.0
293.6	11.8	0.0	-.042	.316	279.6	74.0
357.8	42.1	0.0	-.138	.185	314.6	69.0
357.8	35.9	0.0	-.119	.197	307.3	69.0
353.9	30.4	0.0	-.101	.212	301.5	69.0
353.9	21.8	0.0	-.074	.228	288.2	70.0

Tabelle 1: L/D = 140, D = 0,7 cm

Table 1:

$\dot{m}$	$\Delta\vartheta_E$	$\Delta\vartheta_A$	x_E	x_A	q_{BO}	P
Massenfluß	Eintr.-Unter-kühlung	Austr.-Unter-kühlung	Eintr.-Qualität	Austr.-Qualität	max.Heizfl.-Belastung	Druck
Mass Flow Rate	Inlet Sub-cooling	Outlet Sub-cooling	Inlet-Quality	Outlet-Quality	Burn Out Heatflux	Pressure
$g/cm^2\ s$	$^\circ C$	$^\circ C$	-	-	W/cm^2	ata
352.3	10.8	0.0	-.037	.251	276.1	69.0
352.2	3.0	0.0	-.010	.272	269.3	70.0
234.4	25.8	0.0	-.106	.292	225.1	97.0
234.4	36.1	0.0	-.147	.259	228.7	98.0
234.3	44.7	0.0	-.179	.243	237.5	98.0
233.2	17.7	0.0	-.075	.307	214.0	98.0
229.6	8.7	0.0	-.038	.355	205.3	98.0
229.5	1.6	0.0	-.007	.346	193.7	99.0
288.5	43.2	0.0	-.173	.189	251.1	98.0
291.3	32.6	0.0	-.132	.212	242.1	97.0
291.4	20.5	0.0	-.085	.239	228.5	97.0
291.4	11.2	0.0	-.048	.264	219.3	97.0
286.6	5.4	0.0	-.023	.278	207.7	98.0
286.6	0.0	0.0	.030	.328	204.6	98.0
345.2	25.3	0.0	-.105	.172	230.1	98.0
345.1	23.0	0.0	-.096	.185	233.4	98.0
346.5	13.0	0.0	-.055	.214	224.7	97.0
347.3	0.0	0.0	.004	.259	212.2	98.0
346.1	39.4	0.0	-.158	.150	257.6	97.0
348.7	52.9	0.0	-.207	.118	273.7	97.0
350.4	52.2	0.0	-.203	.133	285.8	96.0

Tabelle 2: L/D = 140, D = 0,7 cm
Table 2:

$\dot{m}$	$\Delta\vartheta_E$	$\Delta\vartheta_A$	x_E	x_A	q_{BO}	P
Massenfluß	Eintr.-Unter-kühlung	Austr.-Unter-kühlung	Eintr.-Qualität	Austr.-Qualität	max.Heizfl.-Belastung	Druck
Mass Flow Rate	Inlet Sub-cooling	Outlet Sub-cooling	Inlet-Quality	Outlet-Quality	Burn Out Heatflux	Pressure
$g/cm^2\,s$	$^\circ C$	$^\circ C$	-	-	W/cm^2	ata
231.9	9.6	0.0	-.043	.190	128.1	101.0
225.5	17.9	0.0	-.078	.170	132.7	101.0
225.3	15.2	0.0	-.066	.172	127.4	101.0
238.0	7.1	0.0	-.025	.116	92.4	70.9
239.3	11.8	0.0	-.041	.114	106.8	70.8
320.5	5.3	0.0	-.018	.121	121.9	69.0
314.1	13.1	0.0	-.045	.116	137.5	69.0
313.5	11.1	0.0	-.038	.109	126.0	69.0
372.2	7.5	0.0	-.026	.132	159.1	70.5
369.0	7.2	0.0	-.025	.138	163.3	70.5
373.4	5.7	0.0	-.020	.138	159.3	71.0

Tabelle 3: L/D = 140, D = 0,7 cm
Table 3:

m	x_E	x_A	q_{BO}	p_{EM}
Massenfluß	Eintr.-Qualität	Austr.-Qualität	max. Heizfl.-Belastung	Druck
Mass Flow Rate	Inlet-Quality	Outlet-Quality	Burnout Heatflux	Pressure
$g/cm^2 s$	–	–	W/cm^2	at
223.2	.158	.405	254.8	68.0
229.2	.121	.297	245.3	69.0
241.1	.085	.337	279.0	70.0
231.7	.054	.332	297.5	68.0
237.4	.009	.293	308.0	70.0
237.7	-.010	.280	320.0	68.0
240.1	-.039	.232	300.9	68.0
241.1	-.134	.200	373.6	68.0
241.1	-.111	.214	362.3	68.5
241.1	-.082	.233	351.0	68.5
304.1	-.095	.162	362.3	68.0
280.5	.119	.341	287.3	68.0
278.6	.101	.325	287.3	68.8
278.4	.102	.322	284.0	67.9
273.4	.088	.326	300.9	67.9
273.4	.047	.292	309.6	67.9
293.1	.026	.257	311.2	68.5
276.6	.020	.257	297.5	72.5
279.1	.022	.259	300.9	71.5
284.6	-.002	.239	318.2	68.5

Tabelle 4: L/D = 80, D = 0,7 cm
Rohre mit langer Einlaufstrecke

Table 4: L/D = 80, D = 0,7 cm
Channels with long inlet section

m	x_E	x_A	q_{BO}	p_{EM}
Massenfluß	Eintr.-Qualität	Austr.-Qualität	max. Heizfl.-Belastung	Druck
Mass Flow Rate	Inlet-Quality	Outlet-Quality	Burnout Heatflux	Pressure
$g/cm^2 s$	-	-	W/cm^2	at
286.3	-.033	.207	318.6	68.5
329.2	-.082	.285	311.4	66.5
331.7	.026	.236	323.7	66.5
333.4	.012	.222	325.5	66.5
333.4	-.018	.197	334.4	66.5
333.1	-.055	.164	340.2	67.0
343.0	-.098	.139	377.6	67.0
334.9	-.113	.129	377.6	67.0
325.0	.059	.258	300.9	66.0

Tabelle 5: L/D = 80, D = 0,7 cm
Rohre mit langer Einlaufstrecke

Table 5: L/D = 80, D = 0,7 cm
Channels with long inlet section

m	$\Delta\vartheta_E$	$\Delta\vartheta_A$	x_E	x_A	q_{BO}	P
Massenfluß	Eintr.-Unter-kühlung	Austr.-Unter-kühlung	Eintr.-Qualität	Austr.-Qualität	max.Heizfl.-Belastung	Druck
Mass Flow Rate	Inlet Sub-cooling	Outlet Sub-cooling	Inlet-Quality	Outlet-Quality	Burn Out Heatflux	Pressure
$g/cm^2\ s$	$°C$	$°C$	–	–	W/cm^2	ata
232.8	.1	0.0	0.000	.189	177.7	100.5
242.1	.6	0.0	-.003	.205	205.1	100.5
240.9	5.8	0.0	-.026	.191	210.9	101.0
239.2	2.3	0.0	-.010	.208	210.0	101.0
240.2	9.3	0.0	-.041	.181	214.6	101.0
236.9	7.3	0.0	-.033	.201	223.2	101.0
285.7	2.0	0.0	-.009	.178	215.2	101.0
290.0	1.5	0.0	-.007	.168	204.3	101.0
289.1	8.6	0.0	-.038	.137	204.9	101.0
291.5	13.3	0.0	-.058	.141	234.0	100.5
292.5	10.7	0.0	-.047	.139	220.8	100.5
351.8	17.4	0.0	-.075	.098	245.6	101.0
351.0	15.4	0.0	-.067	.105	243.7	101.0
343.4	15.4	0.0	-.067	.110	245.0	101.0
349.9	13.1	0.0	-.058	.112	239.1	101.0
348.7	3.8	0.0	-.017	.144	227.6	101.1
348.8	10.0	0.0	-.044	.112	220.5	100.5

Tabelle 6: L/D = 80, D = 0,7 cm
Rohre mit langer Einlaufstrecke

Table 6: L/D = 80, D = 0,7 cm
Channels with long inlet section

$\dot{m}$	$\Delta\vartheta_E$	$\Delta\vartheta_A$	x_E	x_A	q_{BO}	P
Massenfluß	Eintr.-Unter-kühlung	Austr.-Unter-kühlung	Eintr.-Qualität	Austr.-Qualität	max.Heizfl.-Belastung	Druck
Mass Flow Rate	Inlet Sub-cooling	Outlet Sub-cooling	Inlet-Quality	Outlet-Quality	Burn Out Heatflux	Pressure
$g/cm^2\ s$	$^{\circ}C$	$^{\circ}C$	–	–	W/cm^2	ata
288.6	18.7	0.0	-.044	.262	514.3	21.4
288.6	32.6	0.0	-.078	.235	527.9	21.2
288.6	37.9	0.0	-.088	.227	535.5	19.0
289.9	55.9	0.0	-.130	.181	526.2	20.5
327.4	30.5	0.0	-.074	.202	517.7	25.0
325.9	33.6	0.0	-.082	.200	528.3	23.8
326.6	41.9	0.0	-.099	.186	540.8	21.8
332.7	51.2	0.0	-.121	.167	556.3	22.2
333.5	56.2	0.0	-.132	.157	561.8	21.0
293.2	11.3	0.0	-.029	.272	484.4	33.5
290.4	23.7	0.0	-.062	.253	501.2	33.5
290.4	34.6	0.0	-.090	.235	517.4	33.5
291.3	48.9	0.0	-.125	.205	520.5	33.0
340.9	17.0	0.0	-.044	.225	506.2	32.5
340.1	25.5	0.0	-.066	.209	514.3	32.5
339.2	34.4	0.0	-.089	.198	535.5	32.5
341.6	47.3	0.0	-.121	.169	545.1	32.5
288.8	9.3	0.0	-.028	.252	406.1	33.5
288.8	19.3	0.0	-.059	.227	414.2	33.5
288.8	26.3	0.0	-.078	.216	430.7	31.0

Tabelle 7: L/D = 80, D = 0,7 cm

Rohre mit langer Einlaufstrecke. Meßwerte zur Bestimmung des Einflusses von p auf $q_{B.O.}$.

Table 7: L/D = 80, D = 0,7 cm

Channels with long inlet section. Data to determine the effect of p on $q_{B.O.}$.

m	$\Delta\vartheta_E$	$\Delta\vartheta_A$	x_E	x_A	q_{BO}	p
Massenfluß	Eintr.-Unter-kühlung	Austr.-Unter-kühlung	Eintr.-Qualität	Austr.-Qualität	max.Heizfl.-Belastung	Druck
Mass Flow Rate	Inlet Sub-cooling	Outlet Sub-cooling	Inlet-Quality	Outlet-Quality	Burn Out Heatflux	Pressure
g/cm^2 s	$^{\circ}C$	$^{\circ}C$	-	-	W/cm^2	ata
288.8	41.5	0.0	-.121	.188	452.1	51.0
289.7	40.0	0.0	-.115	.189	450.4	49.0
341.8	11.3	0.0	-.033	.196	403.6	48.0
341.9	13.8	0.0	-.040	.207	435.3	48.0
341.9	33.7	0.0	-.097	.167	463.6	48.0
341.9	48.1	0.0	-.139	.132	470.7	50.5
288.9	19.6	0.0	-.066	.200	361.6	69.0
288.9	27.1	0.0	-.091	.181	368.5	69.0
287.0	38.5	0.0	-.130	.156	380.1	72.5
288.9	7.0	0.0	-.024	.236	354.1	69.0

Tabelle 8: L/D = 80, D = 0,7 cm

Rohre mit langer Einlaufstrecke . Meßwerte zur Bestimmung des Einflusses von p auf $q_{B:O}$.

Table 8: L/D = 80, D = 0,7 cm

Channels with long inlet section. Data to determine the effect of p on $q_{B.O.}$

m	$\Delta\vartheta_E$	$\Delta\vartheta_A$	x_E	x_A	q_{BO}	P
Massenfluß	Eintr.-Unter-kühlung	Austr.-Unter-kühlung	Eintr.-Qualität	Austr.-Qualität	max.Heizfl.-Belastung	Druck
Mass Flow Rate	Inlet Sub-cooling	Outlet Sub-cooling	Inlet-Quality	Outlet-Quality	Burn Out Heatflux	Pressure
$g/cm^2\ s$	$^{\circ}C$	$^{\circ}C$	–	–	W/cm^2	ata
295.4	24.1	0.0	-.082	.132	290.5	70.8
292.7	15.1	0.0	-.052	.160	285.5	69.5
299.6	15.3	0.0	-.052	.159	292.3	69.2
313.2	20.1	0.0	-.068	.145	307.8	69.5
299.6	11.3	0.0	-.039	.151	264.1	68.5
312.9	11.3	0.0	-.039	.149	272.3	69.0
298.2	15.3	0.0	-.053	.127	246.8	70.0
297.4	24.1	0.0	-.082	.156	327.2	70.0
304.2	29.9	0.0	-.100	.141	336.4	69.5
304.3	30.8	0.0	-.104	.135	334.6	70.0
306.6	12.8	0.0	-.044	.144	265.8	70.0
301.2	13.8	0.0	-.048	.150	274.0	70.5

Tabelle 9: L/D = 80, D = 0,7 cm

Werte aus Untersuchungen über den Einfluß der Loopanordnung auf $q_{B.O.}$

Table 9: L/D = 80, D = 0,7 cm

Data from tests to study influence of loop layout on $q_{B.O.}$

$\dot m$	$\Delta\vartheta_E$	$\Delta\vartheta_A$	x_E	x_A	q_{BO}	P
Massenfluß	Eintr.-Unter-kühlung	Austr.-Unter-kühlung	Eintr.-Qualität	Austr.-Qualität	max.Heizfl.-Belastung	Druck
Mass Flow Rate	Inlet Sub-cooling	Outlet Sub-cooling	Inlet-Quality	Outlet-Quality	Burn Out Heatflux	Pressure
g/cm^2 s	°C	°C	-	-	W/cm^2	ata
239.1	3.9	0.0	-.014	.187	219.7	71.0
240.2	7.5	0.0	-.026	.183	229.9	71.0
245.9	9.8	0.0	-.034	.157	216.5	70.0
250.5	3.6	0.0	-.013	.146	164.3	72.0
261.5	27.3	0.0	-.092	.170	325.3	70.0
259.4	12.7	0.0	-.045	.194	282.5	71.5
250.7	18.3	0.0	-.063	.210	314.8	70.0
316.2	18.1	0.0	-.062	.121	265.8	70.0
285.7	5.5	0.0	-.019	.112	173.7	70.0
295.3	10.1	0.0	-.035	.155	264.1	69.0
319.8	23.8	0.0	-.081	.146	333.3	70.0
283.9	20.3	0.0	-.069	.173	316.2	70.0
304.8	21.8	0.0	-.077	.142	300.9	74.5
304.5	20.1	0.0	-.068	.159	319.3	69.5
305.6	30.6	0.0	-.103	.142	343.6	70.0
305.6	26.0	0.0	-.088	.130	305.8	70.5
331.0	16.8	0.0	-.058	.121	272.3	70.0
345.7	18.1	0.0	-.061	.143	326.1	69.0
345.7	17.8	0.0	-.061	.135	312.3	70.0

Tabelle 10:   L/D = 80, D = 0,7 cm

Werte aus Untersuchungen über den Einfluß der Loopanordnung auf $q_{B.0.}$

Table 10:   L/D = 80, D = 0,7 cm

Data from tests to study influence of loop layout on $q_{B.0.}$

m	$\Delta\vartheta_E$	$\Delta\vartheta_A$	x_E	x_A	q_{BO}	
Massenfluß	Eintr.-Unter-kühlung	Austr.-Unter-kühlung	Eintr.-Qualität	Austr.-Qualität	max.Heizfl.-Belastung	Druck
Mass Flow Rate	Inlet Sub-cooling	Outlet Sub-cooling	Inlet-Quality	Outlet-Quality	Burn Out Heatflux	Pressure
$g/cm^2\ s$	$^\circ C$	$^\circ C$	-	-	W/cm^2	ata
232.8	2.0	0.0	-.007	.181	201.4	70.0
235.0	2.5	0.0	-.009	.190	215.7	69.5
235.1	9.3	0.0	-.034	.167	218.0	69.5
301.4	5.9	0.0	-.021	.173	266.8	71.5
300.0	13.0	0.0	-.045	.162	264.8	71.0
363.0	2.2	0.0	-.008	.160	281.3	70.5
366.8	2.2	0.0	-.008	.160	281.3	71.0
360.4	.2	0.0	0.000	.110	193.6	71.0
361.4	14.8	0.0	-.051	.126	293.3	71.0
283.0	5.5	0.0	-.021	.196	269.1	82.0
287.3	13.8	0.0	-.052	.161	267.4	82.0
344.0	20.8	0.0	-.077	.107	278.0	81.0
352.3	14.9	0.0	-.056	.114	262.3	81.5
344.3	14.7	0.0	-.055	.125	272.0	81.5
345.4	21.2	0.0	-.078	.102	274.4	80.0
295.6	5.7	0.0	-.023	.176	248.3	90.5
279.8	14.5	0.0	-.058	.158	255.3	90.5
355.3	5.7	0.0	-.023	.130	232.4	87.0
351.9	8.0	0.0	-.034	.125	232.4	93.5
352.5	8.7	0.0	-.036	.130	245.3	91.5

Tabelle 11: L/D = 80, D = 0,7 cm
Rohre ohne Einlaufstrecke

Table 11: L/D = 80, D = 0,7 cm
Channels without inlet section

m	$\Delta\vartheta_E$	$\Delta\vartheta_A$	x_E	x_A	q_{BO}	P
Massenfluß	Eintr.-Unter-kühlung	Austr.-Unter-kühlung	Eintr.-Qualität	Austr.-Qualität	max.Heizfl.-Belastung	Druck
Mass Flow Rate	Inlet Sub-cooling	Outlet Sub-cooling	Inlet-Quality	Outlet-Quality	Burn Out Heatflux	Pressure
$g/cm^2\ s$	$^{\circ}C$	$^{\circ}C$	–	–	W/cm^2	ata
347.1	8.7	0.0	-.036	.132	244.7	91.5
237.8	9.9	0.0	-.044	.186	221.1	100.0
241.8	7.9	0.0	-.035	.181	211.5	100.0
239.5	3.8	0.0	-.017	.200	210.3	100.0
231.2	.3	0.0	-.001	.222	208.2	100.0
233.6	1.9	0.0	-.009	.212	207.9	100.5
287.5	5.3	0.0	-.024	.171	227.0	100.0
291.2	5.3	0.0	-.024	.174	233.6	100.0
271.5	15.4	0.0	-.067	.150	237.5	100.0
342.7	10.6	0.0	-.047	.129	242.7	101.0
347.8	16.8	0.0	-.073	.101	244.7	100.5

Tabelle 12: L/D = 80, D = 0,7 cm
Rohre ohne Einlaufstrecke

Table 12: L/D = 80, D = 0,7 cm
Channels without inlet section

m	x_E	x_A	q_{BO}	p_{EM}
Massenfluß	Eintr.- Qualität	Austr.- Qualität	max. Heizfl.- Belastung	Druck
Mass Flow Rate	Inlet- Quality	Outlet- Quality	Burnout Heatflux	Pressure
$g/cm^2 s$	-	-	W/cm^2	at
236.9	.152	.317	372.1	68.0
235.7	.101	.278	397.5	68.0
233.3	.179	.349	377.8	68.0
235.2	.231	.399	372.1	71.0
225.8	.140	.329	409.2	67.0
233.3	.072	.256	411.8	67.0
234.4	.064	.252	422.0	67.0
240.3	.014	.203	436.7	67.0
298.6	-.003	.155	453.4	67.0
324.8	.130	.258	399.8	67.0
328.8	.069	.199	411.8	66.0
330.3	-.009	.131	447.2	66.0
324.9	.016	.156	436.7	66.0
318.2	-.032	.117	457.9	67.0
300.9	.152	.198	133.0	70.0
295.4	.165	.288	346.8	69.0
297.8	.139	.271	373.8	69.0
297.9	.104	.244	397.5	67.0
300.7	.041	.191	432.3	67.0
283.8	.058	.217	432.3	67.0

Tabelle 13: L/D = 40, D = 0,7 cm
Rohre mit langer Einlaufstrecke

Table 13: L/D = 40, D = 0,7 cm
Channels with long inlet section

m	x_E	x_A	q_{BO}	p_{EM}
Massenfluß	Eintr.-Qualität	Austr.-Qualität	max. Heizfl.-Belastung	Druck
Mass Flow Rate	Inlet-Quality	Outlet-Quality	Burnout Heatflux	Pressure
$g/cm^2 s$	-	-	W/cm^2	at
288.6	.045	.202	432.3	67.0
287.1	.037	.198	442.8	67.0
337.4	.140	.255	372.1	68.0
296.9	-.076	.070	367.5	97.5
297.7	.102	.208	266.0	96.5
301.8	.049	.168	301.8	97.5
292.2	.062	.190	315.2	97.5
294.2	.038	.172	330.1	97.5
294.2	.039	.169	319.4	97.5
291.6	.154	.266	276.2	97.0
296.8	.070	.172	254.5	96.5

Tabelle 14: L/D = 40, D = 0,7 cm
Rohre mit langer Einlaufstrecke

Table 14: L/D = 40, D = 0,7 cm
Channels with long inlet section

m	$\Delta\vartheta_E$	$\Delta\vartheta_A$	x_E	x_A	q_{BO}	P
Massenfluß	Eintr.-Unter-kühlung	Austr.-Unter-kühlung	Eintr.-Qualität	Austr.-Qualität	max.Heizfl.-Belastung	Druck
Mass Flow Rate	Inlet Sub-cooling	Outlet Sub-cooling	Inlet-Quality	Outlet-Quality	Burn Out Heatflux	Pressure
$g/cm^2\ s$	$^\circ C$	$^\circ C$	–	–	W/cm^2	ata
215.5	8.3	0.0	-.029	.138	342.1	70.0
216.6	4.5	0.0	-.016	.145	333.3	69.5
241.0	15.3	0.0	-.052	.137	435.8	69.5
243.4	12.1	0.0	-.041	.143	428.3	69.0
238.7	10.5	0.0	-.037	.149	420.9	70.0
232.8	5.0	0.0	-.017	.172	420.9	69.0
204.2	5.5	0.0	-.019	.125	283.2	69.5
206.9	9.3	0.0	-.032	.130	319.8	69.5
206.3	9.5	0.0	-.033	.122	304.2	70.5
298.8	3.0	0.0	-.010	.135	412.8	70.0
298.8	13.8	0.0	-.048	.102	426.6	70.0
296.0	29.1	0.0	-.098	.065	458.7	70.0
296.4	21.3	0.0	-.073	.082	435.6	70.0
297.7	17.6	0.0	-.060	.091	428.3	69.5
294.8	12.3	0.0	-.043	.109	424.4	70.0
286.0	5.5	0.0	-.019	.132	411.8	70.0
298.7	0.0	0.0	.050	.192	406.2	66.5
296.9	3.3	0.0	-.011	.135	413.5	69.5
296.8	8.5	0.0	-.030	.120	422.7	70.0
338.7	5.5	0.0	-.019	.108	411.8	69.0

Tabelle 15: L/D = 40, D = 0,7 cm

Werte aus Untersuchungen über den Einfluß der Loopanordnung auf $q_{B.O.}$

Table 15: L/D = 40, D = 0,7 cm

Data from tests to study influence of loop layout on $q_{B.O.}$

$\dot{m}$	$\Delta\vartheta_E$	$\Delta\vartheta_A$	x_E	x_A	q_{BO}	P
Massenfluß	Eintr.-Unter-kühlung	Austr.-Unter-kühlung	Eintr.-Qualität	Austr.-Qualität	max.Heizfl.-Belastung	Druck
Mass Flow Rate	Inlet Sub-cooling	Outlet Sub-cooling	Inlet-Quality	Outlet-Quality	Burn Out Heatflux	Pressure
$g/cm^2\ s$	^oC	^oC	–	–	W/cm^2	ata
335.9	7.8	0.0	-.027	.103	417.4	69.0
340.4	13.0	0.0	-.045	.086	424.8	70.0
343.5	16.3	0.0	-.056	.077	434.1	70.0
344.4	19.8	0.0	-.068	.065	435.3	70.0
343.0	23.8	0.0	-.081	.055	443.4	70.0
343.4	27.6	0.0	-.093	.046	454.7	70.0
344.4	30.6	0.0	-.103	.035	451.0	70.0
344.3	34.1	0.0	-.114	.029	468.4	70.0
345.3	39.4	0.0	-.131	.017	486.0	70.0
343.7	45.3	0.0	-.150	.001	494.0	70.0
343.1	50.1	3.0	-.165	-.010	500.1	70.5
344.1	52.3	3.4	-.171	-.012	518.3	70.0
237.8	13.7	0.0	-.060	.110	337.1	100.0
243.6	3.6	0.0	-.016	.137	311.1	100.0
240.1	8.5	0.0	-.037	.123	321.9	100.5
241.3	11.6	0.0	-.051	.114	333.6	100.0
241.3	18.6	0.0	-.080	.093	348.5	100.5
241.3	25.1	0.0	-.106	.075	365.2	100.5

Tabelle 16: L/D = 40, D = 0,7 cm

Werte aus Untersuchungen über den Einfluß der Loopanordnung auf $q_{B.O.}$

Table 16: L/D = 40, D = 0,7 cm

Data from tests to study influence of loop layout on $q_{B.O.}$

$\dot{m}$	$\Delta\vartheta_E$	$\Delta\vartheta_A$	x_E	x_A	q_{BO}	P
Massenfluß	Eintr.-Unter-kühlung	Austr.-Unter-kühlung	Eintr.-Qualität	Austr.-Qualität	max.Heizfl.-Belastung	Druck
Mass Flow Rate	Inlet Sub-cooling	Outlet Sub-cooling	Inlet-Quality	Outlet-Quality	Burn Out Heatflux	Pressure
$g/cm^2 \ s$	^oC	^oC	–	–	W/cm^2	ata
213.9	2.8	0.0	-.010	.188	398.6	69.8
207.9	4.5	0.0	-.016	.170	368.6	69.5
206.6	4.9	0.0	-.017	.163	353.3	69.6
221.6	6.3	0.0	-.022	.166	395.2	70.0
191.6	10.5	0.0	-.037	.182	398.6	70.0
275.7	13.9	0.0	-.048	.115	427.7	70.1
273.5	11.7	0.0	-.040	.122	424.0	69.1
281.2	10.5	0.0	-.037	.122	424.0	70.0
273.5	3.8	0.0	-.013	.151	426.5	69.8
342.2	10.4	0.0	-.036	.096	431.4	70.4
332.0	1.9	0.0	-.007	.135	448.2	70.4
287.5	8.2	0.0	-.032	.117	382.1	66.1
283.5	9.8	0.0	-.039	.115	387.6	66.5
286.2	6.3	0.0	-.025	.125	382.1	66.0
220.7	12.4	0.0	-.054	.121	323.2	101.0
230.4	7.3	0.0	-.033	.130	311.8	101.0
218.5	1.0	0.0	-.004	.158	296.3	101.0
290.4	13.1	0.0	-.058	.084	342.9	101.0
308.1	.2	0.0	-.001	.115	297.7	101.0
301.2	1.0	0.0	-.004	.114	297.7	101.0

Tabelle 17: L/D = 40, D = 0,7 cm
Rohre ohne Einlaufstrecke

Table 17: L/D = 40, D = 0,7 cm
Channels without inlet section

m	$\Delta\vartheta_E$	$\Delta\vartheta_A$	x_E	x_A	q_{BO}	P
Massenfluß	Eintr.-Unter-kühlung	Austr.-Unter-kühlung	Eintr.-Qualität	Austr.-Qualität	max.Heizfl.-Belastung	Druck
Mass Flow Rate	Inlet Sub-cooling	Outlet Sub-cooling	Inlet-Quality	Outlet-Quality	Burn Out Heatflux	Pressure
$g/cm^2\ s$	$^{\circ}C$	$^{\circ}C$	$-$	$-$	W/cm^2	ata
294.3	5.0	0.0	-.023	.105	323.2	101.0
292.9	8.1	0.0	-.036	.102	335.6	101.0
352.4	9.3	0.0	-.041	.074	337.8	101.0
349.2	1.0	0.0	-.004	.105	311.0	101.0
350.5	1.0	0.0	-.004	.106	323.9	101.0
351.9	5.8	0.0	-.026	.086	336.3	101.0
348.2	14.4	0.0	-.063	.059	355.2	101.0
346.4	19.7	0.0	-.085	.038	353.6	101.0
354.1	27.4	0.0	-.116	.016	390.9	100.9
356.3	40.1	3.1	-.165	-.014	446.2	101.0
358.6	50.4	8.6	-.204	-.038	490.6	101.0
358.6	58.0	11.4	-.231	-.050	537.2	100.5
359.7	67.0	17.0	-.263	-.074	565.4	100.5

Tabelle 18: L/D = 40, D = 0,7 cm
Rohre ohne Einlaufstrecke

Table 18: L/D = 40, D = 0,7 cm
Channels without inlet section

m	$\Delta\vartheta_E$	$\Delta\vartheta_A$	x_E	x_A	q_{BO}	P
Massenfluß	Eintr.-Unter-kühlung	Austr.-Unter-kühlung	Eintr.-Qualität	Austr.-Qualität	max.Heizfl.-Belastung	Druck
Mass Flow Rate	Inlet Sub-cooling	Outlet Sub-cooling	Inlet-Quality	Outlet-Quality	Burn Out Heatflux	Pressure
$g/cm^2\ s$	$^\circ C$	$^\circ C$	—	—	W/cm^2	ata
170.8	9.2	0.0	-.032	.185	350.9	71.0
171.8	23.1	0.0	-.079	.149	369.9	70.5
170.5	16.5	0.0	-.057	.164	356.5	71.0
170.6	11.0	0.0	-.038	.153	308.7	70.5
171.9	5.0	0.0	-.017	.174	313.0	69.5
224.1	48.3	0.0	-.159	.039	421.7	70.0
222.3	38.1	0.0	-.127	.061	397.2	70.5
223.4	33.1	0.0	-.111	.075	389.7	70.0
223.3	25.8	0.0	-.087	.091	378.9	70.0
223.6	15.8	0.0	-.054	.117	364.9	70.0
224.3	12.7	0.0	-.044	.118	344.7	71.0
223.6	5.7	0.0	-.020	.142	343.9	71.0
104.8	7.9	0.0	-.035	.203	279.5	100.0
105.6	15.2	0.0	-.065	.265	290.7	100.0
104.9	22.9	0.0	-.097	.259	311.0	100.5
106.8	28.7	0.0	-.120	.237	317.1	100.5
105.2	33.1	0.0	-.137	.245	334.5	100.5
165.2	2.8	0.0	-.013	.191	280.9	100.0
167.2	6.3	0.0	-.028	.176	284.8	100.0
167.2	13.9	0.0	-.061	.153	297.6	100.0

Tabelle 19: $L/D = 40$, $D = 1,1$ cm
Table 19

m	$\Delta\vartheta_E$	$\Delta\vartheta_A$	x_E	x_A	q_{BO}	P
Massenfluß	Eintr.-Unter-kühlung	Austr.-Unter-kühlung	Eintr.-Qualität	Austr.-Qualität	max.Heizfl.-Belastung	Druck
Mass Flow Rate	Inlet Sub-cooling	Outlet Sub-cooling	Inlet-Quality	Outlet-Quality	Burn Out Heatflux	Pressure
g/cm^2 s	$^{\circ}C$	$^{\circ}C$	–	–	W/cm^2	ata
166.9	22.7	0.0	-.096	.136	323.2	100.0
166.9	35.8	0.0	-.148	.095	338.2	100.0
164.8	2.8	0.0	-.013	.171	252.8	100.0
165.9	7.9	0.0	-.035	.158	267.9	100.0
223.5	2.8	0.0	-.013	.126	259.7	100.0
223.7	3.3	0.0	-.015	.132	274.8	100.0
224.1	10.9	0.0	-.048	.109	294.6	100.0
224.6	22.5	0.0	-.096	.045	263.3	100.0
93.7	3.3	0.0	-.023	.209	149.8	141.0
93.8	7.6	0.0	-.051	.195	158.8	141.0
95.3	33.7	0.0	-.195	.094	189.8	141.0
95.4	40.8	0.0	-.230	.072	198.3	141.0
95.8	25.4	0.0	-.152	.129	185.1	141.5
95.3	19.5	0.0	-.120	.156	181.1	141.0
95.2	13.0	0.0	-.084	.186	176.0	142.0
97.1	2.8	0.0	-.019	.226	164.0	141.0
98.4	4.8	0.0	-.032	.212	165.4	141.0
167.3	3.5	0.0	-.025	.131	179.2	141.0
164.7	4.6	0.0	-.031	.135	188.2	141.5
164.8	9.9	0.0	-.064	.117	206.2	141.0

Tabelle 20: L/D = 40, D = 1,1 cm
Table 20

m	$\Delta\vartheta_E$	$\Delta\vartheta_A$	x_E	x_A	q_{BO}	P
Massenfluß	Eintr.-Unter-kühlung	Austr.-Unter-kühlung	Eintr.-Qualität	Austr.-Qualität	max.Heizfl.-Belastung	Druck
Mass Flow Rate	Inlet Sub-cooling	Outlet Sub-cooling	Inlet-Quality	Outlet-Quality	Burn Out Heatflux	Pressure
g/cm² s	°C	°C	-	-	W/cm²	ata
165.0	16.0	0.0	-.101	.09ᵇ	225.4	141.5
165.1	20.8	0.0	-.127	.064	240.3	141.0
169.0	28.6	0.0	-.168	.055	260.5	140.5
163.8	29.4	0.0	-.173	.079	284.0	141.0
165.7	32.7	0.0	-.189	.043	265.1	141.0
221.1	40.5	1.8	-.229	-.013	327.0	141.0
221.0	34.0	0.0	-.196	.008	308.8	141.0
220.7	28.4	0.0	-.168	.024	291.3	141.0
219.7	22.6	0.0	-.137	.042	270.8	141.0
220.4	17.2	0.0	-.107	.056	248.5	140.5
219.8	12.4	0.0	-.080	.071	228.8	141.0
220.2	3.8	0.0	-.026	.106	201.3	141.0
219.7	9.1	0.0	-.060	.088	224.3	141.5

Tabelle 21: L/D = 40, D = 1,1cm
Table 21

m	$\Delta\vartheta_E$	$\Delta\vartheta_A$	x_E	x_A	q_{BO}	P
Massenfluß	Eintr.-Unterkühlung	Austr.-Unterkühlung	Eintr.-Qualität	Austr.-Qualität	max.Heizfl.-Belastung	Druck
Mass Flow Rate	Inlet Subcooling	Outlet Subcooling	Inlet-Quality	Outlet-Quality	Burn Out Heatflux	Pressure
$g/cm^2\ s$	$^{\circ}C$	$^{\circ}C$	−	−	W/cm^2	ata
156.4	20.8	0.0	−.071	.135	323.3	69.5
154.9	14.6	0.0	−.050	.153	317.0	69.0
153.6	12.6	0.0	−.043	.165	317.8	69.5
156.3	0.0	0.0	−.019	.173	301.1	69.0
156.4	0.0	0.0	−.023	.174	310.0	69.0
218.9	2.5	0.0	−.009	.129	302.3	70.0
218.1	5.3	0.0	−.018	.120	305.5	69.0
219.8	14.1	0.0	−.048	.094	314.7	69.5
98.0	3.8	0.0	−.013	.286	298.2	68.0
97.8	11.1	0.0	−.038	.279	312.2	69.0
98.6	13.6	0.0	−.046	.250	293.5	69.5
98.1	24.6	0.0	−.082	.219	298.6	68.0
155.7	46.1	0.0	−.188	.013	278.7	101.0
155.4	40.5	0.0	−.173	.039	282.3	105.8
155.0	29.2	0.0	−.126	.067	258.6	104.0
154.5	22.0	0.0	−.099	.087	245.0	107.5
154.8	17.8	0.0	−.082	.098	236.6	108.0
153.4	7.9	0.0	−.035	.134	229.2	100.0
153.5	14.6	0.0	−.069	.108	229.2	109.5
153.7	4.8	0.0	−.022	.143	222.8	100.0

Tabelle 22: L/D = 40, D = 1,5 cm

Table 22

$\dot{m}$	$\Delta\vartheta_E$	$\Delta\vartheta_A$	x_E	x_A	q_{BO}	P
Massenfluß	Eintr.-Unter-kühlung	Austr.-Unter-kühlung	Eintr.-Qualität	Austr.-Qualität	max.Heizfl.-Belastung	Druck
Mass Flow Rate	Inlet Sub-cooling	Outlet Sub-cooling	Inlet-Quality	Outlet-Quality	Burn Out Heatflux	Pressure
$g/cm^2\ s$	$^{\circ}C$	$^{\circ}C$	–	–	W/cm^2	ata
153.7	8.4	0.0	-.037	.127	222.8	100.0
153.7	2.3	0.0	-.010	.153	222.9	99.0
222.3	27.0	0.0	-.114	.034	290.0	100.0
217.9	18.5	0.0	-.079	.059	266.4	100.0
217.1	34.6	0.0	-.143	.018	308.2	100.0
223.5	42.1	.7	-.172	-.003	330.4	100.0
221.0	8.9	0.0	-.039	.085	242.9	100.0
220.3	1.0	0.0	-.005	.111	225.7	100.0
220.4	51.4	6.2	-.206	-.028	344.9	100.0
99.3	.4	0.0	-.002	.235	206.7	100.5
100.0	7.3	0.0	-.032	.216	219.0	100.0
100.1	15.9	0.0	-.069	.189	227.6	100.0
96.9	25.5	0.0	-.108	.182	247.3	100.0
99.1	34.6	0.0	-.143	.157	262.0	100.0

Tabelle 23: L/D = 40, D = 1,5 cm
Table 23

$\dot{m}$	$\Delta\vartheta_E$	$\Delta\vartheta_A$	x_E	x_A	q_{BO}	P
Massenfluß	Eintr.-Unter-kühlung	Austr.-Unter-kühlung	Eintr.-Qualität	Austr.-Qualität	max.Heizfl.-Belastung	Druck
Mass Flow Rate	Inlet Sub-cooling	Outlet Sub-cooling	Inlet-Quality	Outlet-Quality	Burn Out Heatflux	Pressure
$g/cm^2\ s$	^{o}C	^{o}C	–	–	W/cm^2	ata
242.2	44.8	18.3	-.149	-.063	805.6	71.0
239.3	53.3	25.0	-.175	-.085	836.0	70.8
240.6	48.2	21.3	-.159	-.072	803.6	70.6
242.7	37.1	12.2	-.124	-.042	769.8	70.5
239.9	29.4	5.5	-.099	-.019	744.7	70.8
246.8	1.3	0.0	-.004	.066	687.1	70.3
237.6	4.8	0.0	-.017	.057	687.2	70.6
242.4	10.4	0.0	-.036	.038	708.2	70.7
239.6	17.2	0.0	-.059	.016	712.1	70.7
247.0	22.4	.1	-.076	0.000	729.8	70.3
302.9	54.6	31.2	-.179	-.105	858.0	70.5
304.2	45.3	23.7	-.152	-.081	839.3	70.7
303.0	40.5	19.4	-.135	-.067	802.7	70.7
303.4	34.9	14.7	-.117	-.051	781.8	70.8
300.7	28.8	9.2	-.097	-.032	761.5	70.7
301.6	23.3	4.6	-.079	-.016	741.7	70.0
294.1	2.8	0.0	-.010	.048	643.8	70.3
296.0	4.8	0.0	-.017	.042	682.8	70.3
297.2	9.3	0.0	-.032	.028	687.8	70.3
299.7	13.3	0.0	-.046	.012	692.7	70.5

Tabelle 24: L/D = 10, D = 0,7 cm
Rohre mit langer Einlaufstrecke

Table 24: L/D = 10, D = 0,7 cm
Channels with long inlet section

m	$\Delta\vartheta_E$	$\Delta\vartheta_A$	x_E	x_A	q_{BO}	P
Massenfluß	Eintr.-Unter-kühlung	Austr.-Unter-kühlung	Eintr.-Qualität	Austr.-Qualität	max.Heizfl.-Belastung	Druck
Mass Flow Rate	Inlet Sub-cooling	Outlet Sub-cooling	Inlet-Quality	Outlet-Quality	Burn Out Heatflux	Pressure
$g/cm^2\ s$	$^{\circ}C$	$^{\circ}C$	–	–	W/cm^2	ata
299.5	17.1	0.0	-.059	.001	707.1	70.6
297.9	14.2	0.0	-.049	.012	715.1	70.9
302.8	18.3	.4	-.063	-.001	727.0	70.5
301.0	24.0	5.2	-.082	-.015	745.6	71.0
355.7	43.9	24.3	-.147	-.084	869.1	71.9
354.5	41.0	22.5	-.140	-.076	849.9	72.1
352.4	54.2	32.0	-.179	-.111	919.3	71.7
352.0	49.9	29.4	-.165	-.100	867.5	71.4
350.0	43.7	24.6	-.146	-.084	838.1	71.2
350.1	37.2	19.7	-.125	-.065	822.2	71.4
349.9	1.9	0.0	-.006	.043	600.9	71.2
355.9	6.9	0.0	-.024	.026	707.2	71.2
353.7	12.4	0.0	-.043	.005	701.0	71.4
356.0	16.9	1.6	-.058	-.005	729.0	71.4
352.2	22.1	5.9	-.076	-.021	751.7	71.1
350.2	26.0	8.9	-.089	-.031	750.8	71.2
349.8	31.1	13.2	-.105	-.046	804.4	71.1
232.8	55.3	32.6	-.226	-.136	719.6	100.5
232.8	50.8	27.6	-.205	-.117	696.4	100.5
234.5	44.5	22.6	-.181	-.095	601.9	100.5

Tabelle 25: L/D = 10, D = 0,7 cm
Rohre mit langer Einlaufstrecke

Table 25: L/D = 10, D = 0,7cm
Channels with long inlet section

m	$\Delta\vartheta_E$	$\Delta\vartheta_A$	x_E	x_A	q_{BO}	P
Massenfluß	Eintr.-Unterkühlung	Austr.-Unterkühlung	Eintr.-Qualität	Austr.-Qualität	max.Heizfl.-Belastung	Druck
Mass Flow Rate	Inlet Sub-cooling	Outlet Sub-cooling	Inlet-Quality	Outlet-Quality	Burn Out Heatflux	Pressure
$g/cm^2\,s$	$^\circ C$	$^\circ C$	-	-	W/cm^2	ata
254.5	36.5	16.1	-.151	-.070	649.0	100.5
235.6	31.3	11.8	-.131	-.052	635.7	101.0
233.8	25.5	6.7	-.108	-.030	626.7	101.0
236.2	21.2	3.3	-.091	-.015	613.2	101.0
234.4	0.0	0.0	0.000	.066	551.6	101.0
235.0	4.8	0.0	-.022	.048	567.2	101.0
230.5	9.3	0.0	-.041	.032	582.9	101.0
235.6	13.6	0.0	-.060	.014	597.9	101.0
232.7	21.2	2.9	-.091	-.015	618.8	101.0
244.9	31.3	11.8	-.131	-.052	662.2	101.0
302.1	15.1	1.1	-.067	-.005	651.4	102.0
300.9	58.6	37.7	-.234	-.156	801.3	101.0
299.6	53.1	32.9	-.214	-.137	779.7	101.0
300.1	46.2	26.9	-.189	-.114	759.4	101.0
301.5	39.1	21.1	-.162	-.091	728.4	102.0
302.7	29.8	13.1	-.126	-.058	699.1	101.1
302.2	22.7	7.3	-.098	-.033	663.9	102.0
302.1	.2	0.0	-.001	.055	568.9	102.0
302.6	5.0	0.0	-.023	.033	588.1	102.0
301.2	10.3	0.0	-.046	.013	613.2	102.0

Tabelle 26:   L/D = 10, D = 0,7 cm
Rohre mit langer Einlaufstrecke

Table 26:   L/D = 10, D = 0,7 cm
Channels with long inlet section

m	$\Delta\vartheta_E$	$\Delta\vartheta_A$	x_E	x_A	q_{BO}	P
Massenfluß	Eintr.-Unter-kühlung	Austr.-Unter-kühlung	Eintr.-Qualität	Austr.-Qualität	max.Heizfl.-Belastung	Druck
Mass Flow Rate	Inlet Sub-cooling	Outlet Sub-cooling	Inlet-Quality	Outlet-Quality	Burn Out Heatflux	Pressure
$g/cm^2\ s$	$^{\circ}C$	$^{\circ}C$	—	—	W/cm^2	ata
302.1	15.6	1.5	-.069	-.007	631.4	102.0
347.6	47.8	30.1	-.193	-.126	797.1	100.5
348.7	39.2	22.6	-.161	-.097	771.2	100.5
347.8	32.4	16.8	-.135	-.073	741.4	100.5
349.8	27.5	12.8	-.116	-.056	711.8	100.3
347.8	12.5	.3	-.055	-.001	631.4	100.5
348.2	16.1	3.1	-.070	-.014	659.0	100.5
353.2	20.8	7.4	-.089	-.033	682.8	100.5
351.3	25.2	11.0	-.107	-.049	702.1	101.0
355.5	5.2	0.0	-.023	.027	621.1	100.5
346.1	5.9	0.0	-.027	.026	630.7	100.3
349.3	3.7	0.0	-.016	.033	602.1	100.5
346.9	5.2	0.0	-.023	.026	599.8	100.5
345.4	1.1	0.0	-.005	.044	586.3	100.5
347.3	7.0	0.0	-.031	.019	604.1	100.5
346.5	11.3	0.0	-.049	.005	658.1	100.2
349.6	58.8	39.2	-.233	-.161	865.0	100.2
349.5	53.0	34.4	-.213	-.143	833.4	100.5

Tabelle 27: L/D = 10, D = o,7 cm
Rohre mit langer Einlaufstrecke

Table 27: L/D = 10, D = 0,7 cm
Channels with long inlet section

m	$\Delta\vartheta_E$	$\Delta\vartheta_A$	x_E	x_A	q_{BO}	P
Massenfluß	Eintr.-Unter-kühlung	Austr.-Unter-kühlung	Eintr.-Qualität	Austr.-Qualität	max.Heizfl.-Belastung	Druck
Mass Flow Rate	Inlet Sub-cooling	Outlet Sub-cooling	Inlet-Quality	Outlet-Quality	Burn Out Heatflux	Pressure
$g/cm^2\ s$	$^{\circ}C$	$^{\circ}C$	-	-	W/cm^2	ata
241.1	10.2	0.0	-.035	.045	761.2	71.2
229.8	19.3	0.0	-.066	.024	812.0	70.5
233.3	25.5	0.0	-.086	.002	810.3	70.0
231.6	21.5	0.0	-.073	.014	800.5	70.2
232.2	17.2	0.0	-.059	.027	789.6	70.4
233.7	15.0	0.0	-.052	.034	789.6	70.2
229.9	10.2	0.0	-.035	.050	769.1	70.2
230.0	7.2	0.0	-.025	.060	769.1	70.5
233.6	1.9	0.0	-.007	.074	739.6	70.2
234.0	.7	0.0	-.002	.075	714.5	70.2
290.5	3.5	0.0	-.012	.053	748.9	70.5
289.6	6.2	0.0	-.022	.044	754.3	70.5
297.1	58.8	32.2	-.191	-.108	961.4	70.0
300.0	50.6	25.6	-.166	-.087	922.4	70.0
300.1	43.7	20.0	-.144	-.068	890.1	69.8
295.4	1.7	0.0	-.006	.058	724.4	70.0
295.9	3.7	0.0	-.013	.050	734.3	70.0
293.1	10.8	0.0	-.037	.028	754.3	70.0
298.2	17.5	0.0	-.060	.006	776.4	70.2
348.7	22.3	4.9	-.076	-.017	797.0	70.2

Tabelle 28: L/D = 10, D = 0,7 cm
Rohre ohne Einlaufstrecke

Table 28: L/D = 10, D = 0,7 cm
Channels without inlet section

m	$\Delta\vartheta_E$	$\Delta\vartheta_A$	x_E	x_A	q_{BO}	P
Massenfluß	Eintr.-Unter-kühlung	Austr.-Unter-kühlung	Eintr.-Qualität	Austr.-Qualität	max.Heizfl.-Belastung	Druck
Mass Flow Rate	Inlet Sub-cooling	Outlet Sub-cooling	Inlet-Quality	Outlet-Quality	Burn Out Heatflux	Pressure
$g/cm^2\ s$	^oC	^oC	-	-	W/cm^2	ata
301.5	29.5	8.5	-.099	-.030	820.8	70.2
301.5	38.6	16.4	-.129	-.056	846.9	70.5
341.0	4.0	0.0	-.014	.041	748.9	70.5
342.4	6.0	0.0	-.021	.034	748.9	70.8
342.6	8.0	0.0	-.028	.029	763.7	70.2
353.4	16.0	0.0	-.055	.002	794.4	70.5
346.0	20.3	2.6	-.069	-.009	810.3	70.5
348.6	26.1	7.8	-.088	-.027	831.3	70.5
350.7	33.1	13.8	-.111	-.047	868.3	70.0
347.2	37.9	17.2	-.126	-.059	906.2	69.8
347.6	48.1	26.1	-.158	-.088	950.9	70.0
349.0	55.6	32.2	-.181	-.108	996.6	70.0
351.6	60.6	36.6	-.196	-.122	1019.9	70.0
236.9	60.1	33.2	-.239	-.138	815.2	101.0
238.8	51.8	26.3	-.208	-.111	789.6	100.5
236.6	46.6	21.5	-.190	-.092	785.4	101.0
239.4	24.0	3.7	-.102	-.017	698.4	101.0
238.4	32.3	10.5	-.135	-.047	719.5	101.0
238.2	39.3	16.2	-.162	-.070	746.4	101.0
236.5	70.6	41.6	-.277	-.171	856.8	101.0

Tabelle 29:   L/D = 10, D = 0,7 cm
Rohre ohne Einlaufstrecke

Table 29:   L/D = 10, D = 0,7 cm
Channels without inlet section

m	$\Delta \vartheta_E$	$\Delta \vartheta_A$	x_E	x_A	q_{BO}	P
Massenfluß	Eintr.-Unter-kühlung	Austr.-Unter-kühlung	Eintr.-Qualität	Austr.-Qualität	max.Heizfl.-Belastung	Druck
Mass Flow Rate	Inlet Sub-cooling	Outlet Sub-cooling	Inlet-Quality	Outlet-Quality	Burn Out Heatflux	Pressure
g/cm^2 s	$^{\circ}C$	$^{\circ}C$	–	–	W/cm^2	ata
239.6	15.2	0.0	-.066	.013	653.2	101.0
238.4	6.9	0.0	-.031	.045	624.7	101.1
239.7	3.5	0.0	-.016	.056	609.7	101.0
238.4	2.6	0.0	-.012	.061	594.6	102.5
301.8	68.4	43.6	-.269	-.179	928.1	101.3
300.9	61.8	38.2	-.246	-.158	896.4	101.5
299.2	60.9	36.7	-.242	-.152	916.5	101.0
300.1	46.9	25.2	-.191	-.107	851.9	101.0
299.4	52.6	30.2	-.212	-.127	868.3	101.0
301.7	40.0	19.8	-.164	-.085	815.2	100.5
301.3	35.2	16.0	-.146	-.069	788.9	100.5
300.7	27.1	9.4	-.115	-.042	748.9	100.5
299.7	23.5	6.1	-.100	-.027	743.6	101.0
300.1	17.1	1.0	-.074	-.004	709.3	100.5
299.8	11.3	0.0	-.049	.016	681.0	100.5
296.9	5.3	0.0	-.024	.039	648.2	101.0
302.0	.4	0.0	-.002	.057	613.4	100.5
350.0	68.6	46.4	-.270	-.189	965.4	101.0
350.4	68.1	45.7	-.268	-.166	977.9	101.0
352.1	59.9	38.1	-.239	-.158	970.1	101.0

Tabelle 30: L/D = 10, D = 0,7 cm
Rohre ohne Einlaufstrecke

Table 30: L/D = 10, D = 0,7 cm
Channels without inlet section

$\dot{m}$	$\Delta\vartheta_E$	$\Delta\vartheta_A$	x_E	x_A	q_{BO}	P
Massenfluß	Eintr.-Unter-kühlung	Austr.-Unter-kühlung	Eintr.-Qualität	Austr.-Qualität	max.Heizfl.-Belastung	Druck
Mass Flow Rate	Inlet Sub-cooling	Outlet Sub-cooling	Inlet-Quality	Outlet-Quality	Burn Out Heatflux	Pressure
$g/cm^2\ s$	^{o}C	^{o}C	–	–	W/cm^2	ata
349.9	53.9	33.4	-.216	-.139	920.4	101.0
350.6	39.1	20.7	-.161	-.089	860.6	101.0
352.4	39.1	20.3	-.161	-.087	887.7	101.0
348.5	1.5	0.0	-.007	.047	654.9	101.0
350.0	11.3	0.0	-.050	.007	697.5	101.3
350.9	16.8	2.8	-.073	-.013	725.0	101.2
352.1	23.1	7.9	-.099	-.035	767.2	101.2
352.5	27.2	11.1	-.115	-.049	791.5	101.2
352.5	32.5	15.4	-.136	-.067	825.7	101.3
352.9	34.9	17.4	-.145	-.076	836.2	101.1
352.0	44.0	25.3	-.180	-.108	865.9	101.2

Tabelle 31: L/D = 10, D = 0,7 cm
Rohre ohne Einlaufstrecke

Table 31: L/D = 10, D = 0,7 cm
Channels without inlet section

m	$\Delta\vartheta_E$	$\Delta\vartheta_A$	x_E	x_A	q_{BO}	P
Massenfluß	Eintr.-Unter-kühlung	Austr.-Unter-kühlung	Eintr.-Qualität	Austr.-Qualität	max.Heizfl.-Belastung	Druck
Mass Flow Rate	Inlet Sub-cooling	Outlet Sub-cooling	Inlet-Quality	Outlet-Quality	Burn Out Heatflux	Pressure
$g/cm^2\ s$	$^\circ C$	$^\circ C$	–	–	W/cm^2	ata
237.8	1.7	0.0	-.006	.042	890.8	70.0
238.3	5.5	0.0	-.019	.031	918.7	70.0
238.9	10.3	0.0	-.037	.014	938.4	70.0
239.5	16.0	.6	-.055	-.002	963.1	70.5
240.7	22.3	6.3	-.076	-.022	981.4	70.5
242.3	27.1	10.8	-.092	-.035	991.1	70.0
240.3	34.4	17.1	-.115	-.059	1022.0	70.0
240.2	42.8	24.5	-.142	-.083	1065.8	70.5
303.2	48.1	32.6	-.158	-.109	1119.1	70.0
301.3	43.1	27.9	-.142	-.094	1098.9	70.0
302.1	37.6	22.9	-.125	-.078	1079.6	70.0
303.2	31.3	17.5	-.105	-.060	1038.7	70.0
303.0	6.5	0.0	-.023	.017	930.3	70.0
302.3	2.5	0.0	-.009	.030	896.7	70.0
308.2	13.5	1.7	-.047	-.006	950.7	71.0
308.1	9.0	0.0	-.031	.008	936.4	70.5
302.4	18.8	6.2	-.065	-.022	976.3	71.0
314.6	25.0	12.3	-.085	-.043	1008.6	71.0

Tabelle 32: L/D = 5, D = 0,7 cm
Rohre mit langer Einlaufstrecke

Table 32: L/D = 5, D = 0,7 cm
Channels with long inlet section

$\dot{m}$	$\Delta\vartheta_E$	$\Delta\vartheta_A$	x_E	x_A	q_{BO}	P
Massenfluß	Eintr.-Unter-kühlung	Austr.-Unter-kühlung	Eintr.-Qualität	Austr.-Qualität	max.Heizfl.-Belastung	Druck
Mass Flow Rate	Inlet Sub-cooling	Outlet Sub-cooling	Inlet-Quality	Outlet-Quality	Burn Out Heatflux	Pressure
$g/cm^2\ s$	^{o}C	^{o}C	–	–	W/cm^2	ata
236.8	6.3	0.0	-.022	.161	413.1	69.0
240.8	3.3	0.0	-.011	.166	408.8	69.0
239.8	10.8	0.0	-.037	.152	433.6	69.0
238.6	15.8	0.0	-.054	.135	430.3	69.0
239.1	19.8	0.0	-.067	.138	467.9	69.5
296.8	33.1	0.0	-.110	.070	510.7	69.2
296.9	29.3	0.0	-.098	.083	512.6	69.2
300.5	5.9	0.0	-.020	.134	442.1	69.1
300.5	15.1	0.0	-.052	.110	463.3	69.5
299.7	31.6	0.0	-.106	.072	507.8	69.5
299.7	20.8	0.0	-.071	.102	492.8	69.2
298.8	13.5	0.0	-.047	.109	442.1	70.0
296.6	3.0	0.0	-.010	.141	429.7	69.0
356.8	8.0	0.0	-.028	.109	467.9	69.0
365.5	13.6	0.0	-.047	.092	483.0	69.0
359.3	21.8	0.0	-.074	.075	510.7	69.2
359.2	30.9	0.0	-.103	.054	538.7	69.5
359.4	48.4	0.0	-.158	.015	592.0	69.0
358.7	55.6	0.0	-.180	.001	620.7	69.0
356.3	34.9	0.0	-.116	.044	544.8	69.0

Tabelle 33: L/D = 40, D = 0,7 cm
Drallblech Nr. 1 (Ψ = 75°) am Meßstreckeneintritt

Table 33: L/D = 40, D = 0,7 cm
Twisted tape No. 1 (Ψ = 75°) at test section inlet

m	$\Delta \vartheta_E$	$\Delta \vartheta_A$	x_E	x_A	q_{BO}	P
Massenfluß	Eintr.-Unter-kühlung	Austr.-Unter-kühlung	Eintr.-Qualität	Austr.-Qualität	max.Heizfl.-Belastung	Druck
Mass Flow Rate	Inlet Sub-cooling	Outlet Sub-cooling	Inlet-Quality	Outlet-Quality	Burn Out Heatflux	Pressure
$g/cm^2 \ s$	$^{\circ}C$	$^{\circ}C$	-	-	W/cm^2	ata
346.4	12.3	0.0	-.042	.094	450.6	99.5
241.2	14.7	0.0	-.063	.118	367.8	99.0
241.2	5.9	0.0	-.026	.149	354.1	99.0
241.3	11.9	0.0	-.052	.129	365.4	100.0
241.2	5.1	0.0	-.023	.158	360.1	100.0
241.2	7.3	0.0	-.032	.151	369.4	100.0
245.8	17.6	0.0	-.075	.124	410.8	99.5
240.7	25.5	0.0	-.108	.100	417.4	100.0
354.1	32.0	0.0	-.132	.009	419.0	99.5
354.2	41.4	2.7	-.169	-.012	461.0	100.0
354.2	56.4	4.9	-.223	-.022	595.3	99.0
354.1	30.1	0.0	-.125	.016	426.3	100.0

Tabelle 34: L/D = 40, D = 0,7 cm
Drallblech Nr. 1 (Ψ = 75°) am Meßstreckeneintritt

Table 34: L/D = 40, D = 0,7 cm
Twisted tape No. 1 (Ψ = 75°) at test section inlet

m	x_E	x_A	q_{BO}	p_{EM}
Massenfluß	Eintr.-Qualität	Austr.-Qualität	max. Heizfl.-Belastung	Druck
Mass Flow Rate	Inlet-Quality	Outlet-Quality	Burnout Heatflux	Pressure
$g/cm^2 s$	−	−	W/cm^2	at
292.6	.094	.251	438.7	67.5
292.1	.071	.226	434.4	66.5
293.1	.091	.245	434.4	65.5
293.6	.119	.270	426.0	65.5
287.3	.067	.220	422.0	65.5
292.1	.024	.176	426.0	66.5
289.7	−.030	.143	482.0	67.5
290.8	−.006	.155	451.3	67.5
289.5	−.014	.153	464.4	68.0
287.7	−.044	.149	531.7	68.5
339.7	.161	.294	430.3	68.0
339.7	.131	.266	438.7	67.0
332.9	.112	.247	430.3	68.0
332.9	.097	.235	438.7	67.0
332.9	.068	.205	438.7	67.0
332.9	.059	.196	438.7	67.0
340.4	.028	.166	451.6	67.0
340.4	.004	.148	468.6	67.0
343.0	−.014	.124	456.1	67.0
345.4	−.031	.126	522.5	67.0

Tabelle 35: L/D = 40, D = 0,7 cm
Rohre mit Drallblech Nr. 2 (ψ = 56°) am Meßstreckeneintritt

Table 35: L/D = 40, D = 0,7 cm
Channels with twisted tape No. 2 (ψ = 56°) at test section inlet

m	x_E	x_A	q_{BO}	p_{EM}
Massenfluß	Eintr.-Qualität	Austr.-Qualität	max. Heizfl.-Belastung	Druck
Mass Flow Rate	Inlet-Quality	Outlet-Quality	Burnout Heatflux	Pressure
$g/cm^2 s$	-	-	W/cm^2	at
238.8	.186	.383	448.9	67.5
238.8	.208	.431	508.9	67.5
243.5	.160	.354	451.5	67.5
244.7	.133	.333	468.6	67.5
243.5	.114	.284	397.5	67.5
238.7	.076	.259	417.7	67.5
238.8	.047	.234	426.0	67.5
238.7	.046	.188	324.9	67.5
242.3	.032	.153	279.3	68.0
238.1	.035	.192	358.3	67.5
238.1	.031	.171	317.4	67.5
238.1	.008	.189	412.2	67.5
238.2	-.013	.177	434.6	67.5
237.5	-.022	.173	443.1	68.5
307.8	-.016	.147	422.0	97.5
305.3	.015	.160	374.0	97.5
305.7	-.007	.152	409.8	98.0
304.8	.047	.187	358.5	98.0

Tabelle 36: L/D = 40, D = 0,7 cm
Rohre mit Drallblech Nr. 2 (ψ= 56°) am Meßstreckeneintritt

Table 36: L/D = 40, D = 0,7 cm
Channels with twisted tape No. 2 (ψ= 56°) at test section inlet

$\dot{m}$	$\Delta\vartheta_E$	$\Delta\vartheta_A$	x_E	x_A	q_{BO}	P
Massenfluß	Eintr.-Unter-kühlung	Austr.-Unter-kühlung	Eintr.-Qualität	Austr.-Qualität	max.Heizfl.-Belastung	Druck
Mass Flow Rate	Inlet Sub-cooling	Outlet Sub-cooling	Inlet-Quality	Outlet-Quality	Burn Out Heatflux	Pressure
$g/cm^2\ s$	$^{\circ}C$	$^{\circ}C$	–	–	W/cm^2	ata
239.9	17.8	0.0	-.061	.154	489.3	70.5
244.5	12.8	0.0	-.044	.163	481.3	70.0
239.9	9.7	0.0	-.034	.165	455.7	70.5
238.7	10.8	0.0	-.037	.172	473.4	70.5
241.0	7.8	0.0	-.027	.176	489.7	70.0
239.9	8.5	0.0	-.030	.166	446.6	70.0
313.1	.8	0.0	-.003	.153	465.6	69.5
300.5	2.5	0.0	-.009	.156	473.4	69.0
295.9	1.3	0.0	-.004	.155	450.1	69.0
296.8	3.3	0.0	-.011	.152	462.0	69.0
303.2	7.0	0.0	-.024	.143	485.5	69.0
300.4	10.6	0.0	-.036	.134	489.3	69.0
296.9	8.0	0.0	-.028	.138	465.6	69.0
303.3	19.1	0.0	-.065	.110	505.4	69.0
302.4	23.6	0.0	-.080	.096	505.9	69.0
355.5	15.8	0.0	-.054	.090	489.3	70.0
355.5	13.0	0.0	-.045	.102	497.3	70.0
355.5	45.6	3.3	-.150	-.012	466.1	70.0
357.5	47.1	0.0	-.155	0.000	525.6	70.0
357.7	42.1	0.0	-.139	.005	493.5	70.0

Tabelle 37: L/D = 40, D = 0,7 cm
Drallblech Nr. 2 (ψ = 56°) am Meßstreckeneintritt

Table 37: L/D = 40, D = 0,7 cm
Twisted tape No. 2 (ψ = 56°) at test section inlet

m	$\Delta\vartheta_E$	$\Delta\vartheta_A$	x_E	x_A	q_{BO}	P
Massenfluß	Eintr.-Unterkühlung	Austr.-Unterkühlung	Eintr.-Qualität	Austr.-Qualität	max.Heizfl.-Belastung	Druck
Mass Flow Rate	Inlet Subcooling	Outlet Subcooling	Inlet-Quality	Outlet-Quality	Burn Out Heatflux	Pressure
$g/cm^2\,s$	$^{\circ}C$	$^{\circ}C$	–	–	W/cm^2	ata
356.2	41.6	2.4	-.138	-.006	435.4	70.0
358.0	29.9	0.0	-.100	.060	576.5	69.5
358.5	23.9	0.0	-.081	.0..	5.0..	69.5
357.7	22.1	0.0	-.075	.0.1	530.0	70.0
357.7	9.6	0.0	-.033	.110	489.3	69.0
356.9	6.5	0.0	-.023	.121	469.3	69.5
355.6	6.0	0.0	-.028	.114	451.3	69.0
354.6	1.0	0.0	-.003	.135	469.7	69.0
353.6	4.5	0.0	-.016	.127	451.5	70.0
235.5	9.3	0.0	-.041	.151	376.6	100.6
234.5	12.0	0.0	-.053	.137	373.2	100.5
235.5	16.9	0.0	-.073	.124	3.7.6	100.3
241.7	15.1	0.0	-.066	.123	3.1.1	100.5
297.4	7.5	0.0	-.034	.119	3.0.5	100.4
297.4	9.0	0.0	-.040	.124	405.5	100.5
297.4	15.4	0.0	-.067	.112	442.5	100.3
297.4	18.2	0.0	-.078	.085	411.9	100.5
297.4	21.6	0.0	-.093	.096	473.4	100.4
346.0	1.3	0.0	-.006	.116	383.4	100.0
346.7	4.3	0.0	-.022	.108	375.0	100.0

Tabelle 38: L/D = 40, D = 0,7 cm

Drallblech Nr. 2 (ψ = 56°) am Meßstreckeneintritt

Table 38: L/D = 40, D = 0,7 cm

Twisted tape No. 2 (ψ = 56°) at test section inlet

m	$\Delta\vartheta_E$	$\Delta\vartheta_A$	x_E	x_A	q_{BO}	P
Massenfluß	Eintr.-Unter-kühlung	Austr.-Unter-kühlung	Eintr.-Qualität	Austr.-Qualität	max.Heizfl.-Belastung	Druck
Mass Flow Rate	Inlet Sub-cooling	Outlet Sub-cooling	Inlet-Quality	Outlet-Quality	Burn Out Heatflux	Pressure
$g/cm^2\ s$	$^\circ C$	$^\circ C$	–	–	W/cm^2	ata
347.0	4.5	0.0	-.020	.129	432.6	99.5
345.7	18.0	0.0	-.077	.073	433.3	100.0
344.7	20.7	0.0	-.089	.085	499.3	100.0
344.6	24.4	0.0	-.103	.077	519.4	99.5
352.7	33.2	0.0	-.138	.047	545.3	100.5
354.1	49.6	0.0	-.199	.005	606.3	100.0

Tabelle 39:   L/D = 40, D = 0,7 cm
Drallblech Nr, 2 (ψ = 56°) am Meßstreckeneintritt

Table 39:   L/D = 40, D = 0,7 cm
Twisted tape No. 2 (ψ = 56°) at test section inlet

m	x_E	x_A	q_{BO}	p_{EM}
Massenfluß	Eintr.-Qualität	Austr.-Qualität	max. Heizfl.-Belastung	Druck
Mass Flow Rate	Inlet-Quality	Outlet-Quality	Burnout Heatflux	Pressure
$g/cm^2 s$	-	-	W/cm^2	at
236.1	.120	.351	519.9	68.0
236.3	.174	.403	516.1	68.0
242.0	.087	.298	488.1	68.0
247.6	.061	.267	488.1	67.5
235.9	.053	.245	430.3	69.0
236.1	.030	.227	443.8	67.5
237.4	.012	.218	464.4	68.5
236.3	-.007	.204	478.3	68.0
238.1	-.021	.195	492.4	68.0
294.8	.120	.308	528.2	67.5
294.6	.075	.252	499.8	67.5
294.6	.034	.202	471.5	67.5
294.2	.032	.193	452.5	68.0
294.7	.008	.176	472.3	67.5
294.8	-.003	.167	482.0	67.5
295.0	-.038	.146	522.2	67.5
249.2	.167	.348	379.4	96.5
254.5	.093	.264	366.1	96.5
252.0	.092	.260	357.0	96.5
247.8	.068	.232	342.9	96.5

Tabelle 40: L/D = 40, D = 0,7 cm

Rohre mit Drallblech Nr. 3 (ψ = 48°) am Meßstreckeneintritt

Table 40: L/D = 40, D = 0,7 cm

Channels with twisted tape No. 3 (ψ = 48°) at test section inlet

$\dot{m}$	x_E	x_A	q_{BO}	p_{EM}
Massenfluß	Eintr.-Qualität	Austr.-Qualität	max. Heizfl.-Belastung	Druck
Mass Flow Rate	Inlet-Quality	Outlet-Quality	Burnout Heatflux	Pressure
$g/cm^2 s$	-	-	W/cm^2	at
247.9	.019	.203	384.8	96.5
245.6	.035	.222	388.1	96.5
248.0	.015	.211	410.8	96.5
248.0	-.007	.196	425.6	97.0
247.9	-.039	.175	446.5	98.0
293.6	.129	.300	422.2	97.0
293.2	.071	.216	357.9	97.5
294.6	.071	.225	381.0	97.5
294.9	.018	.185	413.1	97.5
295.0	-.019	.153	429.8	97.5
295.0	-.006	.172	443.1	97.5
295.0	-.019	.166	461.2	97.5
295.1	-.048	.145	481.3	97.5
332.5	.038	.209	483.8	95.0
337.6	.092	.251	456.0	95.0
332.2	.055	.202	413.8	96.0
333.0	.030	.162	372.4	96.0
336.7	-.002	.139	404.1	96.0
334.5	-.022	.128	428.0	96.0
335.0	-.018	.131	426.3	96.5
342.5	.112	.265	442.3	96.0

Tabelle 41: L/D = 40, D = 0,7 cm
Rohre mit Drallblech Nr. 3 (ψ=48°) am Meßstreckeneintritt
Table 41: L/D = 40, D = 0,7 cm
Channels with twisted tape No. 3 (ψ = 48°) at test section inlet

$\dot{m}$	$\Delta\vartheta_E$	$\Delta\vartheta_A$	x_E	x_A	q_{BO}	P
Massenfluß	Eintr.-Unter-kühlung	Austr.-Unter-kühlung	Eintr.-Qualität	Austr.-Qualität	max.Heizfl.-Belastung	Druck
Mass Flow Rate	Inlet Sub-cooling	Outlet Sub-cooling	Inlet-Quality	Outlet-Quality	Burn Out Heatflux	Pressure
$g/cm^2\,s$	^{o}C	^{o}C	–	–	W/cm^2	ata
245.6	7.7	0.0	-.027	.224	282.9	71.0
243.4	14.5	0.0	-.050	.223	304.9	71.0
243.4	18.6	0.0	-.064	.217	314.1	70.0
243.4	26.1	0.0	-.088	.201	323.6	70.0
242.3	54.3	0.0	-.179	.146	331.3	70.0
242.3	50.6	0.0	-.166	.152	353.3	70.0
235.5	44.6	0.0	-.147	.173	347.9	70.0
240.0	39.6	0.0	-.132	.176	339.1	70.0
240.0	37.4	0.0	-.124	.180	335.4	70.0
236.5	28.9	0.0	-.097	.204	327.2	69.5
236.5	28.3	0.0	-.095	.210	331.9	70.0
237.6	23.9	0.0	-.080	.186	292.3	69.0
235.9	21.6	0.0	-.073	.199	296.3	69.5
236.5	18.8	0.0	-.064	.197	284.5	70.0
305.3	58.0	0.0	-.190	.032	380.4	71.0
298.9	37.6	0.0	-.125	.126	345.3	70.0
300.3	30.1	0.0	-.102	.150	330.0	70.5
291.3	22.3	0.0	-.076	.164	322.1	70.0
298.4	10.2	0.0	-.036	.133	299.4	71.0
287.3	1.2	0.0	-.004	.222	298.8	70.0

Tabelle 42: L/D = 80, D = 0,7 cm
Lochblende Nr. 1 am Meßstreckeneintritt

Table 42: L/D = 80, D = 0,7 cm
Orifice plate No. 1 at test section inlet

$\dot{m}$	$\Delta\vartheta_E$	$\Delta\vartheta_A$	x_E	x_A	q_{BO}	P
Massenfluß	Eintr.-Unter-kühlung	Austr.-Unter-kühlung	Eintr.-Qualität	Austr.-Qualität	max.Heizfl.-Belastung	Druck
Mass Flow Rate	Inlet Sub-cooling	Outlet Sub-cooling	Inlet-Quality	Outlet-Quality	Burn Out Heatflux	Pressure
$g/cm^2\ s$	^oC	^oC	–	–	W/cm^2	ata
292.0	16.4	0.0	-.058	.173	306.0	73.0
301.5	6.3	0.0	-.022	.186	289.0	69.5
289.3	11.4	0.0	-.039	.185	299.1	69.3
292.2	15.1	0.0	-.052	.169	297.3	69.5
295.3	17.6	0.0	-.060	.166	307.8	70.0
295.2	22.1	0.0	-.075	.153	309.6	70.0
299.1	27.6	0.0	-.093	.128	304.6	70.0
297.3	34.1	0.0	-.114	.134	339.8	70.0
349.9	10.2	0.0	-.036	.151	300.2	71.0
357.9	14.0	0.0	-.049	.141	311.9	71.0
356.4	19.3	0.0	-.068	.127	319.0	70.0
360.3	32.5	0.0	-.110	.095	338.4	72.0
354.0	42.6	0.0	-.142	.082	352.9	71.0
357.8	32.6	0.0	-.109	.097	339.8	69.5
355.5	23.3	0.0	-.079	.119	323.3	69.5
354.1	17.6	0.0	-.060	.135	318.2	69.5
355.2	9.0	0.0	-.031	.152	300.9	69.5
359.1	6.8	0.0	-.024	.160	304.2	69.3
242.9	53.9	0.0	-.214	.109	318.4	99.0
238.3	45.9	0.0	-.184	.127	300.9	99.0

Tabelle 43: L/D = 80, D = 0,7 cm
Lochblende Nr.1 am Meßstreckeneintritt

Table 43: L/D = 80, D = 0,7 cm
Orifice plate No.1 at test section inlet

m	$\Delta\vartheta_E$	$\Delta\vartheta_A$	x_E	x_A	q_{BO}	P
Massenfluß	Eintr.-Unter-kühlung	Austr.-Unter-kühlung	Eintr.-Qualität	Austr.-Qualität	max.Heizfl.-Belastung	Druck
Mass Flow Rate	Inlet Sub-cooling	Outlet Sub-cooling	Inlet-Quality	Outlet-Quality	Burn Out Heatflux	Pressure
$g/cm^2\ s$	$^{\circ}C$	$^{\circ}C$	–	–	W/cm^2	ata
243.1	35.4	0.0	-.145	.145	284.0	99.0
243.0	28.8	0.0	-.120	.151	267.4	99.0
361.0	62.2	0.0	-.245	.056	413.0	100.0
241.8	7.9	0.0	-.035	.204	233.6	100.0
238.3	23.6	0.0	-.100	.156	249.0	99.5
238.3	23.6	0.0	-.100	.173	263.3	99.5
301.1	41.1	0.0	-.168	.076	297.1	100.0
294.2	52.9	0.0	-.211	.042	301.6	100.0
298.0	47.1	0.0	-.190	.050	289.0	100.0
298.0	37.6	0.0	-.155	.064	287.7	100.0
297.0	29.3	0.0	-.122	.097	263.6	150.0
299.9	18.0	0.0	-.077	.126	246.5	100.0
299.8	5.7	0.0	-.025	.157	220.6	100.5
353.9	21.2	0.0	-.089	.094	264.3	99.2
356.4	23.8	0.0	-.100	.089	274.6	99.0
357.8	34.9	0.0	-.143	.064	300.9	99.1
357.5	42.9	0.0	-.173	.053	329.3	99.0
360.1	51.9	0.0	-.206	.041	362.3	99.0
361.2	62.2	0.0	-.245	.027	397.0	100.0

Tabelle 44:   L/D = 80, D = 0,7 cm
Lochblende Nr. 1 am Meßstreckeneintritt

Table 44: L/D = 80, D = 0,7 cm
Orifice plate No. 1 at test section inlet

$\dot{m}$	$\Delta\vartheta_E$	$\Delta\vartheta_A$	x_E	x_A	q_{BO}	P
Massenfluß	Eintr.-Unter-kühlung	Austr.-Unter-kühlung	Eintr.-Qualität	Austr.-Qualität	max.Heizfl.-Belastung	Druck
Mass Flow Rate	Inlet Sub-cooling	Outlet Sub-cooling	Inlet-Quality	Outlet-Quality	Burn Out Heatflux	Pressure
$g/cm^2 s$	$^\circ C$	$^\circ C$	—	—	W/cm^2	ata
241.1	43.3	0.0	−.144	.086	525.0	70.5
238.7	43.1	0.0	−.142	.091	528.9	69.5
238.7	36.4	0.0	−.121	.110	525.0	69.5
238.7	35.9	0.0	−.119	.108	516.8	69.5
238.7	33.4	0.0	−.111	.112	508.6	69.0
242.2	32.8	0.0	−.110	.110	504.8	70.5
241.0	25.6	0.0	−.086	.130	496.7	69.0
237.5	23.6	0.0	−.079	.139	496.7	68.5
237.5	18.6	0.0	−.063	.149	480.8	69.0
241.0	19.8	0.0	−.068	.142	480.8	70.5
237.5	14.6	0.0	−.050	.159	472.9	69.0
237.5	17.1	0.0	−.058	.150	472.9	69.0
236.3	8.6	0.0	−.029	.172	455.6	69.0
237.5	11.1	0.0	−.038	.165	460.8	69.0
236.3	4.0	0.0	−.014	.185	449.6	69.0
234.0	4.0	0.0	−.014	.185	443.6	69.0
309.6	35.6	0.0	−.118	.059	523.3	69.5
305.1	36.9	0.0	−.123	.059	528.9	70.0
306.0	41.9	0.0	−.138	.049	545.6	69.0
305.1	42.4	0.0	−.140	.046	539.9	69.5

Tabelle 45: L/D = 40, D = 0,7 cm
Lochblende Nr. 2 am Meßstreckeneintritt

Table 45: L/D = 40, D = 0,7 cm
Orifice plate No. 2 at test section inlet

m	$\Delta\vartheta_E$	$\Delta\vartheta_A$	x_E	x_A	q_{BO}	P
Massenfluß	Eintr.-Unter-kühlung	Austr.-Unter-kühlung	Eintr.-Qualität	Austr.-Qualität	max.Heizfl.-Belastung	Druck
Mass Flow Rate	Inlet Sub-cooling	Outlet Sub-cooling	Inlet-Quality	Outlet-Quality	Burn Out Heatflux	Pressure
$g/cm^2\ s$	^oC	^oC	$-$	$-$	W/cm^2	ata
306.0	47.6	0.0	-.156	.035	557.3	69.5
306.0	48.1	0.0	-.158	.035	562.6	70.0
307.8	53.6	0.0	-.175	.028	592.7	69.5
306.0	54.1	0.0	-.176	.022	578.1	69.5
303.2	30.1	0.0	-.101	.078	516.5	69.5
305.1	29.3	0.0	-.099	.078	514.1	70.0
303.3	20.1	0.0	-.068	.105	500.5	69.5
301.4	21.1	0.0	-.071	.100	492.4	69.0
301.5	8.0	0.0	-.028	.133	462.5	69.0
301.5	8.0	0.0	-.028	.133	460.5	70.0
300.5	1.0	0.0	-.003	.155	452.1	70.0
298.4	0.0	0.0	0.000	.156	449.6	69.0
357.4	23.4	0.0	-.086	.062	501.6	69.5
358.2	24.6	0.0	-.084	.064	504.2	70.5
357.4	32.4	0.0	-.108	.045	523.3	69.5
357.5	34.1	0.0	-.113	.042	530.7	69.0
360.5	43.9	0.0	-.144	.015	562.6	69.5
360.7	46.3	0.0	-.154	.015	575.2	71.0
361.5	49.9	0.0	-.163	.009	592.7	69.5
361.5	50.1	0.0	-.162	.009	592.7	68.0

Tabelle 46: L/D = 40, D = 0,7 cm
Lochblende Nr. 2 am Meßstreckeneintritt

Table 46: L/D = 40, D = 0,7 cm
Orifice plate No. 2 at test section inlet

m	$\Delta\vartheta_E$	$\Delta\vartheta_A$	x_E	x_A	q_{BO}	P
Massenfluß	Eintr.-Unter-kühlung	Austr.-Unter-kühlung	Eintr.-Qualität	Austr.-Qualität	max.Heizfl.-Belastung	Druck
Mass Flow Rate	Inlet Sub-cooling	Outlet Sub-cooling	Inlet-Quality	Outlet-Quality	Burn Out Heatflux	Pressure
$g/cm^2\ s$	^oC	^oC	–	–	W/cm^2	ata
353.7	17.3	0.0	-.059	.114	583.2	69.5
356.1	22.3	0.0	-.076	.070	494.1	71.0
356.2	.5	0.0	-.002	.132	457.3	69.5
358.8	.7	0.0	-.002	.129	449.6	69.5
254.6	21.0	0.0	-.090	.095	392.5	101.0
253.5	13.4	0.0	-.059	.122	380.6	101.0
253.5	5.1	0.0	-.023	.154	375.2	100.0
253.5	9.6	0.0	-.042	.134	374.6	100.0
254.6	28.3	0.0	-.119	.072	406.4	100.0
256.8	27.0	0.0	-.114	.078	412.1	100.0
256.8	37.1	0.0	-.153	.054	443.7	100.0
257.9	36.6	0.0	-.151	.056	444.4	100.0
302.5	41.4	0.0	-.169	.022	481.9	100.0
298.8	42.6	0.0	-.174	.021	484.8	100.0
302.5	30.6	0.0	-.127	.050	449.6	100.0
299.7	30.6	0.0	-.127	.044	430.2	100.0
299.8	11.6	0.0	-.051	.104	388.7	100.0
299.8	8.6	0.0	-.038	.118	389.5	100.0

Tabelle 47: L/D = 40, D = 0,7 cm

Lochblende Nr. 2 am Meßstreckeneintritt

Table 47: L/D = 40, D = 0,7 cm

Orifice plate No. 2 at test section inlet

$\dot{m}$	$\Delta\vartheta_E$	$\Delta\vartheta_A$	x_E	x_A	q_{BO}	P
Massenfluß	Eintr.-Unter-kühlung	Austr.-Unter-kühlung	Eintr.-Qualität	Austr.-Qualität	max.Heizfl.-Belastung	Druck
Mass Flow Rate	Inlet Sub-cooling	Outlet Sub-cooling	Inlet-Quality	Outlet-Quality	Burn Out Heatflux	Pressure
$g/cm^2\ s$	^{o}C	^{o}C	–	–	W/cm^2	ata
231.9	39.1	0.0	-.130	.154	312.8	70.0
231.9	28.6	0.0	-.096	.179	303.2	70.0
231.9	18.1	0.0	-.062	.198	285.6	70.0
231.9	6.8	0.0	-.023	.227	276.7	69.0
231.8	1.2	0.0	-.004	.242	270.1	71.0
296.3	39.1	0.0	-.130	.098	320.8	69.5
296.4	45.9	0.0	-.151	.074	316.9	69.5
296.4	31.8	0.0	-.107	.120	319.0	70.0
292.9	18.1	0.0	-.061	.154	300.7	69.0
292.3	7.0	0.0	-.024	.181	285.2	70.0
294.5	4.0	0.0	-.014	.187	280.6	70.0
357.5	32.1	0.0	-.108	.085	327.2	70.0
357.6	42.1	0.0	-.139	.062	343.1	69.5
358.3	50.1	0.0	-.164	.059	379.1	69.5
357.4	20.1	0.0	-.068	.115	311.8	69.5
356.1	7.0	0.0	-.024	.146	289.9	69.0
359.1	0.0	0.0	.096	.259	276.0	70.5
346.4	36.3	0.0	-.150	.065	311.5	100.0
348.8	43.1	0.0	-.175	.047	323.8	100.0
351.4	33.2	0.0	-.138	.075	312.2	100.2

Tabelle 48: L/D = 80, D = 0,8 cm

Versuchsrohr mit sinusförmig verteilter Heizflächenbelastung

Table 48: L/D = 80, D = 0,8 cm

Test channel with sinusoidal heat flux distribution

$\dot{m}$	$\Delta\vartheta_E$	$\Delta\vartheta_A$	x_E	x_A	q_{BO}	P
Massenfluß	Eintr.-Unter-kühlung	Austr.-Unter-kühlung	Eintr.-Qualität	Austr.-Qualität	max.Heizfl.-Belastung	Druck
Mass Flow Rate	Inlet Sub-cooling	Outlet Sub-cooling	Inlet-Quality	Outlet-Quality	Burn Out Heatflux	Pressure
$g/cm^2\ s$	^{o}C	^{o}C	–	–	W/cm^2	ata
348.7	28.0	0.0	-.117	.089	300.4	100.0
348.5	22.5	0.0	-.096	.093	275.0	100.0
348.1	16.2	0.0	-.070	.106	256.4	100.0
347.5	7.9	0.0	-.035	.126	234.0	100.0
347.2	3.8	0.0	-.017	.134	219.6	100.0
294.9	45.1	0.0	-.183	.079	322.0	100.0
295.6	43.1	0.0	-.175	.076	312.2	100.0
298.9	39.1	0.0	-.160	.085	305.1	100.0
299.3	32.1	0.0	-.133	.101	292.2	100.0
293.6	23.5	0.0	-.099	.122	271.9	100.0
295.6	11.8	0.0	-.051	.143	240.8	99.5
292.9	2.7	0.0	-.012	.167	219.4	99.5
232.8	54.7	0.0	-.216	.098	304.4	99.0
237.1	38.9	0.0	-.159	.129	285.6	100.0
233.9	30.8	0.0	-.127	.143	265.3	99.0
234.5	22.3	0.0	-.094	.163	252.8	99.0
231.0	15.7	0.0	-.067	.177	236.6	99.0
231.3	8.1	0.0	-.036	.196	224.8	99.0
234.7	0.0	0.0	.062	.279	212.2	99.0

Tabelle 49: L/D = 80, D = 0,8 cm

Versuchsrohr mit sinusförmig verteilter Heizflächenbelastung

Table 49: L/D = 80, D = 0,8 cm

Test channel with sinusoidal heat flux distribution

$\dot{m}$	$\Delta\vartheta_E$	$\Delta\vartheta_A$	x_E	x_A	q_{BO}	P
Massenfluß	Eintr.-Unter-kühlung	Austr.-Unter-kühlung	Eintr.-Qualität	Austr.-Qualität	max.Heizfl.-Belastung	Druck
Mass Flow Rate	Inlet Sub-cooling	Outlet Sub-cooling	Inlet-Quality	Outlet-Quality	Burn Out Heatflux	Pressure
$g/cm^2\,s$	^{o}C	^{o}C	–	–	W/cm^2	ata
357.6	41.7	0.0	-.124	.009	138.9	54.5
351.5	38.6	0.0	-.115	.012	130.2	54.0
365.1	28.9	0.0	-.087	.020	113.8	54.0
366.1	28.6	0.0	-.086	.016	108.8	54.0
235.6	56.5	0.0	-.185	.006	121.6	70.5
235.1	51.1	0.0	-.168	.004	109.2	70.5
234.2	43.6	0.0	-.144	.018	103.3	70.5
235.1	36.1	0.0	-.121	.014	85.7	70.5
235.1	28.6	0.0	-.097	.023	76.3	70.5
235.5	18.5	0.0	-.064	.026	57.5	70.5
233.8	16.3	0.0	-.056	.033	56.6	70.8
301.1	59.5	0.0	-.194	.012	168.2	70.5
300.8	53.3	0.0	-.175	.009	149.3	70.5
299.2	38.1	0.0	-.127	.024	122.7	70.0
310.4	24.6	0.0	-.083	.030	96.0	69.5
311.1	16.6	0.0	-.057	.062	100.9	69.0
317.2	14.6	0.0	-.050	.054	90.0	69.0
315.0	17.8	0.0	-.061	.023	72.1	69.0
305.2	28.9	0.0	-.097	.015	93.0	69.0
304.5	34.9	0.0	-.116	.015	108.6	69.0

Tabelle 50:   L/D = 140, D = 0,7 cm
Röhre mit langer Einlaufstrecke

Table 50 :   L/D = 140, D = 0,7 cm
Channels with long inlet section

m	$\Delta\vartheta_E$	$\Delta\vartheta_A$	x_E	x_A	q_{BO}	P
Massenfluß	Eintr.-Unter-kühlung	Austr.-Unter-kühlung	Eintr.-Qualität	Austr.-Qualität	max.Heizfl.-Belastung	Druck
Mass Flow Rate	Inlet Sub-cooling	Outlet Sub-cooling	Inlet-Quality	Outlet-Quality	Burn Out Heatflux	Pressure
g/cm^2 s	$^\circ C$	$^\circ C$	-	-	W/cm^2	ata
305.1	44.1	0.0	-.146	.005	124.7	70.0
318.0	51.1	1.4	-.167	-.005	139.6	70.0
305.3	60.1	.8	-.195	-.003	158.2	70.0
351.6	28.0	0.0	-.095	.017	107.3	71.0
369.8	23.0	0.0	-.079	.026	104.8	71.0
351.8	17.5	0.0	-.060	.030	86.7	70.5
373.4	16.0	0.0	-.055	.037	93.7	70.5
358.2	26.5	0.0	-.090	.019	105.8	71.0
352.5	34.1	0.0	-.115	.011	120.4	71.0
344.9	32.8	0.0	-.110	.011	113.6	70.5
349.1	41.9	.1	-.138	0.000	133.3	69.5
350.3	46.6	0.0	-.153	.005	150.8	70.0
348.4	51.8	0.0	-.169	.008	167.8	69.5
348.4	36.6	0.0	-.121	.015	129.4	69.0
230.1	43.1	0.0	-.176	.020	107.4	101.0
223.9	24.7	0.0	-.105	.058	86.9	101.0
226.8	18.9	0.0	-.082	.059	75.6	101.0

Tabelle 51: L/D = 140, D = 0,7 cm

Rohre mit Einlaufstrecke

Table 51: L/D = 140, D = 0,7 cm

Channels with inlet section

m	$\Delta\vartheta_E$	$\Delta\vartheta_A$	x_E	x_A	q_{BO}	P
Massenfluß	Eintr.-Unter-kühlung	Austr.-Unter-kühlung	Eintr.-Qualität	Austr.-Qualität	max.Heizfl.-Belastung	Druck
Mass Flow Rate	Inlet Sub-cooling	Outlet Sub-cooling	Inlet-Quality	Outlet-Quality	Burn Out Heatflux	Pressure
$g/cm^2\ s$	$°C$	$°C$	–	–	W/cm^2	ata
253.7	94.6	13.1	-.301	-.046	294.3	71.9
241.5	91.3	12.4	-.289	-.043	271.3	70.5
242.1	78.4	7.1	-.251	-.025	250.1	70.5
245.0	69.7	6.0	-.225	-.021	228.4	70.5
245.0	58.5	2.4	-.191	-.008	204.2	70.5
238.8	100.4	14.4	-.315	-.050	289.9	70.2
237.3	107.5	18.5	-.335	-.063	295.6	69.9
234.8	110.7	18.9	-.344	-.065	300.8	69.9
234.5	115.1	18.4	-.359	-.064	316.2	71.1
241.6	124.3	20.5	-.386	-.070	347.4	71.2
236.4	137.0	21.0	-.422	-.072	377.3	71.2
242.9	151.8	26.7	-.464	-.091	413.3	71.3
232.9	159.8	23.6	-.487	-.081	430.8	71.2
237.1	55.0	0.0	-.181	.009	206.2	71.0
249.4	43.7	0.0	-.145	.021	189.7	71.1
230.5	37.8	0.0	-.127	.032	167.9	71.0
235.0	30.1	0.0	-.102	.035	147.7	71.3
233.0	27.5	0.0	-.094	.041	144.2	71.2
339.7	91.4	13.0	-.290	-.045	379.4	71.1
281.0	29.8	0.0	-.101	.033	173.1	71.5

Tabelle 52: L/D = 80, D = 0,7 cm

Rohre mit langer Einlaufstrecke

Table 52: L/D = 80, D = 0,7 cm

Channels with long inlet section

m	$\Delta\vartheta_E$	$\Delta\vartheta_A$	x_E	x_A	q_{BO}	P
Massenfluß	Eintr.-Unter-kühlung	Austr.-Unter-kühlung	Eintr.-Qualität	Austr.-Qualität	max.Heizfl.-Belastung	Druck
Mass Flow Rate	Inlet Sub-cooling	Outlet Sub-cooling	Inlet-Quality	Outlet-Quality	Burn Out Heatflux	Pressure
$g/cm^2\ s$	$^{\circ}C$	$^{\circ}C$	-	-	W/cm^2	ata
281.6	36.7	0.0	-.124	.032	200.8	71.2
287.2	40.9	0.0	-.137	.024	211.6	71.4
283.8	43.5	0.0	-.145	.026	223.3	71.5
281.2	46.3	0.0	-.154	.023	227.7	71.3
278.9	51.5	0.0	-.170	.017	239.2	71.2
278.9	56.0	0.0	-.184	.012	241.5	71.0
279.7	64.1	0.0	-.209	.002	269.7	71.1
345.0	69.7	5.0	-.226	-.018	327.2	71.2
346.9	61.5	2.1	-.201	-.007	306.0	71.0
350.6	39.1	0.0	-.131	.009	224.9	71.0
343.5	46.1	0.0	-.153	.001	242.1	71.0
341.9	80.3	8.8	-.258	-.031	353.2	71.2
344.9	99.2	14.4	-.313	-.050	413.7	71.0
341.4	119.9	21.2	-.374	-.073	467.8	71.3
346.5	70.4	6.5	-.227	-.023	323.3	70.9
348.0	62.0	3.7	-.202	-.013	290.1	71.0
344.8	52.3	0.0	-.172	.002	275.3	70.7
347.6	44.8	0.0	-.149	.004	243.9	71.0
345.1	38.2	0.0	-.128	.009	217.7	70.9
347.9	31.2	0.0	-.106	.018	197.8	71.2

Tabelle 53: L/D = 80, D = 0,7 cm
Rohre mit langer Einlaufstrecke

Table 53: L/D = 80, D = 0,7 cm
Channels with long inlet section

m	$\Delta\vartheta_E$	$\Delta\vartheta_A$	x_E	x_A	q_{BO}	P
Massenfluß	Eintr.-Unter-kühlung	Austr.-Unter-kühlung	Eintr.-Qualität	Austr.-Qualität	max.Heizfl.-Belastung	Druck
Mass Flow Rate	Inlet Sub-cooling	Outlet Sub-cooling	Inlet-Quality	Outlet-Quality	Burn Out Heatflux	Pressure
g/cm^2 s	°C	°C	-	-	W/cm^2	ata
339.8	25.5	0.0	-.087	.034	189.2	71.2
341.7	21.5	0.0	-.074	.033	167.5	71.2
232.7	63.3	3.2	-.251	-.014	220.5	101.2
230.0	73.5	6.1	-.287	-.028	239.1	101.1
225.4	81.9	9.0	-.317	-.040	249.9	101.1
232.6	82.6	8.0	-.319	-.036	264.3	101.0
234.0	93.8	10.9	-.358	-.048	290.4	101.0
233.9	98.8	12.4	-.375	-.055	300.2	101.0
234.3	108.4	15.9	-.407	-.069	317.3	101.0
234.0	115.4	18.2	-.431	-.079	330.1	101.1
232.5	121.6	18.7	-.451	-.081	345.1	101.0
232.2	48.0	0.0	-.194	.025	205.2	100.5
230.0	37.5	0.0	-.155	.034	174.8	100.5
226.3	31.9	0.0	-.133	.054	170.7	100.5
236.0	27.0	0.0	-.114	.058	164.0	100.7
235.3	24.1	0.0	-.102	.064	158.2	100.5
245.5	18.0	0.0	-.078	.061	137.9	100.8
229.8	13.7	0.0	-.060	.103	151.0	100.0
297.0	68.4	5.7	-.271	-.026	290.7	102.0
303.1	74.7	6.6	-.293	-.030	318.4	101.8

Tabelle 54: L/D = 80, D = 0,7 cm

Rohre mit langer Einlaufstrecke

Table 54: L/D = 80, D = 0,7 cm

Channels with long inlet section

m	$\Delta\vartheta_E$	$\Delta\vartheta_A$	x_E	x_A	q_{BO}	P
Massenfluß	Eintr.-Unter-kühlung	Austr.-Unter-kühlung	Eintr.-Qualität	Austr.-Qualität	max.Heizfl.-Belastung	Druck
Mass Flow Rate	Inlet Sub-cooling	Outlet Sub-cooling	Inlet-Quality	Outlet-Quality	Burn Out Heatflux	Pressure
$g/cm^2\ s$	$^{\circ}C$	$^{\circ}C$	–	–	W/cm^2	ata
347.7	58.7	1.6	-.234	-.007	316.2	101.1
349.4	73.0	6.1	-.285	-.027	361.2	101.1
348.3	78.6	8.0	-.305	-.036	376.0	101.0
347.4	84.8	9.4	-.327	-.042	397.0	101.0
349.2	91.1	12.1	-.349	-.053	413.4	101.1
348.0	96.0	13.3	-.365	-.058	428.4	101.0
346.8	102.5	16.4	-.387	-.071	439.2	101.0
345.8	103.0	15.3	-.389	-.067	446.7	101.0
344.7	106.5	16.1	-.401	-.070	456.9	101.0
344.8	57.6	1.4	-.230	-.006	309.6	101.0
348.8	47.9	0.0	-.194	.008	284.0	101.0
345.2	39.3	0.0	-.162	.025	260.8	100.9
343.2	31.9	0.0	-.134	.043	244.1	101.2
341.1	23.1	0.0	-.099	.045	197.8	100.8
338.2	21.7	0.0	-.093	.053	199.5	101.0
336.5	17.8	0.0	-.077	.069	198.1	100.8
351.5	19.4	0.0	-.084	.047	185.8	101.0

Tabelle 55: L/D = 80, D = 0,7 cm
Rohre mit langer Einlaufstrecke

Table 55: L/D = 80, D = 0,7 cm
Channels with long inlet section

m	$\Delta\vartheta_E$	$\Delta\vartheta_A$	x_E	x_A	q_{BO}	P
Massenfluß	Eintr.-Unter-kühlung	Austr.-Unter-kühlung	Eintr.-Qualität	Austr.-Qualität	max.Heizfl.-Belastung	Druck
Mass Flow Rate	Inlet Sub-cooling	Outlet Sub-cooling	Inlet-Quality	Outlet-Quality	Burn Out Heatflux	Pressure
$g/cm^2\ s$	$^\circ C$	$^\circ C$	–	–	W/cm^2	ata
230.1	77.9	9.6	-.249	-.033	226.8	70.0
229.4	72.5	7.6	-.232	-.026	216.5	70.0
229.7	59.6	4.2	-.192	-.015	187.7	69.0
229.3	52.1	1.7	-.169	-.006	172.3	69.0
228.4	13.3	0.0	-.046	.051	102.1	70.0
233.3	14.8	0.0	-.051	.044	102.1	70.0
230.9	16.6	0.0	-.057	.042	106.2	69.5
232.8	23.8	0.0	-.081	.027	116.4	70.0
233.5	30.1	0.0	-.101	.016	126.7	70.0
232.3	35.4	0.0	-.118	.004	131.4	70.0
231.8	42.1	.1	-.139	0.000	147.6	69.5
298.2	46.1	1.3	-.152	-.005	201.4	70.5
299.0	74.5	8.8	-.238	-.031	284.5	70.0
301.0	67.8	7.4	-.218	-.026	265.1	70.0
299.4	59.1	5.3	-.192	-.019	237.8	70.0
298.1	51.8	3.7	-.170	-.013	214.2	70.0
301.8	31.8	0.0	-.107	.010	162.6	70.5
309.2	6.5	0.0	-.023	.152	248.3	70.5
306.5	15.8	0.0	-.054	.034	124.7	71.0
299.1	17.0	0.0	-.059	.033	126.4	71.5

Tabelle 56: L/D = 80, D = 0,7 cm
Rohre ohne Einlaufstrecke

Table 56: L/D = 80, D = 0,7 cm
Channels without inlet section

m	$\Delta\vartheta_E$	$\Delta\vartheta_A$	x_E	x_A	q_{BO}	P
Massenfluß	Eintr.-Unter-kühlung	Austr.-Unter-kühlung	Eintr.-Qualität	Austr.-Qualität	max.Heizfl.-Belastung	Druck
Mass Flow Rate	Inlet Sub-cooling	Outlet Sub-cooling	Inlet-Quality	Outlet-Quality	Burn Out Heatflux	Pressure
g/cm^2 s	^{o}C	^{o}C	–	–	W/cm^2	ata
302.2	20.9	0.0	-.073	.032	144.7	73.0
296.0	24.6	0.0	-.083	.033	159.1	69.5
296.0	27.1	0.0	-.092	.031	167.1	70.5
358.3	78.7	9.7	-.251	-.034	356.5	70.0
356.7	73.7	8.7	-.236	-.030	336.2	70.0
360.0	66.0	7.7	-.214	-.027	307.3	70.5
361.4	15.5	0.0	-.054	.028	137.2	71.0
362.0	19.3	0.0	-.066	.022	147.1	71.0
357.9	23.4	0.0	-.080	.019	162.8	70.9
356.7	29.8	0.0	-.101	.017	193.6	70.5
355.7	33.6	0.0	-.113	.011	203.4	70.5
357.9	41.1	.4	-.137	-.001	221.8	71.0
358.1	50.8	1.9	-.168	-.006	263.2	71.0
358.1	57.5	4.5	-.188	-.016	281.9	70.5
288.5	16.9	0.0	-.063	.045	136.7	82.0
289.9	17.4	0.0	-.065	.049	145.7	82.0
296.0	22.1	0.0	-.082	.043	163.4	82.0
295.8	30.0	0.0	-.110	.033	185.7	81.5
352.2	25.8	0.0	-.094	0.000	145.7	81.0
343.3	40.5	3.5	-.145	-.014	197.5	81.5

Tabelle 57: L/D = 80, D = 0,7 cm
Rohre ohne Einlaufstrecke

Table 57: L/D = 80, D = 0,7 cm
Channels without inlet section

m	$\Delta\vartheta_E$	$\Delta\vartheta_A$	x_E	x_A	q_{BO}	P
Massenfluß	Eintr.-Unter-kühlung	Austr.-Unter-kühlung	Eintr.-Qualität	Austr.-Qualität	max.Heizfl.-Belastung	Druck
Mass Flow Rate	Inlet Sub-cooling	Outlet Sub-cooling	Inlet-Quality	Outlet-Quality	Burn Out Heatflux	Pressure
$g/cm^2\ s$	$^{\circ}C$	$^{\circ}C$	–	–	W/cm^2	ata
340.6	34.3	2.0	-.124	-.008	173.3	81.0
338.1	26.2	0.0	-.096	.009	156.9	81.5
295.2	18.4	0.0	-.073	.048	152.3	90.0
299.4	23.4	0.0	-.092	.040	167.3	90.0
351.8	17.1	0.0	-.069	.046	170.1	91.5
338.8	16.6	0.0	-.067	.046	161.4	91.5
361.1	20.6	0.0	-.082	.037	182.2	91.5
353.3	21.1	0.0	-.084	.037	180.6	91.5
355.2	22.6	0.0	-.090	.032	181.7	91.5
345.5	23.5	0.0	-.093	.060	222.2	91.0
342.9	39.4	0.0	-.152	.012	236.2	91.5
235.7	80.5	5.8	-.311	-.026	269.5	100.5
235.8	69.4	2.1	-.271	-.010	248.1	100.3
238.0	62.3	.1	-.246	-.001	235.1	100.5
238.1	54.9	0.0	-.220	.012	222.6	101.0
238.5	46.8	0.0	-.190	.020	202.0	100.5
237.1	41.9	0.0	-.171	.029	192.0	100.4
237.5	36.6	0.0	-.153	.027	171.9	101.8
235.9	28.3	0.0	-.119	.041	152.8	100.4
237.6	21.1	0.0	-.090	.052	136.7	100.5

Tabelle 58:   L/D = 80, D = o,7 cm
Rohre ohne Einlaufstrecke

Table 58:   L/D = 80, D = 0,7 cm
Channels without inlet section

m	$\Delta\vartheta_E$	$\Delta\vartheta_A$	x_E	x_A	q_{BO}	P
Massenfluß	Eintr.-Unter-kühlung	Austr.-Unter-kühlung	Eintr.-Qualität	Austr.-Qualität	max.Heizfl.-Belastung	Druck
Mass Flow Rate	Inlet Sub-cooling	Outlet Sub-cooling	Inlet-Quality	Outlet-Quality	Burn Out Heatflux	Pressure
$g/cm^2\,s$	$^{\circ}C$	$^{\circ}C$	–	–	W/cm^2	ata
232.4	11.8	0.0	-.052	.088	131.4	100.5
302.7	71.2	6.4	-.277	-.029	302.6	100.0
298.5	65.3	4.6	-.257	-.021	283.3	100.5
297.6	58.2	1.7	-.231	-.008	267.4	100.0
293.2	48.1	0.0	-.194	.006	237.5	100.0
299.9	40.1	0.0	-.164	.008	209.4	100.0
293.5	31.6	0.0	-.131	.030	192.0	100.0
288.0	22.0	0.0	-.093	.049	166.8	100.0
296.1	18.0	0.0	-.077	.057	161.4	100.0
349.6	3.3	0.0	-.015	.150	232.4	101.0
345.8	18.7	0.0	-.081	.052	186.2	101.0
342.1	21.2	0.0	-.091	.061	210.3	101.0
343.1	29.5	0.0	-.124	.036	221.7	101.0
348.3	37.8	0.0	-.157	.011	234.9	101.0
348.7	46.4	0.0	-.189	.003	269.8	101.0
350.3	51.7	1.1	-.207	-.005	284.7	100.0
346.6	60.2	1.9	-.238	-.009	320.0	100.0
342.8	68.2	4.6	-.266	-.021	339.3	100.0
346.9	76.9	7.6	-.297	-.034	368.0	100.0

Tabelle 59: L/D = 80, D = 0,7 cm
Rohre ohne Einlaufstrecke

Table 59: L/D = 80, D = 0,7 cm
Channels without inlet section

m	$\Delta \vartheta_E$	$\Delta \vartheta_A$	x_E	x_A	q_{BO}	P
Massenfluß	Eintr.-Unter-kühlung	Austr.-Unter-kühlung	Eintr.-Qualität	Austr.-Qualität	max.Heizfl.-Belastung	Druck
Mass Flow Rate	Inlet Sub-cooling	Outlet Sub-cooling	Inlet-Quality	Outlet-Quality	Burn Out Heatflux	Pressure
$g/cm^2 \, s$	$^{\circ}C$	$^{\circ}C$	-	-	W/cm^2	ata
242.5	13.5	0.0	-.047	.048	106.2	71.0
237.9	11.7	0.0	-.041	.072	123.2	71.0
240.2	15.0	0.0	-.052	.036	97.4	71.0
240.2	16.5	0.0	-.057	.035	102.1	71.0
239.0	17.8	0.0	-.061	.042	113.7	71.0
241.2	36.4	0.0	-.121	.020	157.4	70.0
235.6	25.6	0.0	-.087	.031	128.5	70.0
236.8	17.3	0.0	-.059	.043	111.5	70.0
241.4	20.3	0.0	-.069	.038	120.0	70.0
305.6	20.1	0.0	-.068	.042	155.3	70.0
311.9	26.8	0.0	-.091	.023	163.4	70.0
311.9	26.8	0.0	-.091	.026	168.5	70.0
313.7	29.6	0.0	-.100	.054	222.4	70.0
314.6	33.6	0.0	-.113	.040	221.8	70.0
318.1	39.9	0.0	-.132	.027	232.8	70.0
315.5	47.3	0.0	-.156	.020	255.8	70.0
273.0	27.6	0.0	-.093	.038	164.7	70.0
273.4	28.6	0.0	-.096	.037	168.5	70.0
274.0	32.9	0.0	-.110	.040	189.7	70.0
301.1	38.1	0.0	-.127	.071	273.7	70.0

Tabelle 60: L/D = 80, D = 0,7 cm
Werte aus Untersuchungen über den Einfluß
der Loopanordnung auf $q_{B.O.}$

Table 60: L/D = 80, D = 0,7 cm
Data from tests to study influence of loop
layout on $q_{B.O.}$

m	$\Delta\vartheta_E$	$\Delta\vartheta_A$	x_E	x_A	q_{BO}	P
Massenfluß	Eintr.-Unter-kühlung	Austr.-Unter-kühlung	Eintr.-Qualität	Austr.-Qualität	max.Heizfl.-Belastung	Druck
Mass Flow Rate	Inlet Sub-cooling	Outlet Sub-cooling	Inlet-Quality	Outlet-Quality	Burn Out Heatflux	Pressure
g/cm^2 s	°C	°C	-	-	W/cm^2	ata
294.5	26.3	0.0	-.089	.026	157.2	70.0
293.6	28.3	0.0	-.095	.028	167.1	70.0
291.2	32.1	0.0	-.108	.022	175.0	70.0
294.3	32.1	0.0	-.107	.024	178.4	69.5
294.2	25.1	0.0	-.085	.045	177.0	69.5
306.0	21.3	0.0	-.072	.020	130.9	69.5
293.6	15.1	0.0	-.052	.047	134.3	69.0
297.7	19.5	0.0	-.066	.033	137.9	69.2
293.6	24.1	0.0	-.081	.028	148.5	69.2
296.2	28.1	0.0	-.094	.041	185.7	69.0
298.6	33.9	0.0	-.113	.031	198.3	69.5
293.8	36.1	0.0	-.120	.028	200.8	69.5
297.4	42.1	0.0	-.138	.010	204.8	69.0
303.0	46.5	0.0	-.153	.018	238.7	70.4
302.9	36.1	0.0	-.120	.049	236.0	70.0
303.9	37.3	0.0	-.125	.030	216.5	70.5
307.5	41.8	0.0	-.139	.046	260.1	70.5
313.8	23.6	0.0	-.081	.034	165.2	70.8
296.0	28.6	0.0	-.097	.035	178.9	70.8
294.5	34.6	0.0	-.116	.028	195.4	71.0

Tabelle 61: L/D = 80, D = 0,7 cm
Werte aus Untersuchungen über den Einfluß
der Loopanordnung auf $q_{B.0.}$

Table 61: L/D = 80, D = 0,7 cm
Data from tests to study influence of loop
layout on $q_{B.0.}$

$\dot{m}$	$\Delta\vartheta_E$	$\Delta\vartheta_A$	x_E	x_A	q_{BO}	P
Massenfluß	Eintr.-Unter-kühlung	Austr.-Unter-kühlung	Eintr.-Qualität	Austr.-Qualität	max.Heizfl.-Belastung	Druck
Mass Flow Rate	Inlet Sub-cooling	Outlet Sub-cooling	Inlet-Quality	Outlet-Quality	Burn Out Heatflux	Pressure
$g/cm^2\,s$	$^{\circ}C$	$^{\circ}C$	–	–	W/cm^2	ata
236.4	30.1	0.0	-.101	.058	173.1	70.0
240.0	30.1	0.0	-.101	.061	178.9	70.0
240.0	38.4	0.0	-.127	.054	200.8	70.0
240.2	42.6	0.0	-.141	.062	223.9	70.0
240.9	48.8	0.0	-.160	.063	248.3	70.0
240.6	52.6	0.0	-.171	.052	248.3	69.5
294.1	48.6	0.0	-.161	.110	364.1	71.0
298.3	39.4	0.0	-.131	.037	229.9	70.0
298.9	45.1	0.0	-.149	.047	269.1	70.0
298.7	50.8	0.0	-.167	.040	283.8	70.0
299.3	56.1	0.0	-.183	.038	304.2	70.0
298.8	63.0	0.0	-.204	.034	327.2	70.0
299.3	67.0	0.0	-.215	.040	352.7	69.5
362.5	53.5	0.0	-.177	.060	392.1	71.5
362.8	52.8	0.0	-.172	.038	351.0	69.2
362.2	47.8	0.0	-.156	.034	318.2	69.2
360.2	41.6	0.0	-.138	.029	277.2	70.0
361.0	36.3	0.0	-.120	.050	283.8	69.2
238.3	42.8	0.0	-.173	.070	234.8	99.5
240.1	39.1	0.0	-.160	.070	223.1	100.0

Tabelle 62: L/D = 80, D = 0,7 cm
Lochblende Nr.1 am Meßstreckeneintritt

Table 62: L/D = 80, D = 0,7 cm
Orifice plate No. 1 at test section inlet

m	$\Delta\vartheta_E$	$\Delta\vartheta_A$	x_E	x_A	q_{BO}	P
Massenfluß	Eintr.-Unter-kühlung	Austr.-Unter-kühlung	Eintr.-Qualität	Austr.-Qualität	max.Heizfl.-Belastung	Druck
Mass Flow Rate	Inlet Sub-cooling	Outlet Sub-cooling	Inlet-Quality	Outlet-Quality	Burn Out Heatflux	Pressure
$g/cm^2\ s$	$^\circ C$	$^\circ C$	-	-	W/cm^2	ata
240.2	1.7	0.0	-.006	.158	180.9	70.5
241.3	8.5	0.0	-.030	.139	187.5	70.5
241.3	13.5	0.0	-.047	.098	161.4	70.5
215.7	22.8	0.0	-.078	.099	175.7	70.5
242.5	28.3	0.0	-.096	.072	186.8	70.5
242.5	36.1	0.0	-.121	.054	195.3	70.5
242.5	47.6	0.0	-.157	.040	219.5	70.3
252.6	55.0	0.0	-.180	.017	229.1	70.2
289.7	7.5	0.0	-.026	.133	212.3	70.5
291.6	10.3	0.0	-.036	.126	217.5	70.5
291.6	27.3	0.0	-.093	.085	237.6	70.5
291.6	23.0	0.0	-.079	.095	233.2	71.0
291.6	19.0	0.0	-.065	.105	228.5	71.0
292.6	31.3	0.0	-.106	.051	211.3	71.0
293.5	38.3	0.0	-.128	.040	227.2	71.0
293.6	44.3	0.0	-.147	.041	253.3	71.0
295.4	52.3	0.0	-.172	.026	268.9	71.0
286.9	47.6	0.0	-.157	.042	262.2	71.0
349.7	52.3	0.0	-.172	.014	299.3	70.5
349.7	49.8	0.0	-.164	.019	293.8	70.5

Tabelle 63: L/D = 80, D = 0,7 cm
Mit Lochblende am Meßstreckenaustritt

Table 63: L/D = 80, D = 0,7 cm
With orifice plate at test section outlet

m	$\Delta\vartheta_E$	$\Delta\vartheta_A$	x_E	x_A	q_{BO}	P
Massenfluß	Eintr.-Unter-kühlung	Austr.-Unter-kühlung	Eintr.-Qualität	Austr.-Qualität	max.Heizfl.-Belastung	Druck
Mass Flow Rate	Inlet Sub-cooling	Outlet Sub-cooling	Inlet-Quality	Outlet-Quality	Burn Out Heatflux	Pressure
$g/cm^2\ s$	$^{\circ}C$	$^{\circ}C$	–	–	W/cm^2	ata
346.5	41.9	0.0	-.139	.021	256.3	70.1
346.6	33.6	0.0	-.113	.033	232.0	70.5
346.5	36.1	0.0	-.121	.024	231.2	70.5
346.5	26.1	0.0	-.088	.072	256.3	70.5
346.6	19.0	0.0	-.065	.091	250.0	70.5
345.8	5.5	0.0	-.019	.138	249.7	70.5
345.8	10.8	0.0	-.037	.119	248.9	70.5
345.8	8.2	0.0	-.029	.112	223.3	70.5
239.3	8.2	0.0	-.037	.219	246.9	100.5
239.2	5.7	0.0	-.025	.200	218.1	100.5
239.1	11.4	0.0	-.050	.187	227.9	101.0
239.2	20.5	0.0	-.088	.142	222.0	101.0
239.2	17.2	0.0	-.075	.163	228.6	101.0
241.5	26.1	0.0	-.111	.108	213.1	100.8
241.5	37.2	0.0	-.154	.074	221.8	100.8
241.5	45.9	0.0	-.187	.061	241.0	101.0
240.4	50.4	0.0	-.204	.057	252.1	101.0
294.1	49.1	0.0	-.199	.049	293.1	101.0
292.3	53.9	0.0	-.216	.031	291.6	101.0
292.2	38.3	0.0	-.158	.055	250.7	101.0

Tabelle 64: L/D = 80, D = 0,7 cm

Mit Lochblende am Meßstreckenaustritt

Table 64: L/D = 80, D = 0,7 cm

With orifice plate at test section outlet

$\dot{m}$	$\Delta\vartheta_E$	$\Delta\vartheta_A$	x_E	x_A	q_{BO}	P
Massenfluß	Eintr.-Unter-kühlung	Austr.-Unter-kühlung	Eintr.-Qualität	Austr.-Qualität	max.Heizfl.-Belastung	Druck
Mass Flow Rate	Inlet Sub-cooling	Outlet Sub-cooling	Inlet-Quality	Outlet-Quality	Burn Out Heatflux	Pressure
g/cm^2 s	^{o}C	^{o}C	–	–	W/cm^2	ata
291.1	31.4	0.0	-.131	.075	241.9	100.5
291.2	27.0	0.0	-.114	.102	253.6	101.0
291.3	17.8	0.0	-.077	.135	249.4	100.5
291.5	6.4	0.0	-.029	.180	246.2	100.5
339.5	3.5	0.0	-.016	.168	252.4	101.0
342.3	9.3	0.0	-.041	.144	255.1	101.0
342.5	17.2	0.0	-.075	.125	274.9	101.0
347.6	25.5	0.0	-.108	.097	288.0	101.0
347.9	33.3	0.0	-.139	.059	276.9	101.0
349.9	41.8	0.0	-.172	.047	308.0	101.0
351.6	49.9	0.0	-.202	.034	333.9	101.0
340.0	28.0	0.0	-.118	.087	280.7	101.0

Tabelle 65:   L/D = 80, D = 0,7 cm
Mit Lochblende am Meßstreckenaustritt

Table 65:   L/D = 80, D = 0,7 cm
With orifice plate at test section outlet

$\dot{m}$	$\Delta\vartheta_E$	$\Delta\vartheta_A$	X_E	X_A	q_{BO}	P	Δ_P
Massenfluß	Eintr.-Unter-kühlung	Austr.-Unter-kühlung	Eintr.-Qualität	Austr.-Qualität	max.Heizfl.-Belastung	Druck	Druckverl.am Meßstrecken-eintritt
Mass Flow Rate	Inlet Sub-cooling	Outlet Sub-cooling	Inlet-Quality	Outlet-Quality	Burn Out Heatflux	Pressure	Pressure Drop at the Inlet of the Test-section
g/cm² s	°C	°C	-	-	W/cm²	ata	mmHg
292.5	1.3	0.0	-.004	.211	336.9	69.0	0.00
292.6	7.0	0.0	-.024	.088	175.7	69.0	0.00
292.6	12.3	0.0	-.042	.066	170.0	68.0	0.00
296.3	13.1	0.0	-.044	.109	244.5	67.5	360.00
293.5	12.9	0.0	-.044	.186	361.8	67.5	410.00
294.5	12.6	0.0	-.042	.191	370.0	67.0	660.00
294.5	13.6	0.0	-.046	.112	249.7	68.0	307.00
294 5	26.6	0.0	-.089	.063	240.0	68.5	305.00
292.6	24.4	0.0	-.081	.107	296.2	68.0	658.00
297.2	23.4	0.0	-.078	.169	394.2	67.5	1075.00
286.1	21.1	0.0	-.071	.183	389.6	68.5	970.00
291.6	25.1	0.0	-.084	.039	193.1	69.0	0.00
291.6	36.4	0.0	-.120	.024	225.5	69.0	0.00
294.5	38.1	0.0	-.126	.041	263.5	68.5	300.00
293.5	37.7	0.0	-.124	.104	358.2	68.0	683.00
297.3	37.1	0.0	-.122	.119	383.9	68.5	1020.00
297.3	35.7	0.0	-.117	.119	377.4	67.5	890.00
296.2	48.1	0.0	-.158	.088	389.6	69.5	882.00
291.6	45.9	0.0	-.150	.120	421.2	68.5	1045.00
293.5	47.1	0.0	-.154	.075	360.0	69.0	685.00

Tabelle 66: L/D = 71,5, D = 0,7 cm
Drosselstelle am Meßstreckeneintritt

Table 66: L/D = 71,5, D = 0,7 cm
Throttling point at test section inlet

m	$\Delta\vartheta_E$	$\Delta\vartheta_A$	X_E	X_A	q_{BO}	P	Δ_P
Massenfluß	Eintr.-Unter-kühlung	Austr.-Unter-kühlung	Eintr.-Qualität	Austr.-Qualität	max.Heizfl.-Belastung	Druck	Druckverl.am Meßstrecken-eintritt
Mass Flow Rate	Inlet Sub-cooling	Outlet Sub-cooling	Inlet-Quality	Outlet-Quality	Burn Out Heatflux	Pressure	Pressure Drop at the Inlet of the Test-section
$g/cm^2\,s$	^{o}C	^{o}C	-	-	W/cm^2	ata	mmHg
M	DTEM	DTAM	XEM	XAM	Q	PEM	PDR
293.5	47.4	0.0	-.154	.034	296.2	68.5	296.00
293.5	48.8	0.0	-.160	.021	283.2	70.0	780.00
296.4	48.8	0.0	-.160	.023	289.7	70.0	47.00
296.4	48.1	0.0	-.158	.026	290.5	70.0	0.00
341.8	41.4	0.0	-.135	.095	422.2	67.0	1190.00
341.8	41.2	0.0	-.134	.083	399.9	67.0	1050.00
337.6	40.2	0.0	-.131	.053	334.3	67.0	610.00
337.6	41.2	0.0	-.134	.032	302.8	68.0	264.00
336.0	39.2	0.0	-.128	.017	262.0	68.0	0.00
337.8	32.9	0.0	-.109	.125	423.0	69.0	0.00

Tabelle 67: L/D = 71,5 , D = 0,7 cm
Drosselstelle am Meßstreckeneintritt

Table 67: L/D = 71,5, D = o,7 cm
Throttling point at test section inlet

$\dot{m}$	$\Delta\vartheta_E$	$\Delta\vartheta_A$	X_E	X_A	q_{BO}	P	ΔP
Massenfluß	Eintr.-Unter-kühlung	Austr.-Unter-kühlung	Eintr.-Qualität	Austr.-Qualität	max.Heizfl.-Belastung	Druck	Druckverl.am Meßstrecken-eintritt
Mass Flow Rate	Inlet Sub-cooling	Outlet Sub-cooling	Inlet-Quality	Outlet-Quality	Burn Out Heatflux	Pressure	Pressure Drop at the Inlet of the Test-section
$g/cm^2\ s$	^{o}C	^{o}C	-	-	W/cm^2	ata	mmHg
243.9	13.6	0.0	-.046	.172	284.8	68.0	185.00
243.9	13.1	0.0	-.045	.084	169.3	68.0	0.00
255.0	26.6	0.0	-.089	.075	224.6	68.0	204.00
255.0	8.6	0.0	-.029	.195	307.5	68.0	194.00
255.0	40.4	0.0	-.132	.057	258.8	68.0	194.00
255.0	35.2	0.0	-.116	.062	243.7	68.0	199.00
249.5	45.2	0.0	-.146	.067	286.4	67.5	363.00
255.0	46.6	0.0	-.152	.034	254.3	68.5	199.00
249.5	28.2	0.0	-.093	.112	275.2	67.5	370.00
249.5	37.2	0.0	-.122	.079	269.7	67.5	363.00
249.5	17.1	0.0	-.057	.196	340.3	67.0	565.00
249.5	19.4	0.0	-.065	.189	340.3	67.5	370.00
249.5	31.4	0.0	-.103	.111	288.0	66.5	560.00
249.5	24.9	0.0	-.083	.173	343.8	67.0	560.00
249.5	40.4	0.0	-.131	.085	290.4	67.0	560.00
249.5	42.2	0.0	-.137	.128	355.4	67.5	743.00
249.5	38.2	0.0	-.125	.140	355.4	67.5	743.00
249.5	30.9	0.0	-.102	.164	356.4	67.0	743.00

Tabelle 68: L/D = 71,5, D = 0,7 cm
Drosselstelle am Meßstreckeneitritt

Table 68: L/D = 71,5, D = 0,7 cm
Throttling point at test section inlet

m	$\Delta\vartheta_E$	$\Delta\vartheta_A$	X_E	X_A	q_{BO}	P	Δ_P
Massenfluß	Eintr.-Unterkühlung	Austr.-Unterkühlung	Eintr.-Qualität	Austr.-Qualität	max.Heizfl.-Belastung	Druck	Druckverl.am Meßstrecken-eintritt
Mass Flow Rate	Inlet Sub-cooling	Outlet Sub-cooling	Inlet-Quality	Outlet-Quality	Burn Out Heatflux	Pressure	Pressure Drop at the Inlet of the Test-section
$g/cm^2\ s$	^oC	^oC	-	-	W/cm^2	ata	mmHg
243.3	43.7	0.0	-.142	.013	203.2	68.0	0.00
296.3	36.4	0.0	-.119	.090	334.2	67.5	556.00
296.3	30.2	0.0	-.099	.128	363.6	67.0	556.00
296.3	19.4	0.0	-.065	.159	356.3	67.5	556.00
296.3	27.4	0.0	-.091	.133	356.3	67.5	556.00
296.3	18.6	0.0	-.063	.157	350.1	68.0	556.00
296.3	22.4	0.0	-.075	.145	350.1	68.0	556.00
296.3	20.6	0.0	-.070	.118	297.8	68.5	370.00
296.3	24.6	0.0	-.083	.081	260.4	69.0	370.00
296.3	26.1	0.0	-.087	.080	266.6	68.5	370.00
296.3	26.9	0.0	-.090	.066	248.2	68.5	370.00
296.3	30.6	0.0	-.102	.054	263.4	68.5	370.00
296.3	42.6	0.0	-.140	.023	258.1	69.0	278.00
296.3	34.9	0.0	-.116	.038	244.5	69.0	278.00
296.3	24.6	0.0	-.083	.081	259.6	69.0	278.00
296.3	26.9	0.0	-.090	.074	259.6	69.0	278.00
296.3	18.1	0.0	-.061	.156	344.7	69.0	278.00
296.3	18.1	0.0	-.061	.092	243.0	69.0	278.00
296.3	20.6	0.0	-.070	.088	249.7	69.0	278.00
296.3	22.6	0.0	-.076	.081	249.7	69.0	278.00

Tabelle 69: L/D = 71,5, D = 0,7 cm
Drosselstelle am Meßstreckeneintritt

Table 69: L/D = 71,5, D = 0,7 cm
Throttling point at test section inlet

$\dot{m}$	$\Delta\vartheta_E$	$\Delta\vartheta_A$	X_E	X_A	q_{BO}	P	Δ_P
Massenfluß	Eintr.-Unter-kühlung	Austr.-Unter-kühlung	Eintr.-Qualität	Austr.-Qualität	max.Heizfl.-Belastung	Druck	Druckverl.am Meßstrecken-eintritt
Mass Flow Rate	Inlet Sub-cooling	Outlet Sub-cooling	Inlet-Quality	Outlet-Quality	Burn Out Heatflux	Pressure	Pressure Drop at the Inlet of the Test-section
g/cm^2 s	°C	°C	-	-	W/cm^2	ata	mmHg
296.3	24.1	0.0	−.081	.082	259.6	69.0	278.00
296.3	23.9	0.0	−.080	.084	260.4	69.0	278.00
296.3	19.6	0.0	−.066	.082	235.6	69.0	185.00
296.3	21.4	0.0	−.072	.076	235.6	69.0	185.00
296.3	15.8	0.0	−.054	.081	214.8	69.0	93.00
296.3	17.3	0.0	−.059	.076	214.8	69.0	93.00
296.3	9.6	0.0	−.033	.189	350.9	69.0	95.00
296.3	14.3	0.0	−.049	.173	350.9	69.0	93.00
296.3	9.6	0.0	−.033	.191	354.5	69.0	185.00
296.3	14.3	0.0	−.049	.175	354.5	69.0	125.00
296.3	24.1	0.0	−.081	.033	182.0	69.0	0.00
296.3	39.7	0.0	−.130	.109	379.2	68.0	741.00
296.3	40.4	0.0	−.132	.085	343.0	68.0	648.00
296.3	39.7	0.0	−.130	.072	321.2	68.0	556.00
296.3	37.9	0.0	−.124	.043	265.8	68.0	370.00
296.3	38.6	0.0	−.128	.052	243.0	69.0	185.00
296.3	38.1	0.0	−.126	.003	212.8	68.5	0.00
296.3	20.9	0.0	−.070	.093	258.9	68.5	278.00
296.3	21.1	0.0	−.071	.164	373.6	68.5	370.00
296.3	25.1	0.0	−.084	.151	373.6	68.5	370.00

Tabelle 70: L/D = 71,5, D = 0,7 cm
Drosselstelle am Meßstreckeneintritt

Table 70: L/D = 71,5, D = 0,7 cm
Throttling point at test section inlet

m	$\Delta\vartheta_E$	$\Delta\vartheta_A$	X_E	X_A	q_{BO}	P	Δ_P
Massenfluß	Eintr.-Unter- kühlung	Austr.-Unter- kühlung	Eintr.- Qualität	Austr.- Qualität	max.Heizfl.- Belastung	Druck	Druckverl.am Meßstrecken- eintritt
Mass Flow Rate	Inlet Sub- cooling	Outlet Sub- cooling	Inlet- Quality	Outlet- Quality	Burn Out Heatflux	Pressure	Pressure Drop at the Inlet of the Test- section
$g/cm^2\ s$	^oC	^oC	$-$	$-$	W/cm^2	ata	mmHg
296.3	25.1	0.0	-.084	.056	222.6	69.0	185.00
296.3	25.1	0.0	-.084	.037	192.5	68.5	0.00
296.3	47.9	0.0	-.155	.091	392.3	67.5	1019.00
296.3	48.9	0.0	-.158	.099	408.6	67.5	926.00
296.3	48.6	0.0	-.158	.090	393.3	68.0	833.00
296.3	48.1	0.0	-.156	.081	377.4	68.0	741.00
296.3	48.1	0.0	-.156	.041	312.8	67.5	556.00
296.3	48.4	0.0	-.157	.031	298.9	68.5	370.00
296.3	48.9	0.0	-.159	.016	278.0	69.0	185.00
296.3	49.1	0.0	-.160	.006	263.5	69.0	0.00
296.3	47.4	0.0	-.155	.013	266.5	69.0	0.00
353.6	44.9	0.0	-.145	.039	350.9	67.0	722.00
348.1	35.2	0.0	-.115	.072	350.9	67.0	722.00
351.3	28.2	0.0	-.093	.097	359.0	67.0	731.00
349.7	16.4	0.0	-.055	.125	340.3	67.0	734.00
346.5	16.4	0.0	-.055	.129	343.8	67.0	565.00
349.7	24.4	0.0	-.081	.107	355.4	67.0	565.00
352.8	28.7	0.0	-.094	.090	351.8	67.0	565.00
352.8	34.7	0.0	-.114	.070	350.1	67.0	565.00
349.7	41.2	0.0	-.134	.044	335.1	67.0	556.00

Tabelle 71: L/D = 71,5, D = 0,7 cm
Drosselstelle am Meßstreckeneintritt

Table 71: L/D = 71,5, D = 0,7 cm
Throttling point at test section inlet

m	$\Delta\vartheta E$	$\Delta\vartheta A$	X_E	X_A	q_{BO}	P	ΔP
Massenfluß	Eintr.-Unter-kühlung	Austr.-Unter-kühlung	Eintr.-Qualität	Austr.-Qualität	max.Heizfl.-Belastung	Druck	Druckverl.am Meßstrecken-eintritt
Mass Flow Rate	Inlet Sub-cooling	Outlet Sub-cooling	Inlet-Quality	Outlet-Quality	Burn Out Heatflux	Pressure	Pressure Drop at the Inlet of the Test-section
$g/cm^2\ s$	^oC	^oC	–	–	W/cm^2	ata	mmHg
349.7	41.7	0.0	-.136	.02?	30?.5	?7.?	370.00
349.7	31.7	0.0	-.104	.060	309.?	67.5	370.00
349.7	23.9	0.0	-.080	.090	319.?	67.?	370.00
349.7	17.4	0.0	-.053	.124	343.?	67.5	370.00
349.7	11.1	0.0	-.038	.141	336.?	67.?	370.00
349.7	13.9	0.0	-.047	.132	336.?	67.5	370.00
349.7	12.9	0.0	-.044	.138	340.4	68.0	185.00
349.7	15.?	0.0	-.053	.128	340.4	68.0	185.00
349.7	24.1	0.0	-.081	.059	262.?	68.0	185.00
349.7	33.9	0.0	-.112	.030	266.6	68.0	185.00
349.7	41.2	0.0	-.134	.017	284.?	68.0	185.00
247.5	15.4	0.0	-.067	.093	185.3	100.0	0.00
244.1	14.2	0.0	-.062	.135	224.1	100.0	94.00
244.1	13.?	0.0	-.058	.172	262.5	100.0	181.00
244.1	13.7	0.0	-.060	.175	265.?	100.0	273.00
245.2	13.?	0.0	-.060	.177	271.5	99.5	370.00
240.6	24.5	0.0	-.103	.14?	279.7	100.0	750.00
241.?	24.0	0.0	-.102	.140	281.6	100.0	560.00
241.?	24.0	0.0	-.102	.13?	272.2	100.0	372.00
247.5	24.8	0.0	-.105	.102	238.?	100.0	178.00

Tabelle 72: L/D = 71,5, D = 0,7 cm
Drosselstelle am Meßstreckeneintritt

Table 72: L/D = 71,5, D = 0,7 cm
Throttling point at test section inlet

$\dot{m}$	$\Delta\vartheta_E$	$\Delta\vartheta_A$	X_E	X_A	q_{BO}	P	Δ_P
Massenfluß	Eintr.-Unter-kühlung	Austr.-Unter-kühlung	Eintr.-Qualität	Austr.-Qualität	max.Heizfl.-Belastung	Druck	Druckverl.am Meßstrecken-eintritt
Mass Flow Rate	Inlet Sub-cooling	Outlet Sub-cooling	Inlet-Quality	Outlet-Quality	Burn Out Heatflux	Pressure	Pressure Drop at the Inlet of the Test-section
$g/cm^2\ s$	^{o}C	^{o}C	-	-	W/cm^2	ata	mmHg
M	DTEM	DTAM	XEM	XAM	G	PEM	PDR
247.5	24.8	0.0	-.105	.050	190.4	100.0	0.00
247.5	36.3	0.0	-.150	.036	215.6	100.0	60.00
241.3	36.5	0.0	-.151	.067	245.3	100.5	190.00
239.4	37.3	0.0	-.154	.101	284.5	101.0	370.00
245.2	37.7	0.0	-.156	.120	315.6	100.5	557.00
245.7	37.2	0.0	-.153	.130	330.1	99.5	755.00
247.5	6.4	0.0	-.037	.167	258.8	100.0	0.00

Tabelle 73: L/D = 71,5, D = 0,7 cm
Drosselstelle am Meßstreckeneintritt

Table 73: L/D = 71,5, D = 0,7 cm
Throttling point at test section inlet

$\dot{m}$	$\Delta\vartheta_E$	$\Delta\vartheta_A$	x_E	x_A	q_{BO}	P
Massenfluß	Eintr.-Unter-kühlung	Austr.-Unter-kühlung	Eintr.-Qualität	Austr.-Qualität	max.Heizfl.-Belastung	Druck
Mass Flow Rate	Inlet Sub-cooling	Outlet Sub-cooling	Inlet-Quality	Outlet-Quality	Burn Out Heatflux	Pressure
$g/cm^2 \; s$	$°C$	$°C$	-	-	W/cm^2	ata
259.2	49.6	9.1	-.165	-.032	322.8	71.6
256.3	49.4	9.4	-.164	-.033	314.7	71.6
249.2	49.5	12.5	-.166	-.044	283.5	72.8
236.8	42.8	5.0	-.143	-.018	278.6	72.0
236.7	43.8	5.4	-.147	-.019	283.2	72.0
236.0	37.5	2.8	-.127	-.010	258.4	72.0
233.4	39.5	1.8	-.133	-.006	276.9	71.5
360.6	82.1	21.0	-.264	-.072	648.1	71.8
183.9	82.8	19.9	-.265	-.068	340.2	71.2
181.3	83.3	19.5	-.267	-.067	340.2	71.2
140.0	82.3	21.8	-.263	-.075	248.2	71.2
151.8	69.8	16.8	-.226	-.058	239.9	71.3
232.3	108.6	32.7	-.340	-.110	502.9	71.0
228.7	106.3	28.8	-.334	-.098	508.6	71.2
305.4	41.7	0.0	-.139	.010	432.3	71.1
301.2	66.0	14.5	-.216	-.051	466.5	72.3
297.2	63.0	11.1	-.206	-.039	465.6	71.5
296.7	63.2	10.4	-.206	-.036	473.9	71.5
295.3	63.6	10.9	-.208	-.038	470.2	71.6
290.1	121.4	55.5	-.378	-.183	533.0	71.5

Tabelle 74: L/D = 40, D = 0,7 cm
Rohre mit langer Einlaufstrecke

Table 74: L/D = 40, D = 0,7 cm
Channels with long inlet section

m	$\Delta \vartheta_E$	$\Delta \vartheta_A$	x_E	x_A	q_{BO}	P
Massenfluß	Eintr.-Unter-kühlung	Austr.-Unter-kühlung	Eintr.-Qualität	Austr.-Qualität	max.Heizfl.-Belastung	Druck
Mass Flow Rate	Inlet Sub-cooling	Outlet Sub-cooling	Inlet-Quality	Outlet-Quality	Burn Out Heatflux	Pressure
g/cm^2 s	$^{\circ}C$	$^{\circ}C$	–	–	W/cm^2	ata
279.5	65.4	14.5	-.214	-.051	427.9	72.0
276.1	70.8	15.1	-.231	-.053	460.0	72.2
278.6	76.6	18.0	-.247	-.062	483.0	71.7
279.0	53.4	9.9	-.176	-.035	371.0	71.6
279.2	44.8	5.4	-.150	-.019	342.0	71.8
278.6	37.7	2.2	-.127	-.008	312.1	72.2
278.4	30.0	0.0	-.102	.008	291.0	72.0
277.1	22.3	0.0	-.077	.034	289.7	72.1
276.2	17.7	0.0	-.061	.035	251.3	72.0
277.0	12.6	0.0	-.044	.041	224.0	72.2
284.8	77.2	16.4	-.248	-.057	513.5	71.3
287.0	82.7	19.2	-.265	-.066	535.9	71.3
287.5	92.8	24.1	-.295	-.083	573.4	71.3
286.5	100.9	26.9	-.318	-.092	610.8	71.2
287.2	108.3	30.4	-.341	-.104	640.1	71.8
287.8	115.8	32.9	-.362	-.111	677.4	71.3
288.5	119.9	34.8	-.374	-.117	696.2	71.3
288.5	126.2	36.7	-.393	-.124	727.5	71.9
288.0	129.7	39.2	-.402	-.132	731.7	71.7
229.8	48.3	7.0	-.162	-.025	293.7	72.8

Tabelle 75: L/D = 40, D = 0,7 cm
Rohre mit langer Einlaufstrecke

Table 75: L/D = 40, D = 0,7 cm
Channels with long inlet section

$\dot{m}$	$\Delta\vartheta_E$	$\Delta\vartheta_A$	x_E	x_A	q_{BO}	P
Massenfluß	Eintr.-Unter-kühlung	Austr.-Unter-kühlung	Eintr.-Qualität	Austr.-Qualität	max.Heizfl.-Belastung	Druck
Mass Flow Rate	Inlet Sub-cooling	Outlet Sub-cooling	Inlet-Quality	Outlet-Quality	Burn Out Heatflux	Pressure
$g/cm^2\ s$	$^{\circ}C$	$^{\circ}C$	–	–	W/cm^2	ata
237.9	41.0	2.6	-.138	-.009	287.5	72.0
239.3	45.7	6.0	-.153	-.021	295.2	72.7
238.1	53.7	8.5	-.178	-.030	330.1	72.5
238.8	64.9	13.8	-.213	-.049	367.0	72.7
231.3	71.5	17.1	-.233	-.060	375.4	72.6
231.5	71.3	16.2	-.232	-.057	380.9	72.4
230.9	79.4	20.4	-.258	-.071	402.4	72.9
229.3	90.2	24.3	-.289	-.084	440.6	72.5
229.3	100.2	27.5	-.320	-.095	481.3	72.9
228.1	106.3	29.2	-.337	-.100	505.4	72.8
227.4	113.7	31.5	-.359	-.108	533.9	72.8
226.4	121.1	33.3	-.380	-.114	564.2	72.8
227.0	128.7	33.0	-.402	-.113	614.1	72.8
234.4	134.7	37.8	-.420	-.128	638.2	72.9
232.1	139.7	36.9	-.433	-.125	669.1	72.7
228.6	120.7	31.5	-.376	-.107	578.5	71.3
275.3	60.7	13.1	-.200	-.046	396.9	72.8
280.9	48.6	7.8	-.162	-.028	353.3	71.8
279.7	51.3	7.8	-.170	-.028	373.9	71.8
279.4	58.7	10.9	-.193	-.038	405.8	71.7

Tabelle 76: L/D = 40, D = 0,7 cm
Rohre mit langer Einlaufstrecke

Table 76: L/D = 40, D = 0,7 cm
Channels with long inlet section

$\dot{m}$	$\Delta\vartheta_E$	$\Delta\vartheta_A$	x_E	x_A	q_{BO}	P
Massenfluß	Eintr.-Unter-kühlung	Austr.-Unter-kühlung	Eintr.-Qualität	Austr.-Qualität	max.Heizfl.-Belastung	Druck
Mass Flow Rate	Inlet Sub-cooling	Outlet Sub-cooling	Inlet-Quality	Outlet-Quality	Burn Out Heatflux	Pressure
$g/cm^2\ s$	$^\circ C$	$^\circ C$	–	–	W/cm^2	ata
243.5	43.7	.6	-.147	-.002	330.1	73.0
243.6	41.6	0.0	-.141	.006	336.7	72.9
242.3	35.9	0.0	-.122	.014	310.7	72.7
240.8	30.2	0.0	-.103	.025	291.9	72.2
355.3	61.0	11.1	-.200	-.039	536.6	71.8
354.9	69.1	14.2	-.225	-.049	584.1	71.7
353.4	76.5	17.1	-.247	-.059	622.8	71.9
353.5	84.1	21.1	-.270	-.073	653.3	72.0
353.7	90.3	22.5	-.288	-.077	698.6	71.5
353.7	97.7	26.3	-.310	-.090	730.6	71.8
354.0	103.4	29.5	-.327	-.101	751.6	71.8
354.8	110.2	33.5	-.346	-.113	776.0	71.7
354.1	115.4	36.1	-.361	-.122	796.3	71.5
353.8	122.0	40.0	-.380	-.134	818.3	71.7
352.6	127.7	42.0	-.398	-.141	848.7	72.0

Tabelle 77: L/D = 40, D = 0,7 cm
Rohre mit langer Einlaufstrecke

Table 77: L/D = 40, D = 0,7 cm
Channels with long inlet section

$\dot{m}$	$\Delta\vartheta_E$	$\Delta\vartheta_A$	x_E	x_A	q_{BO}	P
Massenfluß	Eintr.-Unter-kühlung	Austr.-Unter-kühlung	Eintr.-Qualität	Austr.-Qualität	max.Heizfl.-Belastung	Druck
Mass Flow Rate	Inlet Sub-cooling	Outlet Sub-cooling	Inlet-Quality	Outlet-Quality	Burn Out Heatflux	Pressure
$g/cm^2\ s$	$^\circ C$	$^\circ C$	$-$	$-$	W/cm^2	ata
299.6	121.6	59.4	-.380	-.195	519.0	71.8
357.4	82.2	19.7	-.262	-.068	656.2	70.8
330.9	68.0	14.2	-.221	-.050	533.9	71.6
329.2	74.9	18.1	-.242	-.063	554.7	71.5
363.4	81.9	21.5	-.263	-.074	643.9	71.5
362.9	81.5	21.1	-.262	-.073	643.9	71.6
362.0	82.4	21.5	-.265	-.074	648.1	71.6
336.2	114.2	34.2	-.360	-.116	765.3	72.5
321.6	114.5	42.5	-.360	-.143	654.8	72.1
317.3	111.8	40.6	-.352	-.137	639.3	72.3

Tabelle 78: L/D = 40, D = 0,7 cm
Rohre mit langer Einlaufstrecke

Table 78: L/D = 40, D = 0,7 cm
Channels with long inlet section

m	$\Delta\vartheta_E$	$\Delta\vartheta_A$	x_E	x_A	q_{BO}	P
Massenfluß	Eintr.-Unter-kühlung	Austr.-Unter-kühlung	Eintr.-Qualität	Austr.-Qualität	max.Heizfl.-Belastung	Druck
Mass Flow Rate	Inlet Sub-cooling	Outlet Sub-cooling	Inlet-Quality	Outlet-Quality	Burn Out Heatflux	Pressure
$g/cm^2\ s$	$^{\circ}C$	$^{\circ}C$	–	–	W/cm^2	ata
413.5	107.2	43.6	-.403	-.178	769.5	101.0
390.7	102.9	36.2	-.389	-.150	770.6	101.2
391.4	94.5	32.4	-.361	-.136	727.5	101.3
392.6	88.5	29.1	-.340	-.123	704.9	101.3
388.8	79.4	22.6	-.309	-.097	680.4	101.4
388.4	75.7	20.8	-.296	-.090	660.7	101.8
381.6	63.7	14.1	-.254	-.062	602.8	101.8
392.5	33.2	0.0	-.139	0.000	452.1	101.9
395.7	33.1	1.1	-.139	-.005	437.8	101.8
393.1	44.5	5.7	-.183	-.026	509.7	101.9
393.0	50.3	8.7	-.204	-.039	535.7	101.9
391.9	57.8	12.5	-.232	-.056	570.9	101.9

Tabelle 79: L/D = 40, D = 0,7 cm
Rohre mit langer Einlaufstrecke

Table 79: L/D = 40, D = 0,7 cm
Channels with long inlet section

$\dot{m}$	$\Delta\vartheta_E$	$\Delta\vartheta_A$	x_E	x_A	q_{BO}	P
Massenfluß	Eintr.-Unter-kühlung	Austr.-Unter-kühlung	Eintr.-Qualität	Austr.-Qualität	max.Heizfl.-Belastung	Druck
Mass Flow Rate	Inlet Sub-cooling	Outlet Sub-cooling	Inlet-Quality	Outlet-Quality	Burn Out Heatflux	Pressure
$g/cm^2\,s$	$°C$	$°C$	–	–	W/cm^2	ata
100.1	41.9	0.0	−.139	.005	136.6	70.0
100.2	42.1	3.7	−.139	−.013	119.8	70.0
100.2	42.6	0.0	−.141	.016	149.9	70.0
100.1	34.6	0.0	−.116	.030	138.5	70.0
100.1	28.3	0.0	−.095	.040	129.0	70.0
100.1	20.8	0.0	−.071	.056	121.3	70.0
100.1	13.0	0.0	−.045	.066	105.9	70.0
100.9	9.0	0.0	−.031	.071	98.8	70.5
100.9	6.7	0.0	−.024	.076	95.4	70.5
172.0	55.6	10.5	−.182	−.037	235.4	70.5
172.6	48.6	5.7	−.160	−.020	228.1	70.5
172.6	41.1	2.2	−.137	−.008	210.2	70.5
171.7	36.1	0.0	−.121	.006	207.2	70.5
172.4	30.1	0.0	−.102	.018	195.6	71.0
171.4	21.1	0.0	−.072	.039	181.2	70.5
170.6	14.3	0.0	−.049	.051	163.6	70.5
170.5	31.8	0.0	−.107	.046	248.5	70.5
170.5	31.3	0.0	−.105	.039	234.2	70.0
224.4	29.1	0.0	−.098	.018	248.3	70.5
224.2	35.9	0.0	−.120	.005	265.6	70.0

Tabelle 80: L/D = 40, D = 1,1 cm
Rohre mit langer Einlaufstrecke

Table 80: L/D = 40, D = 1,1 cm
Channels with long inlet section

m	$\Delta\vartheta_E$	$\Delta\vartheta_A$	x_E	x_A	q_{BO}	P
Massenfluß	Eintr.-Unter-kühlung	Austr.-Unter-kühlung	Eintr.-Qualität	Austr.-Qualität	max.Heizfl.-Belastung	Druck
Mass Flow Rate	Inlet Sub-cooling	Outlet Sub-cooling	Inlet-Quality	Outlet-Quality	Burn Out Heatflux	Pressure
$g/cm^2\ s$	$^{\circ}C$	$^{\circ}C$	–	–	W/cm^2	ata
224.4	43.6	4.1	-.144	-.014	275.1	70.0
219.0	19.8	0.0	-.068	.036	217.3	70.5
224.2	15.3	0.0	-.053	.044	207.2	70.0
105.2	39.6	0.0	-.162	.117	244.8	100.0
105.6	48.2	0.0	-.193	.070	232.7	99.0
224.9	40.4	.4	-.165	-.002	304.6	100.0
97.3	5.3	0.0	-.024	.139	132.1	100.0
97.3	5.8	0.0	-.026	.135	130.7	100.0
97.2	8.4	0.0	-.037	.135	140.0	100.0
97.2	14.4	0.0	-.063	.100	132.4	100.0
97.2	23.3	0.0	-.099	.097	158.5	100.0
97.2	30.6	0.0	-.127	.073	162.4	100.0
97.2	40.1	0.0	-.164	.037	163.6	100.0
97.5	46.6	0.0	-.188	.020	170.2	100.0
99.8	53.2	1.7	-.212	-.008	169.7	100.0
166.4	18.7	0.0	-.080	.067	204.7	100.0
166.6	27.8	0.0	-.117	.050	232.0	100.0
166.9	40.6	0.0	-.166	.011	246.4	100.0
167.0	51.7	4.2	-.207	-.019	261.1	100.0
223.9	31.6	0.0	-.131	.029	300.6	100.0

Tabelle 81: L/D = 40, D = 1,1,cm
Rohre mit langer Einlaufstrecke

Table 81: L/D = 40, D = 0,7 cm
Channels with long inlet section

m	$\Delta\vartheta_E$	$\Delta\vartheta_A$	x_E	x_A	q_{BO}	P
Massenfluß	Eintr.-Unter-kühlung	Austr.-Unter-kühlung	Eintr.-Qualität	Austr.-Qualität	max.Heizfl.-Belastung	Druck
Mass Flow Rate	Inlet Sub-cooling	Outlet Sub-cooling	Inlet-Quality	Outlet-Quality	Burn Out Heatflux	Pressure
$g/cm^2\ s$	^{o}C	^{o}C	–	–	W/cm^2	ata
93.8	14.7	0.0	-.093	.130	144.4	141.0
93.8	20.3	0.0	-.125	.108	150.0	141.5
93.8	27.9	0.0	-.165	.082	159.7	141.0
93.2	35.2	0.0	-.203	.060	168.5	141.0
95.6	42.1	0.0	-.238	.023	170.9	142.0

Tabelle 82: L/D = 40, D = 1,1 cm
Rohre mit langer Einlaufstrecke

Table 82: L/D = 40, D = 1,1 cm
Channels with long inlet section

m	$\Delta\vartheta_E$	$\Delta\vartheta_A$	x_E	x_A	q_{BO}	P
Massenfluß	Eintr.-Unter-kühlung	Austr.-Unter-kühlung	Eintr.-Qualität	Austr.-Qualität	max.Heizfl.-Belastung	Druck
Mass Flow Rate	Inlet Sub-cooling	Outlet Sub-cooling	Inlet-Quality	Outlet-Quality	Burn Out Heatflux	Pressure
$g/cm^2\ s$	$^{\circ}C$	$^{\circ}C$	-	-	W/cm^2	ata
97.2	41.1	0.0	-.136	.012	144.2	69.5
97.9	30.1	0.0	-.101	.028	127.3	69.5
98.1	22.6	0.0	-.077	.035	110.0	69.5
98.3	12.6	0.0	-.043	.137	178.4	69.5
98.5	4.8	0.0	-.017	.164	179.1	69.0
98.1	34.4	0.0	-.114	.072	183.6	69.0
97.7	37.9	0.0	-.125	.088	210.2	69.0
96.0	45.4	0.0	-.149	.053	194.4	69.0
155.5	39.9	0.0	-.132	.036	262.0	69.0
158.0	32.1	0.0	-.107	.048	247.9	69.0
156.6	17.1	0.0	-.058	.032	142.7	69.5
155.8	22.6	0.0	-.077	.029	167.4	69.5
157.1	31.4	0.0	-.105	.010	182.1	69.5
157.3	38.1	0.0	-.127	.001	202.4	70.0
157.5	47.6	5.7	-.156	-.020	215.0	69.5
155.9	54.1	8.9	-.176	-.031	226.4	69.5
221.6	53.1	11.3	-.174	-.039	297.4	70.0
220.0	48.1	8.1	-.158	-.028	285.9	70.0
220.5	23.6	0.0	-.080	.018	219.0	70.0
219.8	28.6	0.0	-.096	.014	243.7	70.0

Tabelle 83: L/D = 40, D = 1,5 cm
Rohre mit langer Einlaufstrecke

Table 83: L/D = 40, D = 1,5 cm
Channels with long inlet section

$\dot{m}$	$\Delta\vartheta_E$	$\Delta\vartheta_A$	x_E	x_A	q_{BO}	P
Massenfluß	Eintr.-Unter-kühlung	Austr.-Unter-kühlung	Eintr.-Qualität	Austr.-Qualität	max.Heizfl.-Belastung	Druck
Mass Flow Rate	Inlet Sub-cooling	Outlet Sub-cooling	Inlet-Quality	Outlet-Quality	Burn Out Heatflux	Pressure
$g/cm^2\ s$	$^\circ C$	$^\circ C$	–	–	W/cm^2	ata
98.0	0.0	0.0	.030	.332	298.2	68.0
97.8	1.0	0.0	-.003	.314	312.2	69.0
98.6	20.1	0.0	-.068	.087	154.5	69.5
156.4	26.1	0.0	-.088	.118	323.3	69.5
156.3	9.1	0.0	-.031	.160	301.1	69.0
156.4	11.8	0.0	-.041	.156	310.0	69.0
218.9	7.0	0.0	-.024	.113	302.3	70.0
218.1	9.6	0.0	-.033	.106	305.5	69.0
99.3	4.4	0.0	-.020	.217	206.7	100.5
153.7	15.4	0.0	-.072	.099	222.8	110.0
153.7	6.6	0.0	-.029	.135	222.9	99.0
153.7	11.9	0.0	-.056	.115	222.8	110.0
220.3	36.4	0.0	-.121	.002	272.2	70.0
99.3	42.6	0.0	-.174	.089	229.7	100.0
100.0	53.4	0.0	-.213	.066	246.3	100.0
98.9	52.3	0.0	-.212	.020	201.7	100.5

Tabelle 84: L/D = 40, D = 1,5 cm
Rohre mit langer Einlaufstrecke

Table 84: L/D = 40, D = 1,5 cm
Channels with long inlet section

$\dot{m}$	$\Delta\vartheta_E$	$\Delta\vartheta_A$	x_E	x_A	q_{BO}	P
Massenfluß	Eintr.-Unter-kühlung	Austr.-Unter-kühlung	Eintr.-Qualität	Austr.-Qualität	max.Heizfl.-Belastung	Druck
Mass Flow Rate	Inlet Sub-cooling	Outlet Sub-cooling	Inlet-Quality	Outlet-Quality	Burn Out Heatflux	Pressure
$g/cm^2 \ s$	$^\circ C$	$^\circ C$	−	−	W/cm^2	ata
231.8	10.5	0.0	−.037	.097	294.9	70.0
215.5	13.5	0.0	−.047	.051	202.4	70.0
216.8	19.1	0.0	−.065	.036	208.4	70.0
218.1	21.8	0.0	−.074	.008	170.6	69.5
217.4	28.9	0.0	−.097	.012	226.4	69.5
219.3	39.1	0.0	−.130	.004	279.8	69.5
236.5	52.1	6.8	−.170	−.023	328.0	69.5
238.8	51.3	4.2	−.168	−.015	346.8	70.0
243.5	48.4	4.0	−.158	−.014	333.9	69.5
234.0	44.8	1.8	−.148	−.006	313.8	70.0
234.1	38.1	0.0	−.127	.002	286.4	70.0
244.8	34.9	0.0	−.116	.007	289.2	69.5
244.9	29.9	0.0	−.100	.020	281.8	69.5
245.7	23.9	0.0	−.081	.039	281.4	69.5
245.1	18.6	0.0	−.063	.050	267.0	69.0
203.2	42.6	1.1	−.141	−.004	263.9	70.0
201.9	35.9	0.0	−.120	.012	252.6	70.0
207.0	28.1	0.0	−.095	.009	204.8	70.0
204.8	16.8	0.0	−.058	.026	163.0	70.0
204.0	15.0	0.0	−.052	.040	178.2	70.2

Tabelle 85: L/D = 40, D = 0,7 cm
Rohre ohne Einlaufstrecke

Table 85: L/D = 40, D = 0,7 cm
Channels without inlet section

$\dot{m}$	$\Delta\vartheta_E$	$\Delta\vartheta_A$	x_E	x_A	q_{BO}	P
Massenflu	Eintr.-Unter-kühlung	Austr.-Unter-kühlung	Eintr.-Qualität	Austr.-Qualität	max.Heizfl.-Belastung	Druck
Mass Flow Rate	Inlet Sub-cooling	Outlet Sub-cooling	Inlet-Quality	Outlet-quality	Burn Out Heatflux	Pressure
g/cm^2 s	°C	°C	—	—	W/cm^2	ata
245.0	60.1	5.7	-.195	-.020	405.8	70.0
237.9	67.0	7.0	-.216	-.024	431.4	70.2
234.5	70.2	7.0	-.226	-.024	446.6	70.2
233.3	74.9	7.1	-.239	-.025	473.4	69.9
234.0	58.7	6.6	-.191	-.023	370.7	69.9
239.8	54.3	4.6	-.177	-.016	366.2	70.0
223.9	49.6	0.0	-.163	0.000	345.7	69.8
227.5	44.0	0.0	-.145	.002	318.6	69.9
227.0	36.5	0.0	-.122	.021	309.2	70.4
236.1	29.6	0.0	-.100	.017	262.9	70.0
232.9	19.9	0.0	-.068	.040	239.4	70.1
223.5	14.9	0.0	-.051	.039	193.2	70.1
234.0	13.2	0.0	-.046	.043	199.4	70.2
227.9	11.5	0.0	-.040	.049	194.4	70.2
222.8	14.4	0.0	-.050	.036	183.3	70.1
221.6	12.8	0.0	-.044	.046	190.5	70.0
302.4	23.8	0.0	-.081	.028	313.7	70.7
303.9	27.5	0.0	-.093	.022	332.4	70.7
303.7	36.6	0.0	-.123	.014	394.8	70.8
304.0	43.9	0.0	-.146	.005	436.5	70.6

Tabelle 86: L/D = 40, D = 0,7 cm
Rohre ohne Einlaufstrecke

Table 86: L/D = 40, D = 0,7 cm
Channels without inlet section

m	$\Delta\vartheta_E$	$\Delta\vartheta_A$	x_E	x_A	q_{BO}	P
Massenfluß	Eintr.-Unter-kühlung	Austr.-Unter-kühlung	Eintr.-Qualität	Austr.-Qualität	max.Heizfl.-Belastung	Druck
Mass Flow Rate	Inlet Sub-cooling	Outlet Sub-cooling	Inlet-Quality	Outlet-Quality	Burn Out Heatflux	Pressure
$g/cm^2\,s$	$°C$	$°C$	$-$	$-$	W/cm^2	ata
207.1	20.0	0.0	-.068	.015	164.5	70.2
293.2	44.3	5.4	-.146	-.019	354.2	70.0
283.5	34.6	0.0	-.115	.002	316.9	69.5
289.4	28.8	0.0	-.097	.011	300.3	70.0
285.5	17.1	0.0	-.059	.043	277.7	70.0
297.6	50.3	2.9	-.165	-.010	435.8	70.0
298.4	48.3	2.0	-.159	-.007	428.3	70.0
297.4	48.1	1.7	-.158	-.006	428.3	70.0
298.4	45.1	0.0	-.149	.006	439.8	70.0
298.0	40.6	0.0	-.135	.015	424.8	70.0
299.1	36.6	0.0	-.122	.028	428.3	70.0
299.6	34.3	0.0	-.115	.029	410.1	70.5
297.4	31.1	0.0	-.104	.044	419.1	70.0
298.1	27.8	0.0	-.094	.049	404.5	70.5
296.2	25.1	0.0	-.085	.049	379.7	70.0
297.9	14.3	0.0	-.049	.038	249.6	70.0
299.7	19.6	0.0	-.067	.026	267.0	70.0
305.3	27.3	0.0	-.092	.018	322.4	70.0
307.8	36.9	0.0	-.123	.008	385.0	70.0
303.7	46.3	0.0	-.153	0.000	439.8	70.0

Tabelle 87: L/D = 40, D = 0,7 cm
Rohre ohne Einlaufstrecke

Table 87: L/D = 40, D = 0,7 cm
Channels without inlet section

$\dot{m}$	$\Delta\vartheta_E$	$\Delta\vartheta_A$	x_E	x_A	q_{BO}	p
Massenfluß	Eintr.-Unter-kühlung	Austr.-Unter-kühlung	Eintr.-Qualität	Austr.-Qualität	max.Heizfl.-Belastung	Druck
Mass Flow Rate	Inlet Sub-cooling	Outlet Sub-cooling	Inlet-Quality	Outlet-Quality	Burn Out Heatflux	Pressure
$g/cm^2\ s$	$^{\circ}C$	$^{\circ}C$	–	–	W/cm^2	ata
303.8	50.1	1.1	-.165	-.004	462.1	70.3
301.9	56.4	3.4	-.184	-.012	490.2	70.3
304.1	61.8	6.3	-.201	-.022	512.6	70.3
301.9	64.8	8.3	-.210	-.029	515.4	70.5
298.7	64.6	9.6	-.209	-.033	495.4	70.3
301.9	68.7	11.7	-.221	-.041	515.4	70.2
301.7	73.6	13.5	-.236	-.047	540.3	70.4
302.9	77.4	15.9	-.247	-.055	551.7	70.0
284.1	15.4	0.0	-.053	.035	239.4	69.8
291.3	14.8	0.0	-.051	.034	235.1	70.0
349.3	41.2	3.3	-.137	-.012	414.0	70.4
345.4	35.3	.2	-.118	-.001	383.4	70.7
347.6	28.7	0.0	-.097	.012	359.3	70.4
343.6	18.8	0.0	-.064	.020	277.6	70.5
352.3	43.5	2.0	-.144	-.007	456.0	69.9
340.0	49.1	4.7	-.161	-.016	466.1	69.8
355.8	54.8	7.9	-.179	-.028	509.2	70.0
357.3	60.3	10.3	-.195	-.036	539.4	69.7
340.8	70.2	13.4	-.226	-.046	578.5	70.2
356.8	74.3	18.1	-.237	-.062	593.4	69.8

Tabelle 88: $L_\gamma/D = 40$, D = 0,7 cm
Rohre ohne Einlaufstrecke

Table 88: L/D = 40, D = 0,7 cm
Channels without inlet section

m	$\Delta \vartheta_E$	$\Delta \vartheta_A$	x_E	x_A	q_{30}	P
Massenfluß	Eintr.-Unter-kühlung	Austr.-Unter-kühlung	Eintr.-Qualität	Austr.-Qualität	max.Heizfl.-Belastung	Druck
Mass Flow Rate	Inlet Sub-cooling	Outlet Sub-cooling	Inlet-Quality	Outlet-Quality	Burn Out Heatflux	Pressure
$g/cm^2\ s$	$^{\circ}C$	$^{\circ}C$	–	–	W/cm^2	ata
294.3	54.3	6.5	-.197	-.026	446.0	86.0
296.6	50.1	4.0	-.183	-.016	436.7	86.0
297.4	42.0	0.0	-.156	.001	414.3	86.9
293.3	32.4	0.0	-.122	.031	398.9	86.5
289.4	24.1	0.0	-.092	.048	361.2	86.2
290.9	16.5	0.0	-.064	.052	301.0	85.5
288.6	13.0	0.0	-.050	.056	275.1	85.5
229.0	19.4	0.0	-.084	.054	262.6	101.0
234.5	17.9	0.0	-.077	.057	263.2	100.9
228.2	26.2	0.0	-.111	.041	288.6	101.0
233.3	32.0	0.0	-.134	.031	321.7	101.0
233.0	37.0	0.0	-.153	.021	337.8	100.9
235.7	46.1	5.8	-.188	-.026	315.0	101.0
240.1	51.9	4.7	-.209	-.021	373.5	101.0
237.0	59.1	7.8	-.236	-.035	394.7	101.3
235.3	65.9	11.0	-.260	-.048	412.6	101.0
235.3	65.8	9.5	-.260	-.042	423.4	101.2
299.9	38.7	.5	-.160	-.002	390.9	100.8
294.5	28.0	0.0	-.118	.040	387.6	101.0
297.9	19.9	0.0	-.086	.051	339.4	101.0

Tabelle 89: L/D = 40, D = 0,7 cm
Rohre ohne Einlaufstrecke

Table 89: L/D = 40, D = 0,7 cm
Channels without inlet section

m	$\Delta\vartheta_E$	$\Delta\vartheta_A$	x_E	x_A	q_{BO}	P
Massenfluß	Eintr.-Unter-kühlung	Austr.-Unter-kühlung	Eintr.-Qualität	Austr.-Qualität	max.Heizfl.-Belastung	Druck
Mass Flow Rate	Inlet Sub-cooling	Outlet Sub-cooling	Inlet-Quality	Outlet-Quality	Burn Out Heatflux	Pressure
$g/cm^2\ s$	$^\circ C$	$^\circ C$	–	–	W/cm^2	ata
300.8	47.3	0.0	-.156	.002	451.0	70.5
237.8	21.2	0.0	-.090	.046	271.2	100.0
237.7	28.3	0.0	-.119	.035	306.1	100.0
239.0	38.1	0.0	-.156	.008	329.1	100.0
247.6	46.6	4.7	-.188	-.021	345.3	100.0
243.6	44.5	3.1	-.181	-.014	337.1	100.5
240.1	32.6	0.0	-.135	.038	346.9	100.0
240.1	38.0	0.0	-.156	.011	336.5	100.5
237.8	17.2	0.0	-.074	.053	253.5	100.0
291.6	16.9	0.0	-.073	.068	344.6	101.0
297.1	25.0	0.0	-.106	.033	346.1	101.0
300.6	34.3	0.0	-.143	.012	387.1	101.0
301.5	43.9	3.7	-.179	-.017	405.3	101.0
298.7	55.4	9.1	-.222	-.040	449.6	101.0
293.1	69.3	15.9	-.271	-.069	492.4	100.5
296.4	75.9	18.4	-.294	-.079	528.9	100.0
295.0	84.0	22.2	-.322	-.094	558.0	99.9

Tabelle 90:   L/D = 40, D = 0,7 cm
Rohre ohne Einlaufstrecke

Table 90:   L/D = 40, D = 0,7 cm
Channels without inlet section

m	$\Delta\vartheta_E$	$\Delta\vartheta_A$	x_E	x_A	q_{BO}	P
Massenfluß	Eintr.-Unterkühlung	Austr.-Unterkühlung	Eintr.-Qualität	Austr.-Qualität	max.Heizfl.-Belastung	Druck
Mass Flow Rate	Inlet Subcooling	Outlet Subcooling	Inlet-Quality	Outlet-Quality	Burn Out Heatflux	Pressure
$g/cm^2\ s$	^{o}C	^{o}C	–	–	W/cm^2	ata
301.3	61.6	8.3	-.199	-.029	485.5	69.5
346.4	52.6	6.4	-.172	-.022	489.8	70.0
345.5	43.8	2.4	-.145	-.008	446.6	70.0
346.4	35.1	0.0	-.117	.004	401.1	70.0
346.8	25.6	0.0	-.086	.019	350.1	69.5
346.3	16.8	0.0	-.058	.034	302.9	70.0
241.3	44.4	0.0	-.180	.013	389.6	100.0
241.3	32.0	0.0	-.132	.035	337.5	99.2
241.2	18.3	0.0	-.078	.061	282.2	99.5
241.2	27.7	0.0	-.118	.051	337.5	102.0
241.3	29.9	0.0	-.126	.063	379.5	101.5
241.2	31.3	0.0	-.124	.053	367.0	93.0
241.3	38.6	0.0	-.158	.035	389.2	100.0
241.2	45.6	0.0	-.185	.014	401.1	100.0
241.2	30.9	0.0	-.129	.064	388.9	100.5
241.3	32.8	0.0	-.136	.050	375.6	100.0
240.6	50.4	0.0	-.203	.017	442.2	100.0

Tabelle 91: L/D = 40, D = 0,7 cm

Drallblech Nr.1 (Ψ = 75°) am Meßstreckeneintritt

Table 91: L/D = 40, D = 0,7 cm

Twisted tape No. 1 (Ψ = 75°) at test section inlet

$\dot{m}$	$\Delta\vartheta_E$	$\Delta\vartheta_A$	x_E	x_A	q_{BO}	P
Massenfluß	Eintr.-Unter-kühlung	Austr.-Unter-kühlung	Eintr.-Qualität	Austr.-Qualität	max.Heizfl.-Belastung	Druck
Mass Flow Rate	Inlet Sub-cooling	Outlet Sub-cooling	Inlet-Quality	Outlet-Quality	Burn Out Heatflux	Pressure
$g/cm^2 s$	^{o}C	^{o}C	–	–	W/cm^2	ata
238.5	56.3	8.8	-.183	-.031	344.0	69.5
238.4	42.3	0.0	-.139	.003	323.9	69.2
238.3	36.8	0.0	-.122	.016	314.0	69.2
238.3	30.4	0.0	-.102	.023	283.3	69.5
239.1	23.9	0.0	-.081	.053	306.2	69.5
238.7	12.1	0.0	-.041	.054	218.5	69.0
238.1	18.6	0.0	-.063	.046	249.9	69.5
240.1	25.1	0.0	-.085	.034	271.9	70.0
238.3	32.6	0.0	-.109	.032	320.5	70.0
238.4	40.1	0.0	-.133	.021	350.1	69.5
238.2	50.8	0.0	-.167	.007	392.6	70.0
299.7	36.4	0.0	-.120	.032	436.0	69.0
302.0	41.8	0.0	-.138	.029	480.9	69.2
302.1	49.9	0.0	-.163	.014	510.7	69.5
302.2	54.3	0.0	-.177	.006	526.1	69.5
299.1	17.3	0.0	-.059	.037	275.5	70.0
299.5	22.1	0.0	-.075	.027	292.3	70.0
305.3	31.4	0.0	-.105	.007	327.8	69.0
303.8	50.4	8.5	-.164	-.029	388.9	69.0
303.6	50.4	4.7	-.164	-.016	425.3	69.0

Tabelle 92: L/D = 40, D = 0,7 cm

Drallblech Nr. 1 (Ψ = 75°) am Meßstreckeneintritt

Table 92: L/D = 40, D = 0,7 cm

Twisted tape No. 1(Ψ = 75°) at test section inlet

m	$\Delta\vartheta_E$	$\Delta\vartheta_A$	x_E	x_A	q_{BO}	P
Massenfluß	Eintr.-Unter-kühlung	Austr.-Unter-kühlung	Eintr.-Qualität	Austr.-Qualität	max.Heizfl.-Belastung	Druck
Mass Flow Rate	Inlet Sub-cooling	Outlet Sub-cooling	Inlet-Quality	Outlet-Quality	Burn Out Heatflux	Pressure
$g/cm^2\ s$	$^{\circ}C$	$^{\circ}C$	–	–	W/cm^2	ata
239.9	15.5	0.0	-.054	.047	231.2	70.5
238.7	18.0	0.0	-.062	.031	212.2	70.5
239.3	22.3	0.0	-.076	.011	198.2	70.5
244.5	23.5	0.0	-.081	.029	253.7	71.0
244.5	30.3	0.0	-.102	.008	256.4	70.5
239.3	30.8	.2	-.104	-.001	233.8	71.0
239.9	37.3	1.5	-.125	-.005	270.9	71.0
238.7	36.1	0.0	-.121	.004	282.9	70.5
238.7	40.8	0.0	-.136	.001	310.7	70.5
239.9	39.6	.4	-.132	-.001	295.2	70.0
238.8	41.6	1.2	-.138	-.004	301.4	70.0
238.8	41.9	0.0	-.139	.001	317.1	70.0
298.8	35.8	0.0	-.119	.004	349.9	69.2
298.7	29.9	0.0	-.100	.008	309.9	69.5
301.1	26.1	0.0	-.088	.008	275.5	69.0
299.1	19.1	0.0	-.065	.028	267.8	69.5
356.2	18.3	0.0	-.063	.037	339.8	70.5
355.4	20.3	0.0	-.069	.030	336.7	70.0
354.7	24.8	0.0	-.084	.010	320.5	70.0
355.4	28.1	0.0	-.095	.005	336.7	70.0

Tabelle 93: L/D = 40, D = 0,7 cm

Drallblech No. 2 (Ψ = 56°) am Meßstreckeneintritt

Table 93: L/D = 40, D = 0,7 cm

Twisted tape No. 2 (Ψ = 56°) at test section inlet

m	$\Delta\vartheta_E$	$\Delta\vartheta_A$	x_E	x_A	q_{BO}	P
Massenfluß	Eintr.-Unter-kühlung	Austr.-Unter-kühlung	Eintr.-Qualität	Austr.-Qualität	max.Heizfl.-Belastung	Druck
Mass Flow Rate	Inlet Sub-cooling	Outlet Sub-cooling	Inlet-Quality	Outlet-Quality	Burn Out Heatflux	Pressure
$g/cm^2\ s$	$^\circ C$	$^\circ C$	-	-	W/cm^2	ata
355.4	25.1	0.0	-.085	.010	323.6	70.0
241.8	36.4	0.0	-.151	.018	339.8	100.8
241.8	35.3	0.0	-.147	.007	310.7	101.0
241.8	29.3	0.0	-.123	.020	289.9	101.0
241.7	26.4	0.0	-.112	.067	359.5	100.5
240.0	24.1	0.0	-.102	.055	315.2	100.5
242.3	21.3	0.0	-.091	.051	288.5	100.5
242.9	2.1	0.0	-.010	.173	370.4	100.5
242.9	3.0	0.0	-.014	.166	364.3	101.0
241.2	32.9	0.0	-.137	.032	340.0	100.5
241.2	32.8	0.0	-.136	.013	301.0	100.3
241.2	45.1	1.9	-.184	-.009	350.4	101.0
241.2	44.4	0.0	-.181	.002	367.1	100.7
298.9	43.3	0.0	-.176	.010	465.6	100.3
297.5	41.8	1.2	-.171	-.005	409.2	100.6
297.5	29.3	0.0	-.123	.018	349.7	100.3
297.4	23.4	0.0	-.100	.050	371.7	100.5
297.4	26.4	0.0	-.112	.067	442.5	100.5
297.4	0.0	0.0	.081	.230	366.5	100.4
297.2	.2	0.0	-.001	.144	359.6	101.0

Tabelle 94: L/D = 40, D = 0,7 cm
Drallblech Nr. 2 (Ψ = 56°) am Meßstreckeneintritt

Table 94: L/D = 40, D = 0,7 cm
Twisted tape No. 2 (Ψ = 56°) at test section inlet

m	$\Delta\vartheta_E$	$\Delta\vartheta_A$	x_E	x_A	q_{BO}	P
Massenfluß	Eintr.-Unter-kühlung	Austr.-Unter-kühlung	Eintr.-Qualität	Austr.-Qualität	max.Heizfl.-Belastung	Druck
Mass Flow Rate	Inlet Sub-cooling	Outlet Sub-cooling	Inlet-Quality	Outlet-Quality	Burn Out Heatflux	Pressure
$g/cm^2 \ s$	$^{\circ}C$	$^{\circ}C$	–	–	W/cm^2	ata
298.8	32.8	0.0	-.136	.028	409.2	100.3
298.8	30.8	0.0	-.129	.014	356.5	100.3
298.8	37.6	0.0	-.155	0.000	387.6	100.3
298.8	35.6	0.0	-.147	.021	420.6	100.4
354.7	49.8	3.3	-.201	-.015	546.2	100.5
357.3	40.6	.3	-.166	-.001	488.6	100.0
353.0	38.9	0.0	-.159	.017	521.2	100.0
352.7	32.2	0.0	-.134	.005	409.2	100.5
352.3	25.5	0.0	-.108	.026	394.7	100.0
347.0	35.8	1.8	-.148	-.008	402.1	100.0
347.7	37.6	.5	-.155	-.002	439.7	100.0
341.5	37.6	0.0	-.155	.023	506.6	100.0

Tabelle 95: L/D = 40, D = 0,7 cm
Drallblech Nr. 2 (ψ = 56°) at test section inlet

Table 95: L/D = 40, D = 0,7 cm
Twisted tape No. 2 (ψ = 56°) at test section inlet

m	$\Delta\vartheta_E$	$\Delta\vartheta_A$	X_E	X_A	q_{BO}	P	Δ_P
Massenfluß	Eintr.-Unter-kühlung	Austr.-Unter-kühlung	Eintr.-Qualität	Austr.-Qualität	max.Heizfl.-Belastung	Druck	Druckverl.am Meßstrecken-eintritt
Mass Flow Rate	Inlet Sub-cooling	Outlet Sub-cooling	Inlet-Quality	Outlet-Quality	Burn Out Heatflux	Pressure	Pressure Drop at the Inlet of the Test-section
$g/cm^2\ s$	^{o}C	^{o}C	-	-	W/cm^2	ata	mmHg
289.7	40.4	0.0	-.133	.094	628.4	68.5	560.00
289.7	40.9	0.0	-.135	.095	635.4	69.0	472.00
288.7	44.9	0.0	-.147	.084	635.4	68.5	473.20
289.7	49.1	0.0	-.160	.078	658.1	69.0	467.50
288.7	52.4	0.0	-.170	.068	655.9	69.0	467.50
295.4	52.4	0.0	-.170	.070	676.7	69.0	565.00
293.5	47.6	0.0	-.156	.069	628.4	69.0	552.00
289.7	41.9	0.0	-.138	.069	571.3	69.0	552.00
288.7	34.1	0.0	-.113	.089	558.7	68.5	555.20
288.7	28.9	0.0	-.097	.111	571.3	69.0	552.00
288.7	15.3	0.0	-.052	.131	506.7	69.0	302.50
288.7	19.3	0.0	-.066	.105	471.0	69.5	302.50
288.7	23.6	0.0	-.080	.084	451.9	69.5	302.50
288.7	29.9	0.0	-.100	.074	478.9	69.5	302.50
289.7	33.1	0.0	-.110	.064	482.6	69.0	302.50
289.7	29.9	0.0	-.100	.092	529.5	69.0	374.00
288.7	33.1	0.0	-.110	.087	543.7	69.0	373.10
291.6	40.4	0.0	-.133	.058	533.3	69.5	373.10
299.1	40.1	0.0	-.132	.044	502.9	69.0	189.80
298.2	34.1	0.0	-.113	.044	447.8	69.0	189.80

Tabelle 96: L/D = 40, D = 0,7 cm
Drosselstelle am Meßstreckeneintritt

Table 96: L/D = 40, D = 0,7 cm
Throttling point at test section inlet

m	$\Delta\vartheta_E$	$\Delta\vartheta_A$	X_E	X_A	q_{BO}	P	ΔP
Massenfluß	Eintr.-Unter-kühlung	Austr.-Unter-kühlung	Eintr.-Qualität	Austr.-Qualität	max.Heizfl.-Belastung	Druck	Druckverl.am Meßstrecken-eintritt
Mass Flow Rate	Inlet Sub-cooling	Outlet Sub-cooling	Inlet-Quality	Outlet-Quality	Burn Out Heatflux	Pressure	Pressure Drop at the Inlet of the Test-section
$g/cm^2\ s$	^oC	^oC	-	-	W/cm^2	ata	mmHg
298.2	16.3	0.0	-.056	.120	500.5	69.5	189.80
298.2	17.8	0.0	-.061	.086	418.3	69.0	190.70
298.2	23.1	0.0	-.078	.064	405.3	69.5	188.90
298.2	27.1	0.0	-.091	.059	427.4	69.0	188.90
298.2	31.6	0.0	-.106	.051	446.0	70.0	188.90
288.7	30.4	0.0	-.102	.049	414.3	69.5	94.40
288.7	22.6	0.0	-.077	.057	368.1	69.5	94.40
294.5	17.6	0.0	-.060	.116	494.9	69.5	92.60
295.4	11.0	0.0	-.038	.138	494.9	69.5	92.60
293.5	12.8	0.0	-.044	.076	336.3	69.5	0.00
293.5	23.6	0.0	-.080	.045	351.2	70.0	0.00
293.5	34.1	0.0	-.114	.036	420.0	70.0	0.00
293.5	44.8	0.0	-.148	.019	467.4	70.0	0.00
293.5	51.8	0.0	-.171	.007	494.9	71.0	0.00
344.1	43.9	0.0	-.144	.029	567.9	68.5	370.40
344.1	44.1	0.0	-.145	.028	568.5	69.0	277.80
345.7	32.9	0.0	-.108	.038	487.8	67.5	277.80
339.2	21.6	0.0	-.072	.069	461.4	67.5	277.80
337.6	24.4	0.0	-.081	.059	455.5	68.0	278.70
338.4	18.9	0.0	-.064	.093	508.6	68.5	278.70

Tabelle 97: L/D = 40, D = 0,7 cm
Drosselstelle am Meßstreckeneintritt

Table 97: L/D = 40, D = 0,7 cm
Throttling point at test section inlet

m	$\Delta\vartheta_E$	$\Delta\vartheta_A$	X_E	X_A	q_{BO}	P	ΔP
Massenfluß	Eintr.-Unter-kühlung	Austr.-Unter-kühlung	Eintr.-Qualität	Austr.-Qualität	max.Heizfl.-Belastung	Druck	Druckverl.am Meßstrecken-eintritt
Mass Flow Rate	Inlet Sub-cooling	Outlet Sub-cooling	Inlet-Quality	Outlet-Quality	Burn Out Heatflux	Pressure	Pressure Drop at the Inlet of the Test-section
g/cm^2 s	^oC	^oC	-	-	W/cm^2	ata	mmHg
337.6	14.6	0.0	-.050	.105	499.2	68.5	185.20
337.6	19.1	0.0	-.065	.065	419.8	68.5	185.20
337.6	26.1	0.0	-.087	.062	483.9	68.5	185.20
337.6	32.4	0.0	-.108	.049	507.1	69.0	182.40
337.6	39.1	0.0	-.129	.040	544.5	68.5	184.30
335.9	38.1	0.0	-.126	.032	507.7	68.5	91.70
337.6	33.1	0.0	-.110	.033	464.0	69.0	95.60
337.6	26.1	0.0	-.088	.038	407.0	69.0	95.60
337.6	17.3	0.0	-.059	.095	496.1	69.0	92.60
335.9	10.1	0.0	-.034	.118	490.6	68.5	92.60
338.2	8.6	0.0	-.029	.122	490.6	69.0	93.50
344.1	34.1	0.0	-.113	.043	515.6	68.5	370.30

Tabelle 98: L/D = 40, D = 0,7 cm

Drosselstelle am Meßstreckeneintritt

Table 98: L/D = 40, D = 0,7 cm

Throttling point at test section inlet

m	$\Delta\vartheta_E$	$\Delta\vartheta_A$	x_E	x_A	q_{BO}	P	Δ_P
Massenfluß	Eintr.-Unter-kühlung	Austr.-Unter-kühlung	Eintr.-Qualität	Austr.-Qualität	max.Heizfl.-Belastung	Druck	Druckverl.am Meßstrecken-eintritt
Mass Flow Rate	Inlet Sub-cooling	Outlet Sub-cooling	Inlet-Quality	Outlet-Quality	Burn Out Heatflux	Pressure	Pressure Drop at the Inlet of the Test-section
$g/cm^2\ s$	^oC	^oC	-	-	W/cm^2	ata	mmHg
98.4	46.1	0.0	-.152	.042	181.7	70.5	18.00
98.4	40.6	0.0	-.135	.040	163.6	70.5	18.00
98.4	32.3	0.0	-.109	.055	153.0	70.5	18.00
98.4	23.6	0.0	-.080	.067	137.6	70.0	18.00
98.4	11.5	0.0	-.040	.096	127.0	70.0	18.00
97.9	5.7	0.0	-.020	.117	128.2	70.0	18.00
101.1	18.8	0.0	-.064	.230	282.0	70.0	926.00
102.0	14.8	0.0	-.051	.237	278.1	70.5	926.00
100.2	9.8	0.0	-.034	.258	278.1	69.5	926.00
99.6	3.5	0.0	-.012	.272	270.4	69.0	926.00
99.8	28.4	0.0	-.095	.208	287.7	69.0	926.00
99.9	39.6	0.0	-.131	.197	311.5	69.0	926.00
102.2	41.4	0.0	-.136	.223	349.8	69.0	1204.00
102.1	32.4	0.0	-.108	.229	327.6	69.0	1204.00
102.1	24.9	0.0	-.084	.268	342.3	69.0	1204.00
102.1	13.8	0.0	-.047	.303	340.3	69.0	1204.00
101.7	3.0	0.0	-.010	.312	312.5	69.0	1204.00
99.9	8.3	0.0	-.029	.334	345.5	69.0	1204.00
100.8	7.5	0.0	-.026	.232	247.4	69.5	463.00
99.9	.5	0.0	-.002	.285	272.2	69.5	463.00

Tabelle 99: L/D = 40, D = 1,1 cm
Drosselstelle am Meßstreckeneintritt

Table 99: L/D = 40, D = 1,1 cm
Throttling point at test section inlet

—

$\dot{m}$	$\Delta\vartheta_E$	$\Delta\vartheta_A$	X_E	X_A	q_{BO}	P	Δ_p
Massenfluß	Eintr.-Unter-kühlung	Austr.-Unter-kühlung	Eintr.-Qualität	Austr.-Qualität	max.Heizfl.-Belastung	Druck	Druckverl.am Meßstrecken-eintritt
Mass Flow Rate	Inlet Sub-cooling	Outlet Sub-cooling	Inlet-Quality	Outlet-Quality	Burn Out Heatflux	Pressure	Pressure Drop at the Inlet of the Test-section
g/cm² s	°C	°C	–	–	W/cm²	ata	mmHg
167.6	9.6	0.0	-.033	.209	358.3	69.0	1194.00
100.0	28.4	0.0	-.095	.036	115.7	69.5	18.00
100.1	16.3	0.0	-.056	.066	107.7	69.5	18.00
100.1	17.6	0.0	-.060	.085	128.3	69.5	204.00
100.2	16.8	0.0	-.057	.209	235.3	69.5	389.00
100.2	17.6	0.0	-.060	.230	255.8	69.5	574.00
99.4	6.8	0.0	-.023	.235	226.6	69.5	574.00
100.3	6.8	0.0	-.023	.236	229.4	69.5	389.00
99.8	2.7	0.0	-.010	.219	200.6	69.5	199.00
99.3	10.3	0.0	-.035	.202	207.7	69.5	199.00
99.3	18.6	0.0	-.063	.081	126.6	69.5	199.00
99.3	15.3	0.0	-.052	.102	135.1	69.5	199.00
100.3	15.3	0.0	-.052	.202	224.4	69.5	389.00
100.2	24.9	0.0	-.084	.113	174.0	69.5	389.00
100.3	27.6	0.0	-.093	.082	154.4	69.5	389.00
100.3	34.1	0.0	-.114	.069	162.0	69.5	389.00
100.2	34.9	0.0	-.116	.109	198.9	69.5	565.00
100.2	29.6	0.0	-.099	.138	209.7	69.5	565.00
100.3	24.9	0.0	-.084	.158	213.8	69.5	565.00
100.2	24.1	0.0	-.081	.305	340.5	69.5	852.00

Tabelle 100: L/D = 43,1, D = 1,1 cm
Drosselstelle am Meßstreckeneintritt

Table 100: L/D = 43,1, D = 1,1 cm
Throttling point at test section inlet

$\dot{m}$	$\Delta \vartheta_E$	$\Delta \vartheta_A$	x_E	x_A	q_{BO}	P	Δp
Massenfluß	Eintr.-Unter-kühlung	Austr.-Unter-kühlung	Eintr.-Qualität	Austr.-Qualität	max.Heizfl.-Belastung	Druck	Druckverl.am Meßstrecken-eintritt
Mass Flow Rate	Inlet Sub-cooling	Outlet Sub-cooling	Inlet-Quality	Outlet-Quality	Burn Out Heatflux	Pressure	Pressure Drop at the Inlet of the Test-section
$g/cm^2 s$	^oC	^oC	-	-	W/cm^2	ata	mmHg

M	DTEM	DTAM	XEM	XAM	Q	PEM	PDR
99.9	10.0	0.0	-.035	.239	259.7	69.5	463.00
99.9	16.1	0.0	-.055	.224	264.7	69.5	463.00
99.0	24.1	0.0	-.081	.214	278.2	69.5	463.00
99.0	42.6	0.0	-.140	.155	278.1	69.5	463.00
99.5	30.1	0.0	-.101	.210	293.7	69.5	463.00

Tabelle 101: L/D = 40, D = 1,1 cm
Drosselstelle am Meßstreckeneintritt

Table 101: L/D = 40, D = 1,1 cm
Throttling point at test section inlet

m	$\Delta \vartheta_E$	$\Delta \vartheta_A$	X_E	X_A	q_{BO}	P	Δp
Massenfluß	Eintr.-Unter-kühlung	Austr.-Unter-kühlung	Eintr.-Qualität	Austr.-Qualität	max.Heizfl.-Belastung	Druck	Druckverl.am Meßstrecken-eintritt
Mass Flow Rate	Inlet Sub-cooling	Outlet Sub-cooling	Inlet-Quality	Outlet-Quality	Burn Out Heatflux	Pressure	Pressure Drop at the Inlet of the Test-section
$g/cm^2\ s$	^oC	^oC	-	-	W/cm^2	ata	mmHg
174.2	58.1	4.8	-.189	-.017	262.3	70.0	82.00
172.6	49.8	1.8	-.164	-.006	237.9	70.0	82.00
172.5	43.1	0.0	-.142	.005	224.4	70.0	82.00
172.8	34.9	0.0	-.117	.019	207.0	70.0	82.00
172.8	27.3	0.0	-.092	.036	195.1	70.0	82.00
172.8	18.1	0.0	-.062	.055	177.9	70.0	82.00
172.8	0.0	20.6	-.291	-.071	331.7	71.0	82.00
172.8	1.0	0.0	-.003	.214	331.7	69.0	269.00
171.9	6.3	0.0	-.022	.204	341.7	70.0	269.00
172.7	20.1	0.0	-.068	.099	254.2	70.0	269.00
172.7	32.9	0.0	-.110	.043	252.6	70.0	269.00
172.7	40.1	0.0	-.133	.019	231.1	70.0	269.00
172.7	47.3	0.0	-.156	.002	240.2	70.0	269.00
173.2	48.1	0.0	-.158	.018	269.3	70.0	454.00
173.2	41.1	0.0	-.136	.033	257.7	70.0	454.00
173.4	31.9	0.0	-.106	.062	258.5	69.0	454.00
173.1	22.1	0.0	-.075	.099	266.1	69.0	454.00
170.7	9.6	0.0	-.033	.195	343.5	69.0	454.00
172.0	11.6	0.0	-.040	.168	345.8	69.0	454.00
171.6	6.5	0.0	-.022	.204	342.6	69.0	639.00

Tabelle 102: L/D = 43,1, D = 1,1 cm
Drosselstelle am Meßstreckeneintritt

Table 102: L/D = 43,1, D = 1,1 cm
Throttling point at test section inlet

m	$\Delta\vartheta_E$	$\Delta\vartheta_A$	X_E	X_A	q_{BO}	P	ΔP
Massenfluß	Eintr.-Unter-kühlung	Austr.-Unter-kühlung	Eintr.-Qualität	Austr.-Qualität	max.Heizfl.-Belastung	Druck	Druckverl.am Meßstrecken-eintritt
Mass Flow Rate	Inlet Sub-cooling	Outlet Sub-cooling	Inlet-Quality	Outlet-Quality	Burn Out Heatflux	Pressure	Pressure Drop at the Inlet of the Test-section
$g/cm^2\,s$	°C	°C	–	–	W/cm^2	ata	mmHg
171.4	9.3	0.0	-.032	.193	340.8	68.5	639.00
171.3	15.3	0.0	-.052	.185	359.3	69.0	639.00
171.3	19.1	0.0	-.065	.174	361.1	69.0	639.00
168.7	28.4	0.0	-.095	.064	237.9	68.5	639.00
167.8	36.1	0.0	-.120	.053	256.5	69.0	639.00
169.1	44.1	0.0	-.145	.043	280.8	69.0	639.00
172.0	48.1	0.0	-.157	.051	316.6	69.0	824.00
172.5	44.9	0.0	-.147	.058	312.3	69.0	824.00
173.4	39.9	0.0	-.132	.062	295.9	69.0	824.00
173.3	32.9	0.0	-.110	.068	271.0	69.5	824.00
173.8	18.9	0.0	-.064	.171	360.2	69.0	824.00
171.7	19.9	0.0	-.067	.175	367.7	69.0	1009.00
172.5	22.1	0.0	-.075	.174	378.2	69.0	1009.00
171.7	27.4	0.0	-.092	.148	363.5	69.0	1009.00
172.0	36.6	0.0	-.121	.134	387.9	69.0	1009.00
172.7	45.9	0.0	-.150	.067	331.7	69.0	1009.00
171.2	46.6	0.0	-.153	.073	340.8	69.0	1194.00
171.2	39.9	0.0	-.132	.097	344.9	69.0	1194.00
170.9	33.4	0.0	-.111	.145	386.9	69.0	1194.00
169.2	22.1	0.0	-.075	.173	369.6	69.0	1194.00

Tabelle 103: L/D = 43,1, D = 1,1 cm
Drosselstelle am Meßstreckeneintritt

Table 103: L/D = 43,1, D = 1,1 cm
Throttling point at test section inlet

m	$\Delta\vartheta_E$	$\Delta\vartheta_A$	X_E	X_A	q_{BO}	P	Δ_P
Massenfluß	Eintr.-Unter-kühlung	Austr.-Unter-kühlung	Eintr.-Qualität	Austr.-Qualität	max.Heizfl.-Belastung	Druck	Druckverl.am Meßstrecken-eintritt
Mass Flow Rate	Inlet Sub-cooling	Outlet Sub-cooling	Inlet-Quality	Outlet-Quality	Burn Out Heatflux	Pressure	Pressure Drop at the Inlet of the Test-section
$g/cm^2\,s$	^{o}C	^{o}C	-	-	W/cm^2	ata	mmHg
249.5	30.9	0.0	-.102	.164	356.4	67.0	743.00
249.5	38.2	0.0	-.125	.140	355.4	67.5	743.00
249.5	42.2	0.0	-.137	.128	355.4	67.5	743.00
249.5	40.4	0.0	-.131	.085	290.4	67.0	560.00
249.5	31.4	0.0	-.103	.111	288.0	66.5	560.00
249.5	24.9	0.0	-.083	.173	343.3	67.0	560.00
249.5	17.1	0.0	-.057	.196	340.3	67.0	565.00
249.5	19.4	0.0	-.065	.189	340.3	67.5	370.00
249.5	28.2	0.0	-.093	.112	275.2	67.5	370.00
249.5	37.2	0.0	-.122	.079	269.7	67.5	363.00
249.5	45.2	0.0	-.146	.067	286.4	67.5	363.00
255.0	46.6	0.0	-.152	.034	254.3	68.5	199.00
255.0	40.4	0.0	-.132	.057	258.8	68.0	194.00
255.0	35.2	0.0	-.116	.062	243.7	68.0	199.00
255.0	26.6	0.0	-.089	.075	224.6	68.0	204.00
255.0	8.6	0.0	-.029	.195	307.5	68.0	194.00
243.9	13.6	0.0	-.046	.172	284.8	68.0	185.00
243.9	13.1	0.0	-.045	.084	169.3	68.0	0.00
243.9	24.9	0.0	-.083	.043	165.0	68.0	0.00
243.3	36.9	0.0	-.121	.024	190.4	68.0	0.00

Tabelle 104: L/D = 43,1, D = 1,1 cm
Drosselstelle am Meßstreckeneintritt

Table 104: L/D = 43,1, D = 1,1 cm
Throttling point at test section inlet

m	$\Delta\vartheta_E$	$\Delta\vartheta_A$	X_E	X_A	q_{BO}	P	Δ_P
Massenfluß	Eintr.-Unter-kühlung	Austr.-Unter-kühlung	Eintr.-Qualität	Austr.-Qualität	max.Heizfl.-Belastung	Druck	Druckverl.am Meßstrecken-eintritt
Mass Flow Rate	Inlet Sub-cooling	Outlet Sub-cooling	Inlet-Quality	Outlet-Quality	Burn Out Heatflux	Pressure	Pressure Drop at the Inlet of the Test-section
$g/cm^2\ s$	^{o}C	^{o}C	-	-	W/cm^2	ata	mmHg
97.6	50.9	0.0	-.165	.031	182.7	68.5	57.00
96.6	41.4	0.0	-.136	.038	160.5	68.5	57.00
96.5	28.7	0.0	-.095	.061	144.8	68.0	57.00
96.5	19.9	0.0	-.067	.090	145.2	68.5	57.00
96.4	11.6	0.0	-.040	.118	145.7	68.5	57.00
97.4	8.6	0.0	-.029	.169	184.7	68.0	187.00
96.1	1.3	0.0	-.004	.250	233.0	69.0	187.00
96.4	5.8	0.0	-.020	.183	187.6	68.0	193.00
96.9	18.1	0.0	-.061	.091	141.6	68.5	193.00
97.1	14.1	0.0	-.048	.109	145.5	68.5	375.00
96.5	9.1	0.0	-.031	.150	166.8	68.5	375.00
96.5	6.6	0.0	-.023	.171	178.4	68.5	375.00
95.7	4.5	0.0	-.016	.212	208.5	68.5	375.00
95.7	1.0	0.0	-.003	.230	213.4	68.5	372.00
97.2	4.0	0.0	-.014	.204	202.6	68.5	640.00
97.3	5.0	0.0	-.017	.193	195.6	68.5	644.00
96.6	7.6	0.0	-.026	.187	196.7	68.5	639.00
96.7	13.1	0.0	-.045	.138	169.0	68.5	639.00
96.0	17.1	0.0	-.058	.094	139.8	68.5	625.00
96.9	18.6	0.0	-.063	.111	161.0	68.5	928.00

Tabelle 105:   L/D = 40, D = 1,5 cm
Drosselstelle am Meßstreckeneintritt

Table 105:   L/D = 40, D = 1,5 cm
Throttling point at test section inlet

m	$\Delta\vartheta_E$	$\Delta\vartheta_A$	X_E	X_A	q_{BO}	P	Δ_P
Massenfluß	Eintr.-Unter-kühlung	Austr.-Unter-kühlung	Eintr.-Qualität	Austr.-Qualität	max.Heizfl.-Belastung	Druck	Druckverl.am Meßstrecken-eintritt
Mass Flow Rate	Inlet Sub-cooling	Outlet Sub-cooling	Inlet-Quality	Outlet-Quality	Burn Out Heatflux	Pressure	Pressure Drop at the Inlet of the Test-section
$g/cm^2\,s$	^oC	^oC	–	–	W/cm^2	ata	mmHg
96.8	14.1	0.0	-.048	.155	187.3	68.5	935.00
96.7	9.6	0.0	-.033	.184	200.4	69.0	935.00
96.2	6.6	0.0	-.023	.188	194.0	68.5	935.00
95.3	8.1	0.0	-.028	.168	178.4	68.5	1194.00
97.5	12.6	0.0	-.043	.150	179.6	69.0	1194.00
97.5	22.1	0.0	-.075	.077	141.8	68.5	1222.00
97.8	24.1	0.0	-.081	.286	341.6	69.5	648.00
97.4	26.4	0.0	-.089	.281	342.3	69.5	648.00
97.8	29.6	0.0	-.099	.276	349.5	68.5	648.00
97.7	19.1	0.0	-.065	.296	336.1	68.5	648.00
97.4	10.1	0.0	-.035	.312	321.7	69.0	648.00
98.0	3.3	0.0	-.011	.325	314.4	68.5	667.00
157.6	28.9	0.0	-.096	.136	349.5	67.7	620.00
157.5	21.6	0.0	-.072	.153	340.2	67.2	620.00
157.3	17.9	0.0	-.060	.161	333.1	68.2	620.00
157.2	13.1	0.0	-.045	.171	324.8	67.7	620.00
154.1	6.8	0.0	-.023	.187	310.7	68.2	620.00
157.1	5.6	0.0	-.019	.190	314.4	68.2	630.00
157.3	1.3	0.0	-.004	.198	304.1	68.2	630.00
154.8	10.1	0.0	-.034	.182	319.6	68.2	630.00

Tabelle 106:   L/D = 40, D = 1,5 cm
Drosselstelle am Meßstreckeneintritt

Table 106:   L/D = 40, D = 1,5 cm
Throttling point at test section inlet

$\dot{m}$	$\Delta\vartheta_E$	$\Delta\vartheta_A$	X_E	X_A	q_{BO}	P	ΔP
Massenfluß	Eintr.-Unter-kühlung	Austr.-Unter-kühlung	Eintr.-Qualität	Austr.-Qualität	max.Heizfl.-Belastung	Druck	Druckverl.am Meßstrecken-eintritt
Mass Flow Rate	Inlet Sub-cooling	Outlet Sub-cooling	Inlet-Quality	Outlet-Quality	Burn Out Heatflux	Pressure	Pressure Drop at the Inlet of the Test-section
g/cm² s	°C	°C	-	-	W/cm²	ata	mmHg
154.9	14.1	0.0	-.048	.179	336.1	68.2	630.00
155.0	20.4	0.0	-.069	.145	317.1	68.2	630.00
155.0	25.4	0.0	-.085	.140	332.4	68.7	630.00
155.4	20.1	0.0	-.068	.021	132.6	68.7	630.00
155.4	37.9	0.0	-.125	.018	213.3	68.7	630.00
155.3	37.6	0.0	-.124	.026	222.9	68.7	630.00
155.5	44.1	0.0	-.145	.018	241.1	68.7	630.00
156.5	53.9	0.0	-.175	.022	293.1	68.7	815.00
156.2	45.9	0.0	-.149	.026	263.0	68.2	815.00
156.0	35.1	0.0	-.116	.102	324.8	68.7	815.00
155.8	23.7	0.0	-.079	.151	343.6	67.2	815.00
158.5	37.6	0.0	-.124	.052	267.3	68.7	815.00
224.8	47.6	0.0	-.155	.020	376.4	68.0	787.00
224.3	38.1	0.0	-.126	.024	320.6	68.5	787.00
223.6	27.4	0.0	-.092	.076	358.1	68.5	787.00
220.4	15.1	0.0	-.051	.110	340.9	67.5	787.00
222.0	3.8	0.0	-.013	.139	323.4	68.0	787.00
225.6	8.8	0.0	-.030	.121	326.2	68.0	509.00
225.1	13.3	0.0	-.046	.111	336.7	69.5	509.00
225.3	17.9	0.0	-.060	.099	343.7	68.0	509.00

Tabelle 107: L/D = 40, D = 1,5 cm
Drosselstelle am Meßstreckeneintritt

Table 107: L/D = 40, D = 1,5 cm
Throttling point at test section inlet

m	$\Delta\vartheta_E$	$\Delta\vartheta_A$	X_E	X_A	q_{BO}	P	Δ_P
Massenfluß	Eintr.-Unter-kühlung	Austr.-Unter-kühlung	Eintr.-Qualität	Austr.-Qualität	max.Heizfl.-Belastung	Druck	Druckverl.am Meßstrecken-eintritt
Mass Flow Rate	Inlet Sub-cooling	Outlet Sub-cooling	Inlet-Quality	Outlet-Quality	Burn Out Heatflux	Pressure	Pressure Drop at the Inlet of the Test-section
$g/cm^2\ s$	$^{\circ}C$	$^{\circ}C$	-	-	W/cm^2	ata	mmHg
M	DTEM	DTAM	XEM	XAM	Q	PEM	PDM
225.8	24.4	0.0	−.081	.085	359.6	68.0	509.00
226.3	31.6	0.0	−.105	.028	289.8	68.5	509.00
230.6	37.6	0.0	−.124	.021	320.5	68.5	509.00
223.0	36.4	0.0	−.120	.029	319.3	68.5	324.00
223.1	36.1	0.0	−.119	.021	299.6	68.5	324.00
222.7	30.4	0.0	−.101	.021	261.6	68.5	0.00
222.5	22.6	0.0	−.076	.064	299.0	68.0	324.00
222.1	13.9	0.0	−.047	.113	340.9	68.0	324.00
221.5	5.8	0.0	−.020	.134	326.9	68.5	324.00
221.1	3.0	0.0	−.010	.144	326.9	68.5	324.00

Tabelle 108: L/D = 40, D = 1,5 cm
Drosselstelle am Meßstreckeneintritt

Table 108: L/D = 40, D = 1,5 cm
Throttling point at test section inlet

m	$\Delta\vartheta_E$	$\Delta\vartheta_A$	x_E	x_A	q_{BO}	P
Massenfluß	Eintr.-Unter-kühlung	Austr.-Unter-kühlung	Eintr.-Qualität	Austr.-Qualität	max.Heizfl.-Belastung	Druck
Mass Flow Rate	Inlet Sub-cooling	Outlet Sub-cooling	Inlet-Quality	Outlet-Quality	Burn Out Heatflux	Pressure
$g/cm^2\ s$	$^\circ C$	$^\circ C$	-	-	W/cm^2	ata
237.3	32.6	6.0	-.109	-.021	815.9	70.0
239.4	37.4	10.6	-.124	-.037	815.9	70.0
239.7	41.9	14.0	-.139	-.048	846.9	70.0
239.8	47.2	17.9	-.155	-.061	874.1	69.8
233.3	53.8	21.6	-.176	-.074	928.4	70.0
234.6	55.1	23.0	-.180	-.078	928.4	70.0
234.2	30.3	3.8	-.101	-.013	804.4	69.4
236.4	40.9	12.7	-.134	-.043	842.3	68.2
236.4	51.6	21.4	-.166	-.071	880.8	67.0

Tabelle 109:   L/D = 10, D = 0,7 cm
Rohre ohne Einlaufstrecke

Table 109:   L/D = 10, D = 0,7 cm
Channels without inlet section

$\dot{m}$	$\Delta\vartheta_E$	$\Delta\vartheta_A$	X_E	X_A	q_{BO}	P	ΔP
Massenfluß	Eintr.-Unter-kühlung	Austr.-Unter-kühlung	Eintr.-Qualität	Austr.-Qualität	max.Heizfl.-Belastung	Druck	Druckverl.am Meßstrecken-eintritt
Mass Flow Rate	Inlet Sub-cooling	Outlet Sub-cooling	Inlet-Quality	Outlet-Quality	Burn Out Heatflux	Pressure	Pressure Drop at the Inlet of the Test-section
g/cm^2 s	°C	°C	-	-	W/cm^2	ata	mmHg
289.6	41.9	0.0	-.139	.017	429.0	70.0	0.00
302.9	41.9	0.0	-.139	.003	408.6	70.0	53.00
289.6	41.9	0.0	-.139	.020	437.3	70.0	98.00
296.3	42.6	0.0	-.141	.030	481.4	70.0	200.00
291.5	40.7	0.0	-.133	.045	493.8	68.0	302.00
292.4	40.7	0.0	-.133	.061	539.6	68.0	410.00
289.6	40.4	0.0	-.132	.062	534.9	68.0	498.00
289.6	40.4	0.0	-.132	.066	540.5	68.0	620.00
289.6	40.4	0.0	-.132	.067	543.4	68.0	716.00
289.6	40.4	0.0	-.132	.068	546.2	68.0	825.00
289.6	29.4	0.0	-.098	.093	522.1	68.0	630.00
289.6	27.9	0.0	-.093	.092	513.5	68.0	690.00
289.6	27.6	0.0	-.092	.098	524.4	68.0	585.00
289.5	27.6	0.0	-.092	.094	512.8	68.0	490.00
289.5	24.9	0.0	-.083	.107	524.2	68.0	450.00
289.5	24.9	0.0	-.083	.091	478.2	68.0	402.00
289.5	24.4	0.0	-.081	.063	397.8	68.0	292.00
289.5	24.4	0.0	-.081	.053	374.0	68.0	200.00
289.5	24.1	0.0	-.081	.037	327.9	68.0	105.00
289.5	24.6	0.0	-.082	.030	312.6	68.0	20.00

Tabelle 110: L/D = 40, D = 0,7 cm
Drosselstelle am Meßstreckeneintritt

Table 110: L/D = 40, D = 0,7 cm
Throttling point at test section inlet

m	$\Delta\vartheta_E$	$\Delta\vartheta_A$	X_E	X_A	q_{BO}	P	Δ_P
Massenfluß	Eintr.-Unter-kühlung	Austr.-Unter-kühlung	Eintr.-Qualität	Austr.-Qualität	max.Heizfl.-Belastung	Druck	Druckverl.am Meßstrecken-eintritt
Mass Flow Rate	Inlet Sub-cooling	Outlet Sub-cooling	Inlet-Quality	Outlet-Quality	Burn Out Heatflux	Pressure	Pressure Drop at the Inlet of the Test-section
$g/cm^2\ s$	^oC	^oC	-	-	W/cm^2	ata	mmHg
289.5	14.6	0.0	-.050	.052	284.6	68.0	20.00
289.5	15.9	0.0	-.054	.068	339.9	68.0	100.00
289.5	15.9	0.0	-.054	.073	352.5	68.0	200.00
289.5	17.4	0.0	-.059	1.309	3783.1	68.0	300.00
289.5	17.4	0.0	-.059	.090	407.8	68.0	400.00
289.5	18.6	0.0	-.063	.084	403.9	68.0	500.00
289.5	16.6	0.0	-.056	.123	490.1	68.0	600.00
289.5	6.3	0.0	-.022	.150	468.5	68.0	600.00
289.5	7.6	0.0	-.026	.146	468.7	68.0	500.00
289.5	7.6	0.0	-.026	.143	465.7	68.0	400.00
289.5	7.6	0.0	-.026	.142	462.1	68.0	300.00
289.5	7.6	0.0	-.026	.141	464.0	68.0	200.00
289.5	7.6	0.0	-.026	.086	311.7	68.0	100.00
289.5	7.6	0.0	-.026	.081	297.1	68.0	20.00
243.4	13.6	0.0	-.046	.070	271.6	68.0	20.00
243.4	14.4	0.0	-.049	.062	260.3	68.0	100.00
243.4	13.9	0.0	-.047	.100	343.4	68.0	200.00
243.3	13.1	0.0	-.044	.101	336.2	67.5	300.00
243.3	14.4	0.0	-.048	.096	334.0	67.5	400.00
243.3	14.6	0.0	-.049	.099	345.3	67.0	500.00

Tabelle 111: L/D = 40, D = 0,7 cm

Drosselstelle am Meßstreckeneintritt

Table 111: L/D = 40, D = 0,7 cm

Throttling point at test section inlet

$\dot{m}$	$\Delta\vartheta_E$	$\Delta\vartheta_A$	X_E	X_A	q_{BO}	P	ΔP
Massenfluß	Eintr.-Unter-kühlung	Austr.-Unter-kühlung	Eintr.-Qualität	Austr.-Qualität	max.Heizfl.-Belastung	Druck	Druckverl.am Meßstrecken-eintritt
Mass Flow Rate	Inlet Sub-cooling	Outlet Sub-cooling	Inlet-Quality	Outlet-Quality	Burn Out Heatflux	Pressure	Pressure Drop at the Inlet of the Test-section
$g/cm^2\ s$	^oC	^oC	-	-	W/cm^2	ata	mmHg
243.3	15.6	0.0	-.053	.118	392.5	67.5	600.00
243.3	13.6	0.0	-.046	.159	474.2	67.5	700.00
243.3	23.4	0.0	-.078	.108	427.6	67.5	700.00
243.3	24.9	0.0	-.083	.105	433.1	67.5	600.00
243.3	24.9	0.0	-.083	.087	394.6	67.5	500.00
243.3	23.9	0.0	-.080	.078	364.9	67.5	400.00
243.3	23.4	0.0	-.078	.076	357.0	67.0	300.00
243.3	23.4	0.0	-.078	.058	318.7	67.0	200.00
243.4	23.9	0.0	-.080	.057	319.7	67.5	100.00
243.4	23.9	0.0	-.080	.059	324.2	67.5	100.00
243.4	23.4	0.0	-.078	.061	325.0	67.5	10.00
243.4	33.2	0.0	-.109	.031	328.1	67.5	10.00
243.4	33.2	0.0	-.110	.045	360.8	68.0	100.00
243.4	32.7	0.0	-.108	.057	384.7	67.5	200.00
243.3	32.2	0.0	-.106	.075	419.0	67.5	300.00
243.3	32.2	0.0	-.106	.079	428.1	67.5	400.00
243.4	32.7	0.0	-.108	.083	441.0	68.0	500.00
243.3	32.7	0.0	-.108	.081	434.3	68.0	600.00
243.3	32.7	0.0	-.108	.088	450.4	68.0	700.00

Tabelle 112: L/D = 40, D = 0,7 cm
Drosselstelle am Meßstreckeneintritt

Table 112: L/D = 40, D = 0,7 cm
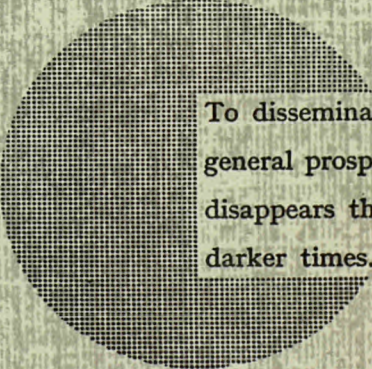Throttling point at test section inlet

To disseminate knowledge is to disseminate prosperity — I mean general prosperity and not individual riches — and with prosperity disappears the greater part of the evil which is our heritage from darker times.

Alfred Nobel

SALES OFFICES

All Euratom reports are on sale at the offices listed below, at the prices given on the back of the front cover (when ordering, specify clearly the EUR number and the title of the report, which are shown on the front cover).

OFFICE CENTRAL DE VENTE DES PUBLICATIONS DES COMMUNAUTES EUROPEENNES
2, place de Metz, Luxembourg (Compte chèque postal Nº 191-90)

BELGIQUE — BELGIË
MONITEUR BELGE
40-42, rue de Louvain - Bruxelles
BELGISCH STAATSBLAD
Leuvenseweg 40-42 - Brussel

DEUTSCHLAND
BUNDESANZEIGER
Postfach - Köln 1

FRANCE
SERVICE DE VENTE EN FRANCE
DES PUBLICATIONS DES
COMMUNAUTES EUROPEENNES
26, rue Desaix - Paris 15e

ITALIA
LIBRERIA DELLO STATO
Piazza G. Verdi, 10 - Roma

LUXEMBOURG
OFFICE CENTRAL DE VENTE
DES PUBLICATIONS DES
COMMUNAUTES EUROPEENNES
9, rue Goethe - Luxembourg

NEDERLAND
STAATSDRUKKERIJ
Christoffel Plantijnstraat - Den Haag

UNITED KINGDOM
H. M. STATIONERY OFFICE
P. O. Box 569 - London S.E.1

EURATOM — C.I.D.
51-53, rue Belliard
Bruxelles (Belgique)